

RONANDER, E

THE PHOTOCHEMISTRY OF URANIUM HEXAFLUORIDE AS
APPLIED TO LASER ISOTOPE SEPARATION

DPhil (Science)

UP

1998

The photochemistry of uranium hexafluoride as applied to laser isotope separation

by

EINAR RONANDER

Thesis Presented in Supplication of the Degree of

DOCTOR OF PHILOSOPHY IN SCIENCE

at the

UNIVERSITY OF PRETORIA

Promoter: Prof. E R Rohwer M.Sc (Stell.)
Ph.D. (RAU)

DEPARTMENT OF CHEMISTRY

December 1998

DEDICATED TO ROLF AND CARL

TABLE OF CONTENTS

	PAGE
SUMMARY	(i)
OPSOMMING	(iv)
ACKNOWLEDGMENTS	(vii)
DECLARATION	(ix)
CHAPTER I	
Introduction and Definition of Concepts	
1.1 Introduction	1
1.2 Lasers in chemical applications	2
1.3 Isotope separation	3
1.4 Scope and Aims of Project	9
1.5 Excitation of the internal modes of energy in polyatomic molecules	10
1.6 Terminology for energies	13
CHAPTER II	
The Unimolecular Decomposition of Uranium Hexafluoride	
2.1 Introduction	15
2.2 Transition state theory and the high pressure limit	17
2.3 Characteristic activated complexes and Arrhenius factors	22
2.4 Model for the loose transition state	23
2.5 Moments of inertia for the transition state	30
2.5.1 Introduction	30
2.5.2 The critical bond length for UF ₆	32
2.6 Comparison of transition state for UF ₆ with spatial configuration derived from thermochemical data	36
2.7 Prediction of unimolecular decay rate under MLIS conditions	43
2.8 Conclusions	47
CHAPTER III	
Vibrational Energy Exchange and the Quenching of the Unimolecular Decay Rate	

3.1	General	49
3.1.1	Rate constants, cross sections and collision numbers	52
3.2	Experimental method for the study of vibrational energy transfer	55
3.2.1	Experimental	55
3.2.2	Results	
3.2.2.1	HF fluorescence - dissociation with $16\mu\text{m}$	62
3.2.2.2	HF fluorescence as a probe for vibrational energy transfer from UF_6^*	62
3.2.3	Long range dipole-dipole interaction mechanism for the vibrational energy exchange in UF_6	65
3.2.4	Discussion and conclusions	70

CHAPTER IV

Measuring Unimolecular Dissociation Rates of UF_6 in a Molecular Beam in a Mass Spectrometer.

4.1	Reaction rates and the fragment ion abundances in a mass spectrometer	74
4.2	Electron impact ionization	76
4.3	Negative surface ionization	82
4.4	Ionization with XeCl Laser	91
4.5	Laser ionization in time-of-flight mass spectrometer	97
4.6	Negative ion formation and the detection in a TOF Mass Spectrometer	109
4.7	Conclusions	115

CHAPTER V

Secondary Chemical Dissociation Reactions following the Laser Instigated Unimolecular dissociation of Uranium Hexafluoride

5.1	Secondary reactions subsequent to the unimolecular dissociation of UF_6	116
5.2	Some basic reactions	116
5.2.1	Radiation with and without methane present	117
5.2.2	Identification of UF_4 in photolysis products	125
5.2.2.1	Infrared spectroscopy	126
5.2.2.2	Ultraviolet and near infrared spectroscopy	138
5.2.2.3	Mass spectrometry	142
5.2.2.4	X-Ray photoelectron spectroscopy (XPS) of laser photolysis products	143
5.2.3	Observation of dissociation products in a static cell by He-Ne laser beam scattering	147

5.3	Secondary reactions for uranium bearing compounds	149
5.4	Reactions of fluorine radical with methane	154
5.5	Reactions of the methyl radical	163
5.6	Secondary reactions following dissociation by ultraviolet laser	165

CONCLUSIONS 183

REFERENCES 185

APPENDIX A

Computing the Density of Vibrational States for UF₆ 192

APPENDIX B

The Rotational Partition Function and the Moments of Inertia for UF₆ 207

PAPERS

- I Laser Isotope Separation and the Concept of Separative Work.
– E Ronander, E R Rohwer and S P van Heerden
- II The TEA-CO₂ Laser in the Chemical Industry.
– E Ronander and E G Rohwer
- III A Long-Range Dipole-Dipole Interaction Mechanism for the Vibrational Energy Exchange in SF₆ and UF₆.
– E Ronander and E R Rohwer
- IV Multiphoton Infrared Dissociation of UF₆ and the Subsequent Ionization of the Photo Fragments in a Time-of-Flight Mass Spectrometer.
– E Ronander, C J Liebenberg and E R Rohwer

SUMMARY

The subject of this dissertation is the very relevant field of laser instigated photochemistry. Its application to the industrially important process of uranium separation is carefully studied and reported. The isotope separation is accomplished by selectively vibrationally exciting the minor isotope, ^{235}U , with an infrared laser. Subsequently, adequate laser energy of another infrared laser/s is coupled to the UF_6 molecule which causes bond rupture. The photochemistry of this laser based process will determine its economical viability. At the onset of this study very scant knowledge about the photochemistry of the uranium hexafluoride molecule was available in the scientific literature and important phenomena were unexplained. Many of these were clarified and explained during the course of this investigation. Furthermore, many previously assumed and accepted aspects concerning the photochemistry of uranium hexafluoride were proven to be incorrect or unsubstantiated.

Firstly, the laser instigated unimolecular dissociation rate of UF_6 was calibrated with experimental data. The RRKM statistical theory was employed to correctly describe the unimolecular dissociation process. Excellent agreement between theory predictions and experimental thermal dissociation data was obtained. This verifies the chosen geometrical configuration of the activated complex as proper and reasonable. A simple bond rupture reaction, where the activated complex is represented by a weak bonding of the UF_5 moiety to a fluorine atom, seems appropriate. In establishing the features of the activated complex, the vibrational frequencies of the UF_5 molecule were allocated to the transition configuration together with two hindered rotations. The U-F bond that is ruptured, is stretched to three times the equilibrium bond length in the activated complex. The well known Whitten Rabinovitch approximation to determine the density of the vibrational states was employed but a less cumbersome formulation for UF_6 was subsequently derived. This methodology was for the first time applied to UF_6 with very good results. Previous two efforts, reported in the scientific literature, were unsuccessful in the sense that agreement between theory and experimental observations was poor. This treatise shows that the unimolecular dissociation rate for UF_6 is at least two orders faster than previously advocated. This impacts very positively

on the entire separation process.

The influence of molecular collisions and the quenching effect this has on the unimolecular dissociation rate must normally be taken cognisance of. In chapter III the transfer of vibrational energy between UF_6 molecules is studied with the aid of a pump and probe experiment. When a hydrogen containing molecule like CH_4 is present in the gas mixture, strong HF fluorescence is detected when the F radical reacts with the former. This can be utilized to measure the transfer rate of vibrational energy. It was established that very fast transfer occurs when CH_4 is present and also the transfer mechanism between UF_6 molecules was identified to be of a long range nature. It is proposed that a dipole-dipole mechanism for vibrational energy exchange is operative. This seems to be confirmed by the inverse temperature dependence with the rate measured. This is in contrast to the hard sphere gas kinetic theory which predicts a direct dependence with temperature. In the final instance, however, the measured transfer rates are still much slower than the unimolecular dissociation rates of UF_6 determined in chapter III and its contribution can consequently be neglected at the envisaged gas density.

Much effort was expended during this study to experimentally measure the unimolecular dissociation rate of UF_6 , after laser excitation, inside a molecular beam apparatus. The measurement technique that is suitable for such an application is the mass spectrometry. However, the requirements to measure in the corrosive environment of UF_6 as well as the very fast time resolution needed, posed terrific challenges. Various ionization techniques to ionize UF_6 and its photo product were developed and tested. A commercial quadrupole mass spectrometer as well as a locally built time-of-flight mass spectrometer was utilized for the detection of ion fragments. It was established that the formation of negative molecular UF_6 ions in a pulsed mode represents the best solution to the requirements. Nevertheless, the actual rates could not be measured due to the demise of the MLIS project. The success of accurately modelling the thermal unimolecular dissociation of UF_6 , to a large degree compensated for this disappointment.

In the last chapter, the secondary reactions following on the unimolecular dissociation of UF_6 , are reported and scrutinized. This section represents a major overhaul of the established picture that prevailed up to this study. At least nineteen different conclusions, stemming from experimental observations, are put forward. Each of these differs profoundly from previously held views on the secondary reactions following laser photolysis of UF_6 . Amongst the more prominent findings are:

1. The presence of the uranium compound, UF_4 , in the laser photolysis products of UF_6 has unambiguously been established. This is true for both infrared and ultraviolet laser photolysis.
2. The internal energy content of nascent photolysis products is extremely important to determine the secondary reactions. Equally important is the rate of internal energy loss in various environments to promote or inhibit reactions.
3. There is a great danger in equating the results of static gas cell irradiations, i.e., repeated laser shots, with the photolysis results in dynamic systems. This has previously led to incorrect interpretations.

OPSOMMING

In hierdie skripsie word die belangrike onderwerp van lasergeïnduseerde fotochemie aangespreek. Die industriële toepassing hiervan vir die laserisotoopskeiding van uraan, word bestudeer en gerapporteer. Die eerste stap in die laserskeidingsproses is die isotoopselktiewe opwekking van die minderheidsisotoop, ^{235}U , met 'n infrarooi laser. Verdere energie word toegevoeg met 'n tweede (en derde) infrarooi laser wat daartoe lei dat die U-F binding in die UF_6 molekule breek. Die fotochemie speel 'n deurslaggewende rol in die ekonomiese lewensvatbaarheid van die isotoopskeidingsproses. By die aanvang van hierdie projek was die kennis van die fotochemie van UF_6 karig en 'n aantal eksperimentele waarnemings kon nie verklaar word nie. Tydens hierdie ondersoek is baie vrae opgeklaar en kan 'n eenduidige model opgestel word. 'n Aantal aanvaarde opvattinge in verband met die fotochemie is ook uitgewys as ongestaaf.

Daar is eerstens indringend gekyk na die unimolekulêre ontbinding van UF_6 soos beskryf deur die RRRM teorie en die daaropvolgende kalibrasie van die model met eksperimentele data. Uitstekende ooreenstemming kon verkry word tussen hierdie statistiese teorie en gemete termieseontbindingswaardes vir die reaksietempo. Dit bevestig dat die geometriese konfigurasie van die geaktiveerde kompleks, wat ontbinding voorafgaan, redelik en aanvaarbaar is. Die konfigurasie is voorgestel as 'n UF_5 molekule met 'n relatief swak binding met die fluoor atoom wat vrykom nadat die U-F-binding gebreek is. Gevolglik is die vibrasiefrekwensies van UF_5 sowel as twee beperkte rotasies toegeken aan die oorgangstoestand om die interne energie voor te stel. Die mate van verlenging van die binding wat opgehef word tydens dissosiasie is vasgestel met toepaslike teoretiese oorwegings. Aanvanklik is die bekende Whitten Rabinovitch formulering gebruik om die digtheid van vibrasievlakke te bereken maar later is 'n wiskundige beskrywing vir UF_6 daargestel wat meer elegant en minder tydrowend is. Die benadering wat in hierdie studie gevolg word om die ontbindingstempo te bereken is vir die eerste maal op UF_6 toegepas en lewer uitstekende resultate. Twee vorige pogings in die wetenskaplike literatuur was onbevredigend en ooreenstemming met eksperimentele waardes was swak. Daar word ook uitgewys dat die unimolekulêre ontbindingstempo vir UF_6 ten minste twee ordes vinniger is as voorheen beweer.

Gelukkig het dit 'n baie positiewe invloed op die industriële gebruik van laserisotoopskeidingsproses.

Normaalweg moet die rol van molekulêre botsings en die gevolglike uitruil van vibrasie-energie tussen UF_6 molekules deeglik in ag geneem word by die ontbindingstempos. Hoofstuk III van hierdie skripsie spreek dan ook hierdie onderwerp aan. 'n Tegniek van vibrasionele opwekking en toetsing is aangewend om die tydsverval van vibrasie energie te bestudeer. In die teenwoordigheid van CH_4 word HF gas gevorm na ontbinding, wat fluoresseer en gevolglik infrarooistraling uitgee. Hierdie straling kan aangewend word om die vibrasionele verval te monitor. Daar is sodoende gevind dat die uitruil van vibrasionele energie tussen UF_6 molekule baie vinnig is - vinniger as wat voorspel kan word met die bekende harde sfeer gas kinetiese teorie van botsings. 'n Uitruilmeganisme wat oor lang afstande tussen molekule effektief is, die sogenaamde dipool-dipool interaksiekragte word voorgestel as verklaring. Die toename in uitruiltempo met afname in gastemperatuur, - die teenoorgestelde word voorgestel deur die botsingsteorie - ondersteun die meganisme. Daar is egter gevind dat die ontbindingstempo van UF_6 so hoog is dat uitruil van vibrasie-energie weglaatbaar is by die betrokke gasdigthede.

Groot aksent is in die eksperimentele werk geplaas op die meting van die ontbindingstempo van UF_6 in 'n molekulêre bundel binne in 'n massaspektrometer. Hierdie metode, wat in die algemeen in besonder geskik is vir sodanige metings, het baie uitdagings gebied vanweë die uiters korrosiewe aard van UF_6 en die vinnige tydoplosvermoë wat verlang word by die ionisasietegniek. Verskeie ionisasietegnieke is gevolglik ontwikkel en geëvalueer. As meetinstrument is twee modelle massaspektrometers gebruik, naamlik: 'n kwadrupoolopstelling sowel as 'n vlugtydmassaspektrometer wat plaaslik ontwikkel is. Die ionisasietegniek waarby negatiewe molekulêre ione, UF_6^- , gevorm word in 'n gepulseerde bedryfswyse is uiteindelik verkies as die mees aanvaarbare tegniek. Nietemin kon die werklike ontbindingstempos nie gemeet word nie as gevolg van die vroeë staking van die verrykkingsprogram. Die sukses wat met die kalibrasie van die teorie in hoofstuk II behaal is, maak tot 'n hoë mate op vir hierdie teleurstelling.

In die laaste hoofstuk word daar intens aandag gegee aan die sekondêre chemiese reaksies wat volg op die lasergeïnduseerde ontbindingsreaksie van UF_6 . Die aanvaarde reaksies word hersien en die resultaat het wye gevolge. Teen die einde van hoofstuk V word 'n opsomming gegee van ten minste negentien belangrike gevolgtrekkings wat drasties verskil van die aanvaarde reaksiemodel. Onder die belangrikste gevolgtrekkings is die volgende:

- a) Die uraan produk UF_4 is positief geïdentifiseer as 'n fotolise produk beide vir infrarooi- en ultravioletlaserbestraling.
- b) Daar is bepaal dat die interne energie van die nuutgevormde fotoliseprodukte 'n deurslaggewende rol speel in die sekondêre reaksies. Ooreenstemmend is die blussing van die interne energie ewe belangrik om reaksies te bevoordeel of te beperk.
- c) Die aanvaarde praktyk om direk te projekteer vanaf die resultate van lasersbestralings in statiese houers na dinamiese gasvloei sisteme, hou ernstige gevaar in. Dit kan tot verkeerde gevolgtrekkings lei.

ACKNOWLEDGMENTS

This treatise was produced with the help, inspiration and stimuli of a number of people to whom I am deeply grateful. I would be remiss in not mentioning the ones who were the most important. It seems fitting to start at the beginning. Dr D M Kemp was responsible for me starting my working career at the Uranium Enrichment Corporation about 21 years ago. His seemingly boundless enthusiasm and passion for good science and more particularly, chemistry, left an enduring impression on me. I am still not sure what made him take a chance on me. Nevertheless, when I was requested to launch the laser isotope separation programme in 1983, it was the start of moving into the field of chemistry from physics. Since that time the UF_6 molecule has kept us engaged to unravel the secrets of its laser photolysis. Dr Kemp has often served as advisor, sounding board and mentor and for this I offer my sincere thanks.

Without a doubt the most important person for the last many years has been my supervisor, prof E R Rohwer. He has always been encouraging, helpful and inspiring. His critical reading of the text of this treatise contributed appreciably to the accuracy and clarity thereof. I have had the opportunity of working together with a number of excellent scientists over many years. A number contributed directly and indirectly to the results reflected in this study. In particular, I would like to express my gratitude to the following colleagues:

Dr Hennie Human - for his contributions to the laser scattering results and fluorescence.

Mr Christo Liebenberg - for the HF fluorescence results and the pump probe experiments.

Dr Willie Meyer- who kindly recorded the infrared spectra of UF_6 photolysis products for me.

Mr Hendrik Strydom- for assistance with the SIMS and ESCA spectra.

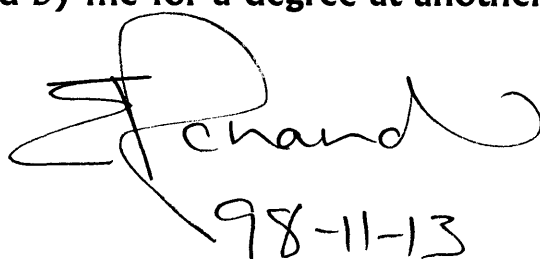
Mr Maarten Venter and

Mr Christo Green - for constructing the time-of-flight mass spectrometer.

The typing of the text was mainly done by my secretary of the last eight years Mrs J Meyer. For her untiring and unruffled assistance I thank her. She has been invaluable. Finally, I would like to thank the Atomic Energy Corporation for the opportunity to embark on this study.

DECLARATION

I declare that the thesis, which I submit with this for the degree of Doctor of Philosophy at the University of Pretoria, is my own work and has not previously been submitted by me for a degree at another university.

Handwritten signature of J. Chand
98-11-13

CHAPTER I

CHAPTER I

INTRODUCTION AND DEFINITION OF TERMS

1.1 INTRODUCTION

Laser-induced chemistry has received much attention in the past two decades. A number of uses of lasers for industrial scale chemical applications has been put forward and investigated. These applications include isotope separation, the purification of chemicals, the chemical modification of surfaces and the generation of catalytic intermediates. Lasers are also used very effectively in the study of reaction dynamics. The applicability of lasers to industrial scale synthesis is determined by economical considerations. In figure 1 [1] the selling price of some of

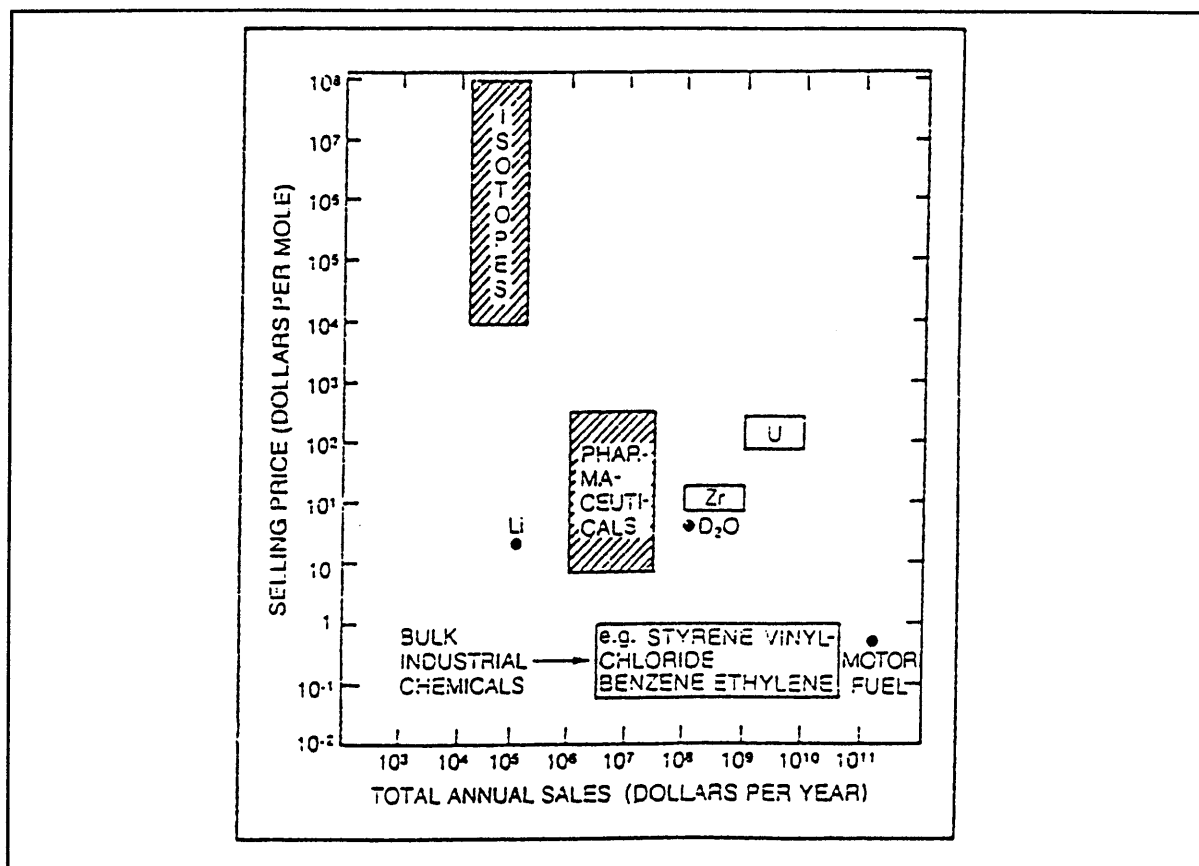


Fig. 1: Selling price compared with annual sales of some selected chemical in the USA.

the relevant chemicals are presented and it indicates that for most high volume chemicals, this is substantially below U\$1 per mole of product. It is also shown that some isotopes have a selling price of U\$10⁴ to 10⁸ per mole. These high value added products are therefore very good candidates for laser based processes. A product with a relatively high intrinsic value and of importance to the nuclear industry is isotopically enriched uranium. The latter has a value of ca U\$100 per mole of product. Due to the increased costs of modern medicines the laser synthesis of some pharmaceuticals is becoming more attractive.

Two aspects that dominate the economy of laser based processes are the quantum yield of the specific reaction and the cost of the laser photons. Another way of expressing the first factor is the specific energy consumption of the reaction, which will be dealt with more extensively in this dissertation. For a typical multiple-IR-photon process the quantum yield can be low and values between 10⁻¹ to 10⁻² are common. The quantum yield of a chemical reaction can be substantially increased if chain reactions are involved or if the laser photon interacts only with one minor component of the process gas. An example of the latter is the selective removal of H₂S from synthesis gas, CO + H₂, using an ArF laser. The second area of concern, namely the reduction of the cost of laser photons, has been intensely researched at the South African Atomic Energy Corporation for the past decade. In general it can be said that CO₂ lasers produce photons much more cheaply than other lasers. The lower cost per photon more than compensates for the low energy per photon (0,1eV) and therefore the greater number of photons required for photodynamical processes.

1.2 LASERS IN CHEMICAL APPLICATIONS

Figure 2 shows a simplified picture of how lasers are used in a photo process. Basically all we are doing is adding laser energy into some kind of chemical reaction. We assume that the addition of laser energy is going to improve the yield (kilogram of product per kilogram of feed material). This will then cost so many MJ (megajoules) of energy per kg of feed (1 MJ = 0,28 kWh).

DOCUMENT NUMBER	VERSION	PAGE	OF
LT100-000000-155-022		2	

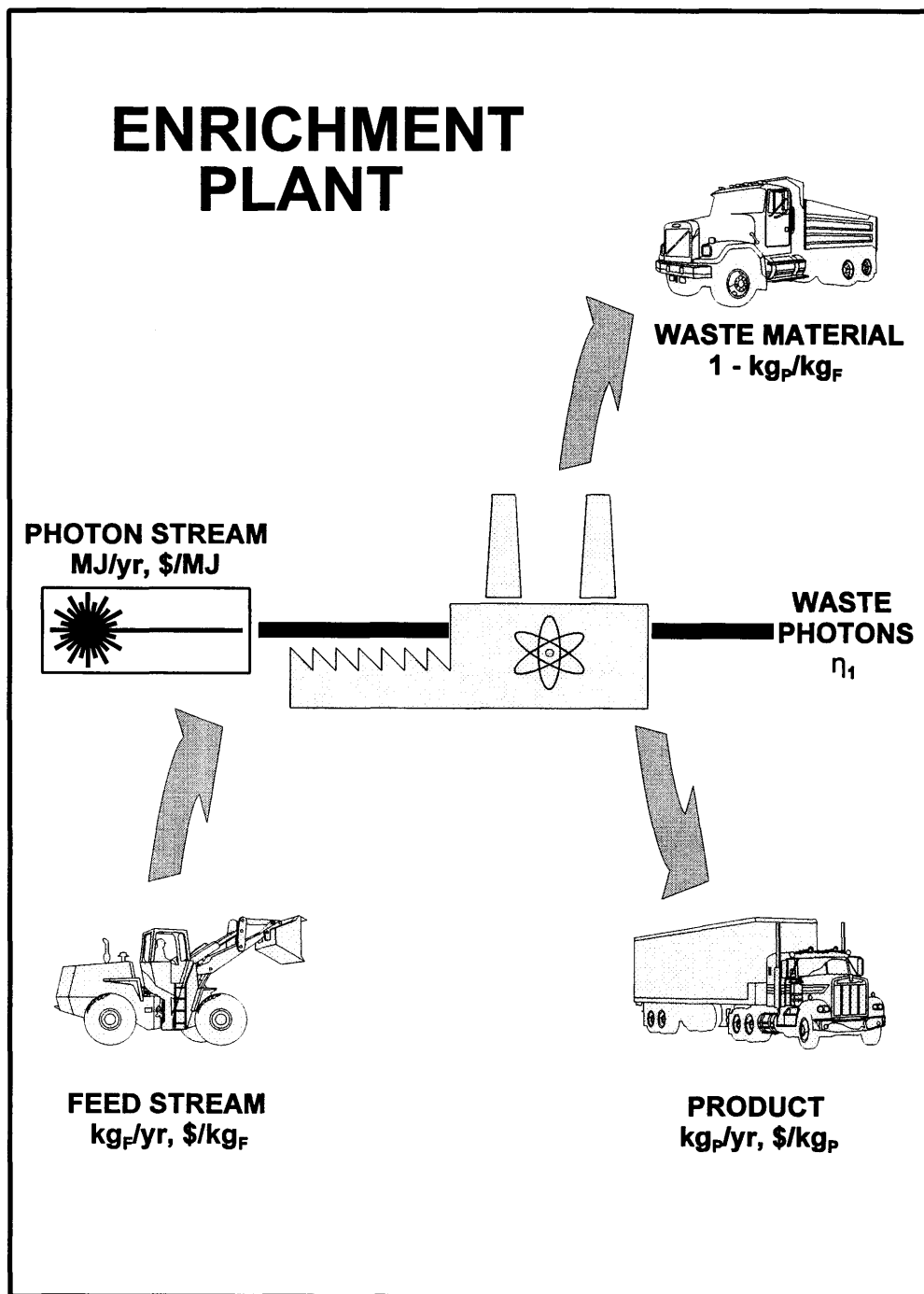


Fig.2: Application of lasers in chemistry.

If we concern ourselves for the moment only with isotope separation the unit cost of production can be expressed in the simple formula below (figure 3).

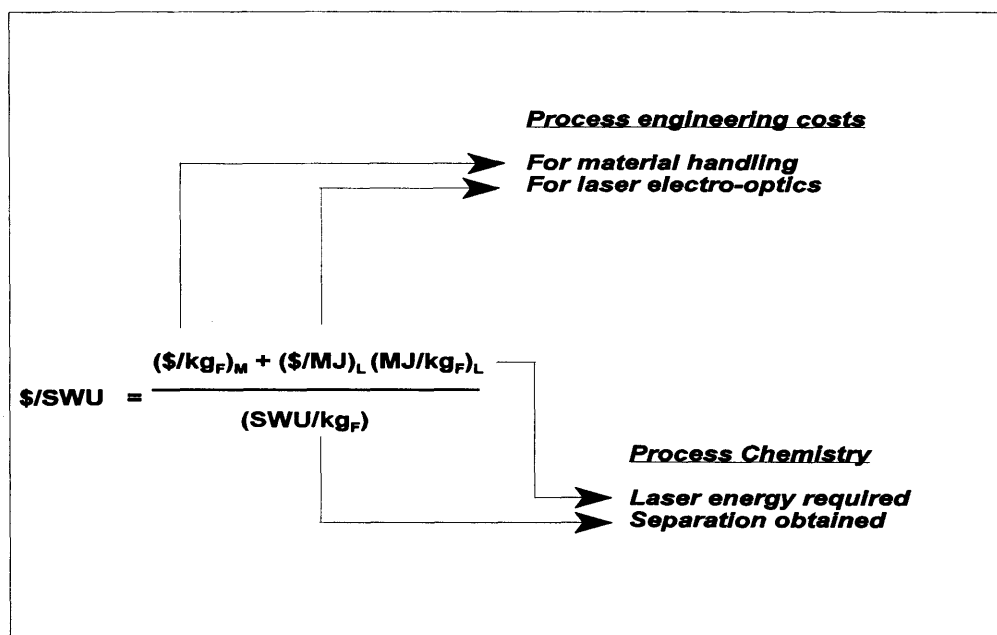


Fig. 3: Expression for the separation cost for uranium enrichment.

The units of separative work, SWU, has been defined specifically to deal with the separation of uranium. This parameter is defined and scrutinized meticulously in a paper produced during the time span of this dissertation, see paper I at the end of the dissertation. The concept of separative work units has been redefined and a methodology to deal with the high degrees of isotope selectivity of the laser based processes have been put forward. Figure 3 shows the US\$/separative work unit (SWU) and shows it divided into two major terms. The $(U\$/kg_F)$ in the first term is the dollars required to process the kg of material through the irradiation zone where it is illuminated by the lasers. Then the basic “yield” of the process or the SWU/kg_F being produced through the process would be represented by the denominator. Thus the first term gives the $U\$/kg_F$ associated with just processing materials through the plant independent of the cost of laser

irradiation. The second term consists of the specific amount of energy in MJ required to illuminate 1 kg of the material (uranium). This is multiplied by the dollars expended for each MJ of that energy.

For the physical chemist the main concern for the parameters in the simple relationship of figure 3, revolves around the specific energy consumption, MJ/kg_F, and the separation achieved. The first parameter is the topic of this dissertation as this is closely tied up with the unimolecular dissociation and subsequent secondary bimolecular reactions in the laser photolysis process.

1.3 ISOTOPE SEPARATION

A number of commercial opportunities exists for isotope selective laser chemistry. For the purpose of this discussion only those isotopes that can be separated with the TEA CO₂ laser will be considered. Table 1 summarizes some of the more important cases (also see paper II).

The best known example of isotope separation is the production of enriched uranium that is used in light water reactors. A process based on the TEA CO₂ laser has been proposed. This is being referred to as the MLIS process which is an acronym for molecular laser isotope separation. In the MLIS process multi-photon absorption in the ν_3 band of UF₆ is used to selectively excite the ²³⁵UF₆ isotope and finally dissociate the UF₆ molecule. Gaseous UF₆ is used since this is the only uranium compound with a sizeable vapour pressure at reasonable temperatures and fluorine as the sole partner exists only as a single isotope. Due to the complexity of the vibrational and rotational spectrum at ambient temperatures, the UF₆ molecule has to be flow cooled to below 100K. This is accomplished by the adiabatic expansion through a nozzle. The resultant molecular beam moves at a high speed of approximately 450 m/s. As a consequence a laser repetition rate of ~12 kHz and average output power of several kilowatt is required to irradiate all the UF₆ (figure 4) based on laser fluence and irradiation volume considerations.

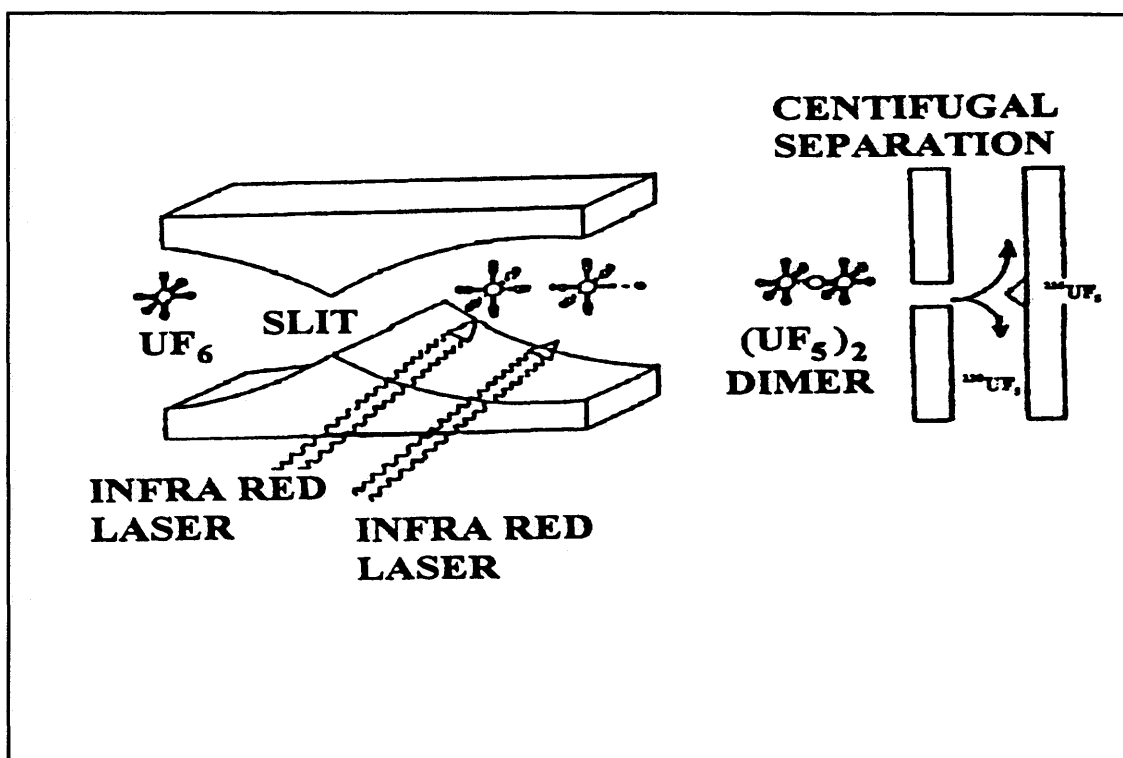


Fig 4: Schematic presentation of the MLIS process.

Figure 5 depicts in a schematic manner the main features of the photochemistry as applied to the separation of uranium isotopes. The laser excitation of the UF_6 occurs at time $t = 0$ and the laser pulses are very short relative to the time frame of the subsequent chemical activity. At the onset of this study the understanding was that the unimolecular decay process extends over 4 to 5 μs . This would allow enough time for collisional transfer of internal energy to impact on the dissociation rate, although this has never been quantified. In this dissertation this picture will be scrutinized for the reason that there remains a number of unexplained experimental observations. A second time span follows the unimolecular dissociation in which a number of secondary reactions can occur. After the time lapse of ca 500 μs all the products of the photolysis process are analyzed in a time-of-flight mass spectrometer and we therefore consider the reactions up to this point. Again a number of experimental observations in this second region remain unexplained. The goals of this dissertation are therefore clear:

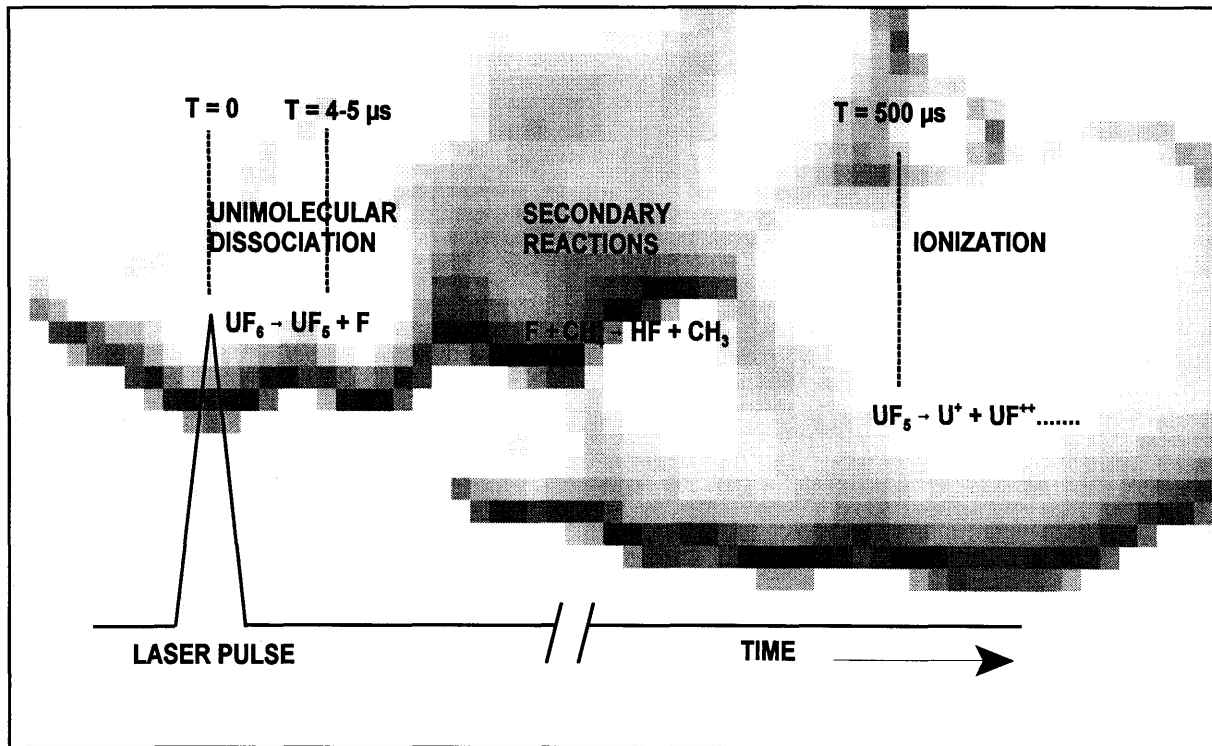


Fig 5: Time span for chemistry mechanism for MLIS.

1. Clarify and quantify the laser instigated unimolecular dissociation rate of UF_6 and calibrate this with experimental data. Previous efforts to this end have been unsuccessful in the sense that the agreement between theory and experimental observation was poor. Simultaneously, clarify the possible contribution of a bimolecular mechanism between UF_6 and the scavenger gas utilized for the fluorine radical annihilation.
2. Quantify and compare with experimental observations the contributions of secondary reactions to the main photolysis process. The loss of yield (cut) of the process is of utmost importance as this impacts critically on the specific energy consumption (MJ/kg_F) and consequently on the unit production cost of separation ($$/SWU$). It is therefore imperative to understand in detail the reaction mechanisms.

Table 1: Laser processes for isotope separation

<i>ELEMENT</i>	<i>APPLICATIONS</i>	<i>LASER PROCESS</i>
HYDROGEN	² H 0,015% na. Heavy water reactors, research applications	T/H separated by TEA CO ₂ laser decomposition of CF ₃ H
	³ H Lumiglow sources	T/D separated by TEA CO ₂ laser decomposition of CCl ₃ H
BORON	¹⁰ B 19,78% na. Safety devices and control rods of nuclear reactors and neutron counter tubes	TEA CO ₂ laser dissociation of BCl ₃ .
CARBON	¹² C Isotopically pure form has special thermal properties (higher conduction) and used in the growth of diamond and DLC coatings.	TEA CO ₂ laser dissociation of CF ₂ HCl (Freon 22). Single step process: 99.99% ¹² C and 72% ¹³ C. Two step process: ¹³ C > 95%
	¹³ C 1,11% na. Medical, biological and agricultural tracer studies and accelerator beam particles.	TEA CO ₂ dissociation of CF ₂ Cl ₂ (Freon 12) with HI as co-reagent. CF ₂ H ₂ product 97% enriched.
NITROGEN	¹⁵ N 0,37% na. Medical, biological and agricultural tracer studies and accelerator beam particles.	TEA CO ₂ laser dissociation of NH ₃
OXYGEN	¹⁷ O 0,037% na. 50% enrichment used for ¹⁷ O NMR, medical diagnostics and studying properties of high T _c superconductors. Both ¹⁷ O and ¹⁸ O used as accelerator beam particles.	TEA CO ₂ laser dissociation of diisopropyl ether.
	¹⁸ O 0,204% na. CO ₂ lasers for LIDAR applications in atmospheric window, production of ¹⁸ F for positron emission tomography (PET) from ¹⁸ O (p,n) ¹⁸ F, PET appears to be a growing medical market.	
SULPHUR	³⁴ S 4,22% na. Environmental pollution dilution studies of SO ₂ and drug metabolism.	TEA CO ₂ dissociation of SF ₆ .
	³⁶ S 0,014% na.	
MOLYBDENUM	⁹⁸ Mo 23,78% na. Required for ^{99m} Tc generator, produced by ⁹⁸ Mo (n,λ) ⁹⁹ Mo.	TEA CO ₂ laser dissociation of MoF ₆ .

1.4 SCOPE AND AIMS OF PROJECT

Before one continues the text and introduces the nomenclature which is indispensable to follow the context of this treatise, it seems advisable to reflect on the scope and aims of the project. This will obviously refer to the status as perceived at the launch of the project. Under the final compilation of the conclusion, the degree of success or achievement will be registered.

At the onset of the project, reliable theoretical estimations of the rate coefficients for the laser instigated unimolecular dissociation of UF_6 were not available. It was clear that a description of the dissociation kinetics must be put forward based on e.g. the RRKM statistical theory. It was imperative to calibrate this model with reliable experimental data. If the dissociation rate could be reliably predicted, especially to cover a wide range of parameters, this would greatly reduce the viability risks involved in scaling up the separation process to industrial scale. The measurement of yield data (also separation data) had become time consuming in the development of the separation process. In an early stage of the project it was concluded that the measurement of the real time dissociation rate in situ in a molecular beam apparatus would be a sensible approach to generate experimental data for the calibration purpose. In principle the mass spectrometer is very suitable for such type of measurements and consequently an evaluation of relevant ionization techniques was launched. Furthermore, an experimental technique applicable to the determination of collisional exchange rates was needed to establish the role of collisions in the unimolecular dissociation rate of UF_6 . In the economical analysis of the separation process the molecular density in the irradiation chamber proves to be crucial. An increased density is highly desirable. However, collisional effects could have a detrimental effect on the separation performance. A quantification of its contribution became essential.

Once the dissociation process was well understood and quantified it was deemed necessary to revisit the mechanism and role of secondary chemical reactions. The chemist was never very comfortable with the excepted hypotheses to explain some chemical phenomena. Some examples were:

DOCUMENT NUMBER	VERSION	PAGE	OF
LT100-000000-155-022		9	

1. In the process gas CH_4 is used as scavenger gas. At the German laboratories of Uranit, that also studied MLIS, the scientists clearly believed that a scavenger gas was not necessary. In South Africa we believed it to be essential to secure a good process yield. This needed clarification.
2. The formation of CH_3F as a reaction product was seen as undesirable and also connected to the loss of selectivity. No sound scientific evidence, however, existed to support this view.
3. An uranium compound that contained the hydrogen atom was consistently detected in solid photolysis products that were analysed by mass spectrometric techniques. No explanation for this had been offered.

It, therefore, became imperative to study in greater detail the secondary reactions following unimolecular dissociation. The gist of the endeavours would be to establish clearly what reaction steps the uranium bearing compounds encounter. It became important to generate a commensurate picture to appropriately explain the experimental observations.

1.5 EXCITATION OF THE INTERNAL MODES OF ENERGY IN POLYATOMIC MOLECULES

Infrared spectroscopy normally refers to quantum transitions between vibration-rotational levels which occur at the minimum of the internuclear distance of the molecular potential energy and also in the ground electronic state. Since the first observation of the multiphoton absorption process and the unique effects arising from this excitation process, considerable theoretical and experimental efforts have been directed towards understanding this phenomenon. The results have led to a physical model of the multiphoton vibrational excitation of molecules by intense infrared radiation, which is at the root of multiphoton infrared photochemistry and its practical applications, e.g. laser isotope separation.

DOCUMENT NUMBER	VERSION	PAGE	OF
LT100-000000-155-022		10	

Figure 6 illustrates schematically the main stages of the infrared multiphoton excitation and subsequent dissociation of a polyatomic molecule such as UF_6 within the framework of the simple model that has been put forward. According to this model, the molecule in the course of its vibrational excitation passes through three distinctly different regions:

1. A region of low-lying discrete vibrational-rotational levels where few transitions are possible from a given initial state.
2. A region of dense vibrational states referred to as the quasi-continuum where a large number of transitions are possible from a given state.
3. The continuum region which extends beyond the dissociation limit where the unimolecular decay of the vibrationally overexcited molecule becomes possible.

At moderate intensities of the laser field, the excitation in the discrete part of the absorption features, proceeds along the line of resonant multistep

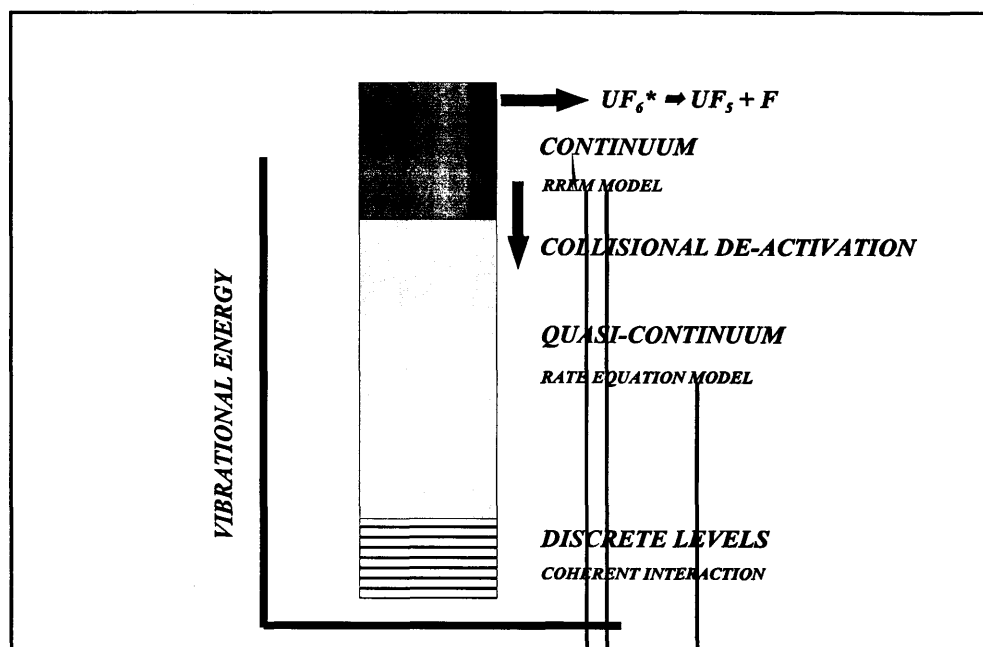


Fig. 6: The three distinct regions associated with the multi-photon excitation of polyatomic molecules.

excitation of molecular vibrations. This resonant absorption can be accomplished despite the anharmonic detuning due to a change in the rotational energy of the molecule, anharmonic splitting of the excited vibrational states etc. At higher laser energies, direct two- and three-photon transitions are possible where resonance is possible between two, or three, simultaneous quantum transitions. As the vibrational energy of the molecule grows, the vibrational energy is very rapidly distributed amongst all the vibrational modes. This occurs above a limit referred to as the stochastization energy. In this fashion a molecule can acquire an energy comparable with the dissociation energy, but this acquired energy will be distributed among many degrees of freedom. This phenomenon allows us to apply statistical theories to describe the dissociation process which, for smaller molecules, must be instigated by collisions. According to the statistical theory of unimolecular decay, RRKM theory, for the weakest molecular bond to break, the vibrational energy of the molecule must be concentrated, as a result of fluctuation, on this bond which requires several vibrational periods. The laser utilized for dissociation usually has a pulse length of 10^{-7} s or shorter which implies a required dissociation rate faster than 10^7 , if dissociation should occur within the laser pulse to limit collisional effects. Consequently, after 10^{-7} s, the molecule should contain energy significantly in excess of its dissociation energy derived from thermochemical data.

For the purpose of laser isotope separation, the isotope selective excitation of molecular vibrations in the discrete region of the vibrational energy ladder is very important. This phenomenon for UF_6 has been extensively studied and modeled at the AEC. The achievement of the theoretical efforts in this regard is nothing less than outstanding. In the quasicontinuum the excitation process can be described by rate equations as was very successfully demonstrated for SF_6 and UF_6 . The third stage of the excitation process and subsequent dissociation of UF_6 is the main topic of this report. To this purpose the RRKM theory will be utilized and appropriate calibration procedures for the decay rate will be scrutinized. Simultaneously the competing processes of collision deactivation, which impacts on the laser energy requirements for dissociation, will be quantified.

1.6 TERMINOLOGY FOR ENERGIES

The RRKM theory predicts the unimolecular decay rate of molecules with statistical mechanics based on the number of ways that a given amount of energy can be distributed between the various degrees of freedom of a polyatomic molecule. To this purpose any fixed amount of energy that cannot be redistributed is clearly of no interest. Examples of such fixed modes or amounts of energy are the translational energy and the zero point energy of a molecule. Distinguished from this form of energy are the non-fixed energies, e.g. vibrational- and rotational energy, that can be freely redistributed. The term active is used to describe the non-fixed degrees of freedom that can all contribute to the reaction rate.

To understand the significance and be able to handle all the different energy terms that will be utilized in this dissertation, they will now be introduced. Figure 7 illustrates the energies involved in the unimolecular reaction of a molecule A [2].

The energized molecule, denoted by A^* represents a molecule that has obtained, e.g. by laser excitation, an excess internal energy, E^* , in the active degrees of freedom exceeding the critical energy value E_0 below which a classical reaction cannot occur. The energy, E^* , comprises both vibrational and rotational energy denoted by E_v^* and E_r^* respectively and clearly

$$E^* = E_v^* + E_r^* \quad (1.1)$$

Note that these energies are measured from the zero-point energy of the ground electronic state of the molecule. The activated complex that precedes the bond rupture reaction is denoted by A^+ and the non-fixed energy of the complex by E^+ . The transformation from an energized molecule to the activated complex “consumes” an amount of energy E_0 to surmount the energy barrier which has thus become fixed. Consequently E^+ and E^* for a corresponding complex and energized molecule are simply related by

$$E^+ = E^* - E_0 \quad (1.2)$$

E^+ contains components of both vibrational and rotational energy denoted by E_v^+ and E_r^+ . It is important to note that non-fixed energy of the energized molecule can become fixed in the translational motion of A^+ along the reaction coordinate;

$$E^+ = E_v^+ + E_r^+ + x \quad (1.3)$$

with x the associated translational energy.

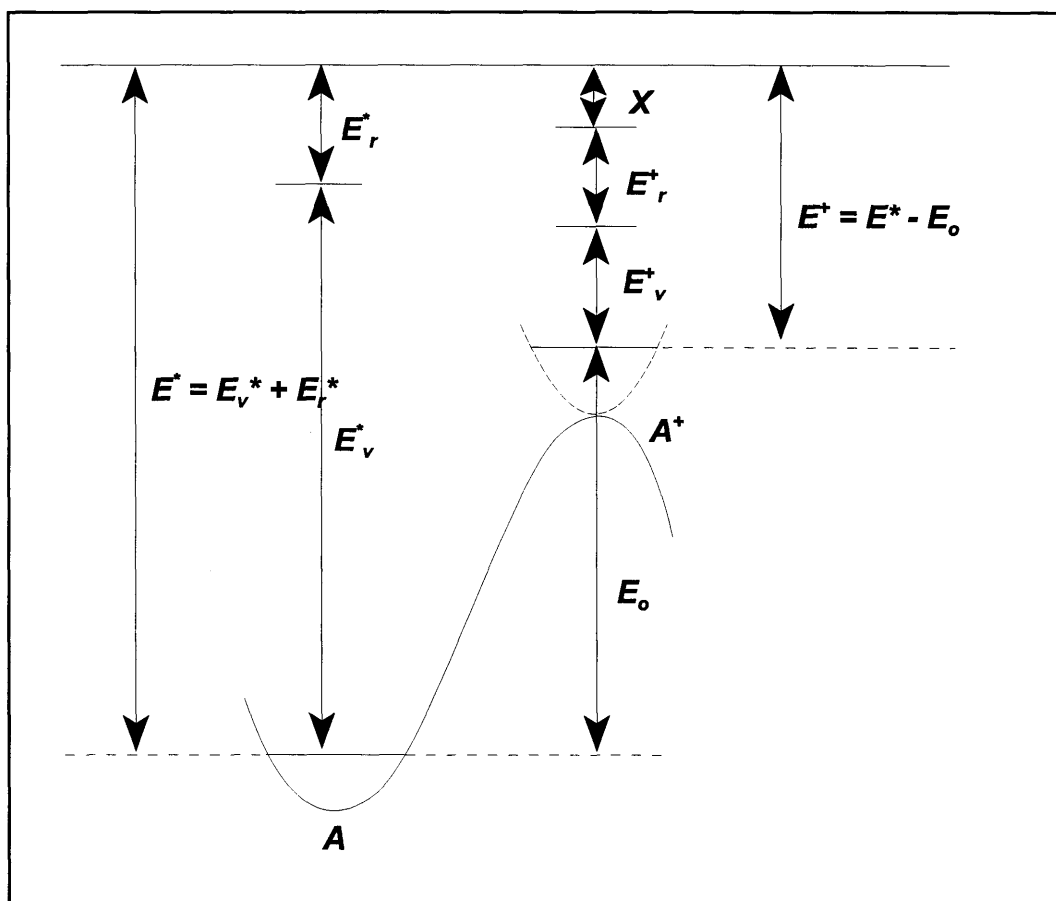


Fig.7: Illustration of energy terminology for a unimolecular reaction.

CHAPTER II

CHAPTER II

THE UNIMOLECULAR DECOMPOSITION OF URANIUM HEXAFLUORIDE

2.1 INTRODUCTION

A gas-phase unimolecular reaction is an apparently simple process: an isolated molecule undergoes a chemical change. However, to understand this process in detail, one requires virtually the full gamut of modern theoretical chemistry. Unimolecular reactions include isomerizations such as that of cyclo-heptatriene to toluene, eliminations such as that of chloroethane and dissociations such as the breaking of the C-H bond in CH_4 . The difference between isomerizations, eliminations and dissociations lies in the form of the potential surfaces, which are illustrated schematically in figure 8 [3].

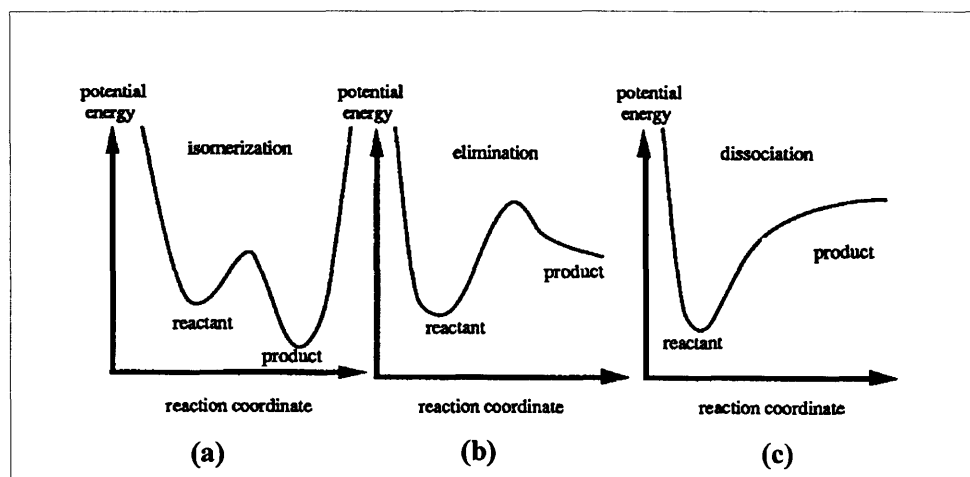


Fig. 8: Potential energy along reaction coordinate for isomerizations, eliminations and dissociations.

The laser dissociation of molecules such as SF_6 and UF_6 is best described by the potential energy along the reaction coordinate as depicted in figure 8(c). This potential energy function shows no or little energy barrier in the reverse direction i.e. for the recombination reaction. The UF_6

molecule that actually undergoes reaction must have a high internal energy at least to exceed the barrier between reactant and product. To reach an internal energy sufficient for reaction requires excitation which is acquired via collisions in the case of the thermal process and via the absorption of laser photons when the dissociation is instigated by laser. For the latter case we can write for UF_6



The actual reaction event then occurs in a second step:



The suggestion that thermally induced unimolecular reactions involve separable reaction and activation steps was first made by Lindemann (1922), who simultaneously pointed out that this assumption leads to the pressure dependence depicted in figure 9 [4].

This dependence involves (1) a high-pressure limit, in which the rate coefficient becomes independent of the pressure; (2) a low-pressure limit, in which the rate coefficient is proportional to the pressure, and (3) a fall off regime which involves the transition from one limit to the other. This means that at low pressures, a unimolecular reaction is of second order overall, being first order with respect to reactant and first order with respect to bath gas. If the reactant is immersed in an inert bath gas, e.g. Ar or N_2 , then the reaction is still first order with respect to reactant; on the other hand, if there is no inert bath gas present, then the reactant acts as its own bath gas and the reaction is then second order with respect to reactant in the low-pressure regime.

The dissociation of UF_6 by laser as applied in the MLIS process takes place at low pressures whilst in this report it will be shown how the functional description of the Arrhenius equation that is applicable in the high-pressure region, can be utilized to describe the properties of the transition state which is essential to determine the rate of reaction (2.2).

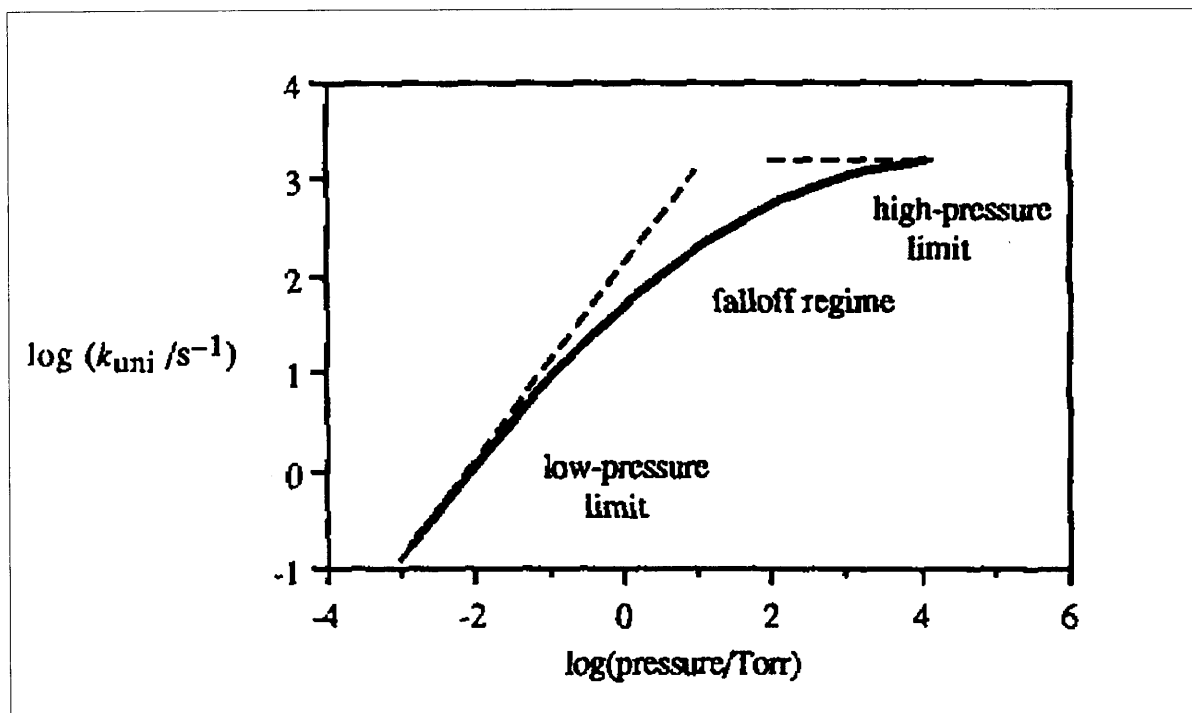


Fig. 9: Schematic illustration of the dependence of the thermal rate coefficient for a unimolecular reaction on the pressure of bath gas. Broken lines indicate high- and low-pressure limiting values.

2.2 TRANSITION STATE THEORY AND THE HIGH PRESSURE LIMIT

Transition state theory is widely used by experimentalists to interpret rate data. This is because it requires no calculations on the dynamics of the reacting system, since the approximations made in the theory enables one to calculate the rate coefficient solely in terms of the statistical properties of the system, specifically the thermodynamics of the activated complex. Moreover, the properties of this activated complex can often be estimated a priori, and thus the theory can be used predictively, both qualitatively and quantitatively. We first need to provide a proper definition of the activated complex, which is synonymous with the transition state, and also define the transition state formula from which the rate coefficient for the high pressure regime can be established.

As previously mentioned, in this report the thermal decomposition rate of UF_6 will be fitted for the high-pressure regime to derive the properties of the activated complex. For this regime the time scales for reaction and for collision energy transfer in an isolated molecule are well separated in a unimolecular system. The collisional activation process can be represented by the step:



with a time duration of $\sim 10^{-13}$ sec. In contrast, the lifetime with respect to reaction of an isolated A^* :



is typically 10^{-9} sec or greater (note that we are specifically referring to the high-pressure regime). Hence collisional activation and deactivation occurs essentially instantaneously relative to the lifetime of an excited molecule with respect to reaction. It is therefore possible to separate the theoretical treatment of the two processes which is the basis of the Lindemann mechanism:

The rate equations that describe these processes are:

$$\frac{d[A]}{dt} = - [M]R_+ [A] + [M]R_- [A^*] \quad (2.5)$$

and

$$\frac{d[A^*]}{dt} = [M]R_+ [A] - [M]R_- [A^*] - k[A^*] \quad (2.6)$$

From the steady state approximation for A*:

$$[A^*] = \frac{[A] [M] R_+}{k_+ [M] R_-} \quad (2.7)$$

follows

$$\frac{d[A]}{dt} = \frac{k [M] R_+}{k + [M] R_-} [A] \quad (2.8)$$

This represents an example of first-order kinetics, with rate coefficient

$$k_{uni} = \frac{k [M] R_+}{k + [M] R_-} \quad (2.9)$$

At high pressures in the limit when $[M] \rightarrow \infty$, the corresponding rate coefficient is given by

$$\lim_{[M] \rightarrow \infty} k_{uni} = k_{uni}^\infty = \frac{k R_+}{R_-} \quad (2.10)$$

Therefore the high-pressure rate coefficient is pressure-independent and the overall rate is dictated by that of the reaction step 2.4. No knowledge of the collisional processes are required to deal with the dissociation rate in this regime.

The transition state formula (for derivation see reference [3]), for the high-pressure rate coefficient is:

$$k_{uni}^\infty = \frac{k_B T}{h} \frac{Q^\ddagger}{Q} \exp(-E_o / k_B T) \quad (2.11)$$

with E_0 = the critical energy of the transition state i.e. its minimum energy; k_B is the Boltzmann constant; h is Planck's constant and T the temperature. Here Q and Q^+ are the partition functions of the reactant and "activated" complex, respectively. We next revise the formula for partition functions. We shall adopt the common assumption that the dynamics of both reactant and of transition state are separable into independent vibrations and rotations. One can therefore write either partition functions as:

$$Q_{tot} = \prod_i Q_i^{vib} \prod_j Q_j^{rot} \quad (2.12)$$

where Q_i^{vib} and Q_j^{rot} are the partition functions for the i^{th} vibrational and j^{th} rotational degrees of freedom. For the activated complex we will have one less degree of freedom because the degree of freedom corresponding to the reaction coordinate is not included in calculating Q^+ .

To find the partition functions it is better to use the quantum mechanical expressions rather than the classical ones. If we assume that each vibration can be treated as that of a simple harmonic oscillator with vibrational frequency ν_i , the quantum partition function is:

$$Q^{vib} = \prod_i (1 - e^{-h\nu_i/k_B T})^{-1} \quad (2.13)$$

The partition function for the rotation of a linear molecule is given by:

$$Q^{rot}(\text{linear molecule}) = \frac{k_B T}{\sigma h c B} \quad (2.14)$$

where σ is the symmetry number, c the speed of light and B the rotational constant. If B is

expressed in the usual units of reciprocal length, e.g. cm^{-1} , $B = h/4\pi cI$, where I is the moment of inertia. For a non-linear molecule, one has instead:

$$Q^{rot} (\text{non-linear molecule}) = \frac{1}{\sigma} \left(\frac{k_B T}{hc} \right)^{3/2} \left(\frac{\pi}{ABC} \right)^{1/2} \quad (2.15)$$

where A , B and C are the three rotational constants for the molecule. A more detail discussion and the methodology to calculate vibrational - and rotational partition functions can be found in Appendix A and B respectively.

The incorporation of symmetry numbers in the transition state formula deserves a short discussion. The straightforward high-pressure transition state formulation, equation (2.1), and also the RRKM formulation refers basically to the dissociation rate by a single reaction path from the reactant molecule to the products. It often happens that there are several paths which are physically distinct but nevertheless completely equivalent in so far as the rate calculation is concerned. Such reaction paths involve activated complexes which are geometrical or optical isomers of each other. In this case the calculated rate must be increased by an appropriate factor known as the statistical factor or reaction path degeneracy denoted by L^+ . This factor is derived from the ratio σ/σ^+ of the symmetry numbers of the rotations, both internal and overall, of the reactant and activated complex. Thus the usual formulation can be written as:

$$k_{\infty}^{uni} = \frac{\sigma}{\sigma^+} \frac{k_B T}{h} \frac{Q^+}{Q} \exp(-E_o/k_B T) \quad (2.16)$$

in which the symmetry numbers are not included in the rotational partition functions (they should not be included twice)[3].

The symmetry number is defined as the total number of independent permutations of identical atoms or groups in a molecule that can be arrived at by simple rigid rotations of the entire

molecule. A simple method of estimating σ is to multiply the symmetries of each of the independent symmetry axes. For the case of the CH_4 molecule where we have four independent threefold symmetry axes the symmetry number $\sigma = 4 \times 3 = 12$. UF_6 has six fourfold axes and $\sigma = 6 \times 4 = 24$. For those who are familiar with point groups and their symmetry designations, table 2 summarizes the symmetry numbers of molecules belonging to different groups [5].

Table 2: Symmetry number for various point groups^a

POINT GROUP	σ	POINT GROUP	σ	POINT GROUP	σ
C_1 C_i C_s	1	D_2 D_{2d} $D_{2h} \equiv V$	4	$C_{\infty v}$	1
C_2 C_{2v} C_{2h}	2	D_3 D_{3d} D_{3h}	6	$D_{\infty h}$	2
C_3 C_{3v} C_{2h}	3	D_4 D_{4d} D_{4h}	8	T, T_d	12
C_4 C_{4v} C_{4h}	4	D_6 D_{6d} D_{6h}	12	O_h	24
C_6, C_{6v}, C_{6h}	6	S_6	3		

^aTaken from G Herzberg, *Molecular Spectra and Molecular Structure*, Van Nostrand, Princeton, N J, 1945. C_j indicates a j -fold axis of symmetry. D_j denotes a molecule of the class C_j with a j -fold axis and J twofold axes at right angles to the C_j axis and at equal angles to each other. T denotes tetrahedral symmetry, and O , octahedral symmetry.

2.3 CHARACTERISTIC ACTIVATED COMPLEXES AND ARRHENIUS FACTORS

The chemical structure, i.e. the spatial configuration, of the activated complex has a pronounced effect on the rate coefficient. Thus the experimentally observed A-factor is strongly indicative of the structure of the transition state. According to the A-factor transition states can be classified into different structures. The simplest type of transition state that is applicable to the dissociation of UF_6 , is the simple bond fission transition state. As can be seen from figure 8 there is no barrier to recombination and the critical energy is equal to the bond dissociation energy. This situation is encountered when the reactant is a closed-shell specie and both the two products are

free radicals. This type of reactions have very high A-factors because the transition state is a very loosely bonded state. Typical A-factors range from 10^{16} to $10^{17.5} \text{ s}^{-1}$ [2, 3].

2.4 A MODEL FOR THE LOOSE TRANSITION STATE

The model given in this section is simplistic, but illustrates the essential features of the rupture of a single bond, and therefore fills an important pedagogical purpose. Consider the simple fission transition state for the CH_4 molecule involved in the decomposition to a methyl radical and a hydrogen radical. This model is schematically depicted in figure 10 which shows that the transition state involves a substantially stretched carbon-hydrogen bond. Current information on the CH_3 radical suggests that there are no significant changes in the C-H bond lengths nor even in H-C-H angles in comparing CH_4 with CH_3 . The CH_3 radical is nearly planar with an angle of $\sim 117^\circ$ for the H-C-H bond angle compared to the corresponding tetrahedral angle of $109,5^\circ$ in CH_4 . The active degrees of freedom in the loose transition state of figure 10 are as follows:

1. The product-like vibrations, i.e. we allocate the vibrations of the methyl radical to the methyl moiety in the transition state.
2. The rotational degrees of freedom about the three principle axes where two moments of inertia are increased by a factor (we will later see that this factor is $\sim 2,2$), determined by the extension of the C-H bond length.
3. A change in external symmetry, where $\sigma^+ = 1$ for the methyl radical must be included in the rotations.
4. The two-dimensional rocking motions of the hydrogen moiety in the methane molecule are treated as a hindered two-dimensional rotation. This stems from the observation that at significant extensions of the C-H bond the restoring forces for the rocking vibrations are not operative. Consequently this mode of energy is rather treated as rotations of the

transition state. It is clear that the hydrogen moiety cannot rotate freely because the methyl fragment will interfere with the rotation and consequently this steric interaction will reduce the solid angle available for the rotation.

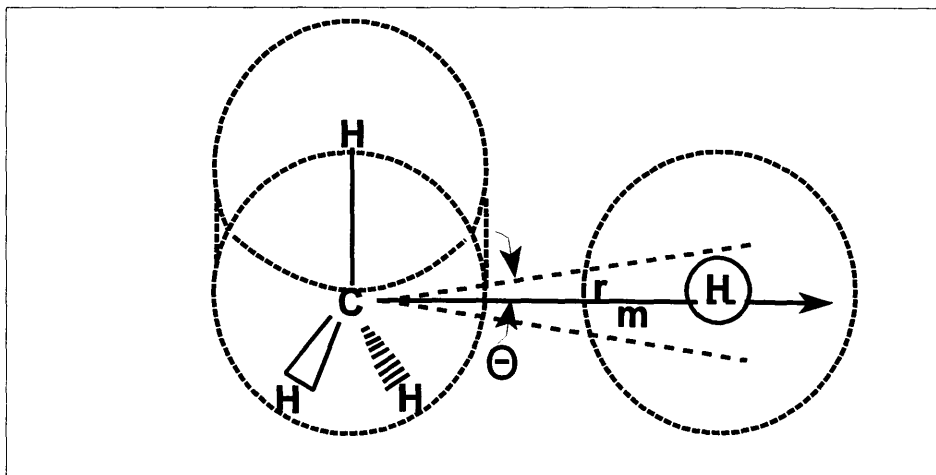


Fig.10: Spatial configuration of the activated complex during the rupture of the C-H bond in CH_4 .

The calculations for points 1 to 3 can be done in a straightforward manner similar to the treatment of the reactant molecule CH_4 . The treatment of the hindered rotations under point 4 merits a more expansive discussion as this will also be utilized for the case of UF_6 . For the transition state one can take a spatial configuration in which the C-H bond has been extended to 2,8 times it's equilibrium distance of 1,1Å or 3,08 Å as shown in figure 10. The extension of 2,8 X will now be substantiated on the basis of the potential of interaction between the methyl fragment and the hydrogen atom. A more sophisticated approach to establish the transition state bond distance is offered for UF_6 but for the present purpose the following approach will suffice.

It has been well established that the interaction potential between the methyl fragment and the hydrogen atom can be represented by a simple Lennard Jones (V_{LJ}) or Morse (V_{M}) or Buckingham potential (V_{BE}) function which depends on the internuclear distance r . Lets consider only the Lennard-Jones potential as similar results are obtained for the other two expressions. If we introduce the dimensionless variable parameter $\rho = r/r_0$ where r_0 is the equilibrium internuclear

distance, then:

$$V_{LJ} = -E_o (2/\rho^6 - 1/\rho^{12}) \quad (2.17)$$

where E_o = the potential energy of interaction at $r = r_o$.

The general shape of the potential is shown below (figure 11).

At $r = r_o$, $V = -E_o$, and this represents a minimum in the potential energy, hence

$$\left(\frac{dV}{d\rho} \right)_{\rho = 1} = 0 \quad (2.18)$$

Around the equilibrium position the vibrational frequency for a harmonic oscillator is related to the force constant, k , and the reduced mass, μ , by

$$\nu = \frac{1}{2\pi} (k/\mu)^{1/2} \quad (2.19)$$

To include the rotational energy in expression (2.17) we must add the energy E_{rot} :

$$E_{rot} = \frac{P_{\theta}^2}{2I_r} = \frac{P_{\theta}^2}{2\mu r^2} = \frac{E_{rot}^o}{\rho^2} \quad (2.20)$$

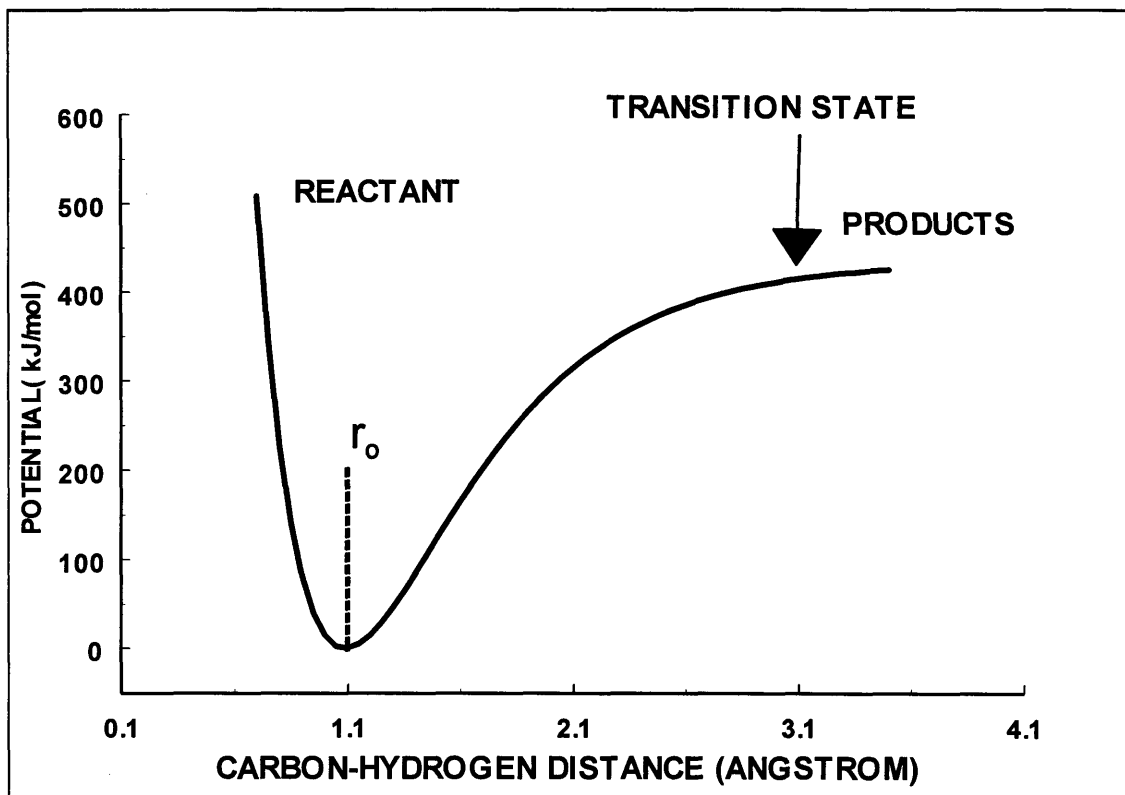


Fig. 11: Morse potential for the C-H bond in CH_4 . $E_0 = 410 \text{ kJ/mole}$ and $r_0 = 1,09 \text{ \AA}$.

where P_θ is the angular momentum which is constant for an isolated molecule. E_{rot}^0 is associated with the rotational energy at $\rho = 1$. At the maximum of the total interaction potential, Lennard-Jones plus centrifugal potentials, we find a natural position to locate the transition state and this occurs where

$$\frac{dV_{\text{tot}}}{d\rho} = 0 \text{ at } \rho = \rho_{\text{max}}$$

Remember that

$$V_{\text{tot}} = V(\rho) + E_{\text{rot}} \quad (2.21)$$

At the relative large internuclear distances consider here the short range repulsive component in the Lennard-Jones potential can be ignored. Consequently

$$\begin{aligned}
 V_{tot} &= -E_o \left(\frac{2}{\rho^6} - \frac{1}{\rho^{12}} \right) + \frac{E_{rot}^o}{\rho^2} \\
 &= -\frac{2E_o}{\rho^6} + \frac{E_{rot}^o}{\rho^2} \quad (\rho \gg 1)
 \end{aligned}
 \tag{2.22}$$

Then

$$\left(\frac{dV_{tot}}{d\rho} \right)_{\rho = \rho_{max}} = 0 = \frac{12E_o}{\rho_{max}^7} - \frac{2E_{rot}^o}{\rho_{max}^3}
 \tag{2.23}$$

At the top of the barrier the average rotational energies = RT, then:

$$\begin{aligned}
 E_{rot}(\rho = \rho_{max}) &= E_{rot}^o / \rho_{max}^2 = RT \\
 \text{or } E_{rot}^o &= RT \rho_{max}^2
 \end{aligned}
 \tag{2.24}$$

Substituting this result into equation (2.23) and solving, we find:

$$\rho_{max} = \left(\frac{6E_o}{RT} \right)^{1/6}
 \tag{2.25}$$

Calculated numerical values for ρ_{max} show that it is very insensitive to either E_o or T because of the small fractional power dependence. In figure 12 this relationship is shown for CH_4 where $E_o = 410$ kJ/mole. For most common values of E_o and T, ρ_{max} lies in the range 2,5 to 3.

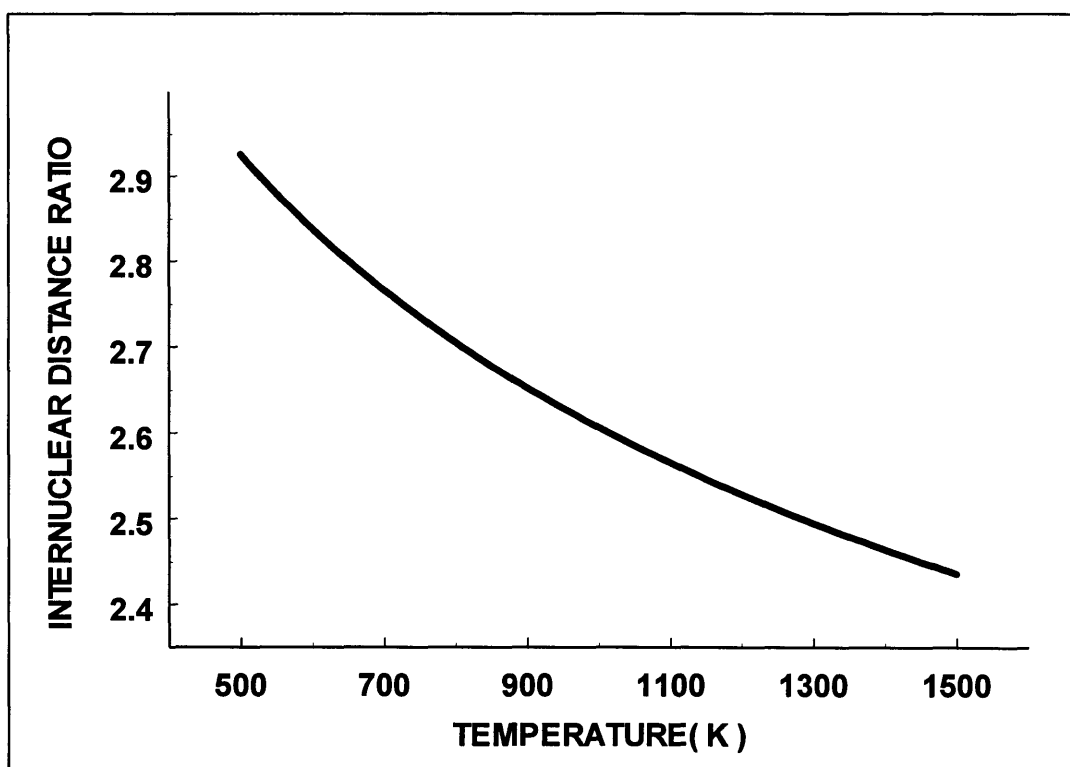


**Fig.12: Temperature dependence for $\rho = r/r_0$ the internuclear distance ratio for CH_4 .
 $E_0 = 410 \text{ kJ/mole}$ and $r_0 = 1,09 \text{ \AA}$.**

Our adopted value of 2,8 mentioned above is thus well supported by this analysis.

Next, we are concerned about the angle in which the hindered rotation of the hydrogen atom can rotate in figure 10. In our simple model we will assume that the C---H bond can bend through an angle θ until the moving H atom makes contact with its neighboring H atoms. This interaction distance will be taken as the van der Waal's radius which for a nonbonded H atom is $1,3\text{\AA}$. Consequently the conical angle θ which represents the solid angle of hindered motion can be geometrically solved to be $\sim 36^\circ$ or $0,62$ radians at $\rho = 2,8$. The two bending motions of the H atom relative to the CH_3 methyl group thus becomes a two-dimensional rotation, restricted to a relative solid angle, $\Delta\Omega/4\pi$, given by

$$\frac{\Delta\Omega}{4\pi} = \frac{1 - \cos \theta}{2} \approx \frac{\theta^2}{4} \quad (\text{for } \theta < 1) \quad (2.26)$$

The resultant moment of inertia for this rotation can be calculated with the relationship

$$\frac{1}{I_r} = \frac{1}{I_1} + \frac{1}{I_2} \quad (2.27)$$

where I_1 , is the moment of inertia of the flat CH_3 group about an axis through the C atom and perpendicular to the plane of figure 10. I_2 is approximately the moment of the C-----H long bond about this same C-atom axis. For the methyl group we have

$$I_1 = 3/2 m_H r_{C-H}^2 \sin^2 (180 - \theta) \sim 1,5 r_{C-H}^2 \text{ amu } \text{Å}^2$$

where $\theta = 109^\circ$ the H--C--H angle in CH_4 and $r_{C-H} \approx 1,1 \text{ Å}$. An internal symmetry number of 3 must be incorporated for the methyl group. Furthermore, $I_2 \sim 7,8 r_{C-H}^2 \text{ amu } \text{Å}^2$ and with $\sigma^+ = 3$ we find

$$I_r / \sigma \sim 0,05 \text{ amu } \text{Å}^2$$

It is also possible to treat the transition complex as a distorted CH_4 molecule with the two bending motions of the long H bond as just lower frequency motions instead of restricted free internal rotations with $\sigma^+ = 3$. To obtain the same result for the entropy change we would have to assign to the two bending frequencies values of $\sim 225 \text{ cm}^{-1}$ each. This frequency is about 1/6 the normal value for such motion, $\sim 3100 \text{ cm}^{-1}$, and implies a 36-fold reduced force constant for the bending motion and a six-fold larger amplitude of motion for such a H-atom.

A similar approach to determine the moments of inertia of the loose transition state for UF_6 will be followed. With the aid of the theory put forward in Appendix B the density of rotational states can consequently be calculated.

2.5 MOMENTS OF INERTIA FOR THE TRANSITION STATE

2.5.1 INTRODUCTION

It has been well established that the overall rotations of molecules can have a marked effect on the unimolecular rate of dissociation. The energy of rotation can change from the reactant molecule to the transition state as the geometry of the molecule changes and hence the moment of inertia, I , changes. In most cases where such effects are worth considering the moment of inertia for the transition state is larger than for the reactant molecule and the rotations release energy into the other (active) degrees of freedom of the molecule. The multiplicity of available quantum states of the activated complex is increased and hence the specific rate constant for dissociation is accordingly increased. Alternatively one can explain the effect by considering the centrifugal part of the rotation energy to overcome the potential energy barrier for dissociation. Effectively the bond energy, E_o , in bond fission reactions is reduced. Let us consider the moment of inertia which directly effects the energy of rotation.

The simplest example of rotational motion is that of the particle of mass, m , rotating in a circle of radius R . The momentum associated with such motion implies a wavefunction of wavelength $\lambda = h/p$. Furthermore, an angular momentum, J , is defined of magnitude $J = pR$ and the kinetic energy of the motion can be expressed as:

$$\text{Kinetic energy} = p^2/2m = J^2/2mR^2 \quad (2.28)$$

In this expression mR^2 is called the moment of inertia, I , which allow us to write:

$$E = J^2/2I \quad (2.29)$$

Not all values of the moment are permitted and when treated quantum mechanically the appropriate expression is:

$$E = n^2h^2/2I \quad n = 0,1,2 \quad (2.30)$$

For a system with more than one atom rotating around an axis the combined moment of inertia is given by

$$(2.31)$$

For the UF_6 molecule which is classified as a spherical top molecule, see figure 13, the moments of inertia around the principal axes A, B and C, chosen as depicted in figure 13. They are all the same, i.e. $I_A = I_B = I_C$. For I_A we have:

$$\begin{aligned} I_A &= mR^2 + mR^2 + mR^2 + mR^2 \\ &= 4mR^2 \end{aligned} \quad (2.32)$$

with $m = 19 \text{ amu}$ = the mass of the fluorine atom. The U-F bond length for the UF_6 molecule is taken as $1,99 \text{ \AA}$ [6]. Consequently the moment of inertia around the A axis is $\sim 301 \text{ amu \AA}^2$. When the moment of inertia is expressed as g cm^2 the conversion $1 \text{ amu \AA}^2 = 1,6604 \times 10^{-40} \text{ g cm}^2$ can be employed. The rotational partition function, which appears in the rate constant for the unimolecular decay, is proportional to the product of the moments of inertia. For the reactant molecule we have

$$\begin{aligned} Q_{rot} &\propto (I_A \cdot I_B \cdot I_C)^{1/2} \\ &= (64m^3 R^6)^{1/2} \end{aligned} \quad (2.33)$$

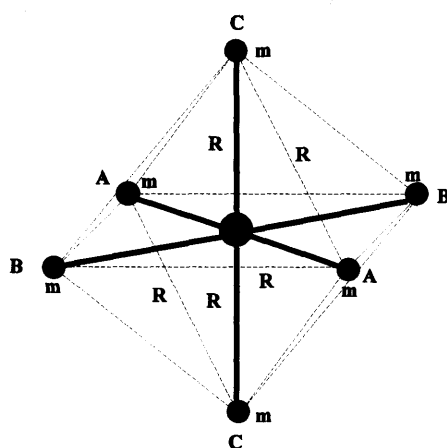


Fig 13: The three principal axes for UF_6 to calculate the moments of inertia.

2.5.2 THE CRITICAL BOND LENGTH FOR UF₆

Before one can calculate the moments of inertia for the activated complex, a realistic estimation of the critical bond length has to be made. In the case of dissociation of UF₆, the model of the loose activated complex will be considered. The earliest procedures assumed that the complex has similar geometry and vibrational frequencies as the reagent molecule UF₆ and additionally to have a large degree of rotational freedom. The first approach was based on a consideration of the forces involved during bond rupture. This involved that the critical bond length was established by balancing the force of attraction between the "atom" with the centrifugal force tending to dissociate the molecule:

$$\frac{-6a}{R_c^7} = J(J + 1) \frac{h^2}{\mu R_c^3} \quad (2.34)$$

where *a* represents the constant in the attractive potential energy expression $V = a/R^6$. In practice a large number of molecules were evaluated to derive an empirical relationship [7, 8]

$$\langle R_c \rangle \approx \frac{\sqrt{\pi}}{\tau(2/3)} \left(\frac{2a}{kT} \right)^{1/6} = 1,309 \left(\frac{2a}{kT} \right)^{1/6} \quad (2.35)$$

Typical values obtained for molecules by utilizing this approach are [8, 9]:

MOLECULE	CRITICAL BOND LENGTH	EQUILIBRIUM BOND LENGTH
CH ₃ - CH ₃	5,2Å	1,5Å
CF ₃ - CF ₃	6,3Å	1,6Å
C ₂ H ₅ - H	4,6Å	1,1Å

These values seemed to be an overestimation of the critical bond length. Bunker and Pattengill [10] subsequently suggested that the critical molecular configuration does not lie at the top of the

energy barrier but rather at a slightly lower value of the radius such that the accessible quantum states per unit energy range is a minimum. When this approach was applied to a variety of molecules the critical configuration occurred typically at bond lengths of 3,5Å in the case of an equilibrium bond distance of 1,2Å and 4,3Å at the maximum of the energy barrier (as given by the Morse potential). This approach led to a significant improvement in the agreement of the RRKM predictions and e.g. Monte Carlo calculations.

The underlining assumption of the second approach forms the basis of modern day analysis of the critical bond length. Detail descriptions can be found in e.g. reference [3] which leads the reader through all the aspects of the methodology. Furthermore, computer codes such as UNIMOL are available to establish values for the critical bond length. As this software was not available to the writer an approach was followed where the analysis was done utilizing the appropriate theory whilst the necessary computing was coded within the Microsoft program AXUM.

A variational approach is followed to establish the critical bond length. Remember that two quantities must be conserved in going from the reagent molecule to the transition state:

1. The total internal energy residing in the internal modes of energy of the reagent molecule must appear in the transition state. Thus, conservation of total energy.
2. The angular momentum in the bond that is extended must also be conserved. As the bond length between the UF_3 moiety and the F atom is extended the moment of inertia associated with this motion is increased. Note that the moments of inertia depends on the square of the bond length which we will denote by r_T . The result is that the partition function contribution of this rotational motion will be increased, i.e. Q_{rot}^+ increases in the transition state formula (2.11). Expressed in another way, the density of states in the activated complex will increase and for a given internal energy distribution in the reagent molecule so will the unimolecular rate of dissociation. However, the energy that is

released from the rotating of the extended bond will also contribute to the dissociation rate. The requirement that the angular momentum be conserved leads to a increased contribution from rotational energy as the critical bond length is extended. Remember that the angular momentum is proportional to the inverse of the squared critical bond length. It can be shown [3] that the microcanonical rates calculated by the RRKM theory as well as the transition state formula (averaged over the Boltzmann distribution) all represent maximum rates. The true rates will then always be given by minimizing the specific rate for given conditions.

Consider the Morse-like potential of figure 14 that describes the change of potential along the reaction co-ordinate that the molecule will experience during simple bond rupturing. Since the density of states of a harmonic oscillator depends on the steepness of the restoring potential, i.e. the magnitude of the force constant, the less steeper the potential becomes the smaller the vibrational energy spacing and hence the larger the density of states.

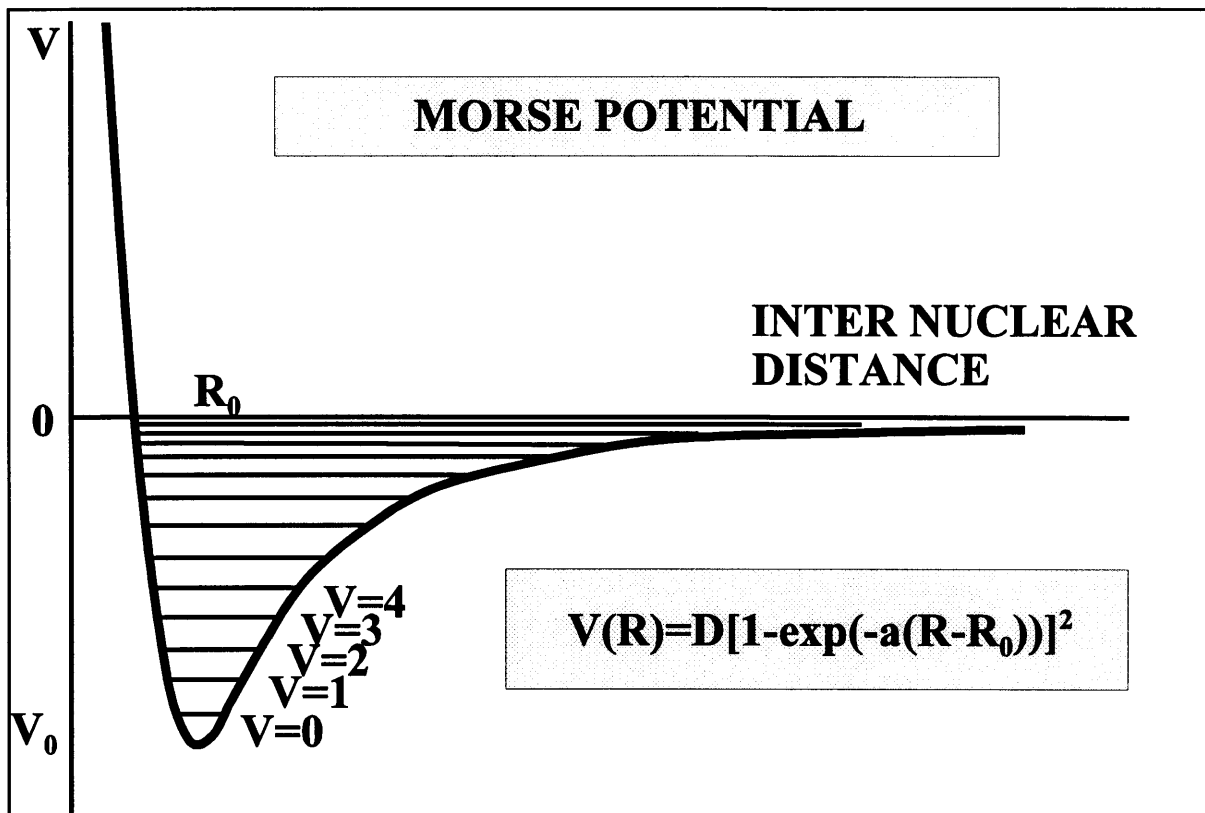


Fig 14: Illustration of the increase in the density of vibrational states as the steepness of the Morse potential decreases towards large internuclear distances.

In terms of the canonical average of $k(E, J)$ the following expression can be utilized to determine the high pressure dissociation rate coefficient [3]:

$$k_{uni}^{\infty} = \frac{k_B T}{h} \frac{Q_{rot}^+ Q_a^+}{Q_{rot} Q_a} e^{-V(r)/k_B T} \quad (2.36)$$

where the subscript a refers to all the active degrees of freedom. This expression will be utilized to determine the value r_T to be used in the calculations for UF_6 .

2.6 COMPARISON OF TRANSITION STATE FOR UF_6 WITH SPATIAL CONFIGURATION DERIVED FROM THERMOCHEMICAL DATA

Previous attempts to describe the spatial configuration of UF_6 during unimolecular dissociation have fallen well short of expectations. Only two publications [11, 12] have reported on such an endeavour and in both cases no comparison with experimental data was attempted. In this section the model and theory offered hitherto will be utilized to compare the predicted transition state with experiment. Real time measurements of the decay rate, or the rate of formation of product species, in situ in a mass spectrometer, is generally very useful for this type of information. In such an experimental setup, molecular beams are employed to generate a well-defined source beam of the molecules of interest. It requires very little effort to spatially match a laser beam to this beam of molecules. Consequently, parameters such as the yield of the reaction etc. are easily derived. This approach was followed from the onset of the experimental planning and an appropriate vacuum chamber and time-of-flight mass spectrometer was constructed for the purpose. During the experimental measurements it became clear that a number of issues reduced the usefulness of the data for comparison with the dissociation rate. These phenomena were investigated thoroughly and some of the results were offered for publication (paper III). A detail description of the effects forms part of this treatise and will emerge later (Chapter IV).

A second approach is to use thermochemical data at high pressure and analyze the properties of the transition state predicted by the experimental data. This avenue was subsequently followed. A literature search produced only one paper [13] where this topic was addressed at the Institute of Physical Chemistry at the University of Göttingen (1978). It is known that this Institute was involved with the MLIS process pursued in Germany. The thermal decomposition of UF_6 diluted in argon was measured in a shock tube at temperatures between 1100 and 1450 K. The concentration of UF_6 was followed by absorption spectroscopy. Measurements of the temperature dependence of the reaction rate indicated that at the experimental conditions applied, the reaction represents that in the high pressure limit. The first order high pressure rate constant is:

$$k_{\text{uni}}^{\infty} = 3,3 \times 10^{16} \exp [-(70,3 \pm 4) \text{ kcal mol}^{-1}/RT] \text{ s}^{-1}$$

$$\begin{aligned} \text{Thus log (Arrhenius coefficient)} &= \log A^{\infty} \\ &= 16,51 \end{aligned}$$

To construct a spatial configuration for the UF_6 molecule and calculate the predicted Arrhenius coefficient, a stepwise methodology will now be presented:

1. Determine the position of the internuclear distance of the U-F bond that will rupture. A model similar to the approach for the methane molecule is used where one U-F bond is stretched and becomes the reaction coordinate. Equation (2.36) will be employed to determine a minimum value for k_{uni}^{∞} and thus the position of the transition state.
2. First, a functional expression for the interaction potential is needed. A Morse potential is proposed and a value for the parameter β must be established:

$$V(r_T) = -E_0 [1 - \exp^{-\beta(r - r_0)}]^2$$

It can be shown that the reaction rate is quite sensitive for the value of β . If the force constant and reduced mass at the equilibrium position is substituted the calculated value for $\beta \sim 1,765$. The most reliable value for $E_0 = 68,8$ kcal/mole was determined by Hildenbrand [14]. In figure 15 the relationship for $V(r_T)$ for a varying U-F bond distance is displayed. It must be pointed out, however, that the force constant at the equilibrium position cannot be strictly applicable at large distances of bond extensions. Accordingly interaction potentials for lower values of β are also shown which would imply a "looser" transition state. If the criteria previously established for CH_4 are applied to UF_6 , a β value of 1,4 to 1,5 seems reasonable.

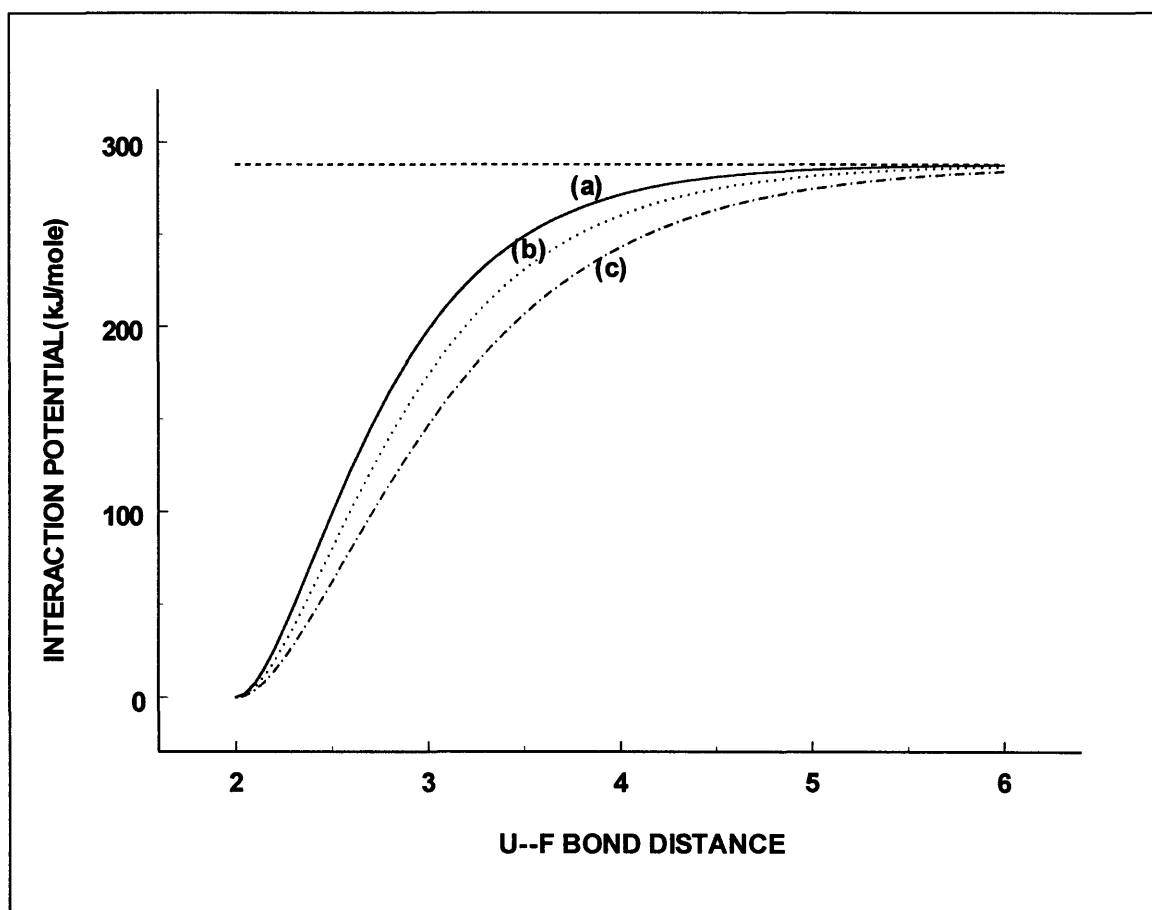


Fig 15: Morse potentials for the U-F bond in UF_6 (a) β -factor of 1,765, (b) β -factor of 1,5 and (c) β -factor of 1,25.

3. The result of the bond extension of one U-F bond is that two moments of inertia for the transition state are increased compared to the reagent molecule. The ratio of the rotational partition functions can be predicted as a function of the bond extension with the theory previously presented. A plot of the ratio is presented in figure 16.
4. For the transition state we propose a configuration where the UF_5 moiety has assumed the vibrational frequencies of the UF_5 molecule in the C_{4v} structure. There will thus be 12 fundamental frequencies plus the frequency in the direction of the reaction coordinate that diminishes. The two additional bending UF_6 frequencies will be treated as hindered two

dimensional rotations. Following our definition of the quantum mechanical vibrational partition function:

Q_{vib}	=	$2,848 \times 10^8$
Q_{vib}^+	=	$7,641 \times 10^6$

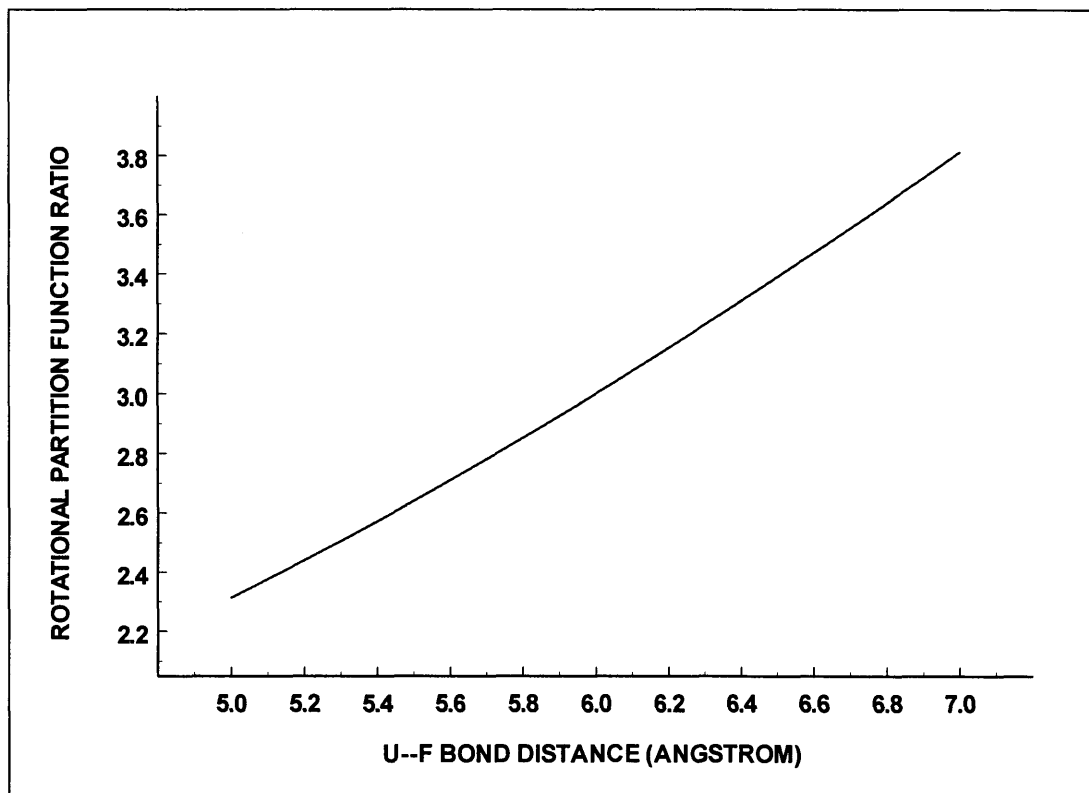


Fig 16: Rotational partition function ratio for undisturbed UF_6 molecule and the transition state. The relationship for the stretched U--F bond is shown.

The vibrational frequencies for UF₅ in table 3 were utilized:

Table 3: Frequencies for the isolated UF₅ molecule

SPECIE	MODE	WAVENUMBER	DEGENERACY
A ₁ IR, Raman	v ₁	648 cm ⁻¹	1
	v ₂	572 cm ⁻¹	1
	v ₃	129 cm ⁻¹	1
B ₁ Raman	v ₄	515 cm ⁻¹	1
	v ₅	99 cm ⁻¹	1
B ₂ Raman	v ₆	201 cm ⁻¹	1
E IR, Raman	v ₇	593 cm ⁻¹	2
	v ₈	201 cm ⁻¹	2
	v ₉	182 cm ⁻¹	2

5. The two-dimensional restricted rotator contributes significantly to the partition function of the active modes. A treatment similar to that for CH₄ is again followed. To calculate the resultant moment of inertia for this rotator we employ the expression:

$$1/I_r = 1/I_1 + 1/I_2$$

The hinderance to rotation is less than for the CH₄ molecule and a 2π solid angle will be permitted. Therefore I₂ ~ 19 x R² where R represents the internuclear distance along the reaction coordinate. A value of 4 x 19 x 2² = 304 amu Å is reasonable for I₁ with the U-F bond length of the UF₅ molecule of ~2Å [15, 16]. In figure 17 the change in the partition function for this hindered two-dimensional rotator as the bond length changes is illustrated. An internal symmetry number of 4 is applicable for the rotator.

6. A statistical factor, L = 6, must be added to equation (2.36) that can be derived from a symmetry number of 24 for UF₆ and 4 for UF₅ (see table 2).

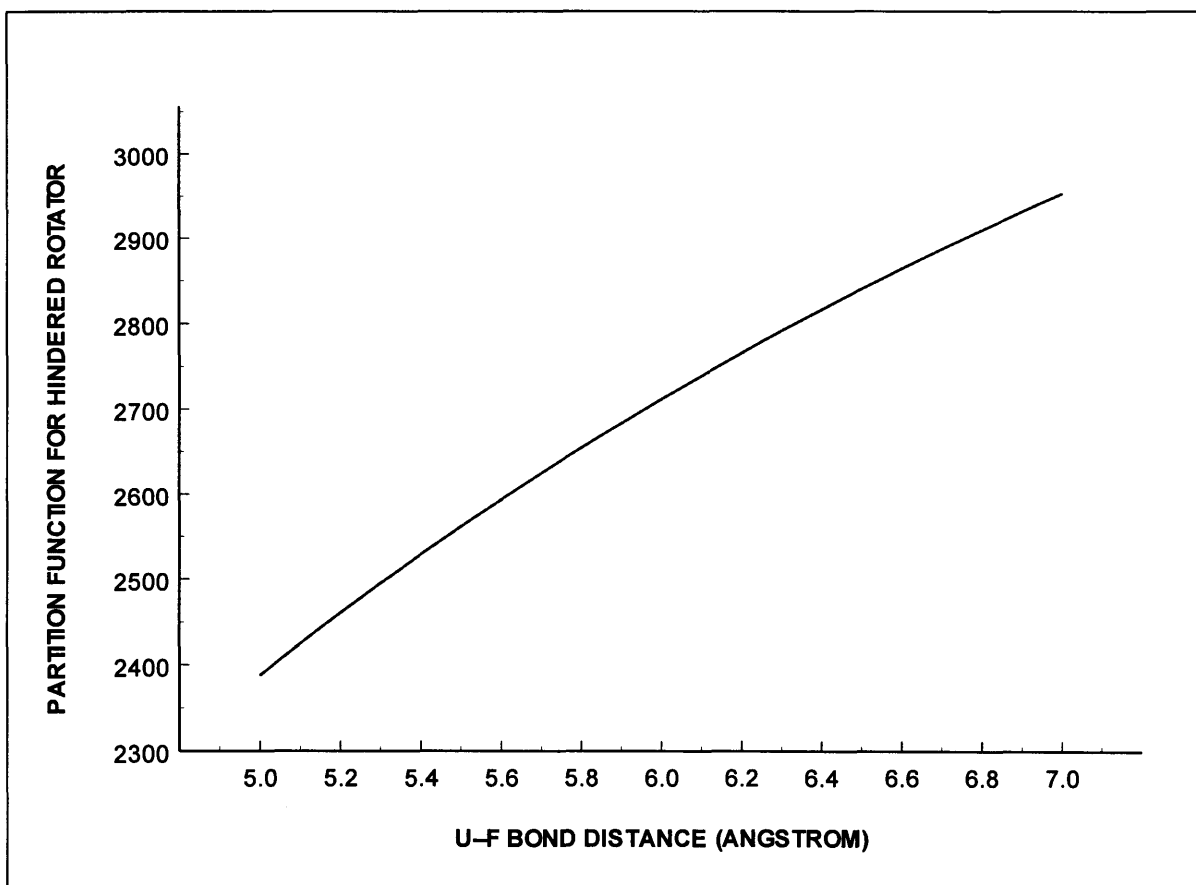


Fig. 17: Rotational partition function for the hindered two-dimensional rotator in the transition state of UF_6 .

7. A temperature of $T = 1250$ K which is about midway in the region of the experimentally reported results seems reasonable.

8. In expression (2.36) for k_{uni} the only variable remains the internuclear distance. The position of the transition state will lie where k_{uni}^∞ is a minimum and this must be established. As the theory predicts a minimum value for the dissociation rate can be found as is illustrated in figure 18. The influence of different β values are also shown. A β value of $\sim 1,45$ will predict a transition state U-F bond length of $\sim 6\text{\AA}$ or 3 times the equilibrium length. This is also slightly larger than the extension that was derived for CH_4 .

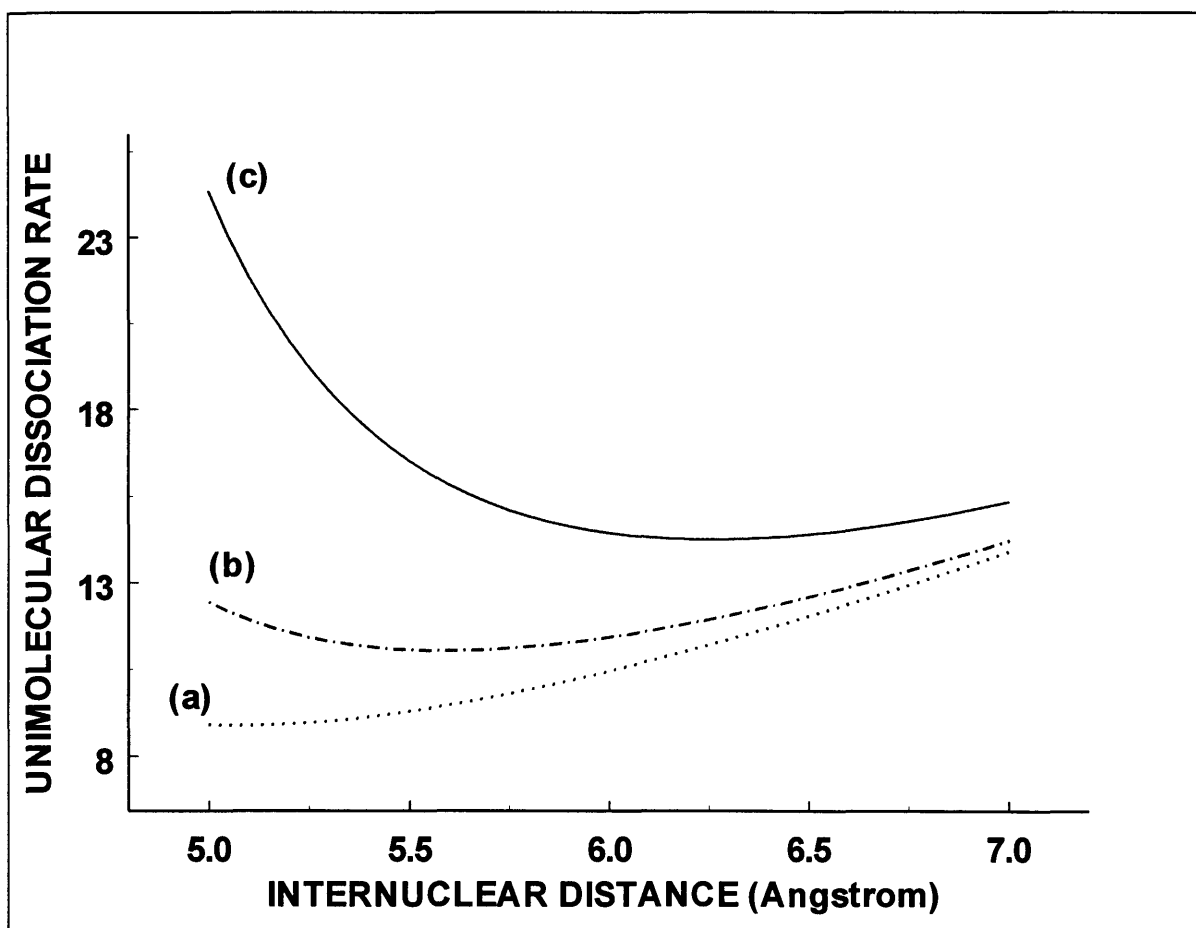


Fig. 18: Unimolecular dissociation rate for UF_6 for different Morse potentials of the U-F bond in the transition state (a) β -factor = 1,765 (b) β -factor = 1,5 and (c) β -factor = 1,25. The minimum position of each curve indicates the position of the transition state.

If the extension for the U-F bond length in the transition state is taken as 3 times the equilibrium length, the following value for the Arrhenius coefficient at high pressures can be predicted:

$$\log A_{\infty} = 16,47$$

This is in excellent accord with the experimental data on the dissociation of UF_6 . Furthermore, the model proposed for the transition state is reasonable and in line with the methodology proposed for simple bond rupture reactions.

The previous attempts [11, 12] to describe the transition state were based on methodology of Benson's rules. In this approach the vibrational frequencies of the transition state were divided into two groups - those that are not affected by the change in spatial configuration and those that are significantly affected. The former group was kept the same as in the undisturbed molecule, whilst for the latter group a percentage change was proposed. This however led to a substantial underestimation on the Arrhenius coefficient.

Work by Rao et al: [11]

$$\log A_{\infty} = 14,43 \text{ (122 x to slow)}$$

Work by Makarov et al: [12]

$$\log A_{\infty} = 14,99 \text{ (33 x to slow)}$$

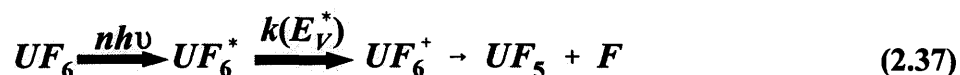
It is clear that the dissociation rate for a given level of excitation is indeed substantially faster than previous predictions (uncalibrated) and that the model that was proposed for UF_6 fell short of acceptable predictions. This model was, incidently, derived from a similar one proposed for the dissociation of SF_6 .

2.7 PREDICTION OF UNIMOLECULAR DECAY RATE UNDER MLIS CONDITIONS

For the final calculation of the laser induced dissociation rates, this treatise has hitherto been concerned to establish an acceptable model for the spatial configuration of the transition state. This was acquired by calibrating the appropriate theory with thermal chemical data. It remains now to predict the unimolecular dissociation rate under MLIS conditions. The density of UF_6 in the process gas mixture varies between 5×10^{14} to 1×10^{16} molecules/cm³ and thus falls in the low pressure regime of our figure 10.

Following the RRKM theory as formulated by Robinson and Holbrook [2] and the energy terminology of section 1.5 we repeat here only the main features of the formulations. The UF_6

molecule will, subsequent to multiphoton excitation by infrared radiation, rapidly randomize this internal energy between all the 15 vibration modes, (3N-6). This energized molecule will furthermore, via the fluctuation of this energy between vibrational modes, concentrate this energy on the weakest bond before rupture. An equal probability for bond rupture with regards to the six U-F bonds is assumed. This activated complex having the appropriate critical molecular spatial configuration, can dissociate readily:



A result of the rapid flow of intramolecular energy is that, for an excited molecule of a particular vibrational energy, E_v^* and angular momentum, J , all states are equally probable, and the micro canonical rate constant is given by

$$k(E_v^*, J) = W(E_v^*, J) / h\rho(E_v^*, J) \quad (2.38)$$

where $W(E_v^*, J)$ is the number of accessible and active internal states associated with motions orthogonal to the reaction coordinate at the transition state, $\rho(E_v^*, J)$ is the density of active states in the molecule, and h is Planck's constant. Expression (2.38) can be rewritten:

$$k(E_v^*, J) = L \frac{Q_{rot}^+}{Q_{rot}^*} \frac{1}{h\rho(E_v^*)} \sum_{e_v^+ = 0}^{E_v^+} \rho(E_v^+)$$

where, the internal energy of the activated complex is defined as (figure 7)

$$E_v^+ = E_v^* - E_0$$

For the UF_6 , E_0 is taken as the U-F bond dissociation energy of 68,8 kcal/mole [14]. Q_{rot}^+ and Q_{rot}^* are the rotational partition functions for the activated complex and the undistorted molecule as previously defined. The density of vibrational states for the undistorted molecule has been analyzed in detail in Appendix A. The density of vibrational quantum states in the activated

complex is $\rho(E_v^+)$ and the sum

$$\sum_{E_v^+ = 0}^{E_v^+} \rho(E_v^+)$$

is the total number of vibrational states in the activated complex up to E_v^+ , which is given by

$$\sum_{E_v^+ = 0}^{E_v^+} \rho(E_v^+) = \frac{[E_v^+ + aE_z^+]^S}{S! \prod_{i=1}^{14} h\nu_i^+}, \text{ with } S = 14$$

for the activated complex.

The above formulations are extensively treated in Appendix A and are known as the Whitten-Rabinovitch approximations. A treatment for the activated complex, to determine the density of vibrational states, similar to that for the undisturbed molecule, is followed. To predict the density of states for the activated complex the following values were used.

$\langle v \rangle$	=	296,5 cm ⁻¹
$\langle v^2 \rangle^{1/2}$	=	371,27 cm ⁻¹
β	=	1,456
E_0	=	68,8 kcal/mole = 24195 cm ⁻¹
E_z^+	=	2075 cm ⁻¹
$S!$	=	8,72 x 10 ¹⁰
$\prod_{i=1}^{14} h\nu_i^+$	=	7,06 x 10 ³¹

The computed values for $\sum_{E_v^+ = 0}^{E_v^+} \rho(E_v^+)$ as a function of the overexcitation above the dissociation energy, 24195 cm⁻¹ for the UF₆⁺ complex is illustrated in the plot of figure 19. Accordingly, the expected rates of dissociation as the internal energy exceeds the threshold limit, can be predicted.

Table 4 summarizes some of the data to illustrate that the unimolecular dissociation rate increases rapidly above the threshold limit. It is in fact at least two orders of magnitude faster than previously anticipated [11]. This aspect is very positive in terms of the anticipated energy consumption of the MLIS process.

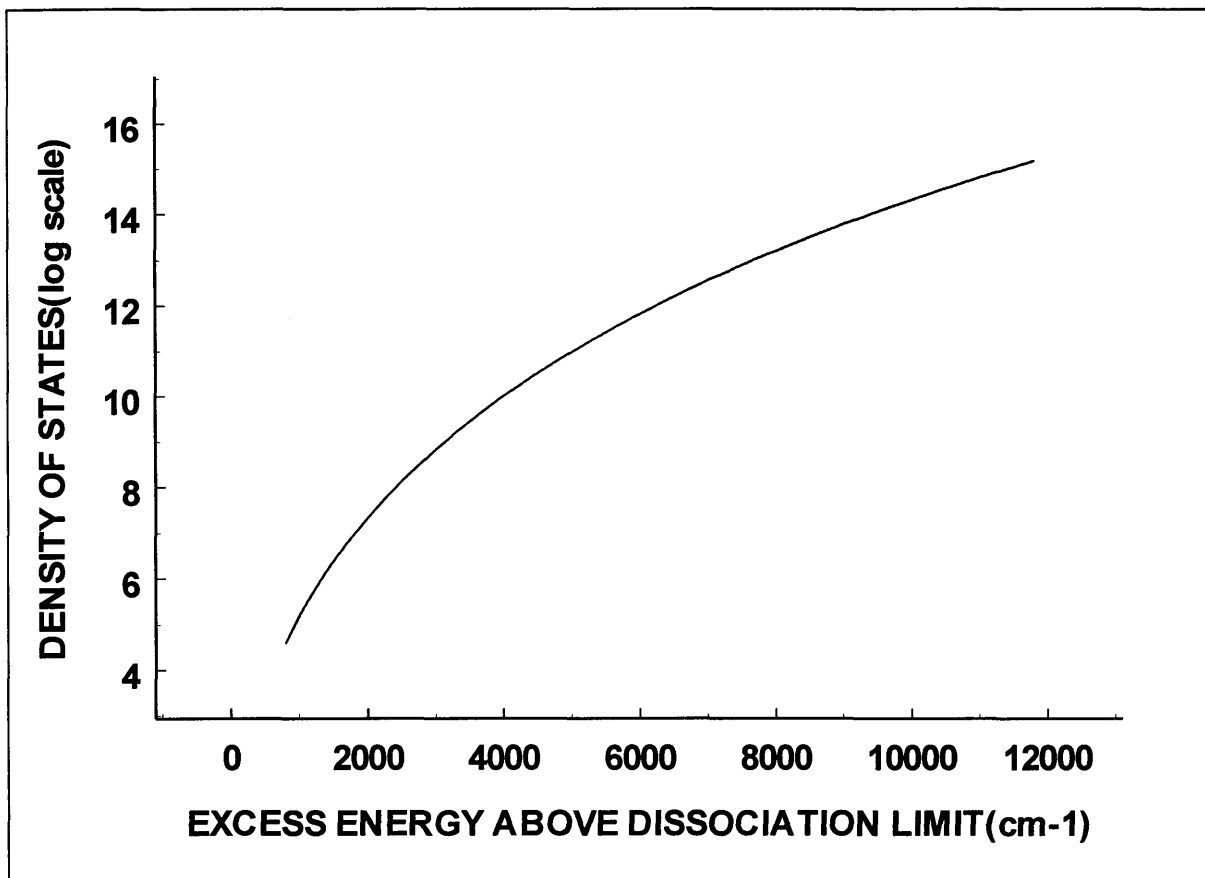


Fig.19: Density of states for the activated complex for the unimolecular dissociation of UF₆.

Table 4: Parameters for the unimolecular dissociation of UF₆

Excess Energy (No of Photons)	$\rho(E_v^*)$	$\Sigma\rho(E_v^*)$	$K_a(E_v^*) s^{-1}$	Lifetime τ(ns)
5	$6,2 \times 10^{14}$	$2,09 \times 10^9$	$1,1 \times 10^6$	909
7	$1,1 \times 10^{15}$	$4,5 \times 10^{10}$	$1,3 \times 10^7$	77
9	$1,85 \times 10^{15}$	$5,4 \times 10^{11}$	$19,2 \times 10^7$	11
10	$2,54 \times 10^{15}$	$1,7 \times 10^{12}$	$2,1 \times 10^8$	4,8
12	$4,28 \times 10^{15}$	$1,3 \times 10^{13}$	$9,6 \times 10^8$	1
13	$5,56 \times 10^{15}$	$3,1 \times 10^{13}$	$1,75 \times 10^9$	0,6
14	$7,15 \times 10^{15}$	$7,4 \times 10^{13}$	$3,2 \times 10^9$	0,3
15	$9,17 \times 10^{15}$	$1,7 \times 10^{14}$	$5,8 \times 10^9$	0,2

2.8 CONCLUSIONS

1. The methodology followed by Lyman [17] to describe the spatial configuration and derive the partition functions for the transition state during the laser dissociation of SF₆ is inadequate and cannot be applied to UF₆.
2. The Arrhenius coefficient that is determined for UF₆ with the methodology of Lyman is more than two orders too small.

3. Following the approach established for a number of bond fission reactions, e.g. CH_4 ; C_2H_6 etc., the calculated Arrhenius coefficient and the experimental value is in excellent accord:

	A_{∞}^{cal}	=	$10^{16,47}$	at 1250 K
and	$A_{\infty}^{\text{exp.}}$	=	$10^{16,52}$	at 1250 K
in	$k_{\infty}^{\text{uni.}}$	=	$A_{\infty} \exp(-E_0/kT)$	

CHAPTER III

CHAPTER III

3. VIBRATIONAL ENERGY EXCHANGE AND THE QUENCHING OF UNIMOLECULAR DECAY RATE

3.1 GENERAL

The molecular route for the separation of uranium isotopes utilizes the technique of flow cooling to decrease the vibrational and rotational temperatures of UF_6 in order to enhance the optical selectivity obtainable in the first selective step of a multi frequency irradiation scheme. This intrinsic selectivity and the subsequent photo dynamics when the molecule is excited through the quasi continuum of vibrational levels to dissociation, impacts critically on the specific energy consumption, expressed as megajoules/kilogram feed material (MJ/kg_F), and the technoeconomics of the separation process. A high molecular density is favoured in the irradiation zone. However, this introduces the aspect of vibrational energy transfer between molecules with the resultant loss in isotopic selectivity. It is therefore imperative to establish a consummate picture of the influence of vibrational exchange processes, during and after the laser pulses, on the photo dynamics of UF_6 .

The molecular density region that is of importance for the MLIS of UF_6 is $\sim 5 \times 10^{14} - 1 \times 10^{16}/\text{cm}^3$ at vibrational temperatures of 70-100 K. It has been shown that for SF_6 , so prevalently used as a good prototype for UF_6 , the selectivity for the minor isotope decreases exponentially when the pressure exceeds 4×10^{-2} torr (5,3 Pa) at 300 K [18, 19]. This represents a density of $2 \times 10^{15}/\text{cm}^3$. It has also been tacitly assumed that the much reduced temperatures that prevail in the irradiation zone will alleviate the detrimental influence of vibrational energy transfer. The latter belief is supported by the predictions of the gas kinetic theory if the collisional diameter [20] for intermolecular vibrational energy exchange is taken as the hard sphere collisional diameter and short range repulsive forces dominate the exchange process.

In our studies into the dissociation dynamics of UF_6 , we have gathered evidence that attractive forces that influence the exchange process over longer distances on the intermolecular potential curve [21] play a significant role at low temperatures.

The Rice-Ramsberger-Kassel-Marcus (RRKM) theory can be used to predict the unimolecular decay rate of UF_6 . Hitherto the influence of collisional transfer of vibrational energy has been neglected as this is regarded as too slow at the density and temperature regions applicable to MLIS. If the overexcitation of a large polyatomic molecule is substantially above the dissociation level, the decomposition will be rapid and the competition of collisional energy transfer processes can be negligible. A higher overexcitation, however, goes at the expense of increased specific energy consumption. A comprehensive study to relate the predictions of the RRKM theory with experimentally measured dissociation rates, which will include collisional effects, has been undertaken to better understand the photo dynamics of UF_6 . This section will deal only with the mechanism of vibrational energy transfer which is very important to allow a proper description of its influence on the selectivity.

Figure 19 shows schematically the ground electronic state of UF_6 together with the excited electronic states that give rise to fluorescence via the A-X- and B-X-bands [22, 23]. The origins of the different fluorescence signals studied are as follows:

1. After infrared multi photon excitation in the ground electronic state, UF_6 dissociates with the formation of a fluorine radical. Adding an appropriate scavenger gas leads to the formation of excited HF which subsequently relaxes by fluorescence and emits 2-3 μm wavelength photons.
2. Excitation with a 248 nm photon, KrF-laser, to the B-X-band, which reaches a directly dissociative state, is followed by very fast unimolecular decay of UF_6 and a similar reaction to 1 can be utilized to obtain a HF fluorescence signal.

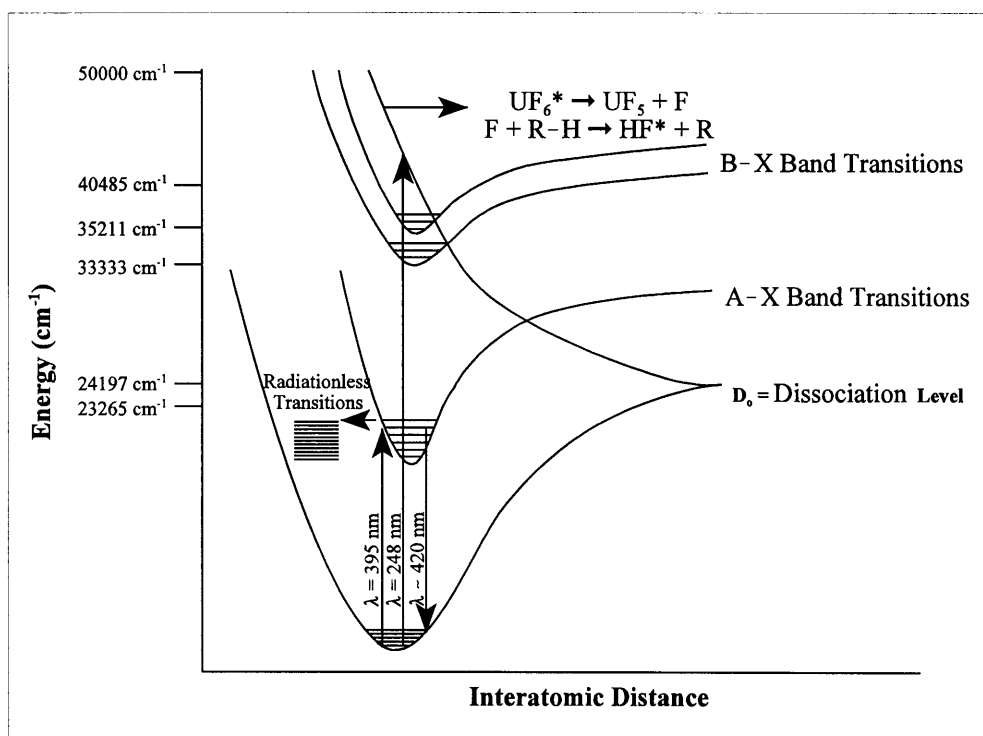


Fig. 19: Schematic presentation of the excitation transitions giving rise to fluorescence in UF_6 .

3. Excitation to the A-X-band with a 395 nm photon gives rise to UF_6 fluorescence which peaks in intensity at 420 nm.

This section describes the experimental configuration to obtain 1 whilst 2 and 3 will be considered when the ultraviolet laser dissociation is discussed later.

Collisional energy transfer between reactant species is essential to support the statistical description of the unimolecular dissociation rate by a thermal rate coefficient at the high-pressure limit (see figure 10). For the laser instigated dissociation of a polyatomic molecule, e.g. UF_6 , this randomization process is ensured by the rapid intramolecular distribution of vibrational energy. The exchange of vibrational energy on an intermolecular basis therefore has a different

implication. Of concern here, is the vibrational energy exchange between highly excited species with less excited specie or bath gas on a time scale which influences the unimolecular dissociation rate. To understand this phenomenon we shall first put forward a semi-classical approximate theory with which to compare experimental measurements. This will allow us to quantify the internal losses due to collisions. [24, 25].

3.1.1 RATE CONSTANTS, CROSS SECTIONS AND COLLISION NUMBERS

In our semi-classical approach for gas phase molecular energy transfer, one considers the relative translational motion in a bimolecular encounter to be purely classical in nature. It also blithely ignores any internal motions, vibrational or rotation, and any effects that the structure of molecule A and B may have on the collision dynamics. In spite of these obvious shortcomings, this approach is extremely valuable for the solution to simple model problems which provide insight into many energy transfer experiments.

In our bimolecular encounter which is defined by an initial relative velocity v_i and impact parameter b , we denote the probability of an $i \rightarrow f$ (initial to final) transition as $P_{if}(b, v_i)$. Then let us suppose that a single system is subject to encounters with random impact parameter. The net effect can be described in terms of a cross-sectional area associated with the energy transfer process, which we may define differentially as $d\sigma_i = P_{if}dA$. The incremental area component, dA , is a small area element through which the interaction occurs. In terms of the impact parameter b , dA is defined as $2\pi b db$. A cross section can now be related to the probability and impact parameter:

$$\sigma_{if}(v_i) = 2\pi \int_0^{\infty} P_{if}(b, v_i) b db \quad (3.1)$$

For two structureless particles subject to a radially-symmetric, e.g. Lennard-Jones, interaction potential we have $P = 1$ if $b \leq d$ and $P = 0$ if $b > d$ where d is the “hard-sphere diameter”. The

cross section then simply becomes:

$$\sigma_{HS} = 2\pi \int_0^d b db = \pi d^2 \quad (3.2)$$

As we are interested in the rate constant for the bimolecular energy transfer process, let's next consider a volume of magnitude V containing at a particular time a concentration $[N_i]$ molecules per cubic centimeter. Energy transfer encounters with B molecules of concentration $[N_B]$ proceeds with time at a finite probability. The change in $[N_i]$, which is negative, $\Delta[N_i]$ during the time interval Δt should equal the number of interactions per unit volume times the fraction where a transfer $i \rightarrow f$ indeed occurs. This latter fraction equals the volume swept out in the time Δt divided by the volume V : $\sigma(v_i)v_i \Delta t/V$. It is the relative velocity that is important here and consequently the above quantity must be averaged over the distribution function for initial relative velocities, $f(v_i)$. Therefore

$$\begin{aligned} \Delta[N_i] &= [\text{number of interacting systems per volume}] \\ &= \frac{1}{V} \int \sigma(v_i) v_i f(v_i) dv_i \Delta t \end{aligned} \quad (3.3)$$

The number of interacting systems per unit volume can be equated to $([N_i]V[N_B]V)/V$ which is equal to $[N_i][N_B]V$. Hence, taking the limit as $\Delta t \rightarrow 0$ we obtain

$$\frac{d[N_i]}{dt} = -k_{if} [N_i][N_B] \quad (3.4)$$

$$\text{where } k_{if} = \int \sigma_{if}(v_i) v_i f(v_i) dv_i \quad (3.5)$$

Here k_{if} is the second-order rate constant for the bimolecular $i \rightarrow f$ energy transfer process and normally has units of $\text{cm}^3 \text{ molecule}^{-1} \text{ sec}^{-1}$. In many experimental situations, $f(v_i)$ is described by a thermal distribution. If we use brackets $\langle \rangle$ to denote thermal average, then $k_{if} = \langle \sigma_{if} v \rangle$.

It is often more convenient to think also in terms of other quantities. We may define cross section $\langle\langle\sigma\rangle\rangle$ so that

$$\langle\langle\sigma\rangle\rangle \equiv k_{if} / \langle v \rangle \equiv \langle \sigma v \rangle / \langle v \rangle \quad (3.6)$$

For hard sphere collisions $\langle\langle\sigma\rangle\rangle = \pi d^2$. The double bracket cross section then gives a number which we can compare with hard sphere cross sections. Similarly a probability per collision can be defined:

$$\langle\langle P \rangle\rangle = \langle\langle\sigma\rangle\rangle / \pi d^2 \quad (3.7)$$

The inverse of this quantity is often called the collision number

$$\langle\langle Z_{if} \rangle\rangle = \langle\langle P_{if} \rangle\rangle^{-1} = \pi d^2 / \langle\langle\sigma\rangle\rangle \quad (3.8)$$

For a system at thermal equilibrium, it may be easily shown [26] that the appropriate distribution of initial relative velocities is

$$f(v) = 4\pi(\mu/2\pi k_B T)^{3/2} v^2 \exp(-\mu v^2/2k_B T) \quad (3.9)$$

where μ is the reduced mass of the two collision partners. From this distribution we derive:

$$\begin{aligned} \langle v \rangle &= (8 k_B T / \pi \mu)^{1/2} \\ \langle v^2 \rangle &= 3 k_B T / \mu \\ \langle v^{-1} \rangle &= (2\mu / \pi k_B T)^{1/2} \end{aligned} \quad (3.10)$$

Consequently, the hard sphere collision rate constant $k = \langle \sigma v \rangle = \pi d^2 (8k_B T / \pi \mu)^{1/2}$ or $k = 4.57 \times 10^{-12} d^2 (T/\mu)^{1/2}$ where d is in Angstroms, T in degrees kelvin and μ in amu. Table 5 shows conversion factors for different units that are sometimes used in the literature [27].

Table : 5 Equivalent Rate Constant and Hard-sphere Bimolecular Encounter Rate Constants for Reduced Mass of 20 amu, Collision Diameter of 4×10^{-8} cm at 300 K

	cm ³ molecule ⁻¹ sec ⁻¹	liter mole ⁻¹ sec ⁻¹	cm ³ molecule ⁻¹ sec ⁻¹	atm ⁻¹ sec ⁻¹	torr ⁻¹ sec ⁻¹	torr ⁻¹ μsec ⁻¹
Equivalent	1	$6,02 \times 10^{20}$	$6,02 \times 10^{23}$	$7,34 \times 10^{21}T^{-1}$	$9,66 \times 10^{18}T^{-1}$	$9,66 \times 10^{12}T^{-1}$
Hard sphere	$2,83 \times 10^{-10}$	$1,7 \times 10^{11}$	$1,7 \times 10^{14}$	$6,9 \times 10^9$	$9,1 \times 10^6$	9,1

From an experimentally measured rate constant, the cross section can be determined from $\langle\langle\sigma\rangle\rangle = k/\langle v \rangle$. For μ in amu and T in degrees Kelvin, this gives $\langle\langle\sigma\rangle\rangle = 6,87 \times 10^{11}(\mu/T)^{1/2}$ k in cm³ molecule⁻¹ sec⁻¹ or $\langle\langle\sigma\rangle\rangle = 7,13 \times 10^{-2}(\mu T)^{1/2}$ k for in usec⁻¹ torr⁻¹.

3.2 EXPERIMENTAL METHOD FOR THE STUDY OF VIBRATIONAL ENERGY TRANSFER

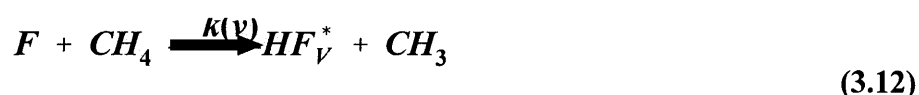
3.2.1 EXPERIMENTAL

A number of experimental techniques have been employed to study and quantify the transfer of vibrational energy between molecules. These methods used to obtain experimental information on the rate coefficient for collisional energy transfer between highly excited reactant molecule and its own specie or a bath gas, can be loosely classified into two categories: “indirect” and “direct”. Indirect experiments involves the observation of the pressure dependence of reaction rate coefficients. The data must be calibrated to yield energy transfer rate coefficients. The simplest example of this calibration is through the fitting of fall off curves (see figure 10). One first fits the observed high-pressure rate coefficient using RRKM theory to obtain $k(E)$. One then fits the pressure dependence in order to find the transfer rate from the master equation for the unimolecular decay rate. Hence the terminology, “indirect”: the data reduction required to obtain energy transfer parameters involves an assumption about the physical model for the reaction parameters.

Direct experiments to obtain energy transfer parameters, involve the measurement of properties which can be directly related to the time dependence of the average energy of the highly excited species, usually under conditions such that no reaction can occur. One example of this approach is the preparation of a highly energetic molecule in its ground electronic state; the time evolution of the emission or absorption spectrum is then monitored as the species undergoes relaxation through collisions with its own specie or a bath gas.

Amongst the direct techniques are the spectroscopic experiments where specific vibrational states are produced and in which specific vibrational states are monitored. This approach is best suited when discrete resolvable energy levels are involved. To study vibrational energy exchange in the quasicontinuum and continuum region of excitation requires a different kind of approach. A pump and probe technique with lasers being utilized to achieve both actions seemed best suited for our purpose.

In the MLIS process a scavenger gas, methane works the best, is brought into play after the U-F bond rupture to annihilate the fluorine radical. From this reaction a vibrationally excited hydrogen fluoride molecule forms which subsequently relaxes by fluorescence and emits 2-3 μm wavelength photons. The fluorescence spectrum is associated with the formation of the excited molecules HF^* in various vibrationally excited states by the reactions:



The temporal behaviour of the fluorescence intensity, I_f , is governed by the concentration of the HF* molecules in the system: $I_f \propto [\text{HF}_v^*]$. From (3.12) and (3.13), we have $[\text{HF}_v^*] = k(v) [\text{CH}_4] [F] - (1/\tau_f) [\text{HF}_v^*]$. The solution of this equation for $[\text{HF}^*]$ has the form:

$$[\text{HF}_v^*] = \frac{k(v) [F] [\text{CH}_4]}{K_a [\text{CH}_4] - 1/\tau_f} [\exp(t/\tau_f) - \exp(K_a [\text{CH}_4] t)] \quad (3.15)$$

where $K_a = \sum k(v)$, and since the concentration of the HF* molecules is small, their lifetime τ_f depends mainly on their collisions with the acceptors. The shape of the fluorescence signal has the form:

$$I_1(t) = C[\exp(-t/\tau_f) - \exp(-t/\tau_r)] \quad (3.16)$$

where $\tau_r = 1/K_a[\text{CH}_4]$.

The shape of the mathematical expression in 3.16 is shown schematically in figure 20. The rise time of the curve preceding the inflexion point is associated with the formation period, thus reaction time, of the HF and the exponential decay following the inflexion point with the vibrational relaxation of the excited HF. The collisional processes that compete with the fluorescence determine this time constant.

Two different sources of 16 μm radiation, to excite the strong ν_3 vibration mode of UF_6 , were used. The first wavelength, L_1 , that was utilized for the multi photon vibrational excitation of UF_6 was generated by four-wave mixing of a 1064 nm Nd:YAG laser and a line tunable 10 μm CO_2 laser in a multipass Raman converter filled with para- H_2 at room temperature [28]. The 1064 nm radiation was filtered from the output beam by a 90 lines/mm diffraction grating and a germanium

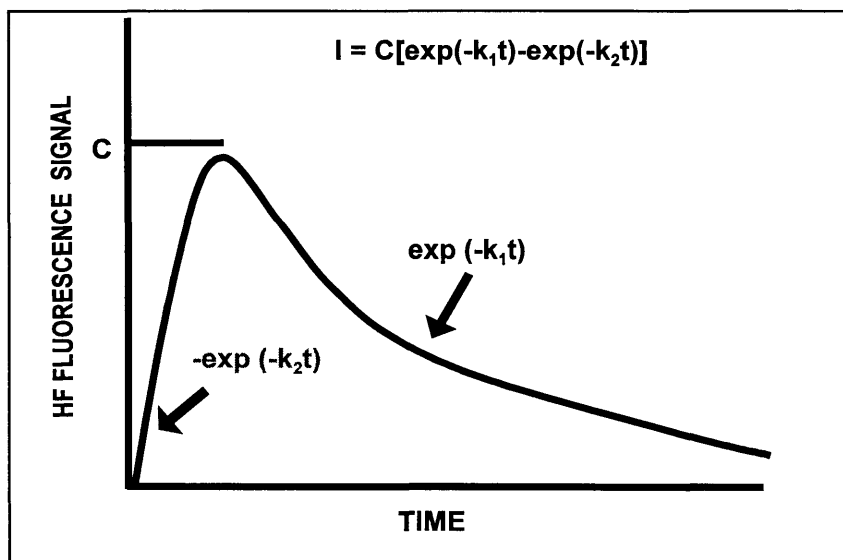


Fig.20: Temporal shape of HF fluorescence signal.

window at the Brewster angle for $16\ \mu\text{m}$. A second wavelength, L_2 , was generated in a similar Raman converter but operated at $77\ \text{K}$ by means of liquid nitrogen [29]. The latter beam contained sufficient energy to dissociate UF_6 via multi photon absorption. Both $16\ \mu\text{m}$ beams were directed collinearly, but counter propagating, through a flow cooling Laval nozzle, as indicated schematically in figure 21. The transverse profile of both $16\ \mu\text{m}$ beams were Gaussian and focussed to $1/e^2$ radii of $\sim 2\ \text{mm}$, with a beam quality factor, M^2 , ~ 1.6 . A fraction of each beam was reflected off a KCl beamsplitter to reference the fluorescence signals and to synchronize the two beams. Altech pyro-electric detectors, PE1 and PE2, were employed as indicated in figure 21.

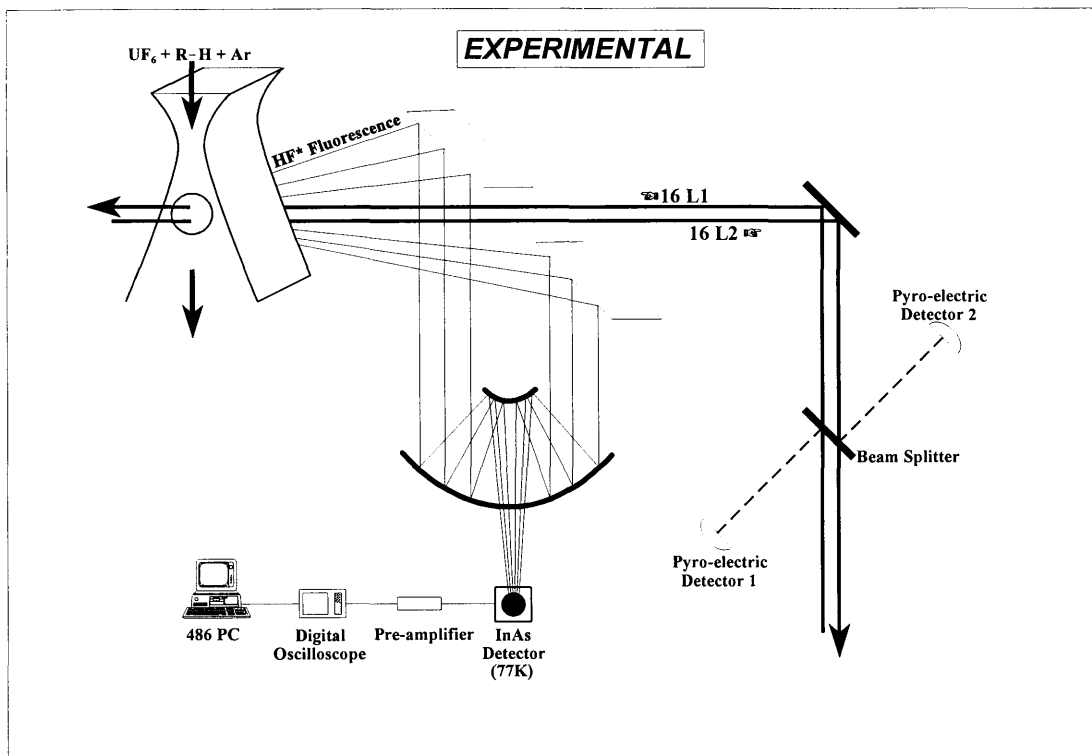


Fig. 21: Schematic presentation of experimental configuration to measure HF* fluorescence.

Various mixtures of UF₆ in Ar as carrier gas were studied with the former ranging from 1 to 4 percent. An appropriate hydrogen containing molecule e.g. H₂ or CH₄, acted as the scavenger gas to remove the fluorine radical. The vibrational temperature was determined by a computer code which was calibrated with spectra obtained with a FTIR-spectrometer [30]. The UF₆ number density at a vibrational temperature of ~100 K was ~2 x 10¹⁵/cm³ in the irradiation region. This was chosen to coincide with experimental conditions that were previously published [31]. The resulting fluorescence, 2-3 μm wavelength, from the excited HF molecules, was collected on the optical axis and directed with a Cassagrain telescope, which focussed the light onto a Boston InAs detector operated at 77 K. Care was exercised to ensure that the total

fluorescence area was imaged onto the sensitive area of the detector. This aspect is in accordance with previous findings that showed that erroneous results are obtained if the experimental setup does not adhere to this condition [32]. From the detector the signal was amplified and recorded, together with the signals from PE1 and PE2, with the aid of a digital oscilloscope and data processing system.

The InAs photo voltaic detector senses the fluorescence emerging from the irradiation zone. If the temporal shape of the fluorescence signal is analyzed to obtain reaction rate information, suitable time resolution of the detector and amplifier system is imperative. This was ascertained by measuring the fast laser pulse from a Nd:YAG laser with the detector system. The scattered laser signal, to protect the detector from damage, with a full width at half maximum intensity, FWHM, of ~ 8 nanoseconds was recorded with the system and is shown in figure 22. The InAs detector is clearly not fast enough to follow the fast rise time of the laser pulse and reflects its own bandwidth which is about 1 MHz, i.e. time constant of $\sim 1 \mu\text{s}$. Any reactions that proceed at a rate faster than this can therefore not be followed on a real time basis. This aspect is important if we analyze, in a later section, reaction rate data.

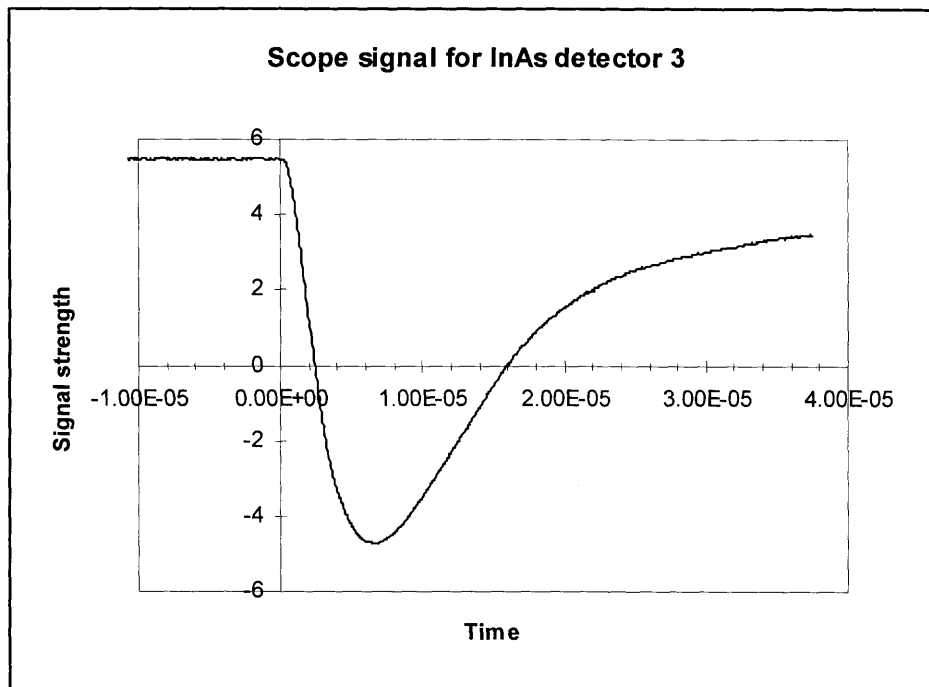
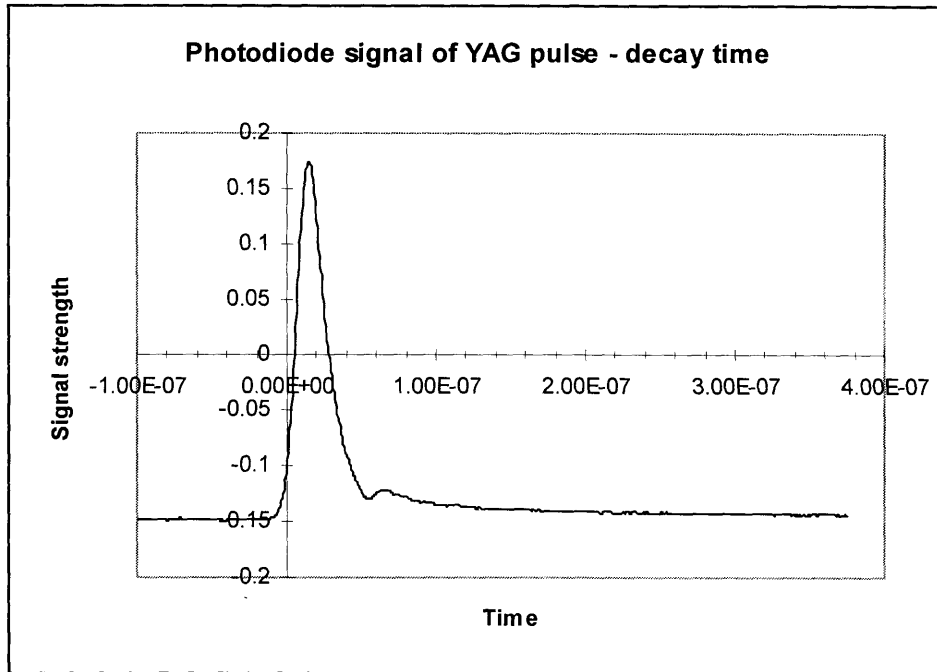


Fig.22 (a) Measured temporal shape of ~8 ns FWHM pulse from Nd:YAG laser. (b) temporal shape as measured by InAs detector.

3.2.2 RESULTS

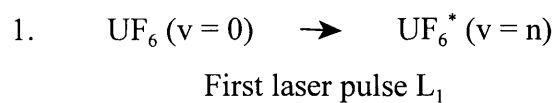
3.2.2.1 HF fluorescence - dissociation with 16 μm

Experiments to characterize the HF fluorescence signal at ambient temperatures were first performed. Figure 23(a)–(d) depicts the time response of the signal in a static condition in the flow cooling nozzle first without any scavenger gas added, figure 23(a), with $\leq 0,023$ torr (3 Pa) CH_4 added, figure 23(b), with a 1:5 ratio of UF_6 : CH_4 added, figure 23(c) and lastly, figure 23(d), with Ar added to 23(c) to the total pressure of $\sim 9,8$ torr (1300 Pa). In all the cases, (a)–(d), the partial pressure of UF_6 was $\sim 0,4$ torr (50 Pa). The slow relaxation process in figure 23(a) corresponds to a $p \tau \sim 85 \mu\text{s torr}$ where p = pressure in torr and τ is the characteristic relaxation time derived from figure 24. This relaxation is derived by ignoring the first $\sim 100 \mu\text{s}$ where clearly another process interferes. The addition of less than 0,023 torr of CH_4 has a significant effect on the fluorescence dynamics in the first 50 μs and a clear fluorescence peak evolves as is shown in figure 23(b-d). Under these conditions the second fluorescence decay shortens significantly and is a function of CH_4 pressure. If the CH_4 concentration is further increased the amplitude of the first part of the signal increases less dramatically and only a $\sim 15\%$ increase results from a ~ 2 torr (250 Pa) CH_4 pressure. Adding argon to the mixture, figure 23(d), the fluorescence signal is suppressed.

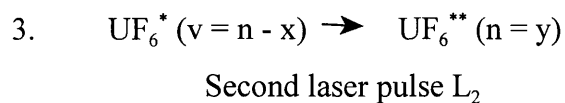
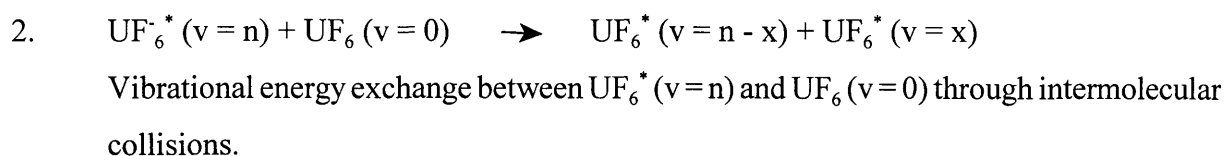
3.2.2.2 HF fluorescence as a probe for vibrational energy transfer from UF_6^*

Two-frequency dissociation measurements were subsequently performed under flow cooled conditions. An appropriate delay time was introduced between the two 16 μm beam pulses and the corresponding HF fluorescence signal was monitored. Reaction mixtures of similar composition were employed and the delay time between the pulses was varied. For each delay time the maximum in the fluorescence trace was measured. Semilog plots of fluorescence intensity (equivalent to relative dissociation yield) versus delay time are given in Figure 25 for two fluences.

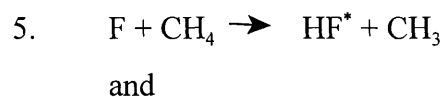
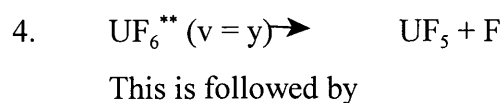
These plots are based on the following reaction scheme of elementary steps and subsequent arguments:



$UF_6^*(v=n)$ is below the threshold for dissociation.



The delay between L_1 and L_2 regulates the period τ available for vibrational energy exchange between $UF_6^*(v=n)$ and $UF_6(v=0)$, while $UF_6^{**}(v=y)$ has sufficient vibrational energy to dissociate by



Through stoichiometry the maximum intensity of fluorescence $\propto [HF^*]$

$$\propto [F]$$

$$\propto [UF_6^{**}(v=y)]$$

$$\propto [UF_6^*(v=n-x)]$$

$$\propto [UF_6^*(v = n)]$$

The rate of vibrational energy exchange by step 2 is given by

$$-\frac{d[UF_6^*(v = n)]}{d\tau} = k[UF_6^*(v = n)][UF_6(v = 0)]$$

$$= k_1[UF_6^*(v = n)]$$

with $k_1 = k[UF_6(v = 0)]$

therefor

$$\ln \sim \frac{[UF_6^*(v = n)]_{\tau}}{[UF_6^*(v = n)]_{\tau=0}} = \ln \sim \frac{[\text{Maximum intensity of fluorescence}]_{\tau}}{[\text{Maximum intensity of fluorescence}]_{\tau=0}} = k_1\tau$$

$$\ln [\text{Maximum intensity of fluorescence}]_{\tau} = k_1\tau + \text{constant}$$

A plot of $\ln [\text{Maximum intensity of fluorescence}]$ versus τ must be linear with slope k_1 in $\mu s^{-1} \text{ torr}^{-1}$

Since

$$k_1 = k [UF_6(v = 0)] \text{ in } \mu s^{-1} \text{ torr}^{-1}$$

therefor

relaxation time for $UF_6 = 1/k_1$ in $\mu s \text{ torr}$.

The striking feature, see table 1, is that the relaxation process at $\sim 100 \text{ K}$ is very fast and substantially exceeds the relaxation rate at room temperature. Furthermore the level of excitation with λ_1 , as shown in figure 25, impacts on the characteristic time - the higher the level of

excitation, the faster the relaxation. Compared to the relaxation when hydrogen is used as scavenger gas [33], methane significantly increases the process and this is more prominent at low temperatures. Table 6 summarizes our results together with relevant data from published literature.

3.2.3 LONG RANGE DIPOLE-DIPOLE INTERACTION MECHANISM FOR THE VIBRATIONAL ENERGY EXCHANGE IN UF₆

The most obvious theory for V-V energy transfer is derived from an exponential repulsive interaction between harmonic oscillators. In this case the integrated probability for V-V energy transfer is directly proportional to the absolute temperature. Mahan [34] was the first to indicate that an alternative mechanism, referred to as long-range dipole-dipole interactions, could induce near resonant V-V transfer in molecules with a strong induced dipole moment. In such cases the attractive part of the interaction potential introduces considerable Fourier components to the interaction potential. An expansion of the dipole moments in a Taylor series relative to the normal vibrational coordinate, confirms that if the dipole derivatives are non-zero, the dipole-dipole potential can indeed couple molecular vibrational states. According to this model, the integrated probability for V-V transfer, exhibits an inverse proportionality to the temperature, as was detected experimentally in our study. Therefore the “collisions” under consideration here are not of the head-on type but are subtle encounters in which one molecule simply passes another with a rather large distance, typically 5-10Å, between them.

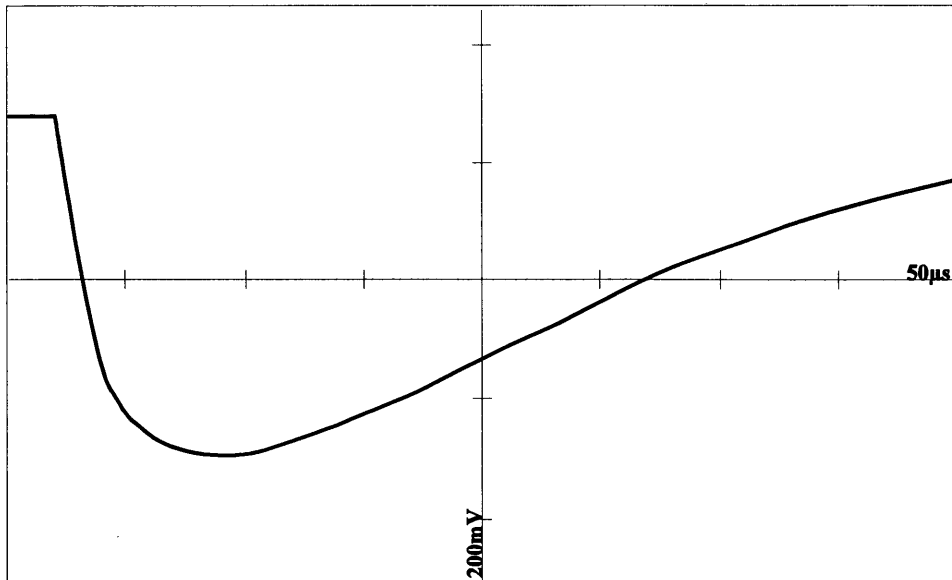


Fig.23(a): HF fluorescence versus time. Oscilloscope trace for ~0,4 torr (50 Pa) UF_6 . HF present as impurity. Temperature is 300 K and dissociation wavelength 16 μm .

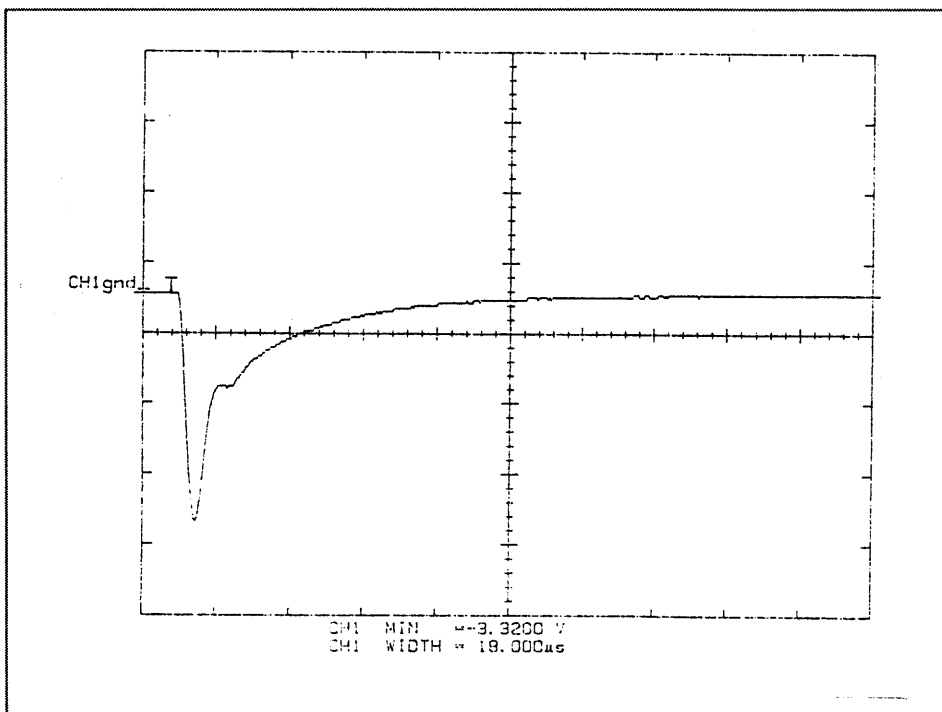


Fig.23(b): HF fluorescence versus time. Oscilloscope trace for ~0,4 torr (50 Pa) UF_6 and ~0,023 torr (3 Pa) CH_4 . Temperature is 300 K and dissociation wavelength 16 μm .

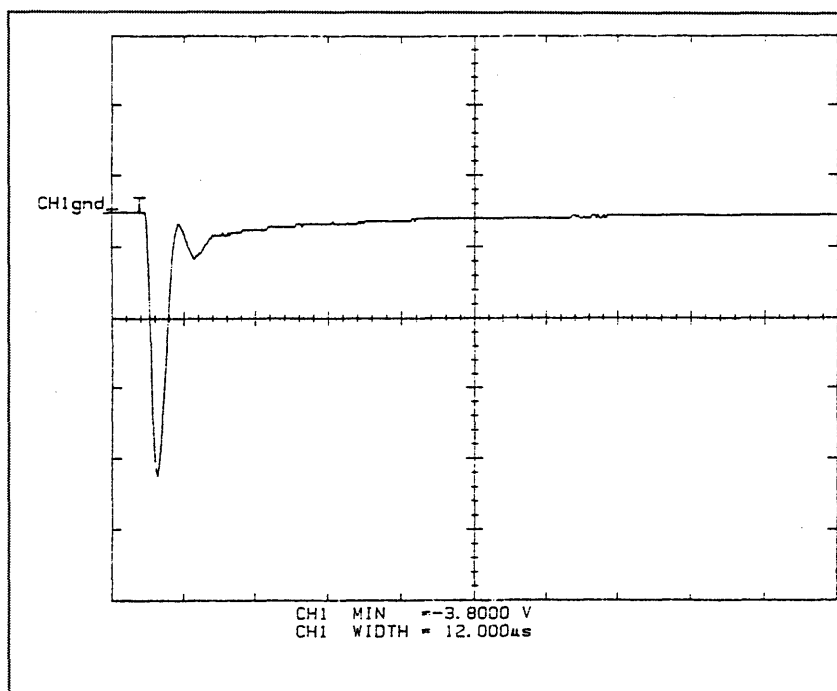


Fig.23(c): HF fluorescence versus time. Oscilloscope trace for ~0,4 torr (50 Pa) UF_6 and 2 torr (266 Pa) CH_4 . Temperature is 300 K and dissociation wavelength 16 μm .

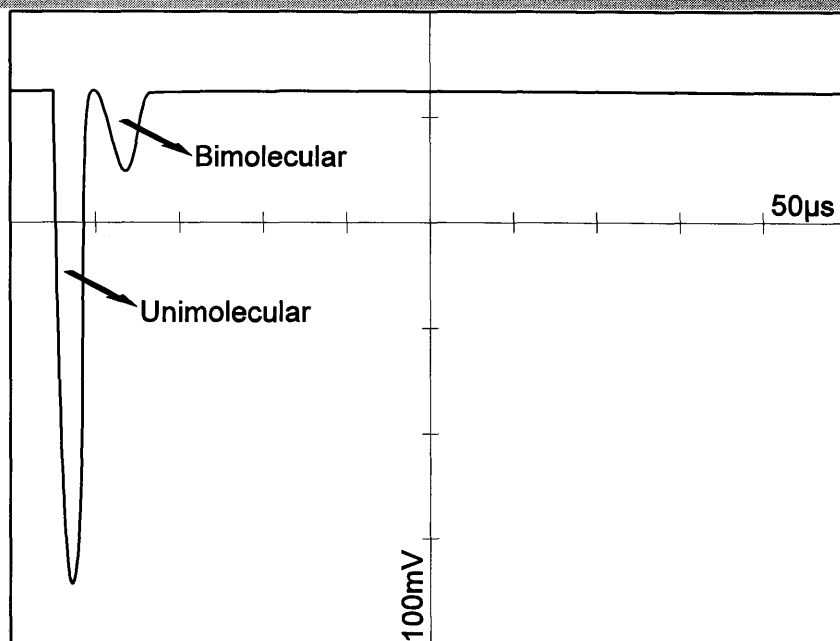


Fig.23(d): HF fluorescence versus time. Oscilloscope trace for ~0,4 torr (50 Pa) UF_6 , 2 torr (266 Pa) scavenger and Argon added to 9,8 torr (1300 Pa). Temperature is 300 K and dissociation wavelength 16 μm .

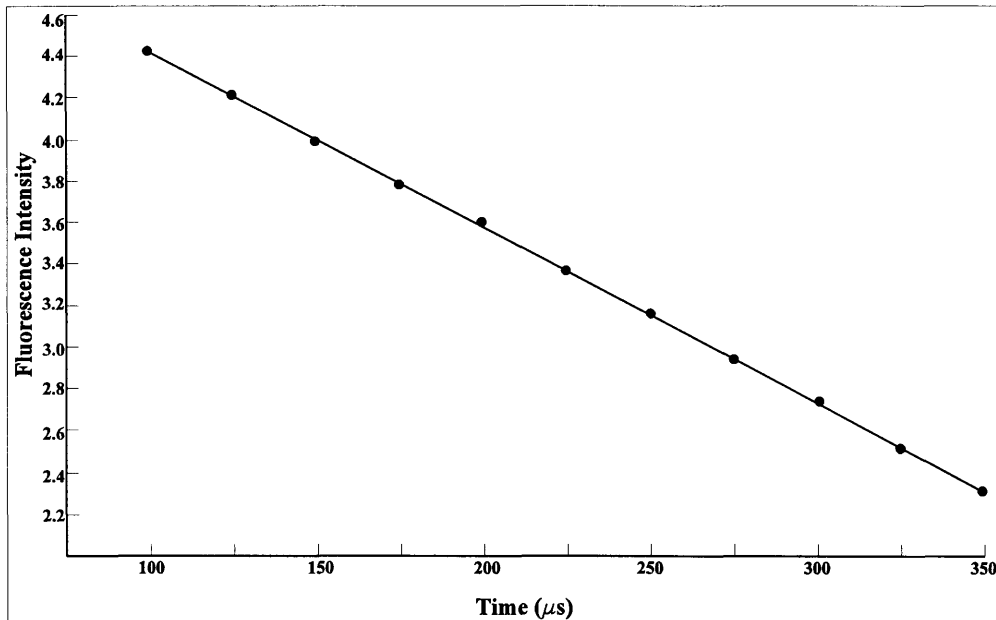


Fig.24: Semilog plot of HF fluorescence decay in figure 23(a). The slope gives a relaxation rate of $\sim 85 \mu\text{s torr}$.

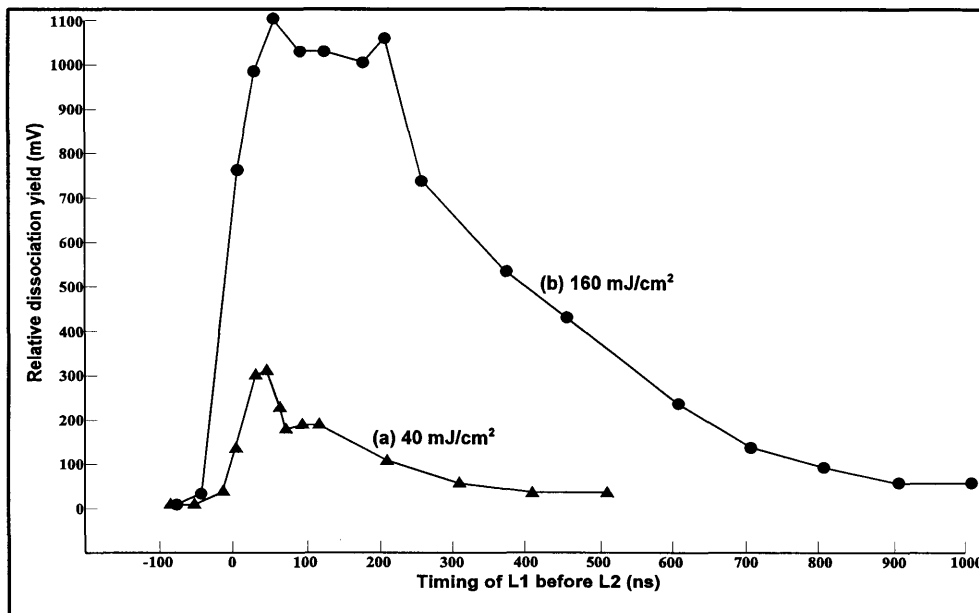


Fig. 25: Peak HF fluorescence versus delay time between two $16 \mu\text{m}$ wavelengths. The two plots are for different intensities of first wavelength (a) 40 mJ/cm^2 (b) 160 mJ/cm^2 .

Table 6: Rate constants for vibrational energy exchange

Gas Composition	Temperature	p.τ	Reference
UF ₆ UF ₆	100 K	0,25μs torr	2
UF ₆ /H ₂ /Ar	300 K	2,9μs torr	1
UF ₆ /H ₂ /Ar	90 K	0,85μs torr	1
UF ₆ /CH ₄ /Ar	300 K	2,5μs torr	this work
UF ₆ /CH ₄ /Ar	100 K	0,75μs torr*	this work
UF ₆ /CH ₄ /Ar	100 K	0,45μs torr**	this word

Different levels of excitation * $\phi\lambda = 40 \text{ mJ/cm}^2$

** $\phi\lambda_2 = 160 \text{ mJ/cm}^2$

Following the descriptions of section 3.1, a simple theory can be put forward to formulate the resonant vibrational energy exchange due to dipole-dipole interactions. The theory gives an energy transfer probability of the form

$$P_{if}(b, \nu) = \sin^2 (A b^{-2} \nu^{-1}) \quad (3.17)$$

where A is a constant that depends on the details of the interaction. If we apply equation (3.1) for the cross section

$$\sigma_{if}(\nu) = \frac{1}{2}\pi^2 A \nu^{-1} \quad (3.18)$$

and the predicted average thermal rate constant is

$$k = \int \nu \sigma(\nu) f(\nu) d\nu = \frac{1}{2}\pi^2 A \quad (3.19)$$

The cross section is

$$\langle\langle\sigma\rangle\rangle = k/\langle\nu\rangle = \frac{1}{2}\pi^2 A (\pi\mu/8k_B T)^{1/2} \quad (3.20)$$

Note that the true average cross section is:

$$\langle\sigma\rangle = \int \sigma(\nu) f(\nu) d\nu = \frac{1}{2}\pi^2 A (2\mu/\pi k_B T)^{1/2} \quad (3.21)$$

which differs by a factor $\pi/4$ from equation 3.20. A very important issue is illustrated by both equations 3.20 and 3.21. Both show that the rate constant for V-V exchange, and also the cross section, increases with decreasing temperature. For hard-sphere collisions the opposite behavior is expected. A long range transfer mechanism can thus be identified on account of two distinct features.

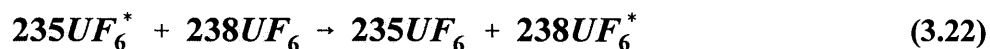
1. The transfer rate reflected in the rate constant is substantially faster than the hard-sphere collision rate derived from the structural diameters of the molecules encountering the exchange.
2. An inverse temperature dependence of the rate constant is exhibited.

3.2.4 DISCUSSION AND CONCLUSIONS

The rate of a unimolecular reaction is in general altered by isotopic substitution in the reactant molecule. A general theory of the kinetic isotope effects has been adequately presented in the literature. Normally, the lighter isotopes, e.g. hydrogen and deuterium, are discussed to review the principles involved. The origin of the kinetic isotope effects lies in the changes in the quantized molecular energy levels which occur when the vibration frequencies and moments of inertia of a molecule are modified by isotopic substitution. These changes, however, are infinitesimal when we consider the isotopes of molecules with high masses such as uranium. An isotope effect which has received little attention in the past is highlighted in this section namely selective excitation by laser. This is of specific importance when the topic of isotope separation is reviewed and the effect of unimolecular dissociation on the enrichment factor is investigated.

The distribution of vibrational energy amongst the ensemble of e.g. UF_6 molecules in the irradiation zone instigated by a laser, takes the general form depicted in figure 26. Due to the selective step excitation in a multifrequency irradiation scheme, such as the MLIS scheme, the

molecules residing in the highest energy segment of this distribution curve, are enriched in $^{235}\text{UF}_6$. They will thus experience the faster rate of unimolecular dissociation. Isotopic scrambling occurs if two different isotopes exchange internal energy as follows:



If the rate of internal energy transfer compares with the dissociation rate then a dilution of the enrichment factor will result. The probability for the $^{238}\text{UF}_6$ to dissociate faster than before the energy transfer, is promoted. This transfer process is of a resonant nature and the long range exchange mechanism is applicable. It is important to understand that the transfer rate can in fact be much faster than the relaxation rates reported here. If two different isotopic molecules exchange energy in the fashion visualized here, no change in the vibrational distribution function will result. All the techniques that have been utilized in the past will consequently indicate no change in measurement since they are not sensitive to isotopic composition. The only way that this effect can be quantified is the measurement of isotopic concentrations of UF_5 product in e.g. a mass spectrometer and then compare this with the predicted spectroscopical selectivity. For UF_6 the data is too scant to further quantify this phenomenon.

During the presentation of a paper contribution at the Quantum Electronic Conference in Sydney (Australia) in 1996 (see paper III), I had interesting discussions with Dr Prior of CSIRO (Australia) and Professor B J Orr from the School of Chemistry, Macquarie University. The first researcher was involved some years ago to study the enrichment of uranium utilizing the molecular complex, uranylhexafluoroacetylacetonate · tetrahydrofuran, $\text{UO}_2(\text{hfacac})_2 \cdot \text{THF}$. They encountered the very problem discussed here to an excessive degree. They measured the absorption features of the two isotopes using isotopically labeled compounds and determined from this the expected enrichment factors. They, however, found it extremely frustrating to observe the “enrichment simply disappearing in static radiation experiments”. This molecule has a molecular mass of 756 which implies a velocity at ambient temperatures substantially slower than UF_6 . Accordingly the contact time, i.e. the duration of “collision”, defined by the ratio of the impact parameter, b , and the velocity, b/v , is larger which promotes the transfer of vibrational

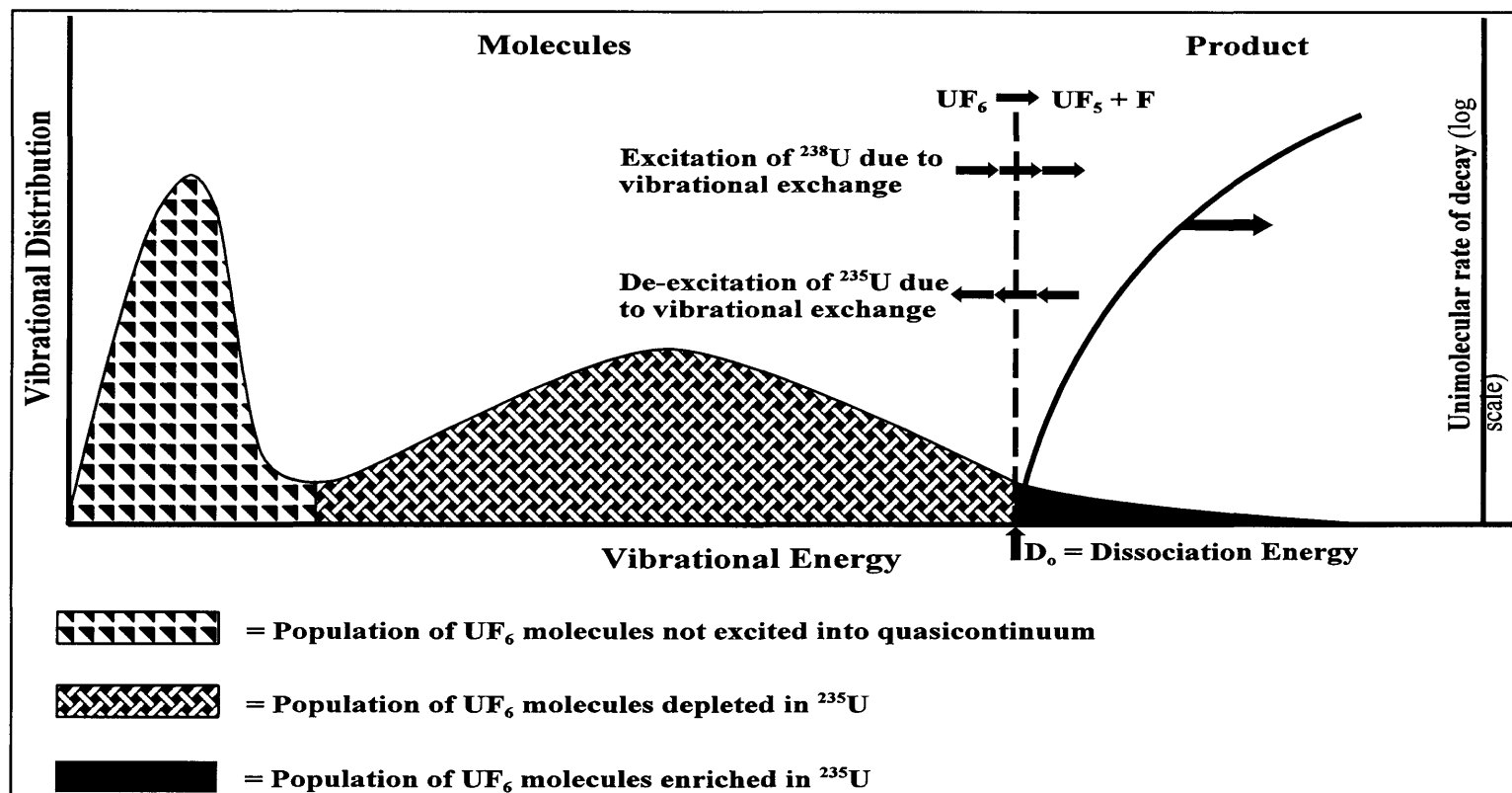


Fig. 26: Schematic of the bi-model vibrational distribution function of UF_6 at the onset of dissociation after excitation by multiphoton infrared absorption.

energy as a result of the long range dipole-dipole mechanism. We can then expect a significant manifestation of the change in unimolecular dissociation rate for isotopic substituted molecules due to the sharing of the excitation energy with the other isotopomers.

In this study the vibrational energy exchange mechanism via dipole-dipole interaction is for the first time identified for the UF_6 system. This clearly demands a different perspective on isotope separation as well as the impact on the unimolecular decay rate of heavier polyatomic molecules. The effect this has on isotope enrichment requires the careful consideration before a economically successful process can be launched.

CHAPTER IV

CHAPTER IV

MEASURING UNIMOLECULAR DISSOCIATION RATES OF UF_6 IN A MOLECULAR BEAM IN A MASS SPECTROMETER

4.1 REACTION RATES AND THE FRAGMENT ION ABUNDANCES IN A MASS SPECTROMETER

As has been shown, the statistical description of the reaction rates, e.g. the unimolecular dissociation rate of UF_6 , by the RRKM theory is very useful. These statistical rate theories have also been applied to the formation of ion fragments in mass spectrometry. For this purpose modifications to the theory are required and these were incorporated in the so-called quasi-equilibrium theory, QET, developed by Rosenstock et al [35]. A number of semi-quantitative applications relating to mass spectrometry can be found in Cook et al.'s book on metastable ions [36].

In this chapter we are concerned only about the formation of ions in a mass spectrometer. The reaction rate of the individual unimolecular reaction defines the product ion abundances in a straightforward manner, which means that from the reaction rates the product ion abundances can be calculated. For the simplest case when the molecular ion has one unimolecular decomposition reaction only, e.g. $UF_6 \rightarrow UF_5 + F$, characterized by the rate constant k , the abundance of UF_6 at time τ is given by:

$$[UF_6] = e^{-k\tau} \quad (4.1)$$

The time lapse τ is measured from the formation of the parent ion and the initial abundance of M , corresponding to time zero, can be normalized to unity. The abundance of UF_5 will consequently be equal to $1 - e^{-k\tau}$. This expression also implies that the half-life of a precursor ion is inversely related to the reaction rate constant

$$\tau_{1/2} = (\ln 2)/k = 0,69/k \quad (4.2)$$

DOCUMENT NUMBER	VERSION	PAGE	OF
LT100-000000-155-022		74	

An illustration of how the rate constant can be determined, is documented for the unimolecular decomposition of $(\text{CF}_3)_3\text{CI}$ in a book by Letokhov et al [37]. The agreement between the predicted rate constants from RRKM theory and the experimentally observed values were within 25-30%. For the purpose of the MLIS process having a closer agreement would be preferable. This is, however, more easily said than accomplished. To measure the abundances of UF_6 and the photo fragments with the mass spectrometric technique, where a variety of ionization techniques were studied and implemented, proved to be a challenging exercise. Numerous features that complicated the interpretation of experimental data had to be negotiated over the past number of years. A few assumptions for the UF_6 system, especially some that appeared in the published literature, were found to be incorrect and had to be discarded. This section reports the endeavours to measure the UF_6 and UF_5 abundances, from the corresponding ions, with the aim to derive the unimolecular decay rates. The added benefit of the mass spectrometer of having isotopic resolution meant that a large portion of the knowledge gained was useful for the measurement of the enrichment factors. This, however, was never the primary concern of this dissertation.

For the purpose of describing the results in a systematic manner it can be divided as follows:

1. Ionization by electron impact and detection in a quadrupole mass spectrometer. Only the positive ions are observed.
2. Negative surface ionization mass spectrometry for the real time monitoring of the UF_6^- molecular ion.
3. Ionization with a XeCl-laser at 308 nm radiation and the observation of the ionization products with a quadrupole mass spectrometer in the positive mode only.

DOCUMENT NUMBER	VERSION	PAGE	OF
LT100-000000-155-022		75	

4. Laser ionization in a locally constructed time-of-flight (TOF) mass spectrometer utilizing a Nd:YAG laser at the fundamental frequency, 1,064 μm wavelength, and its doubled frequency at 532 nm. Detection of ions is in the positive mode.
5. Negative ion formation and detection in the TOF mass spectrometer. The negative ions are produced from low energy photoelectrons that are emitted from a metal surface following laser activation.

4.2 ELECTRON IMPACT IONIZATION

The experimental arrangement for this mode of ion formation and detection consists of a commercially available quadrupole mass spectrometer from Extra Nuclear Laboratories and an appropriate gas inlet system for UF_6 . The quadrupole is housed in the second vacuum chamber of a two-stage differentially pumped configuration. This area will be referred to as the detection chamber and the first one to as the inlet chamber. Figure 27 depicts schematically the lensing system for the electron impact bombardment ionizer. Electron bombardment of background gases creates ions in, or a molecular beam passing through, the ionizing volume. This ionizing volume is located within the ion region “basket”.

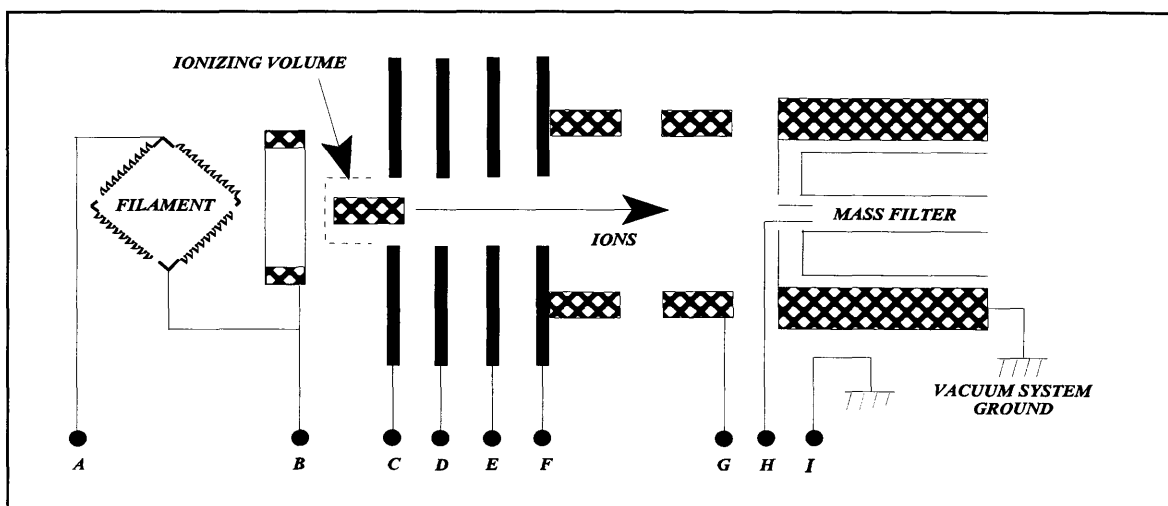


Fig. 27: Schematic illustration of the quadrupole mass spectrometer utilized for UF_6 mass fragment detection.

The filament as indicated in figure 27 is heated by electrical current thereby producing thermal electrons. Four segments of filament is arranged concentric around a cylindrical mesh of thin cold plated wires (“basket”). An appropriate voltage accelerates the electrons inwards to the geometrical axis of the quadruple arrangement where ionization occurs. These ions are then extracted and focussed towards the entrance of the mass filter. At the exit of the quadruple the positive ions are attracted to a channeltron suitable for pulse counting. This channeltron is mounted off-axis to avoid photons and electrons impinging directly on the sensitive area. A pre-amplifier improves the signal and a Nicolet multi-channel analyser records the mass spectra.

The molecular beam of UF_6 was produced effusively either through a 50 μm -diameter pinhole in nickel or from a pulsed valve procured from General Valve. The UF_6 reservoir was at ambient temperature and maintained at a pressure of 0,2-0,3 torr UF_6 for the continuous inlet and at a few torr for the pulse valve. A skimmer with an aperture of typical 1 to 2 mm diameter was placed between

the two chambers. A distance of approximately 40 mm extended between the gas entrance position and the aperture of the skimmer. Behind the skimmer the ionization region was removed by a further 40-50 mm. During operation the pressure in the detection chamber remained below 1×10^{-6} torr while the pressure in the inlet chamber rose to $\sim 1 \times 10^{-5}$ torr. A liquid-nitrogen-cooled plate in the detection chamber significantly improved the UF_6 background signal. It was also possible to detect a modulated beam for the continuous beam mode with a chopper, placed between the inlet and skimmer and with an effective modulation frequency of up to 400 Hz.

In figure 28 a mass spectrum of the background gas is depicted. It represents the fragmentation mass spectrum of the silicone oil used in the diffusion pumps in the initial stage of the investigation. The presence of the strong background signals forced us to replace the diffusion pumps with turbo molecular pumps with nitrogen circulation on the bearings to protect it from the corrosive UF_6 . A positive ion spectrum of UF_6 with the UF_5^+ fragment as the dominant ion can be seen in figure 29. This fragment distribution is typical of the electron impact spectrum of UF_6 where the intensity of ion fragments decreases from UF_5^+ to U^+ . An electron acceleration voltage of 70 to 80-volt

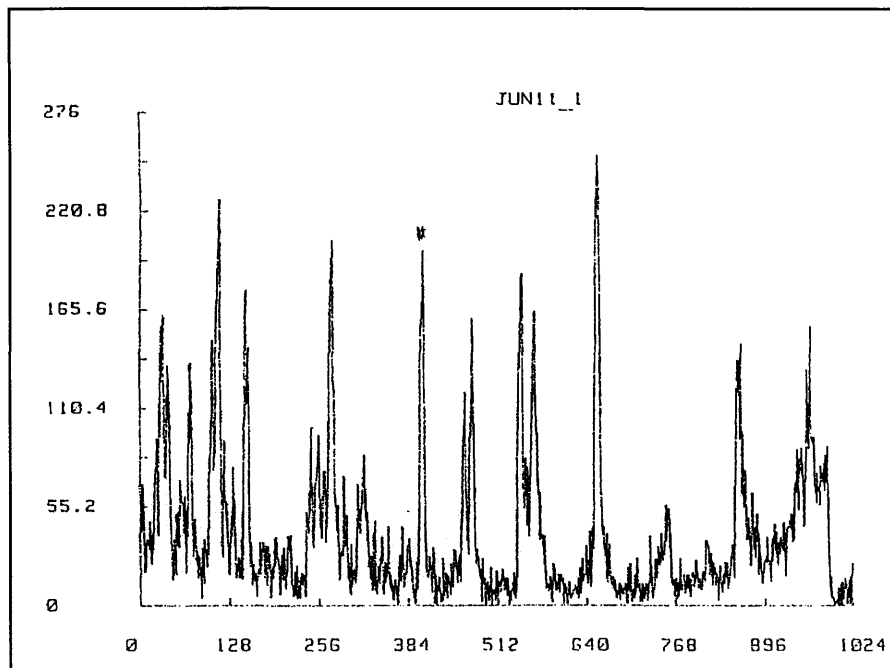


Fig 28: Background mass spectrum of vacuum pump oil in a mass spectrometer. Ionization by electron impact.

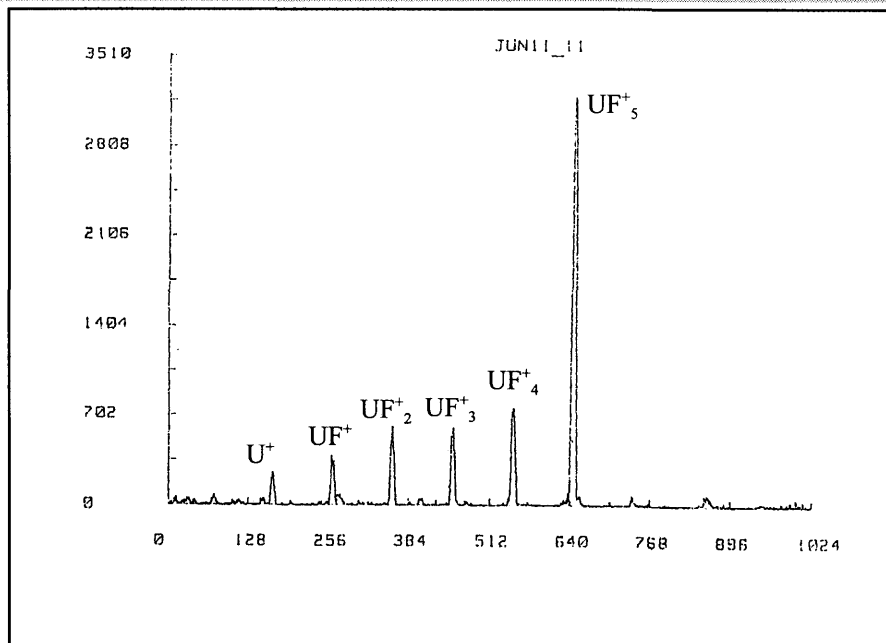


Fig 29: Electron impact ionization mass spectrum of UF_6 in a quadrupole mass spectrometer.

was applied to obtain this distribution. For the purpose to measure the temporal variation of the UF_6 or UF_5 species, the appearance of the prominent UF_5^+ fragment is worrisome. There were two reasons why the electron impact spectrum could not be employed for the purpose set out:

1. Both UF_6 and UF_5 contribute to the UF_5^+ fragment intensity. It is uncertain what the relative contributions are.
2. The fragmentation pattern for UF_6 , and also UF_5 , changes for vibrationally hot molecules. This complicates the situation when an infrared laser instigates dissociation.

Nevertheless, the lense voltage settings and the mass resolution of the quadruple could be optimized in this mode of detection. According to the specifications of the spectrometer a mass range up to 1200 amu was possible with a mass resolution of at least one amu over this range. In figure 30 the UF_5^+ peak is shown under settings for good mass resolution - the calculated resolution is ~ 850 at a (m/e) of 333. This spectrum was recorded for a natural isotopic abundance sample. Figure 31 shows a similar spectrum for a $\sim 20\%$ enriched sample indicating the clear separation between the two isotope fragments.

With the mass spectrometer operating in the positive ion mode, with electron impact ionization, the first isotopic selective dissociation of UF_6 at room temperature was demonstrated at the AEC. This topic, however, is not of direct concern for the present study and will therefore not be recorded here. This mode of operation turned out not to be suitable for the purpose of measuring dissociation rates. Nevertheless, the settings for good results were evaluated. This proved particularly fruitful when at a later stage a mass peak one amu higher than UF_5^+ and U^+ , was consistently detected. Split peaks can result from an excessive voltage setting for the ion region and/or a wide energy spread from an ill-defined ion region. The confidence that an additional mass peak was indeed observed, was boosted by the time spent to optimize the conditions for the positive ion detection.

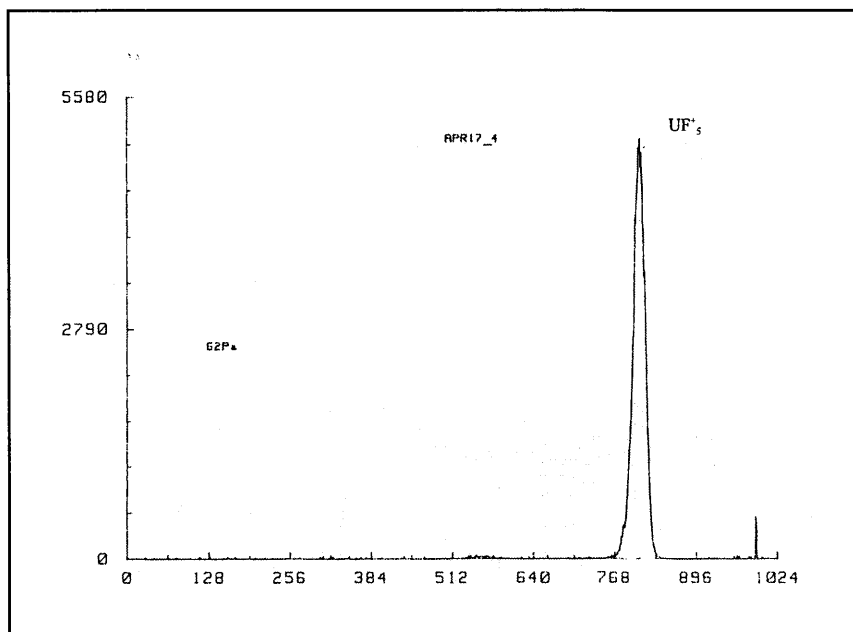


Fig.30: Mass peak of the UF_5^+ ion after electron impact ionization. Numbers on mass axis refers to multichannel numbers and not mass units. The prominent peak is for the 238 isotope and the resolution at mass 333 is 850.

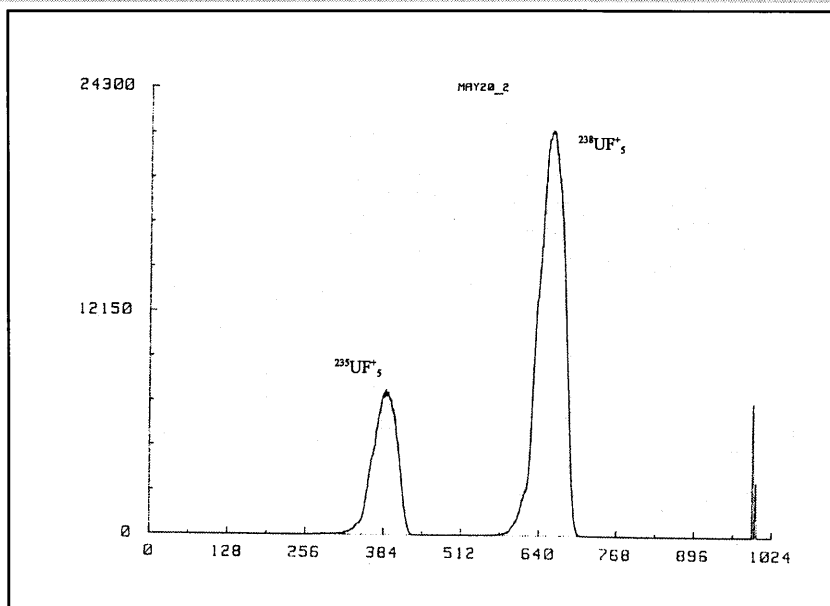


Fig.31: Mass peaks for the two isotopes 235 and 238, of UF_5^+ after electron impact ionization. A 20% enriched sample is shown.

It was furthermore established that XeF_2 , which was synthesized locally, is extremely useful to back-fluorinate solid uranium products that either clogged the 50 μm apertures or modified the electron multiplier operation.

4.3 NEGATIVE SURFACE IONIZATION

Historically, negative surface ionization (NSI) has been the preferred ionization process for performing analysis of halogen compounds due to the high electron affinities of these compounds.

If an electronegative specie, e.g. UF_6 is absorbed on an incandescent metal surface, negative ions can form by electron attachment. This is a very “soft” ionization process and the molecular ions are known to form. If this is the only ion to occur in the mass spectrum it is of course a very desirable situation. The surface ionization efficiency, β , for the thermodynamic equilibrium is expressed by the Saha-Langmuir equation.

$$\beta = [1 + g_o/g_- \exp (\Phi - E_a)/k_B T]^{-1} \quad (4.3)$$

where ϕ is the work function of the surface at which ionization occurs at temperature T , k_B is the Boltzmann constant, E_a is the electron affinity of the emitting chemical species and g_o/g_- is the ratio of the statistical weights of negative ions and the neutral species. As can be deduced from equation (4.3) using elements with high electron affinities is advantageous, on low work function surfaces. For the case that $E_a - \phi > kT$ and the ionization process for the formation of negative ions is exothermic, β is approximately 1. Under this condition the ion yield should theoretically decrease with increasing temperature.

The electron affinity of UF_6 has the remarkably high value of 5,1 eV [38]. Dittner and Datz [38] measured the emission current for virgin platinum and determined a work function of 5,4 eV.

DOCUMENT NUMBER	VERSION	PAGE	OF
LT100-000000-155-022		82	

Consequently the formation of negative ions with a clean Pt wire is very inefficient. The accumulation of surface carbon on the wire, however, significantly improves the efficiency of ion formation. An associated work function of 4,4 eV for the carbonised surface was determined. The selection of Pt as filament material, furthermore, is related to its resistance to the corrosive nature of UF₆. The Pt ionizer consisted of a 1,5 to 2 mm wide Pt ribbon attached to the contact pins of the electron impact arrangement in figure 27. It was aligned with its long dimension perpendicular to the direction of the molecular beam. A current was passed through the ribbon to heat it until it became luminously white-hot. I made no effort to determine the temperature directly but it will be shown that it can be approximately established in an indirect fashion.

Figure 32 shows a mass spectrum for the negative ionization mode where the only component is UF₆⁻ and no UF_n⁻ (n<6) are seen in agreement with Beauchamp [39]. Neither are any ions corresponding to PtF_n⁻ observed. If the current through the Pt filament is gradually increased, as shown in the graph of figure 33, the observed influence on the integrated signal strength differs significantly from that reported by Dittner and Datz [4]. An initial rise in the integrated signal is consistent with the observations of the mentioned researchers but the subsequent drop-off at high temperatures (currents) was not observed by them. A plausible explanation will be given below. If the flux of UF₆ molecules at the Pt ribbon is increased, by increasing the pressure of the effusive source, the signal shows a monotonic rise but “saturates” at the high end side of the flux dependence curve, figure 34.

Due to the simplicity of the negative spectrum, operating the mass filter set for 358 amu = UF₆⁻ mass was straightforward to observe the temporal behaviour of the signal strength. This was particularly useful for the pulsed gas flow mode. In figure 35 such a “gas pulse” is recorded utilizing the major isotopic specie. Due to the inertia of the plunger, the gas pulse is not a

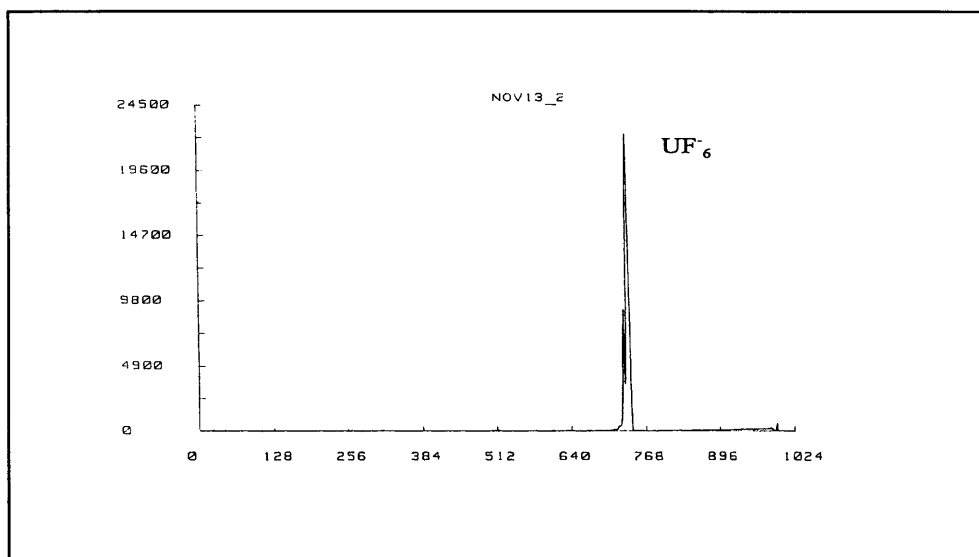


Fig 32: Negative ion fragment spectrum of UF_6 produced by surface ionization from a platinum filament. Only the molecular ion is detected.

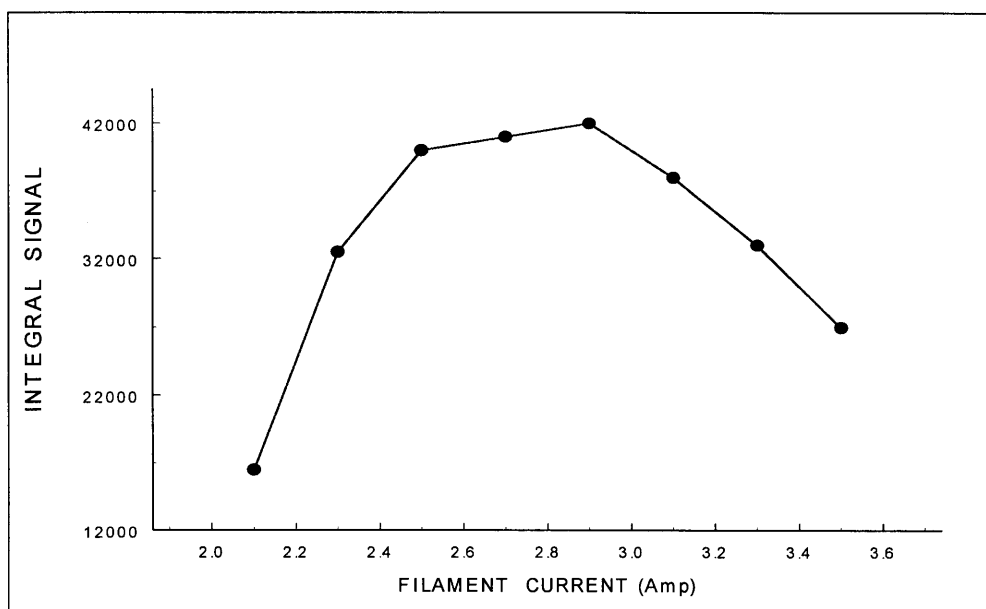


Fig. 33: Molecular ion intensity after surface ionization. The current values are that through the platinum filament.

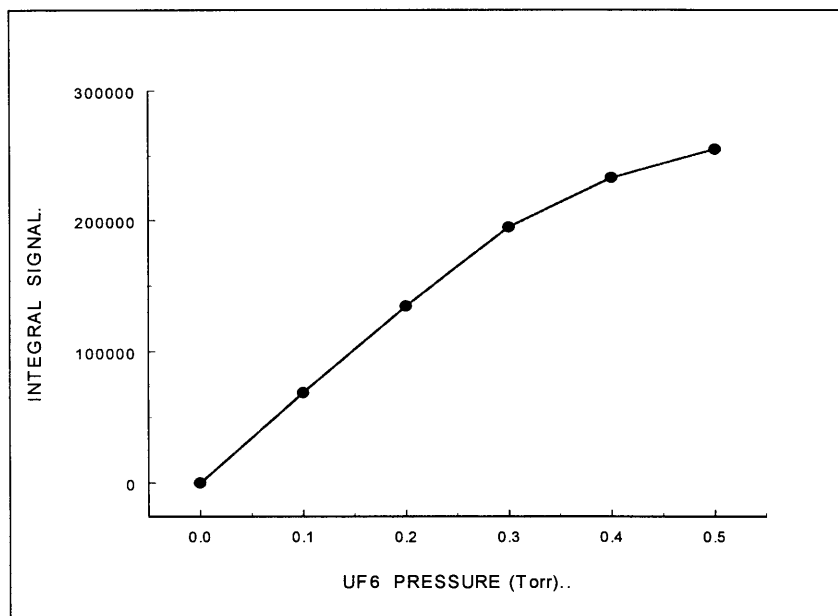


Fig 34: Molecular ion intensity after surface ionization. The pressure values are for the position inside the effusive oven.

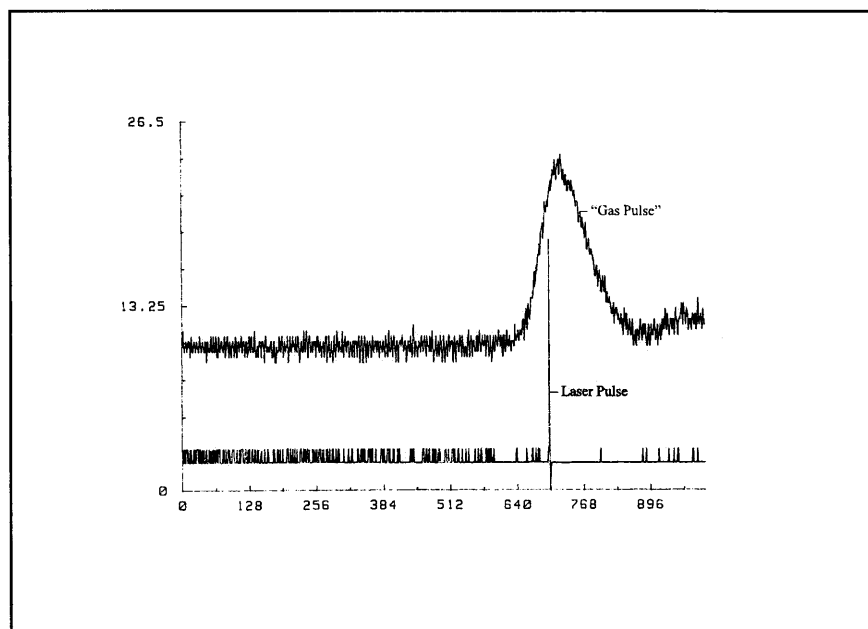


Fig 35: Temporal profile of a UF_6 + carrier gas pulse monitored with the mass filter on the negative molecular ion.

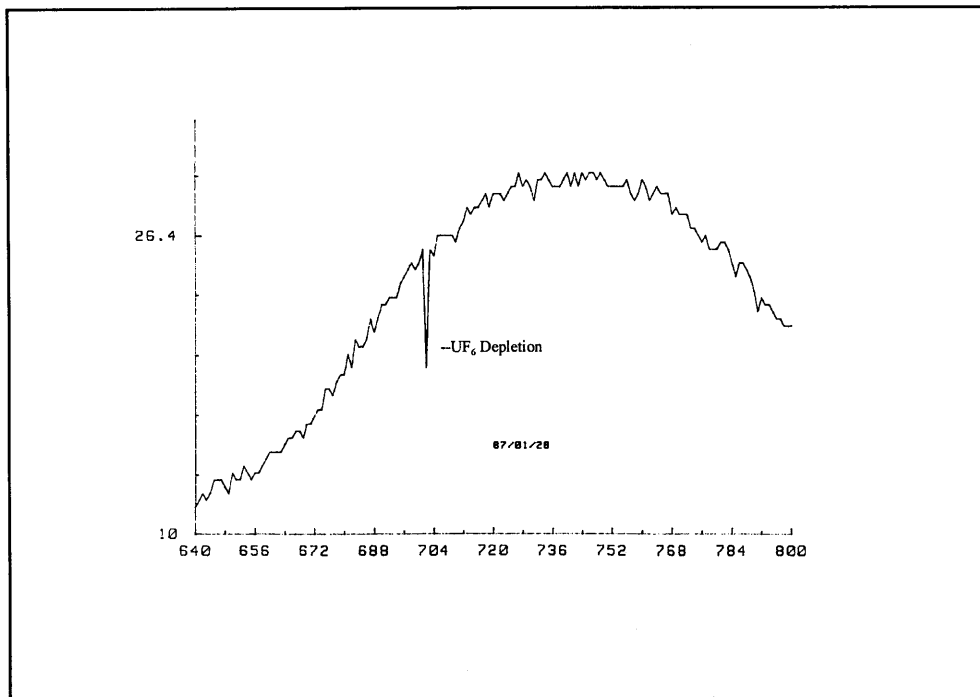


Fig 36: Expanded “gas pulse” monitored by the detection of the negative molecular ion of UF_6 . The time scale represents $1,9 \mu\text{s}/\text{channel}$. The depletion at ~ 704 channel is due to laser dissociation.

“square” pulse with rapidly rising edges. An expanded gas pulse with a time duration of $1,9 \mu\text{s}$ per channel on the multichannel analyser is shown in figure 36. The duration of the gas pulse is approximately $400 \mu\text{s}$. When the UF_6 gas is dissociated by synchronising the laser pulses with the gas pulse, a depletion in the UF_6^- signal can be detected as shown in figure 36. Two infrared $16 \mu\text{m}$ lasers were used which operated on the 16R30 and 16R26 lines. Where the laser beams crossed the molecular beam, the laser beam diameters were approximately 2 mm. From the time duration of the depletion signal and the beam diameter one can calculate a gas velocity of $\sim 475 \text{ m/s}$. This speed is consistent with a speed of 450-500 m/s for the tertiary gas mixture used [40].

A relation between the residence time of the UF₆ molecule on the Pt ribbon and the heat of adsorption, ΔH, has been derived by Frenkel [41]:

$$\tau = \tau_0 \exp (\Delta H/RT) \tag{4.4}$$

where τ₀ is the time of oscillation of the molecules in the adsorbed state normal to the surface. Values for both ΔH and τ₀ have been determined [38]: 33,6 kcal/mole and 3,5 x 10⁻¹³ sec respectively. The residence times calculated with equation (4.4) is shown below.(see table 7)

Table 7 : Residence time of UF₆ on platinum

Temperature (K)	Residence Time (sec)
600	0,51
750	1,9 x 10 ⁻³
900	4,48 x 10 ⁻⁵
1000	6,92 x 10 ⁻⁶
1100	1,50 x 10 ⁻⁶
1200	4,209 x 10 ⁻⁷

Obviously the residence time must be ≤ to the time response of the depleted signal of figure 36 which is ~1,9 μs. Therefore, one can conclude that the temperature of the Pt ribbon is approximately 1100 K. This seems quite plausible for a white-hot metal.

The shape of figure 33 prompts a discussion as this impacts directly on the usefulness of the surface ionization method to measure the dissociation rate of UF₆. The decrease in ion signal for filament currents exceeding ~2,9 A was not detected by Dittner [38]. In the present case, however, the impinging flux of UF₆ molecules are substantially higher than that used in the referenced work:

Dittner and Datz: $\phi = 10^{11}$ molecules/cm² sec.
Present work: $\phi \sim 1 \times 10^{15}$ molecules/cm² sec

From the depletion curve of figure 36 the filament temperature was estimated as ~ 1100 K which is also the optimum position for best sensitivity. The shape of figure 33 can be explained by a effective work function with a shape represented by figure 37. The corresponding shape of the ionization efficiency is illustrated in figure 38. An exaggerated influence of small changes in the work function on the ionization efficiency can be seen. The initial decrease in the work function, figure 37, as the temperature of the filament increases, can be explained by a decrease in residence time on the platinum surface (compare equation 4.4). For a fixed flux of UF₆ molecules impinging on the platinum surface, the surface coverage should decrease with increased temperature as a result of the shorter residence time. The decrease region for the ionization efficiency can be explained by the following descriptions:

1. Increasing emission of electrons from the ionization filament with higher temperatures forms a negative electron cloud around the filament and prevents the UF₆⁻ ion emission.
2. An increase in temperature of the filament is associated with a increased voltage over the filament which can lead to a slight distortion in the electro-optical function of the lenses in the mass spectrometer. This effect was not detected by Dittner. It seems thus more plausible that the much higher flux of UF₆ molecules for our case is the reason for this effect. For maximum sensitivity it is recommended to work at a temperature of ~ 1100 K. This would in turn limit the time resolution for decay data as this cannot be better than the residence time of UF₆ molecules on the platinum surface. This has been estimated as $\sim 1\mu\text{s}$ at 1100K.

According to the results of chapter I, however, the decay time can be substantially faster than a micro-second depending on the degree of over excitation of the UF₆ molecule. It follows

that the surface ionization technique will be useful when the decay rate of UF_6 is not very fast.

In figure 34 we observe that the ionization efficiency does not remain constant as the flux of UF_6 molecules is advanced. Remember here also that the flux of molecules is the product of the density at the filament, and the speed that the gas moves at. When the UF

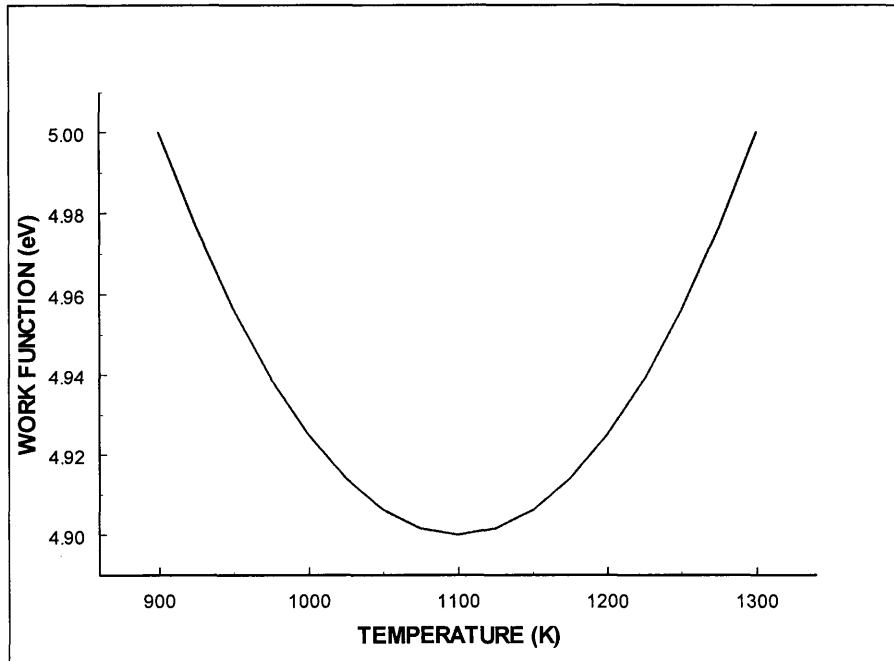


Fig 37: Postulated work function of Pt surface as a function of temperature.

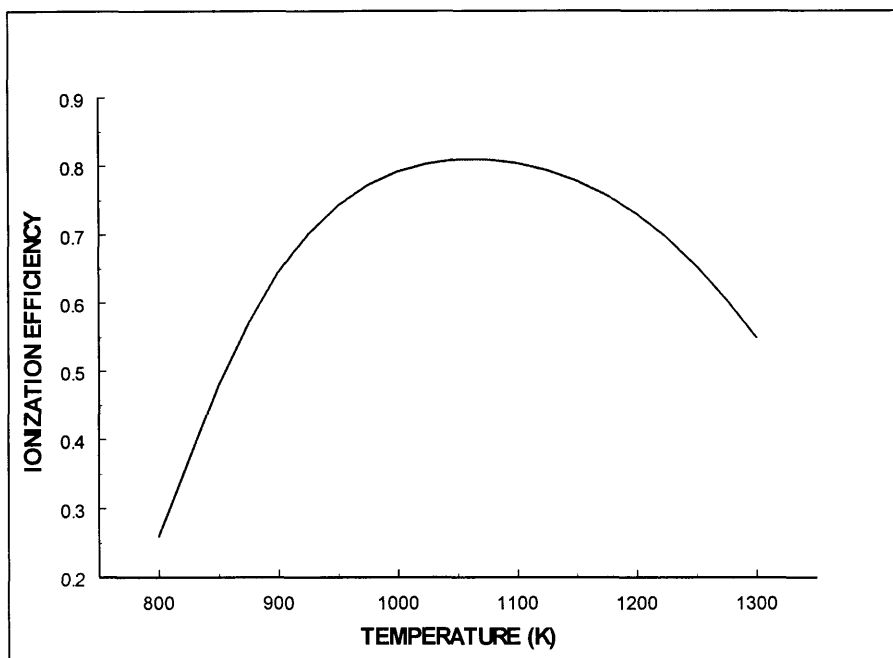


Fig 38: Ionization efficiency of Pt surface for the work function of figure 37.

needs to be flow cooled, as is required in MLIS to enhance the isotope selectivity, the flux of UF_6 molecules are even much larger than that obtained from the effusive source depicted in figure 34. Hence we move further down the saturation realm. When the dissociation yield of the unimolecular decay of UF_6 is measured, it is thus imperative to stay within the limits where a notable change in ion fragment signal is detected for a few percent change in flux of the molecules. The reason for the variable ionization efficiency as the UF_6 concentration fluctuates is most probable connected to a change in surface coverage of the platinum ribbon. This in turn causes an alteration of the work function.

4.4 IONIZATION WITH XeCl LASER

The third MS method used to study the dissociation rate of UF_6 , was ionization of UF_6 or its product UF_5 by a XeCl laser. These lasers emit radiation at 308 nm. Intense laser irradiation often produces energetic fragment ions arising from a Coulombic explosion of multiplying charged parent molecular ions. Remarkable among the reported studies, e.g. that of Wittig et al [42], is the prominence of the singular and multiply charged atomic ions. The mentioned researchers concluded that when UF_6 is dissociated by 266 nm, the nascent UF_5 molecule can be selectively ionized by 532 nm which is the first harmonic of a Nd:YAG laser. An advantage of ionization by laser is the possibility to continuously vary the time difference between the dissociation laser and the ionization laser. It becomes, therefore, straightforward to measure the concentrations of parent ions or product ions as a function of time which can be related to the dissociation rate.

In our experimental setup we used again the quadrupole mass spectrometer with the laser ionization produced in the ion region (look at figure 27). To record a mass spectrum the XeCl laser was run at between 4 and 20 Hz repetition rate, for the effusive source, while the mass filter was slowly scanned in the mass region of interest. In this manner the ion signals of a few laser shots were accumulated in each channel of the multichannel analyser. A recording of the background gas in the mass spectrometer, figure 39, showed strong signals for the diffusion pump oil, which was also detected in the EI spectrum. Fewer fragment ions are, however, detected. Figure 40 is a mass recording when UF_6 is introduced via the effusive source. The dominance of the U^+ ion is a persistent characteristic of this mode of ionization. This is in marked contrast to the EI spectra of UF_6 . The next most prominent component is the UF_2^+ ion which agrees with the finding of Wittig et al [42].

Utilizing a quartz window varied the power density of the ionization laser in the focus region. To continuously vary the power density, the percentage laser transmission was determined beforehand. Different transmissions were achieved by rotating the quartz window to different angles. A

DOCUMENT NUMBER	VERSION	PAGE	OF
LT100-000000-155-022		91	

transmission curve is shown in figure 41 where 90° indicates the perpendicular position. The energies were measured with a Lambda Physik energy meter. The power dependence of the U^+ signal is depicted in figure 42. It exhibits a linear relationship from $\sim 35\%$ of the unattenuated power density. In the region lower than $\sim 35\%$ the signal increases in an exponential manner starting from a threshold of $\sim 25\%$. The unattenuated energy was 175 mJ and the area where ionization occurred $\sim 2 \text{ mm}^2$. Therefore, the threshold fluence is calculated as $2,2 \text{ J/cm}^2$ or $\sim 1,5 \times 10^8 \text{ W/cm}^2$ for a laser pulse length of $\sim 15 \text{ ns}$ at FWHM. This threshold is substantially lower than the fluence region investigated by Armstrong [43] for the third harmonic, 355 nm, and the fourth harmonic, 266 nm, of the Nd:YAG laser. This discrepancy was also seen for the TOF analyses and will be addressed under this section.

DOCUMENT NUMBER	VERSION	PAGE	OF
LT100-000000-155-022		92	

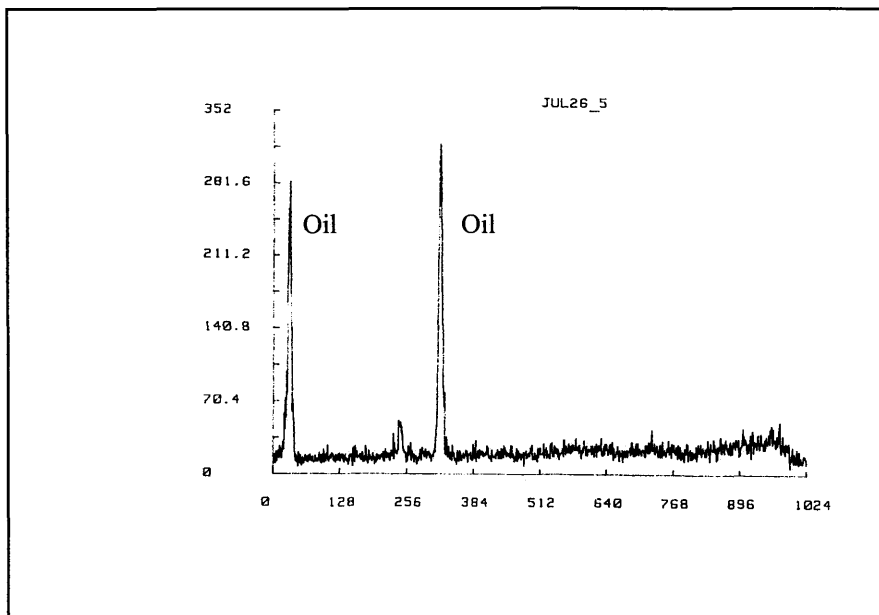


Fig 39: Background spectrum of vacuum pump oil in the mass spectrometer in the positive ion mode when ionization is by a XeCl laser at 308 nm.

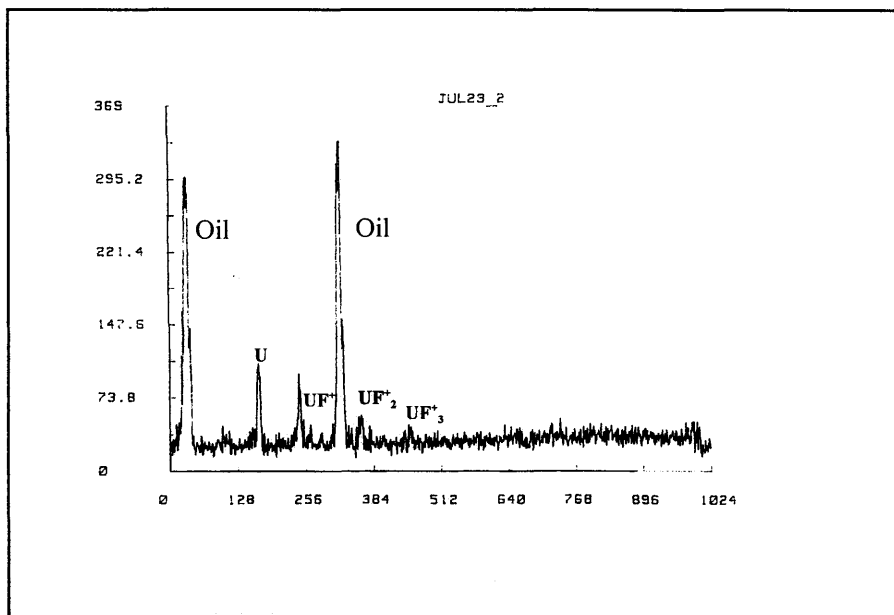


Fig 40: Mass fragment spectrum of UF_6 (plus oil) in the positive ion mode when ionization is by a XeCl laser at 308 nm.

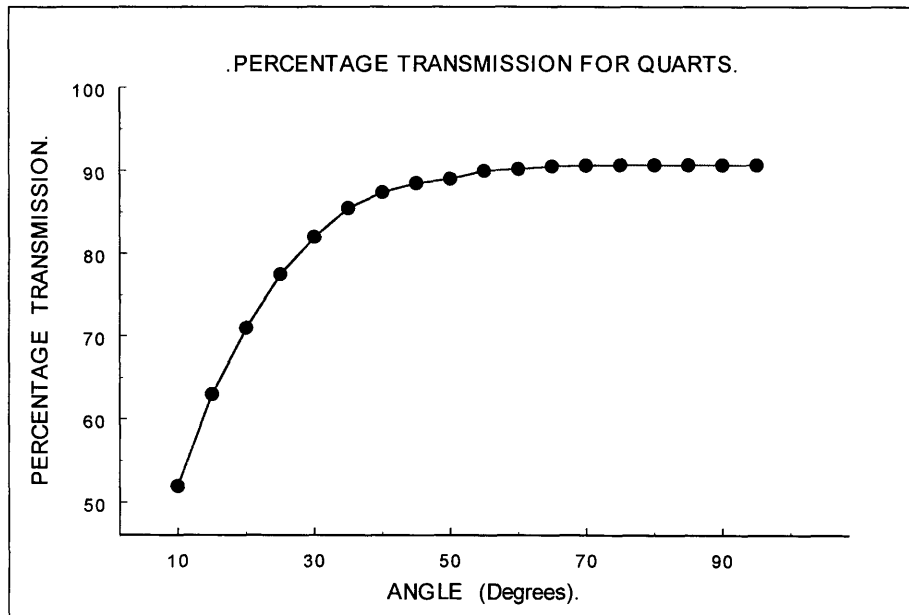


Fig41: Energy transmission curve of quartz for different angles of incidence for the XeCl laser.

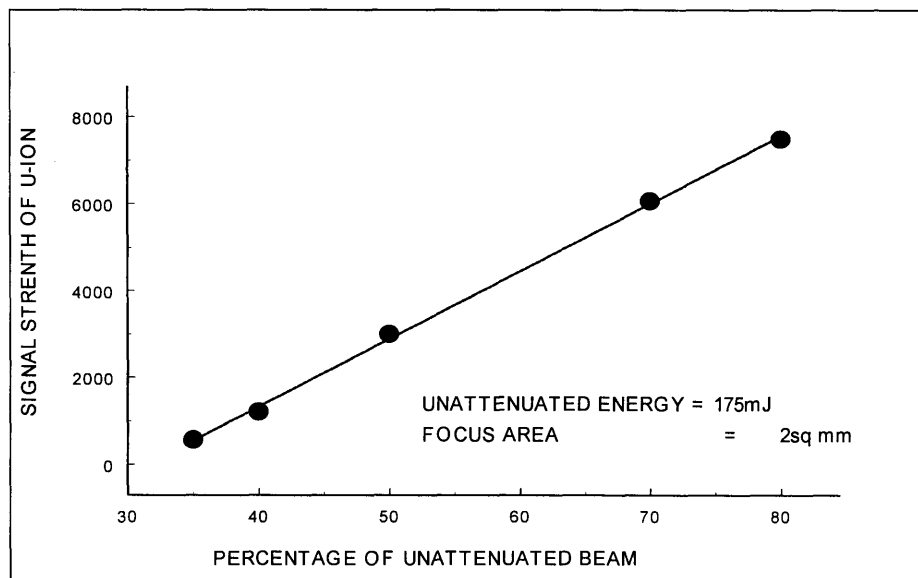


Fig 42: Power dependence of the U⁺ ion fragment for the laser ionization process. The ionization laser is a XeCl laser at 308 nm.

If the density of the UF_6 molecules in the ionization region is increased, by increasing the source pressure, one should observe an increase in the U^+ signal strength. This is indeed the case as is shown in figure 43. The nonlinear behaviour of the signal strength when the pressure is increased is, however, unexpected. At this stage no explanation for this phenomenon will be offered as this

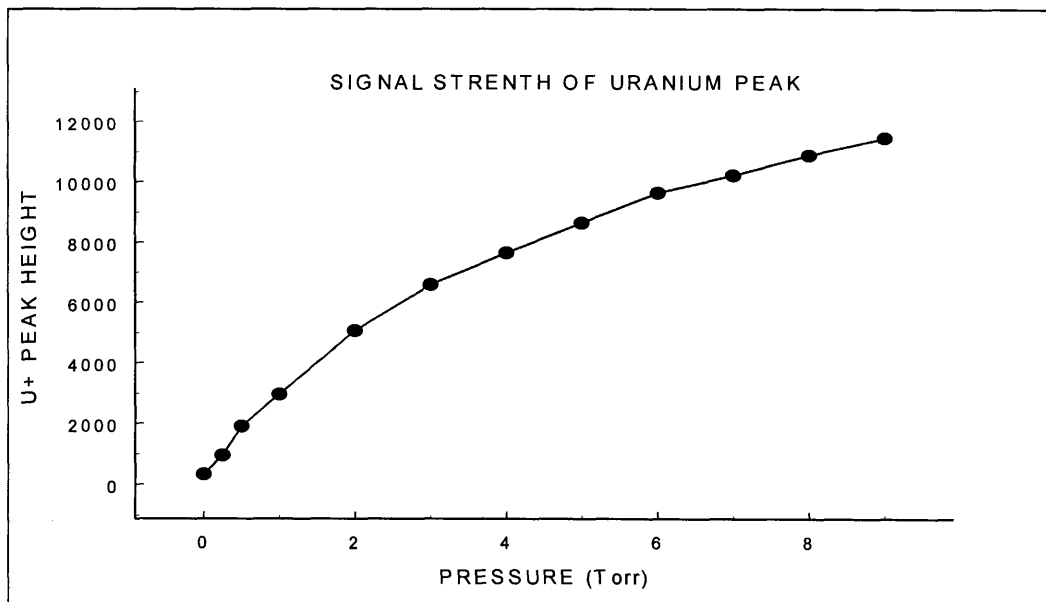


Fig 43: Mass fragment intensity of U^+ ion as a function of source pressure. The ionization laser is a XeCl laser at 308 nm.

was not investigated in detail. Another feature that was observed when CH_4 was added as a scavenger gas is shown in figure 44. An additional mass peak approximately one amu higher than the U^+ peak is seen after laser ionization. It is important to record here that this peak is seen in the gas phase. In later sections the omnipresence of this feature will be discussed as this is important in terms of the secondary reactions that occur subsequently to laser dissociation. This mass peak is consistently observed in the solid phase product and will be identified as the U-H^+ ion.

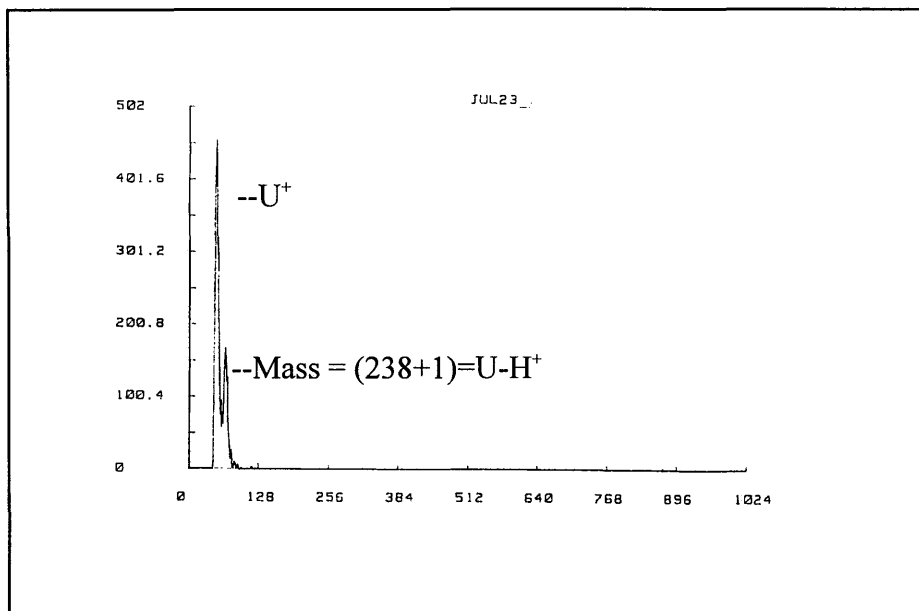


Fig 44: The U^+ fragment ion produced by XeCl laser at 308 nm with a CH_4 scavenger gas added. A prominent ion fragment at 1 amu higher is consistently detected.

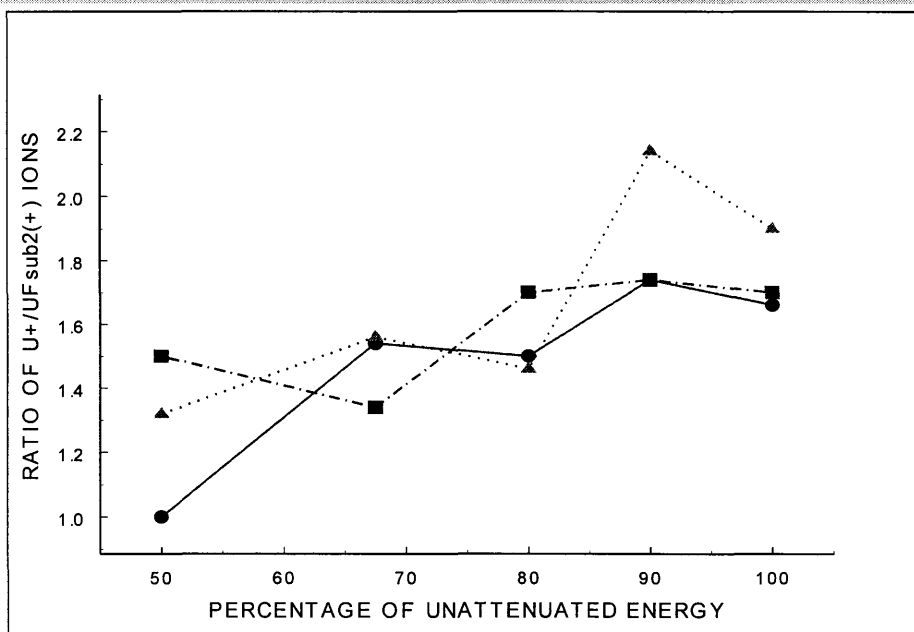


Fig 45: Ratio of U^+ / UF_2^+ ions after laser ionization of UF_6 by XeCl laser. The fluence dependence of this ratio is shown.

A feature of the present mass spectra that is different to that reported by Armstrong [9] is that the U^+ signal is much stronger than the U^{2+} signal in the laser fluence region that was investigated. This is the opposite trend to that reported by Armstrong. This effect could be due to the much lower fluences employed in this study. A plot of the change in the ratio of U^+/UF_2^+ seems to indicate that the abundance is shifted to the U^+ ion as the laser fluence increases (see figure 45). A similar trend from U^+ to U^{2+} seems plausible if the power fluence is substantially increased to the level utilized by Armstrong.

The investigation of the laser ionization technique showed in principal that the dissociation features could be probed on a real time basis. The selectivity between UF_6 and UF_5 needs to be demonstrated and it was decided to rather perform this in a time-of-flight mass spectrometer. It can be expected to achieve a much improved signal strength for the TOF spectrometer as a full mass spectrum is recorded for every laser shot leading to improved detectability. Furthermore, the simultaneous detection of both isotopes in one spectrum would enable one to study any isotopic effects.

4.5 LASER IONIZATION IN TIME-OF-FLIGHT MASS SPECTROMETER

This section will address some phenomena that relate to the analysis of large polyatomic molecules and their photo fragments formed subsequently to a multi photon infrared absorption. The analysis pertains specifically to the time-of-flight mass spectrometer technique when it is utilized to determine, e.g. isotopic concentrations, the yield of a photo reaction, concentrations of specific species etc. Although the molecule UF_6 will be considered to convey the ideas, the processes involved are of a general nature and are deemed to apply to many large polyatomic molecules (see paper IV).

A number of papers [44-47] have recently discussed the direct and real time determination of the separation factor obtained after the multi photon infrared dissociation of UF_6 . The approach is based

DOCUMENT NUMBER	VERSION	PAGE	OF
LT100-000000-155-022		97	

on the selective ionization of the nascent UF_5 product by direct irradiation in a time of flight mass spectrometer. This methodology followed on earlier experimental observations [48,49] which showed that in the case of the dissociation of UF_6 by 266 nm via the B-X band, the UF_5 product can be selectively ionized by radiation at 532 nm. It was subsequently argued that if the ionization laser is set to a fluence, where no ion signal is detected, for UF_6 only in the absence of infrared excitation, the selectivity of the technique towards UF_5 is guaranteed. This is an unfounded conclusion and not in line with the general picture of multi photon excitation and dissociation as it has precipitated over the last two decades. To allow discussion of the present issues, a short review of the salient properties of the infrared multi photon excitation in the ground electronic state of a polyatomic molecule will be given.

In the course of the multi photon excitation (MPE) of polyatomic molecules, a molecule passes through three very distinct regions labelled the initial region of discrete vibrational levels followed by the quasi continuum and the continuum that extends roughly from above the level of dissociation(see chapter I). Experimental observations on the multi photon dissociation (MPD) of SF_6 and UF_6 , like other simple bond rupture reactions, are consistent with the RRKM statistical theory for the description of unimolecular reactions in MPD. In the quasi continuum the internal energy is randomized among all the vibrational modes on a timescale much shorter than the dissociation lifetime. At the onset of dissociation, after the excitation by many infrared photons, the vibrational distribution function of all the molecules in the irradiation zone takes the form as depicted schematically in figure 46. The RRKM theory shows that a substantial over excitation above the dissociation energy is required in order for a large molecule to dissociate, i.e. have a short dissociation lifetime. Thus, when the rate of the dissociation process becomes negligible the internal energy of the irradiated molecules is still substantial. If this energy is largely contained in the irradiation area, which is the case for the conditions prevailing when a laser time-of-flight mass spectrometer is utilized for UF_5 analyses, the following phenomena must surely influence the results:

DOCUMENT NUMBER	VERSION	PAGE	OF
LT100-000000-155-022		98	

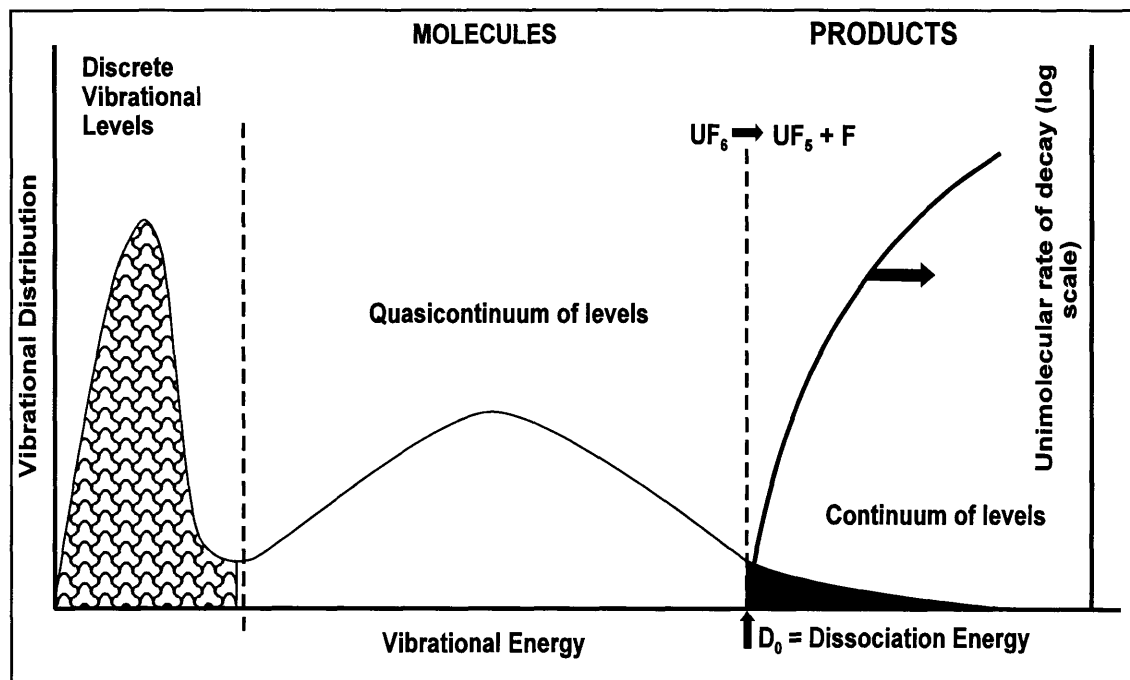


Fig 46: Schematic presentation of the vibrational distribution function for a poly-atomic molecule such as UF_6 following multi photon infrared excitation. The molecules containing internal energy exceeding the dissociation energy, D_0 , can dissociate according to the RRKM theory.

1. The dissociation of vibrationally hot UF_6 molecules by the ionization laser, at fluences below the threshold for photo dissociation of cold UF_6 . An additional amount of UF_5 is formed.
2. The direct ionization of vibrationally hot UF_6 molecules of which the photo ionization cross section differs markedly from vibrationally cold molecules. The additional ions detected are indistinguishable from those used for the detection of UF_5 . The change in the photo ionization cross section for MPE SF_6 in a molecular beam has been used to probe the vibrational energy distribution of SF_6 [50]. Clearly, the simplified picture of the dissociation and ionization processes as totally isolated events, can lead to erroneous interpretation of MS results.

Infrared multi photon excitation (IR-MPE) of room temperature UF_6 was studied using $16 \mu\text{m}$ pulses to excite the strong fundamental ν_3 vibrational mode of UF_6 . These pulses were focussed into the ionization region of a linear Time-of-Flight Mass Spectrometer (TOF-MS), followed by MPI of the dissociation products and mass selection of the resulting ions.

The experimental geometry was such that the direction of gas flow, laser pulses and flight tube were perpendicular to each other. A mixture of a small percentage UF_6 and some carrier gas was prepared in a reservoir and recirculated to maintain its composition. From here the gas mixture was slowly but continuously introduced through a 4 mm dia. orifice into the ionization chamber of the TOF-MS, which was evacuated by a 2000 liter/sec turbo molecular pump. The typical background pressure increased slightly to $\sim 5 \times 10^{-5}$ mbar. This arrangement was suitable for ambient temperature measurements but for flow cooled experiments the setup illustrated in figure 47 was utilized.

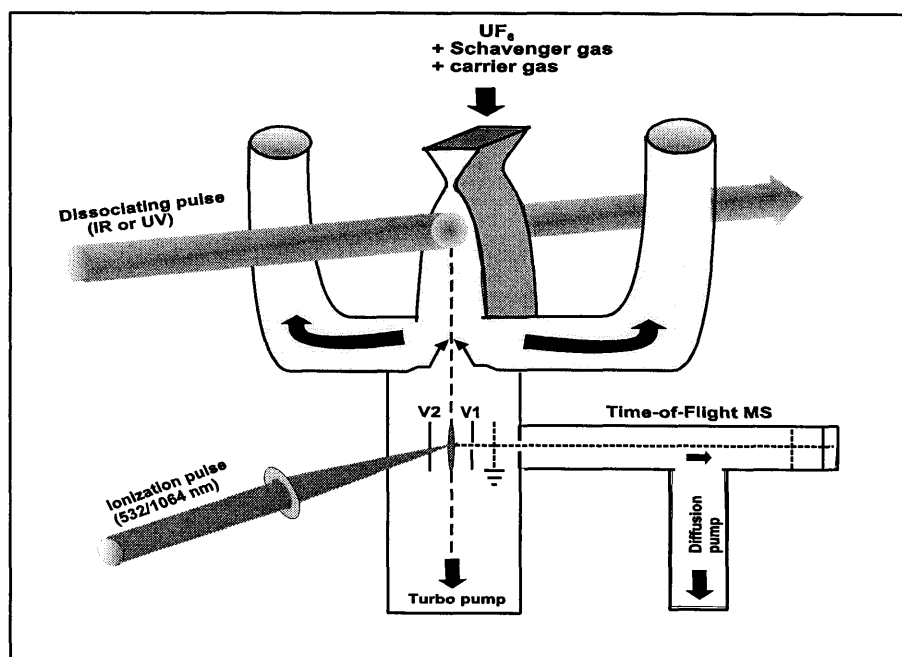


Fig 47: Schematic of the experimental configuration utilized to study the role of vibrational pre-excitation on the ionization spectra of UF_6 .

DOCUMENT NUMBER	VERSION	PAGE	OF
LT100-000000-155-022		100	

A CO₂ oscillator and amplifiers arranged in a master oscillator power amplifier (MOPA) configuration together with the Raman conversion technique was used to generate the 16 μm wavelength radiation. The oscillator was injection mode locked by a CW CO₂ laser, producing a smooth single longitudinal cavity mode. The Raman cell is a Herriot type, 26 pass 77 K para-H₂ cell. The 16 μm output has a Gaussian transverse profile, with an M² beam quality factor of <2. It was focussed inside the TOF-MS with a 1/e² beam radius of 2 mm. At the exit of the ionization chamber, the beam is reflected by a LiF window, and the energy monitored by a Lambda Physic energy meter. A correction was made to relate this value to the actual energy at the centre of the ionization region.

The source for the ionization wavelength was the fundamental, multimode 1064 nm output of a Nd:YAG laser, or alternatively its second harmonic, 532 nm. These pulses were introduced into the TOF-MS, collinearly with the 16 μm, but from the opposite direction. A 300 mm quartz lens focussed the pulses to produce fluences of 200-300 J/cm², respectively. Extreme care was exercised to ensure that the laser fluence was below the MPI threshold of UF₆. The fluences in the focal volume were varied using quartz plate stacks or by adjusting the focal length of the lens. The ionization laser intensity was also monitored in situ by placing a pyro-electric detector in the reflected portion from a LiF window.

A time delay of 0-2 μs was introduced between the 1064 nm pulses and the preceding 16 μm pulses. The ions formed in the volume between the repeller plate and extraction grid as a result of MPD and subsequent MPI were accelerated through a ground grid into the field-free flight tube of the TOF-MS, onto a multichannel plate (MCP) detector. The TOF mass spectra are dominated by the parent U⁺ and U²⁺ ions, of which the ratio could be varied by changing the ionization laser power density. The effective mass resolution at the U²⁺ peak was >300. The output of the MCP detector, together with the respective energy signals were connected to a 540-Tektronix digital storage oscilloscope. Data acquisition and detection were carried out for each photo ionization event. The signal amplitude of the U⁺ ion was taken as an indication of the relative MPE/MPD/MPI yield.

DOCUMENT NUMBER	VERSION	PAGE	OF
LT100-000000-155-022		101	

The time-of-flight mass spectra (TOFMS) of UF_6 , using the focussed light from the Nd:YAG laser or its first fundamental, $\lambda = 532 \text{ nm}$, is dominated by the single and multiple charged uranium ions and not the UF_x^+ fragment ions. This surprising result has been reported previously [39-43] and has led to the postulate of the “giant resonance” transitions [51,52]. Our spectra agree in general with the qualitative features of the previously reported data. However, we also found some distinctly different aspects. The first prominent feature is that the laser fluences employed were at least two orders of magnitude lower than that utilized in reference [52]. This probably stems from the fact that the M^2 parameter was not included in the estimation of the spot size in the latter study, leading to an underestimation of the beam diameter. Whilst only weak ion signals were obtained with the Nd:YAG laser at $\sim 7,6 \times 10^{12} \text{ W/cm}^2$ in the mentioned study, we could detect the mass spectra from $\sim 3 \times 10^{10} \text{ W/cm}^2$. The same feature applies when ionization is instigated by $\lambda = 532 \text{ nm}$. The detected ion signals were similar to that reported in references [42,43] namely U^{2+} , U^+ , and UF_2^+ with the addition of a clear signal at UF^{++} . The latter were approximately one third the strength of the UF^+ ion signal that in turn was about six percent of the dominant signal at U^+ . In the configuration when the ionization is applied downstream of the pre-excitation or dissociation laser, shown in figure 47, the presence of a hydrocarbon scavenger plays a dominant role in the strength of the ion signals [53]. In this position no ion signals were detected when 532 nm radiation was used to ionize the nascent photo fragments of UF_6 even when HF-fluorescence from the formed F radical and a scavenger confirmed that dissociation was indeed occurring. The UF_5 photo fragments produced by, e.g. the 266 nm photo dissociation of UF_6 can contain as much as 1,5 eV of vibrational energy, derived from energy conservation, and at this point it was suspected that this internal energy can play a significant role to overcome the UF_5 ionization potential in especially the collinear experimental setup. If this is applicable to the ionization cross section of the UF_5 photoproduct, then the vibrational content after a multi photon infrared excitation of the parent UF_6 molecule, must show an equally significant effect on its own ionization cross section. The approach to decrease the MPI laser energy to below the threshold of cold UF_6 ionization would then cease to guarantee the selectivity of the ionization for the photo fragments. The magnitude of the dominant U^+ -ion signal was chosen to monitor the

influence of a few parameters on the ionization process. Figure 48 displays the ion signals for a

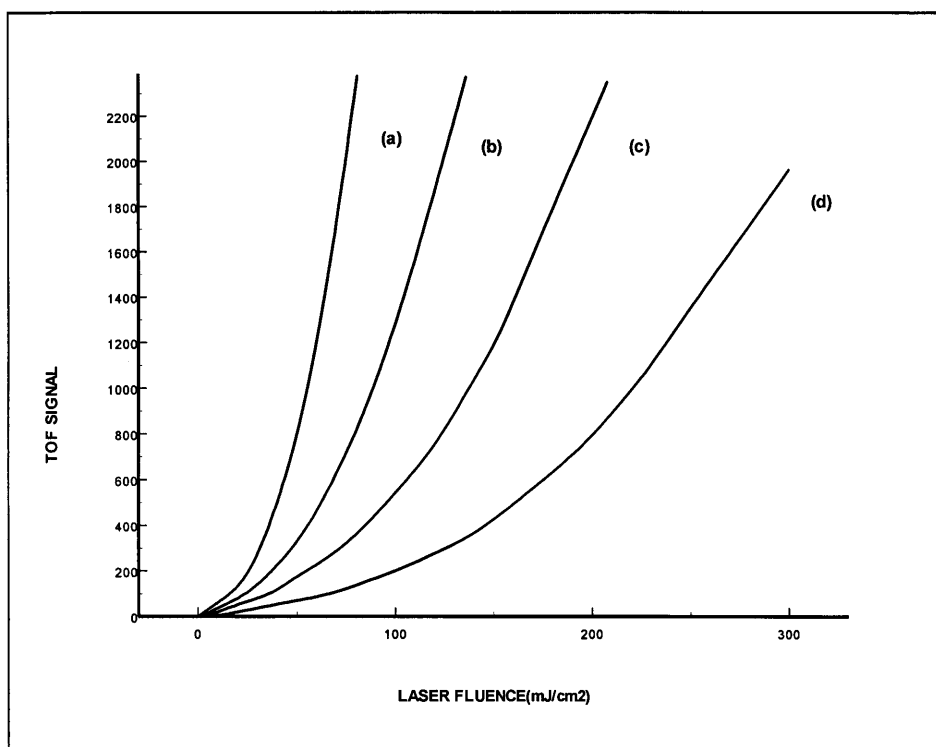


Fig 48: TOFMS signals for UF_6 when ionization is instigated by a Nd:YAG laser (1064 nm) at a constant fluence of $\sim 200 \text{ J/cm}^2$. Pre-excitation is by $16 \mu\text{m}$ radiation for various wavelengths: (a) 16R20 (b) 16R22 (c) 16R28 (d) 16R30. Measurements are for UF_6 at ambient temperature in a co-linear arrangement.

constant Nd:YAG laser (1064 nm) fluence, mJ/cm^2 , whilst the fluence of the $16 \mu\text{m}$ laser is scanned for various wavelengths in the collinear arrangement. The notation, e.g. 16R30 refers to $16 \mu\text{m}$ wavelengths derived from the R30 line of the $10,6 \mu\text{m}$ branch of the CO_2 laser. Prior to the accumulation of the TOF MS spectra, the fluence of the Nd:YAG laser was decreased to the point where no ion signals could be detected when the ionization laser was acting on its own. UF_6 was introduced together with a carrier gas, e.g. helium or argon, where the former constituted 1-5% of the mixture. An effusive inlet introduced the mixture. The temperature was at ambient. A small delay of $\sim 10\text{-}20 \text{ ns}$ between the excitation laser and ionization laser was introduced. It is well-known

that the different 16 μm wavelengths will excite UF_6 with different efficiencies in the discrete region [54,55]. Note that there appears to be virtually no threshold fluence and even values of 10 mJ/cm^2 causes an ion signal which rises rapidly as the fluence of the infrared laser increases. If single wavelength dissociation of UF_6 at room temperature is desired, substantially higher fluences are required. A fluence of 10 mJ/cm^2 mildly excites a UF_6 molecule. Nevertheless, this has a pronounced effect on the ion signals. In figure 49 similar trends are depicted for UF_6 molecules that have been flow cooled to ca 100 K. The ionization process, however, is now not performed in a collinear manner but downstream, with a time delay of $\sim 500 \mu\text{s}$ after the infrared radiation pulse. In this instance, a clear threshold fluence is applicable for each 16 μm wavelength. It is clear from the abovementioned trends that the ion yield is significantly affected by the pre-excitation of the UF_6 molecule and the consequences for isotopic analysis after infrared multi photon dissociation will be

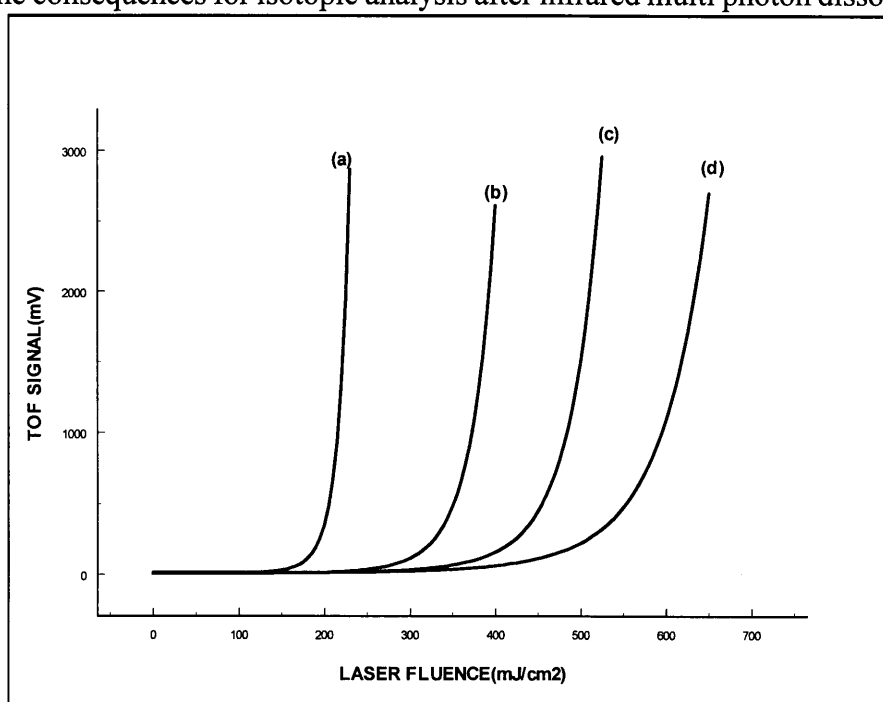


Fig 49: TOFMS signals for UF_6 when ionization is instigated by a Nd:YAG laser (1064 nm) at a constant fluence of $\sim 200 \text{ J}/\text{cm}^2$. Pre-excitation is by 16 μm radiation at various wavelengths: (a) 16R16 (b) 16R20 (c) 16R24 (d) 16R30. Measurements are for UF_6 flow cooled to ca 100 K. A time delay of $\sim 500 \mu\text{s}$ was introduced between pre-excitation and ionization signals.

discussed under the appropriate section. We observed the same trends for the ion yield if the first harmonic at 532 nm was introduced as ionization laser. In the latter case the efficiency of ionization is substantially better, as has been reported before [51,52]. In figure 50 the case for the collinear radiation is depicted. To accentuate the effect even more, a series of graphs is shown in figure 51 where different Nd:YAG ionization fluences are selected and the infrared excitation varied. For any selected ionization fluence the pre-excitation strongly influences the ion yield. Plotting the data on a log scale for the ion signal illustrates clearly the variable “threshold” fluence for the IR dissociation laser to overcome the ionization potential.

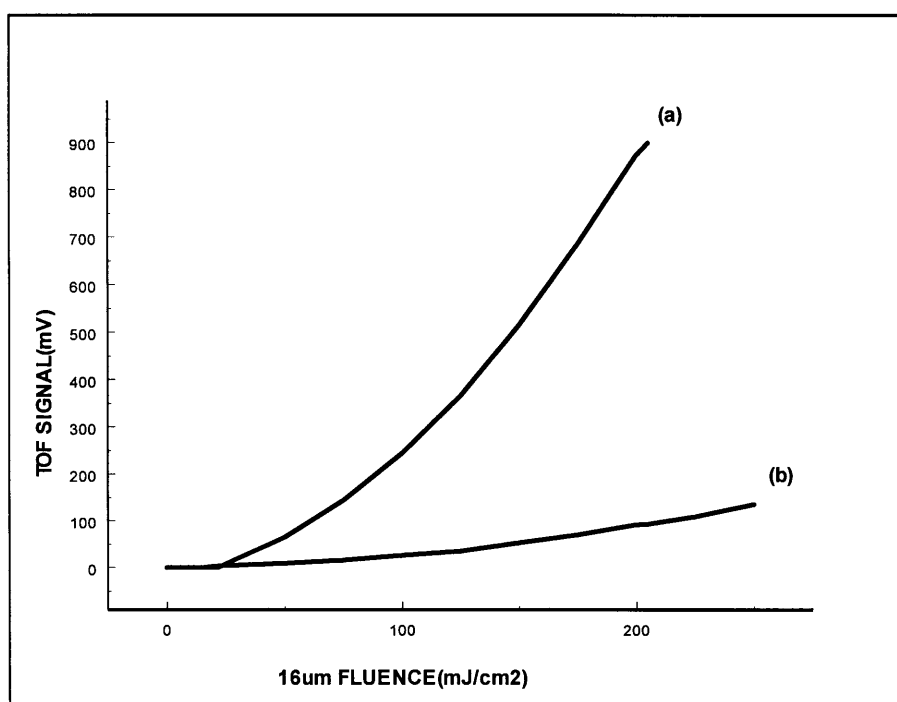


Fig 50: TOFMS signals for UF₆ when ionization is instigated by a Nd:YAG laser at 1064 nm, (a), and the first harmonic of the Nd:YAG laser at 532, (b), respectively. Pre-excitation is by 16 μm radiation at the 16R18 line. The respective fluences of the ionization lasers are ~100 J/cm², (a), and 10 J/cm², (b). The measurements are for UF₆ at ambient temperature in a co-linear arrangement.

Some simple calculations on the average vibrational temperature at the downstream position, to elucidate the contribution of pre-excitation at this position, is desirable. We first assume that the irradiated UF_6 molecules remain largely in the irradiated dimensions as they move downstream. This is a reasonable assumption as the Rayleigh scattering technique, which detects the uranium photo fragments after clustering [53], has previously illustrated this feature. Furthermore, an average vibrational temperature, shortly after irradiation of approximately 2000 K has been determined by Raman scattering techniques [56]. At high temperatures the UF_6 molecules can “store” 15 kT of energy in the vibrational modes whilst all the other modes of energy are equal to 3/2 kT, i.e. rotational and translation. For the case of say 5% UF_6 in He, and an initial flow cooled temperature of ~ 100 K, an equilibrium temperature of 700-800 K will result.

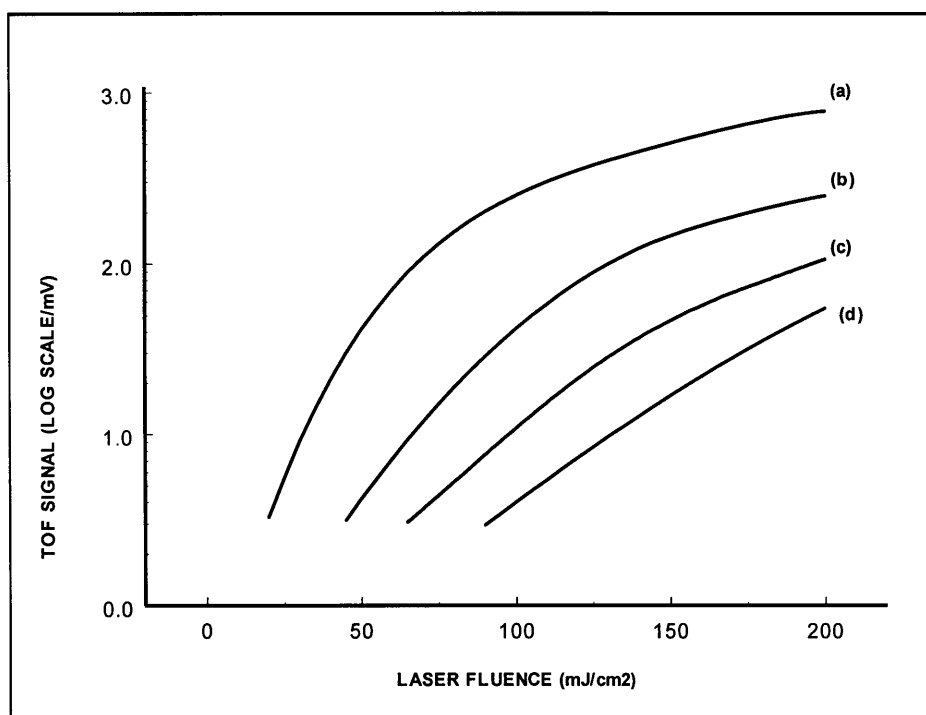


Fig 51: TOFMS signals, presented on a log scale, for UF_6 when ionization is instigated by a Nd:YAG laser (1064 nm) at a different fluence: (a) 280 J/cm², (b) 225 J/cm², (c) 185 J/cm² and (d) 145 J/cm². Pre-excitation is by 16 μm radiation at 16R18 line. Measurements are for UF_6 at ambient temperature in a co-linear arrangement.

From our experimental observations it is certain that such an increase in temperature will affect the ionization signal significantly compared to the flow cooled temperature situation. If a scavenger gas is added, the resultant temperature will be slightly less due to its increased thermal capacity. A discussion of the reported observations should be directed along the giant resonance hypotheses of Armstrong et al [51,52] developed to explain the high level of fragmentation in the laser MS of UF_6 and the schematic presentation of figure 52. The giant resonance proposal has been discussed at length in reference [52] and will not be repeated here. Suffice it to say that the efficient laser excitation of UF_6 molecules to a level of ~ 50 eV is proposed via a resonance with energy in the range of 12-14 eV above the ground state UF_6 . This highly excited molecule then ionizes and fragments, via multiple channels into U^{n+} and UF_x^+ etc.

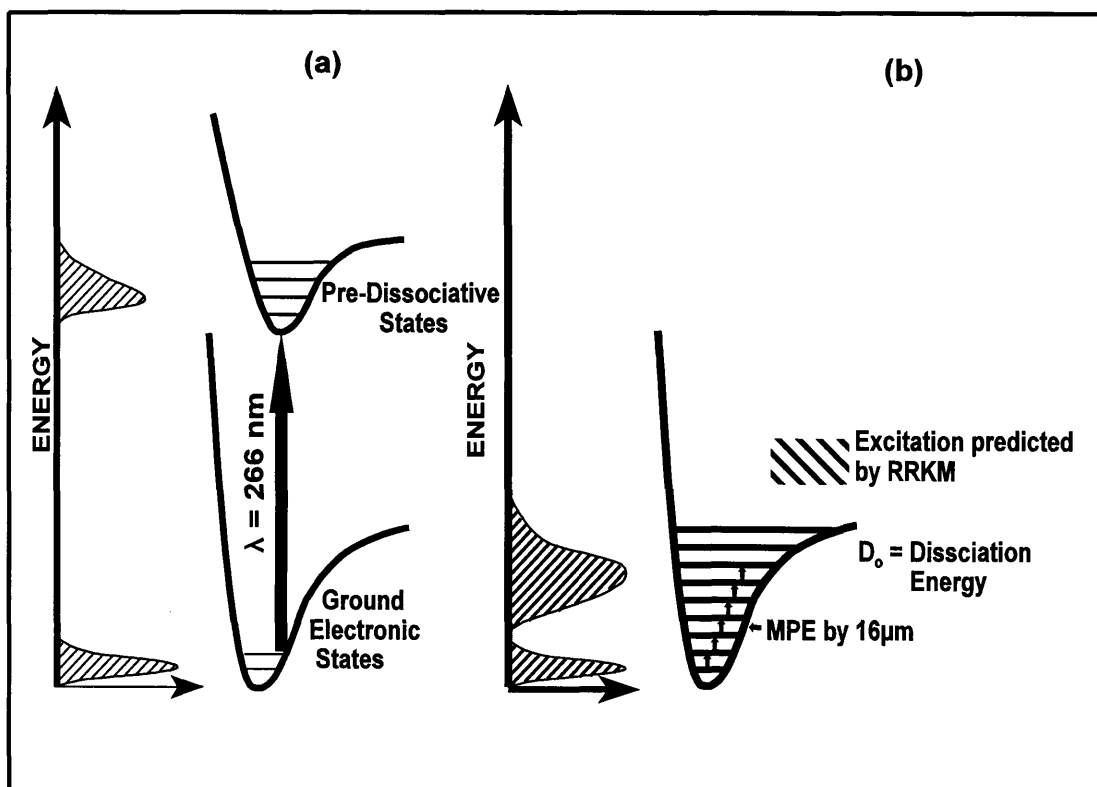


Fig 52: Schematic presentation of the vibrational energy distribution for UF_6 when excitation is instigated by an ultraviolet laser at 266 nm, (a), and multi photon excitation of a infrared laser at $16 \mu\text{m}$ wavelength, (b).

The prominence of the atomic ions seem to be supported by this approach. Figure 52 serves to highlight the different processes involved when dissociation and/or excitation of a UF_6 molecule occur prior to ionization. In the case of UV, 266 nm, excitation the initial vibrational energy distribution is very narrow, representative of either room temperature or flow cooled temperatures. At a wavelength of 266 nm the excitation is to the A-X band and at this wavelength dissociation occurs from the excited electronic states by pre-dissociation [57]. Upon dissociation substantial vibrational, energy, up to 1,5 eV, resides in the UF_5 fragment thereby placing it in the quasi continuum. The remaining UF_6 , in the ground electronic state remains at low levels of vibrational excitation. When the ionization laser is tuned to interact preferentially on the UF_5 photo fragments, selectivity for ionization is possible by virtue of the lower ionization potential, and the vibrational excitation level of the UF_5 molecule. It is also conceivable that if a relatively high pressure of a buffer gas, e.g. Argon, is added to this system that it will affect the ionization yield of the UF_5 , but not UF_6 as was experimentally observed [58] (see figure 70).

Multi photon processes involving the simultaneous annihilation of 266 nm (dissociation of UF_6) and an ionizing wavelength, e.g. 532 nm (detection of UF_5), have previously been excluded if neither of the lasers on its own caused any detectable ion signals. This hypotheses assumes that excitation by 266 nm is to a directly dissociative state which is, in our opinion a debatable issue. The result of reference 24 indicates that pre-dissociation clearly plays a role. The pre-dissociative process requires some time and if the ionization process is instigated whilst a molecule is in the excited state, it follows from our observations and the giant resonance proposal that this pre-excitation will have a significant influence on the ion signals. A model that can be applied to the ionization process (electronic levels) is the analog of the discrete levels and quasi continuum of the vibrational levels in the ground electronic state. The “ease” with which the first resonance in the giant resonance model can be reached, should strongly influence the entire UV multi photon process. This is similar to the case where even mild pre-excitation of the vibrational levels in the multi photon infrared dissociation process has a strong influence on the dissociation yield. From the discussion hitherto

it follows that the claimed selective laser ionization of the UF_5 molecule, immediately after its formation by 266 nm photolysis of UF_6 , is suspect.

Consider the situation when pre-excitation and dissociation proceed via multi photon infrared absorption. The RRKM theory predicts that an over excitation, of 40 to 50 percent above the dissociation energy of 3 eV is required for a UF_6 molecule to dissociate in a short enough time. At the point where the rate of dissociation approaches zero, the average vibrational energy is still substantial, as depicted in figure 52(b). Due to the distribution of the vibrational energy a long high energy tail is characteristic of this process with the result that a portion of the UF_6 molecules can have internal energies up to 4 eV. The UF_5 photo fragment receives less internal energy after dissociation than in the case when dissociation is instigated via 266 nm. Reducing the intensity of the ionization laser to the point where vibrationally cool UF_6 is not detectable, does not guarantee the absence of a signal from the vibrationally excited molecules. The opposite is indeed true, not only does our experimental observation show a significant loss of ionization selectivity of the uranium bearing photo fragment to be analysed, it also implies that this method derives incorrect enrichment factors. The findings of this study have a general impact on the interpretation of molecular beam studies performed by laser ionization MS. Many parameters influence the yields of reactions, including the change in ionization cross section following pre-excitation. From our results the present ionization technique is clearly not suitable to derive decay rates for UF_6 .

4.6 NEGATIVE ION FORMATION AND THE DETECTION IN A TOF MASS SPECTROMETER

From the experience and observations derived hitherto one can design a system that will be suitable for the purpose envisaged. It was clear that the ionization technique must be negative ion formation as this has the desirable feature of molecular ion creation. A schematic layout of the negative ion generation system is shown in figure 53.

DOCUMENT NUMBER	VERSION	PAGE	OF
LT100-000000-155-022		109	

A gold filament is heated to a red-hot temperature to lower the effective work function. At this point no thermal electrons will be emitted. The additional energy needed by the electrons to escape from the surface is supplied by the Nd:YAG laser of ~ 8 ns FWHM pulse length. By controlling, both the temperature of the gold wire and the laser's energy density one can control the electron energy. The latter needs to be very small to have a large electron capture cross section for UF_6^- formation. We chose gold wire for the following reasons:

- (i) It is not chemically attacked by UF_6 and
- (ii) When the gold is at a red-hot temperature it absorbs the $1,064 \mu m$ radiation of the laser.

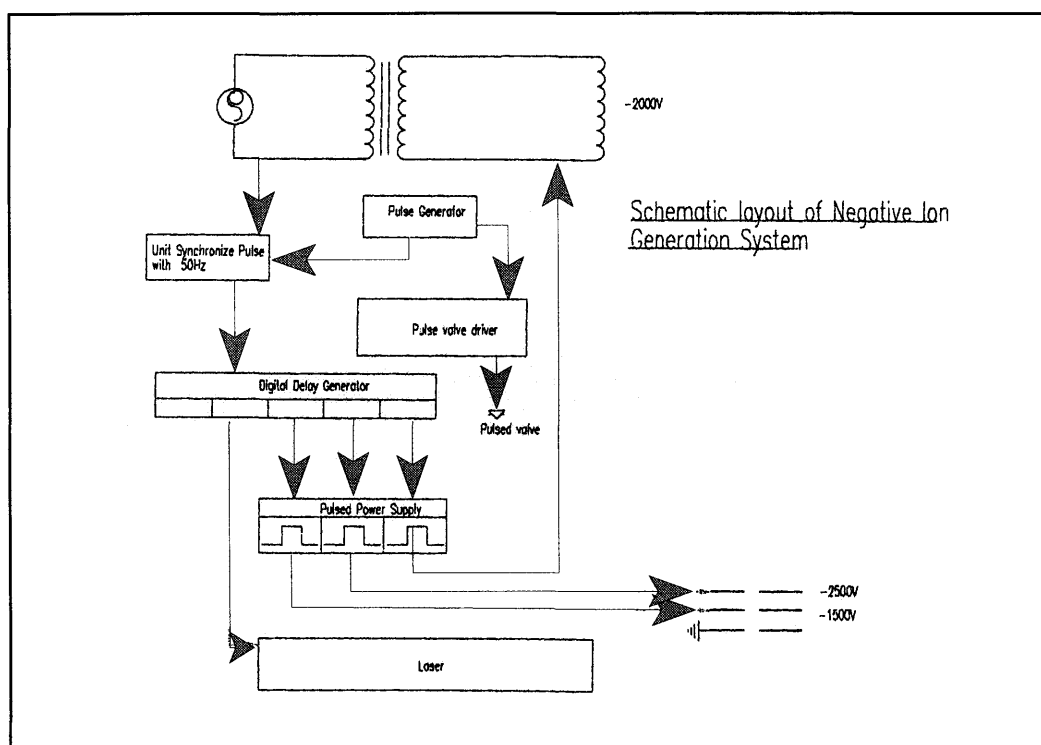


Fig: 53: Schematic layout for negative ion generation by laser with pulsed electro-optics.

In the layout of figure 53 the gold wire filament is heated by 50 Hz AC current via an isolating transformer to the required temperature. In using 50 Hz AC current the following advantages are

immediately apparent. Isolating the current source from the high voltage power supply is easily accomplished. The filament wire can consequently be operated at a voltage close to the repeller plate which will prevent the immediate acceleration of electrons away from the gold wire. An alternative approach is to switch off the current supply just prior to laser triggering. This is a more complicated exercise. Furthermore, the intensity of the electric field at the filament can be selected by synchronising the laser pulse to a chosen potential of the filament (see figure 54). A pulse generator triggers the pulse valve driver and UF_6 plus carrier gas is let into the vacuum through the pulse valve. In parallel, this pulse is synchronised with the AC current source to facilitate the most desirable

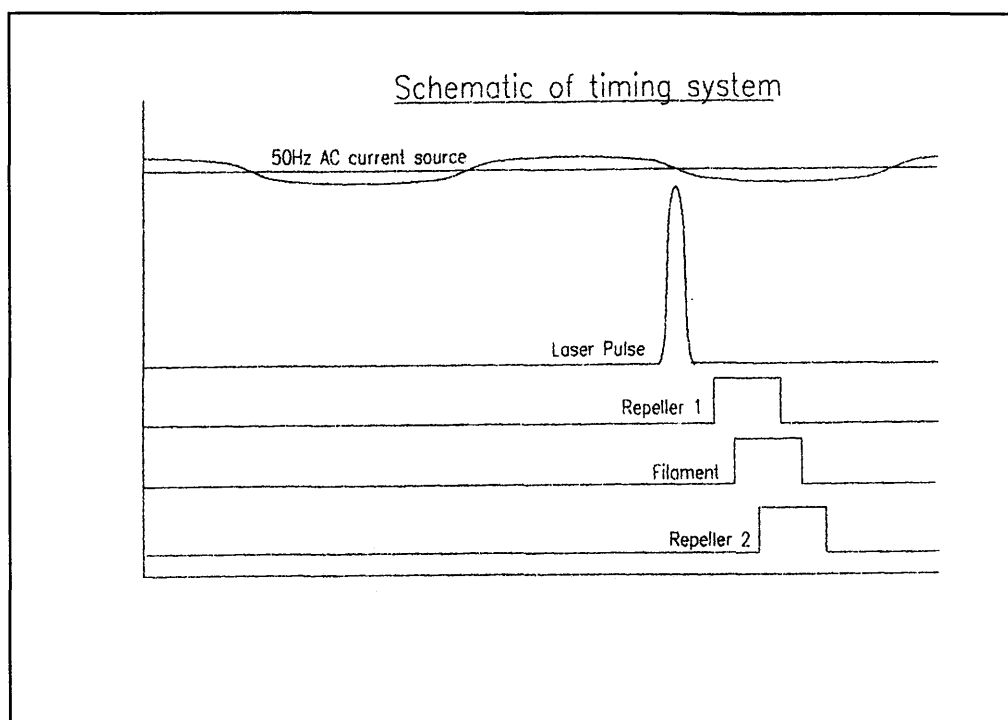


Fig 54: Temporal relationship of alternative current heating of filament, laser pulse and TOF electro-optic voltages.

potential of the filament when emitting electrons. The laser is directed at the gold filament and fired to heat up the spot of impact and subsequently a pulse of electrons are emitted. The weak electric field of the AC current source prevents the electrons from gaining thermal speed. After this event

the plates of the TOFMS need to be raised to be required potential in order to repel the ions in the direction of the detector.

A three channel fast HV switch was constructed for use with the TOF mass spectrometer [59]. The crucial component of each HV switch is the HTS 31-06 solid state switch (Behlke electronics), which is able to switch in the nanosecond range, and the on-time can be controlled by the length of the trigger pulse. Typical voltages up to 3 kV can be switched with ease. Minimum pulse length is 150 ns and repetition rates of 3 MHz is achievable. For operation the solid state switch require a 5V power supply, and for the high voltage charging of an electrode, the charging circuit has to be optimized. This is realized by choosing appropriate values for R_s , R_L , and C indicated in the schematic configuration below.(figure 55)

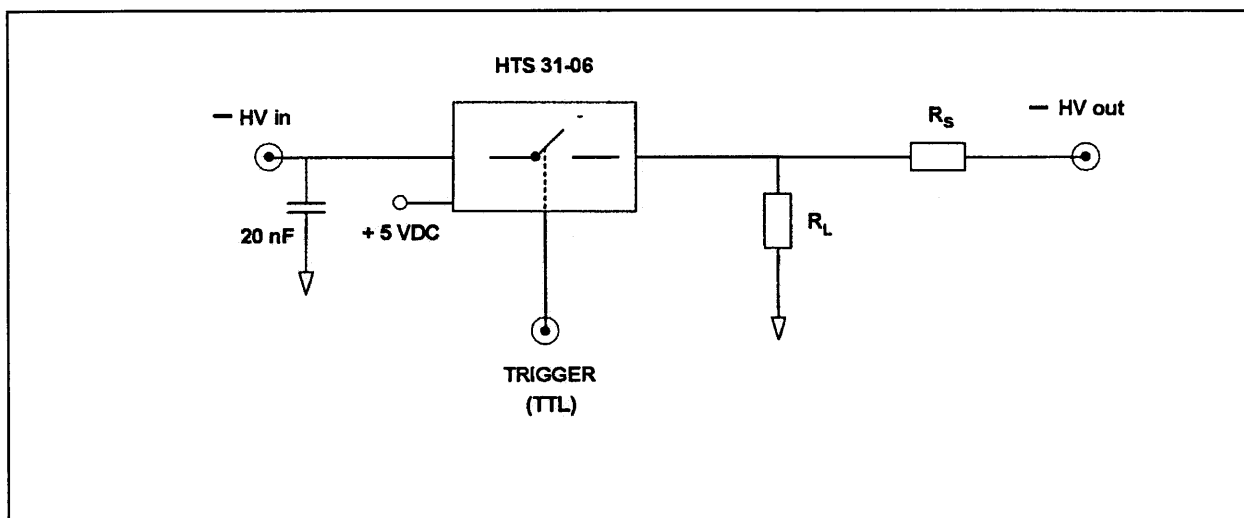


Fig 55: The high voltage switching circuit.

From a typical capacitance of 0,25 nF, this being representative of an electrode in the TOFMS, the switched pulse of 600 V is shown in figure 56. The selected values for the resistances R_L and R_s are indicated.

Some of the results that were obtained can now be reflected. In figure 57 a positive ion fragment spectrum of benzene ionized by the Nd:YAG laser is shown. Note that in this case the voltages to the electrodes were not pulsed but applied continuously. Good mass resolution is obtained. When the voltages are switched some electrical disturbances occurs early on in the mass spectra as can be seen in figure 58. However, the H^+ ion is clearly distinguished from the noise and the higher mass spectrum is clean. This is achieved with a voltage risetime of ~ 90 ns. In figure 59 a negative ion fragment spectrum of toluene ionized at 355 nm, the third harmonic of the Nd:YAG laser, is shown. For the initial detection of negative ions formed as a result of electrons emitted from the filament, we used SF_6 gas and an unfocussed Nd:YAG laser at 1 064 μm radiation. The molecular ion was indeed observed with a very low energy fluence from the laser. Unfortunately further pursuit of this development was curtailed by the sudden termination of the MLIS program in November 1997.

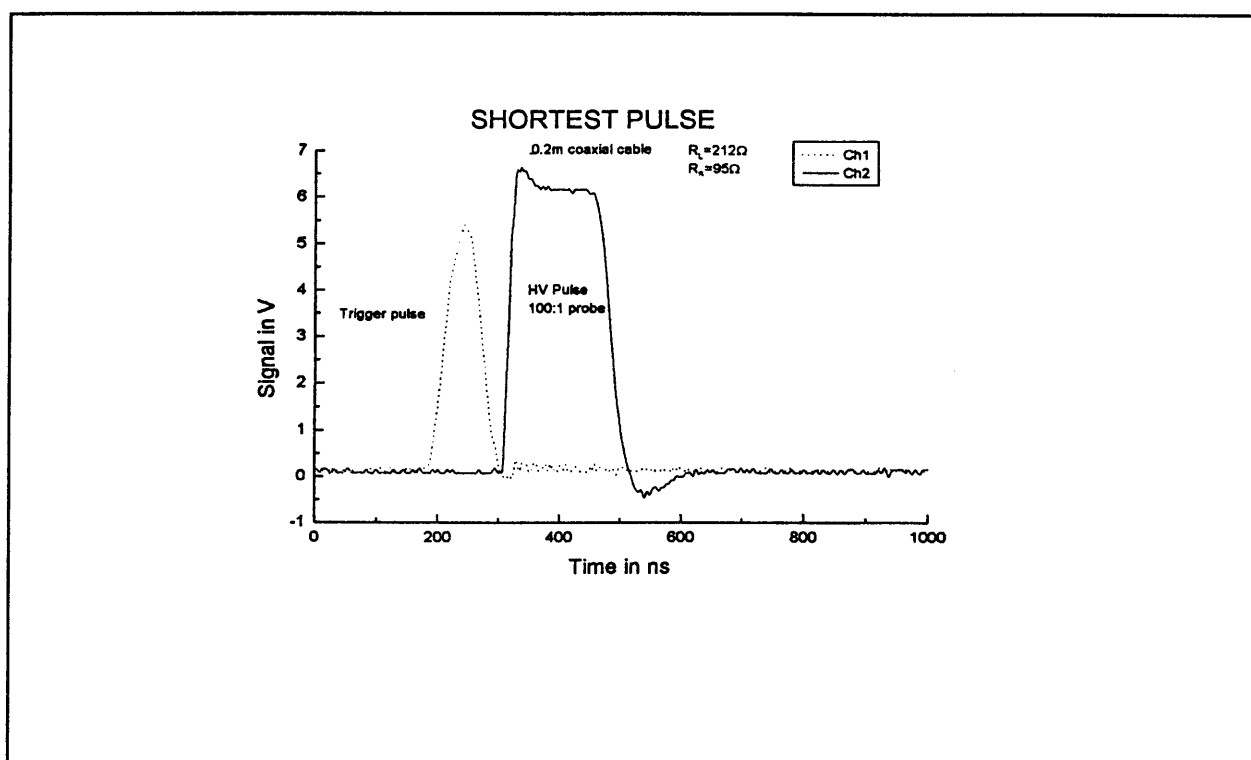


Fig 56: Trigger pulse and high voltage pulse generated for the electro-optics of TOFMS.

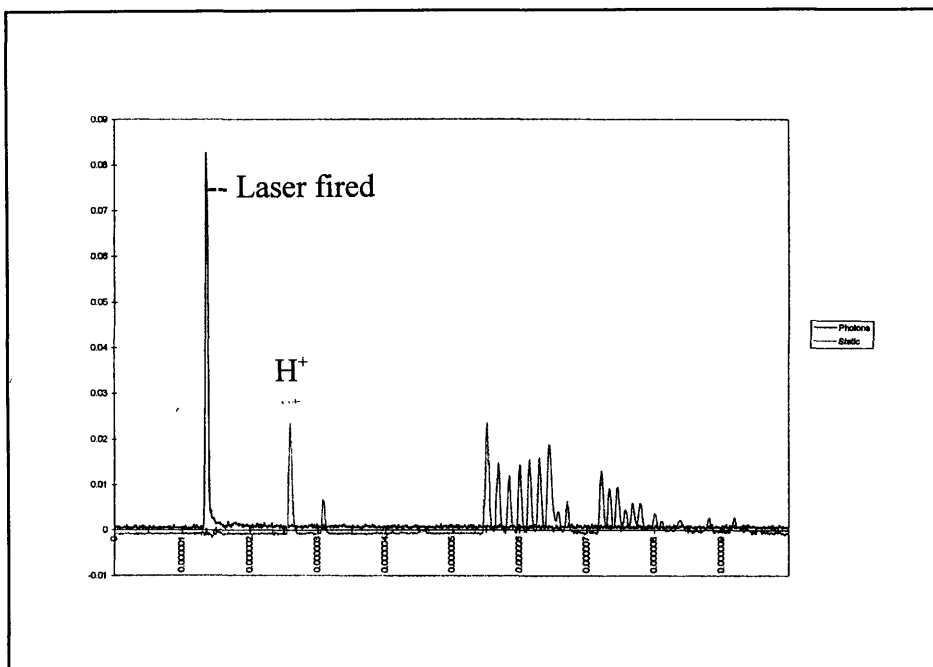


Fig 57: Positive ion spectrum of benzene (static voltages).

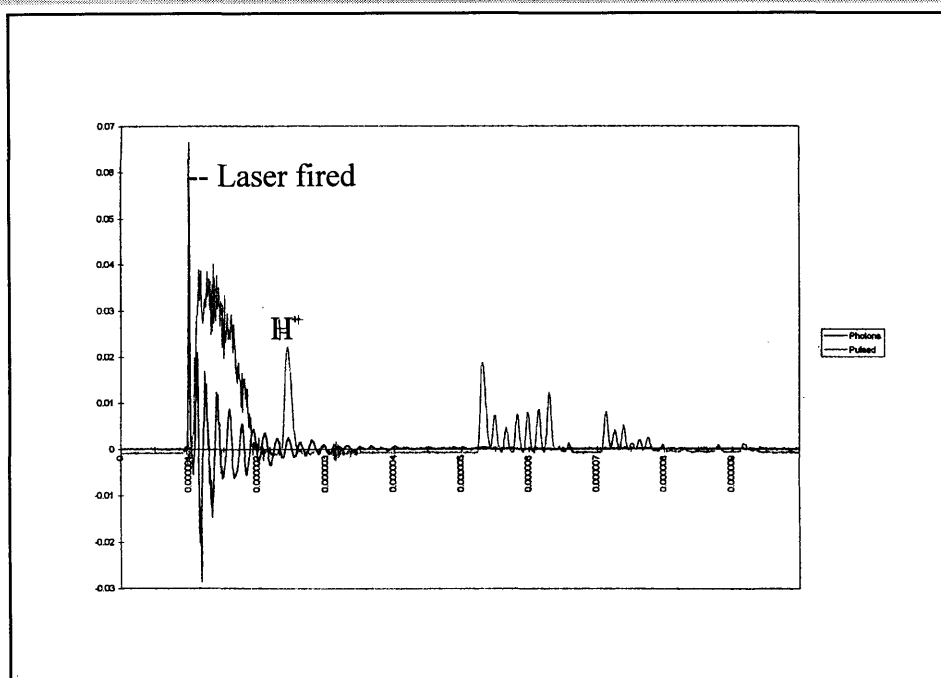


Fig 58: Positive ion spectrum of benzene with pulsed voltages.

DOCUMENT NUMBER

VERSION

PAGE

OF

LT100-000000-155-022

114

4.7 CONCLUSIONS

This chapter reflected on experimental development work since ~1984 in an endeavour to directly measure the laser instigated unimolecular dissociation rate of UF_6 . In the final event this was not achieved. This can be ascribed to the extremely challenging time requirements and the complications when dealing with large poliatomic molecules. The straight forward interpretation of data is flawed with many shortcomings.

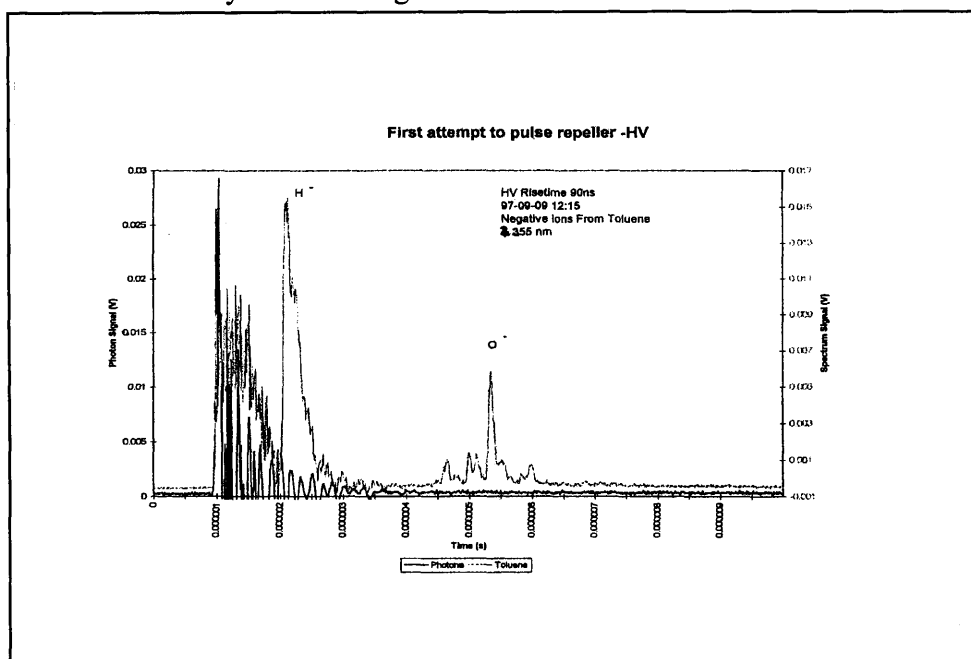


Fig 59: Negative ion spectrum of toluene.

As a result of the lack of direct measurements to calibrate the dissociation rate of UF_6 , it was decided to utilize thermal data for our comparison with experimental data. This procedure was presented in chapter II.

DOCUMENT NUMBER

VERSION

PAGE

OF

LT100-000000-155-022

115

CHAPTER V

CHAPTER V

SECONDARY CHEMICAL REACTIONS FOLLOWING THE LASER INSTIGATED UNIMOLECULAR DISSOCIATION OF URANIUM HEXAFLUORIDE

5.1 SECONDARY REACTIONS SUBSEQUENT TO THE UNIMOLECULAR DISSOCIATION OF UF_6

In this chapter the attention is shifted to the secondary chemical reactions following the unimolecular dissociation of UF_6 by laser. The gist of the endeavours will be to establish clearly what reaction steps the uranium bearing compounds encounter. At the onset of this study there were several experimental observations that could not be fully explained. The data and observations that will be considered here are gleaned from the literature, reports within the AEC which are classified, my own experimental observations, etc. It will be necessary to examine closely a few established concepts and interpretations to elucidate or confirm our present knowledge base of the laser photochemistry of UF_6 .

5.2 SOME BASIC REACTIONS

It has been accepted that the primary uranium bearing compound formed immediately subsequent to multiphoton infrared dissociation is the monomeric species uranium pentafluoride, UF_5 [60-63]. In my experience, which stretches over nearly two decades, this seems a fair conclusion and I am not aware of any observations that can dispute this finding. Amongst many other indicators, the excellent agreement of the RRKM description, refer to chapter I, with the thermal decomposition of UF_6 , confirms the belief that the nascent photolysis product is indeed UF_5 . What happens subsequent to the unimolecular decay now becomes of great importance. Let us first consider the experimental observations during some basic gas phase photolysis.

DOCUMENT NUMBER	VERSION	PAGE	OF
LT100-000000-155-022		116	

5.2.1 RADIATION WITH AND WITHOUT METHANE PRESENT

The scavenger gas CH_4 has been used for an extended period in the MLIS process gas because its presence seemingly leads to a quantum efficiency of ~ 1 . This seems to imply that there is no loss of isotopic selectivity during laser isotope separation due to radicals reacting with unexcited UF_6 . I will now report the results of a few simple, but carefully planned and executed, static cell irradiations to scrutinize some basic reactions.

In figure 60 the experimental layout, not showing the laser system, is schematically depicted [64]. The $16\ \mu\text{m}$ laser system is the same as described in chapter IV. In the optical steering of the laser beam, provision was made for irradiation both under static cell and under dynamic, flow cooled conditions. For now, only the static radiations will be discussed. The laser beam could be reflected in a symmetrical manner by simply tilting the mirror M in figure 60. This ensured that measurements could be performed under identical optical beam parameters for both experiments. At the static cell, which had an orthogonal cross configuration as shown, the laser entered and exited at two ZnSe windows whilst a FTIR was setup to measure the UF_6 pressure via the perpendicular windows (also ZnSe). A MKS Baratron pressure meter suitable for operating with UF_6 was also incorporated in the static cell.

DOCUMENT NUMBER	VERSION	PAGE	OF
LT100-000000-155-022		117	

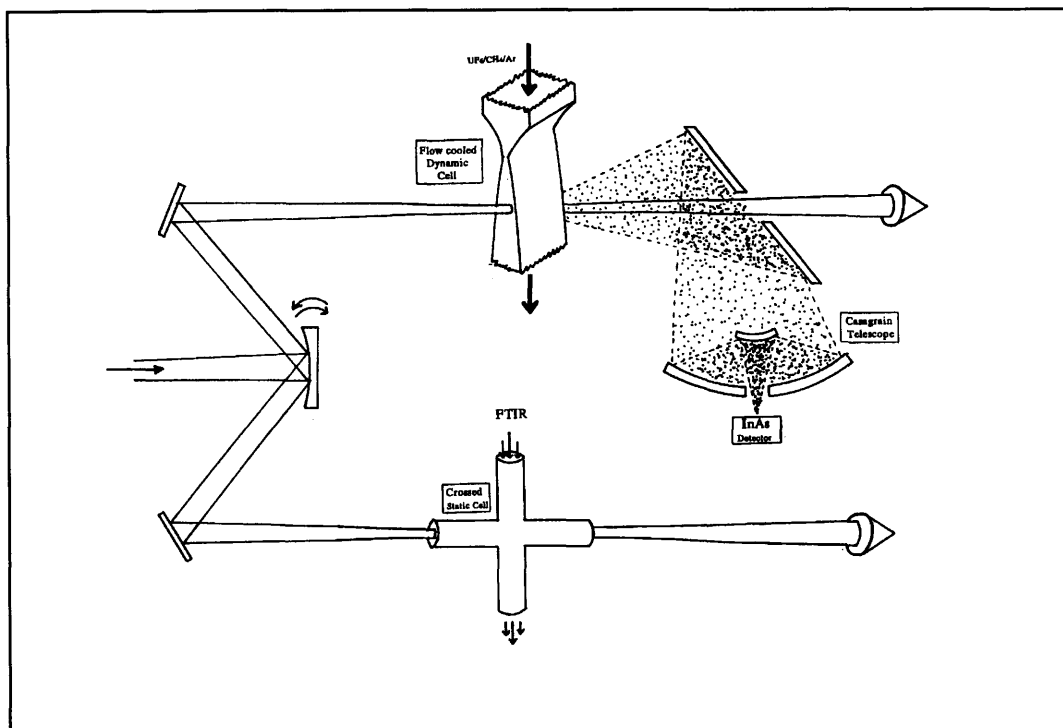


Fig.60: Schematically arrangement depicting the experimental setup for static cell irradiations.

Dissociation of UF_6 was instigated by utilizing the 16R18 laser line at $\sim 620 \text{ cm}^{-1}$. For the comparison purposes a fluence of 650 mJ/cm^2 was used. For this frequency the multiphoton infrared dissociation threshold lies at $\sim 150 \text{ mJ/cm}^2$. A fluence dependence curve for a $\text{UF}_6/\text{CH}_4 = 1/5$ mixture determined in the fluorescence mode is shown for illustrative purposes in figure 61. First, a correlation and calibration between the FTIR spectrometer and the Baratron pressure meter was established. For the former technique the strong ν_3 vibration at $\sim 627 \text{ cm}^{-1}$ was utilized to measure the UF_6 concentration. A correlation between the two techniques can be seen in figure 62 where both measures the depletion of UF_6 and total pressure as many laser shots were accumulated. A linear absorbance curve for UF_6 as measured with the FTIR is shown in figure 63. Only in the very low pressure region is there a slight deviation from linearity. The initial established correlation indicates that the pressure contribution of species other than UF_6 is negligible.

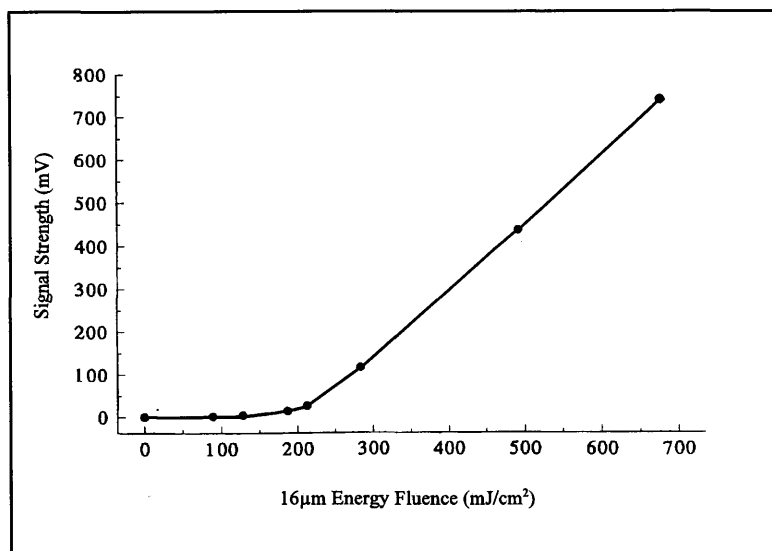


Fig. 61: Energy fluence dependence of the HF fluorescence signal after UF₆/CH₄ photolysis. UF₆ : CH₄ = 1 : 5, P_{tot} = 0,5 kPa and laser wavelength 16R18 [65].

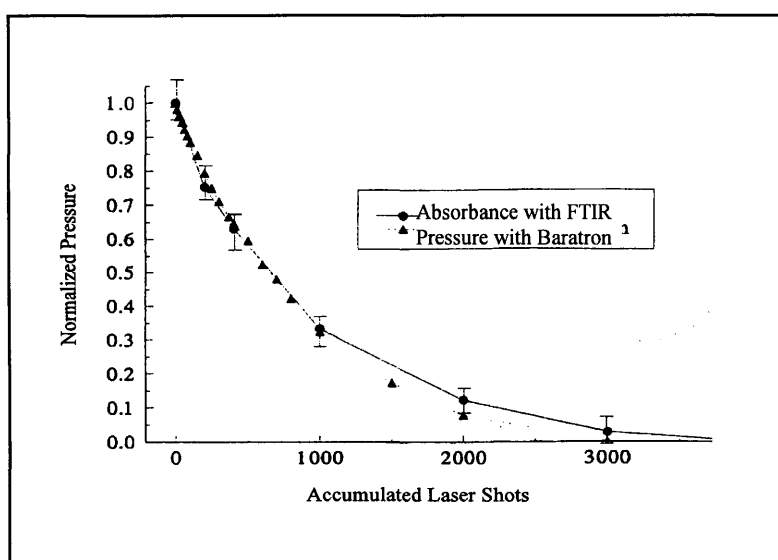


Fig 62: Correlation between UF₆ depletion as measured with FTIR and Baratron pressure meter. UF₆ : CH₄ = 1:5, Energy fluence = 650 mJ/cm² and laser wavelength = 16R18 [65].

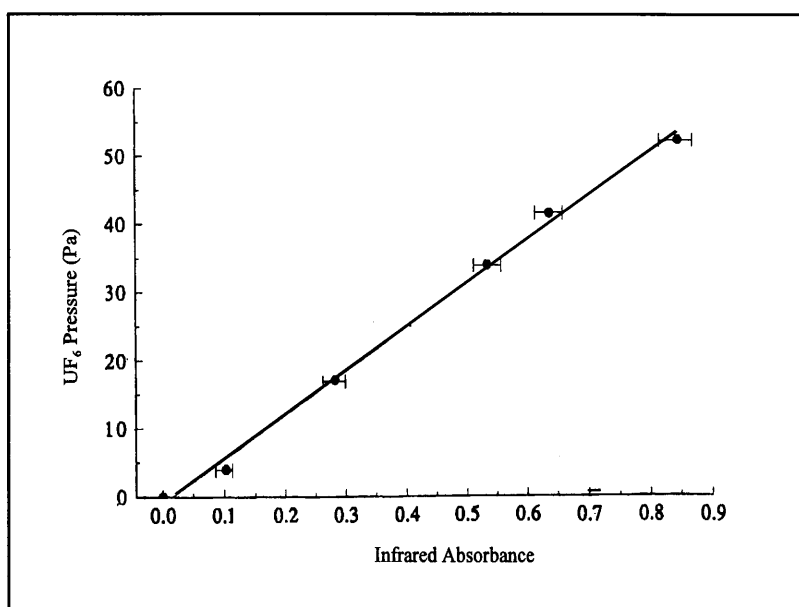


Fig.63: Linear absorbance curve for UF₆ as detected in depletion experiment [65].

In figure 64 a UF₆ depletion curve when the static cell contains initially ~45 Pa UF₆ plus 225 Pa CH₄ is shown. The ratio of UF₆ : CH₄ of 1 : 5 comes from previous experience at the AEC and is deemed to give the maximum HF fluorescence signal. The main features of the depletion curve for UF₆ are:

1. It follows an exponential decay which can be presented by

$$[UF_6] = [UF_6]_0 e^{-bx}$$

where [UF₆] represents concentration, proportional to pressure, and the subscript zero refers to the start concentration. The parameter *b* indicates the percentage dissociation per laser shot and *x* the accumulated number of shots.

2. The UF₆ concentration decreases in a constant fashion until no more UF₆ can be detected.

Representing the natural log of the concentrations ratio against the accumulated number of shots allows us to determine the value of $b \sim 3,6\%$ per shot, see figure 65. If we now repeat our experiment with only neat UF_6 in the irradiation cell we observe again two prominent features:

1. The depletion of UF_6 follows a much slower rate and the percentage/shot decreases from the start and approaches the asymptotic value of $\sim 0,8 - 0,9\%$ /shot, down from the initial $\sim 3\%$ /shot.
2. However, the initial slopes of the two depletion curves are the same and the yield is $\sim 3\%$ /shot for both.

The observations described hitherto illustrates clearly a very important issue. For a flowing gas system, as employed for MLIS, the CH_4 scavenger gas has no beneficial effect in terms of the

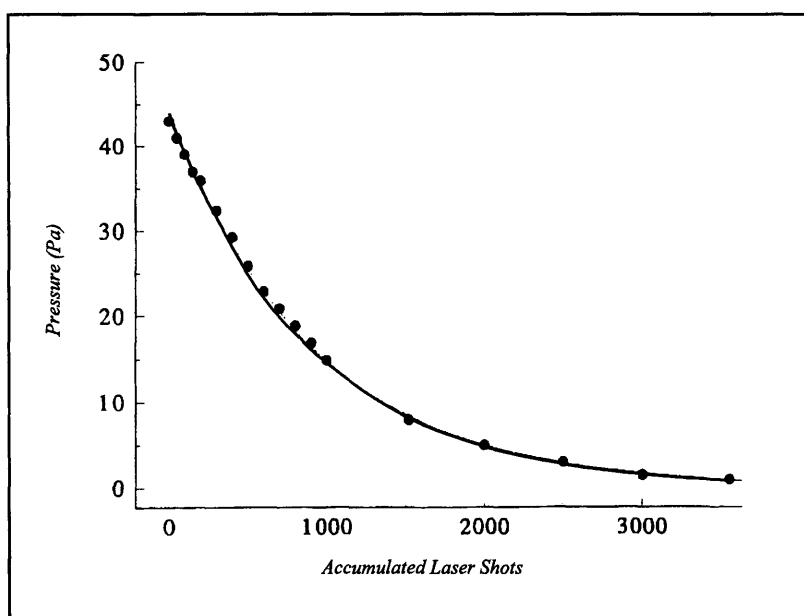


Fig. 64: UF_6 depletion curve during laser photolysis. $\text{UF}_6 : \text{CH}_4 = 1 : 5$, energy fluence = 650 mJ/cm^2 and laser wavelength is 16R18 [65].

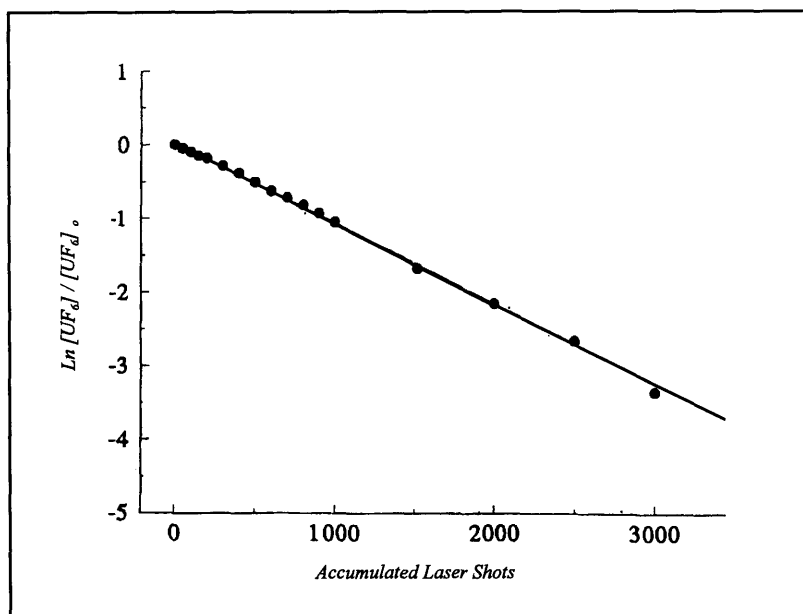


Fig. 65: Logarithmic plot of depletion curve i.e. $\ln[UF_6]/[UF_6]_0$. Conditions from figure 64 [65].

yield of the reaction or quantum efficiency. If we, however, accumulate many laser shots into the same static mixture, the depletion of UF_6 is significantly influenced by the presence of CH_4 . The prevailing interpretation would have it that a recombination reaction between the UF_5 monomer and the F radical is responsible for the retardation in depletion of UF_6 .

From the relative yields of figure 66(a) and (b) one can derive the reaction rate of the reverse reaction. Consider the bimolecular reaction: [66]



If the initial concentrations at $t = 0$ (or no shots) are respectively a , b , c and d and after time t , x (say *mole/l*) have reacted and a second-order rate law is followed:

$$\frac{dx}{dt} = k_r (a - x) (b - x) \quad (5.2)$$

For the case that $a = b$ this differential equation becomes

$$\frac{dx}{dt} = k_r (a - x)^2 \quad (5.3)$$

After integration and the assumption that at $t = 0$, $x = 0$, i.e. the integration constant = $1/a$, the following relationship is valid

$$\frac{x}{a(a - x)} = k_r t \quad (5.4)$$

In figure 66 (a) and (b) the formation of UF_5 is discontinuous, occurring only with each laser shot, which for the experiments ran at 5 Hz. Lets then view the reaction period from one laser shot to the following: The yield with each laser shot can be taken as 3% of the prevailing UF_6 pressure. The laser forms at ~ 35 Pa pressure, where the net yield per shot is $\sim 0,9\%$,

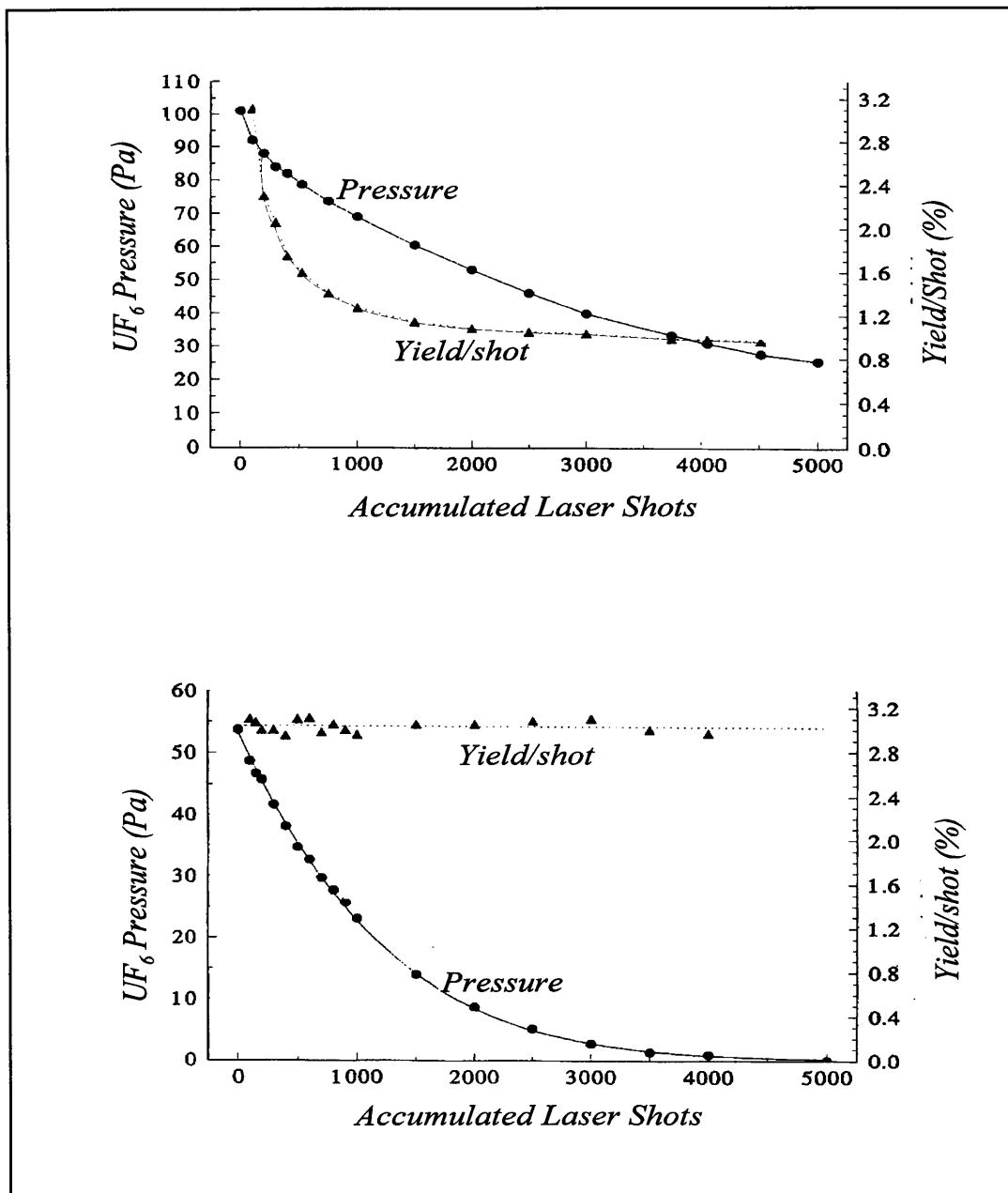


Fig. 66: UF₆ depletion in laser photolysis experiment. Energy fluence = 620 mJ/cm², laser wavelength is 16R18 for (a) neat UF₆ (b) UF₆ : CH₄ = 1 : 5 [65].

Number of UF₅ molecules formed

$$\begin{aligned} 3\% \text{ of } 35 \text{ Pa} &= 1,05 \text{ Pa} \\ &= 2,53 \times 10^{14} \text{ molecules/cm}^3 \text{ at } 300^\circ\text{K} \end{aligned}$$

The reverse reaction, which we have taken as second order, depletes this UF₅ density to 2,1/3 x 2,53 x 10¹⁴ molecules/cm³ in 0,2 second, i.e. 5 Hz. Therefore

$$\begin{aligned} \frac{x}{a(a-x)} &= \frac{1,77 \times 10^{14}}{2,53 \times 10^{14}(2,53 \times 10^{14} - 1,77 \times 10^{14})} \\ \text{or } k_r &= 4,6 \times 10^{-14} \text{ cm}^3 \text{ molecule}^{-1} \text{ sec}^{-1} \\ &= 2,8 \times 10^7 \text{ liter mole}^{-1} \text{ sec}^{-1} \end{aligned}$$

Lyman [67] have estimated the rate of the recombination reaction, between uranium pentafluoride and the F radical at 300 K as ~1,5 x 10⁻¹² cm³ molecule⁻¹ sec⁻¹. If we insert this rate into the calculations, and no other reactions are considered, we would clearly observe no UF₆ depletion at all. Before we can proceed sensibly with the investigation it seems prudent to have a closer inspection of the nature of the uranium bearing compounds in a static environment.

5.2.2 IDENTIFICATION OF UF₄ IN PHOTOLYSIS PRODUCTS

Justification exists for the prevailing belief that the primary and sole uranium bearing compound formed subsequent to infrared laser photolysis is UF₅. It has been tacitly assumed, however, that this compound persist in its nascent configuration and can be collected as such, even if a extended time span has elapsed. Many reports and papers [68,69] have labelled the end uranium product as β - UF₅. In my experimental observations the existence of UF₄ has been clearly identified with the result that the secondary reactions following photolysis of MLIS have to be scrutinized comprehensively. I will now present experimental evidence for the existence of UF₄ in photolysis products.

DOCUMENT NUMBER	VERSION	PAGE	OF
LT100-000000-155-022		125	

5.2.2.1 INFRARED SPECTROSCOPY

Neat UF_6 , UF_6/H_2 mixture and a UF_6/CH_4 mixture were consecutively irradiated with $16\ \mu\text{m}$ wavelength in a three window infrared cell as depicted in figure 67.

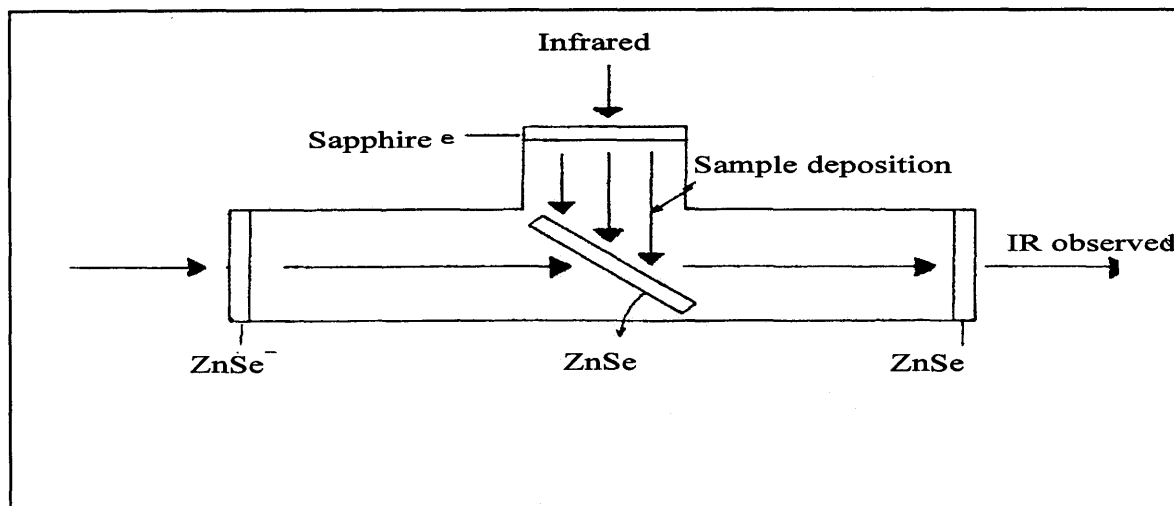


Fig. 67: Irradiation cell arrangement for product collection during infrared laser photolysis.

The irradiation and dissociation of UF_6 with a $16\ \mu\text{m}$ wavelength source was performed. This was carried out first in neat UF_6 and then repeated with hydrogen gas and methane, present as scavengers/co-reactants. The solid product that settles on the ZnSe window of figure 67 was then analysed by FTIR spectroscopy. Spectra representative of the products obtained are shown in figure 68 [70]. The analysis and identification were done by comparison to the known spectra of standard uranium compounds but none fitted to any degree the observed spectra. When an analysis of the monomeric UF_4 molecule was fitted, good agreement was established. Very little is known about the UF_4 molecule and, specifically, about its infrared and Raman spectra. This stems from the difficulty to produce uranium tetrafluoride in the monomeric gaseous phase. Efforts to produce UF_4 as free molecules were reasonably successful in a matrix isolation technique [71]. The problem of the spatial configuration of UF_4 is the first barrier to cross when one wants to establish the expected

spectra. There is as yet no consensus on the structure of UF_4 . As a result of a study by the method of high-temperature gaseous electron diffraction and analysis of the thermochemical characteristics of UF_4 molecules [72-74], the structure of a distorted tetrahedron of C_{2v} symmetry was proposed. On the basis of an analysis of the photo electron spectra of UF_4 vapour [75], however, it was concluded that UF_4 have a tetrahedral configuration in the equilibrium state. The Raman- and IR-spectra of crystalline UF_4 have been recorded and the force constants of the valence force field and of the Urey-Bradley force field were calculated [76] on the basis of the tetrahedral symmetry, T_d . The latter work is, however, clearly erroneous to the extent that the observed spectra could not be reproduced by Prior [77] who indicated that e.g. the 614 cm^{-1} absorption peak does not belong to UF_4 . Furthermore, the calculated force constants for the U--F vibration is out of phase with the values in UF_6 and UF_5 [78,79].

In our analysis we first performed *ab initio* calculations to establish the spatial configuration of the monomeric UF_4 molecule [80]. This confirmed the T_d symmetry as the preferred structure. In any event, the entire body of available experimental data [81-83] showed only a slight deviation of the symmetry from tetrahedral to D_{2d} , C_{3v} or C_{2v} . The optical spectra of UF_4 , on the whole, could be satisfactorily interpreted by assuming a tetrahedral structure [75].

A molecule that undoubtedly has a tetrahedral symmetry is CH_4 . Its infrared spectrum has been well documented and the combination bands identified [84]. We can follow the example of CH_4 to allocate the absorption peaks in the observed spectra of figure 68. First, consider the spectrum obtained when UF_6 is dissociated without any second gas being present:

In the tetrahedral structure the four fluorine nuclei occupy the corners of a regular tetrahedron at whose center lies the uranium nucleus. The symmetry of this arrangement leads to many simplifications in the spectrum as well as to a number of interesting features which are characteristic of the degeneracies of the levels. The system has nine degrees of internal freedom but there are only

four normal frequencies. These may be described in the following manner. The motion corresponding to ν_1 is such that the fluorine nuclei oscillate in phase along the radii of the tetrahedron, that is, directly towards or away from the uranium nucleus which itself remains stationary, see figure 69. This vibration, ν_1 , is a single frequency and the excited levels are non-degenerate. Clearly, the electric moment remains zero throughout the motion and consequently the frequency will be inactive in the infrared. It does appear very strongly in the Raman spectrum. The frequency ν_2 belongs to a different symmetry class. The fluorine nuclei move upon the surface of the sphere which passes through the four corners of the regular tetrahedron. Visualize the normal vibration as follows: two of the fluorine atoms, which we designate as 1 and 2, approach each other while at the same time the atoms 3 and 4 also approach each other by an equal amount. All of these displacements are on the surface of the sphere. In depicting the motion one might have chosen other pairs of nuclei, i.e. 1 and 3, as well as 2 and 4, to approach and recede from each other. The excited levels will be degenerated with the first level exhibiting a two-fold degeneracy. As the uranium nucleus does not move in the motion the ν_2 vibration is also Raman active. A very important feature surfaces, though. Since the intensity of the Raman transition depends upon the off diagonal elements of the polarization tensor we might expect it to be faint. This is in strong contrast with the observation of Kraser and Nurnberg [76] for crystalline UF_4 . This suggests that the mentioned authors have incorrectly interpreted their observed spectra.

The remaining frequencies ν_3 and ν_4 , both belong to the same symmetry class and are active in the infrared and in the Raman spectra. The first motion is such that, two nuclei, say 1 and 2, are displaced directly towards each other while the other pair, 3 and 4 are displaced directly away from each other. Each nuclei can oscillate harmonically in three dimensions and threefold degeneracy is exhibited. The second motion is one in which the central uranium nucleus vibrates harmonically

within a rigid tetrahedron. This is also a three-dimensional harmonic oscillator. For the case of CH₄ we find that

$$\nu_3 > \nu_1 \text{ and } \nu_2 > \nu_3$$

Tumanov [85] determined the values of ν_1 to ν_4 for UF₄ empirically and allocated values to ν_2 and ν_4 to have $\nu_2 < \nu_4$. This I believe to be incorrect. The following values for ν_1 to ν_4 fits very well the spectra of figure 68.

<u><i>On surface</i></u>	<u><i>In gas phase</i></u>
$\nu_1 = 465 \text{ cm}^{-1}$	475 cm^{-1}
$\nu_2 = 215 \text{ cm}^{-1}$	225 cm^{-1}
$\nu_3 = 506 \text{ cm}^{-1}$	520 cm^{-1}
$\nu_4 = 188 \text{ cm}^{-1}$	190 cm^{-1}

The various combination bands, as derived from comparison with CH₄, are as follows (see table 8)

Table 8: Observed transitions for UF₄.

Wavenumber Observed (cm ⁻¹)	Assignment	Species of Upper States
Not in range Not in range Not in range Raman	$v_4 - v_3$ $2v_4$ $v_2 - v_4$ $2v_2$	F_2 $(A_1 + E) + F_2$ $(F_1) + F_2$ $A_1 + E$
588 Very weak Very weak 735 882 In broad background spectrum 1012 1112 1227 1306 1375	$v_2 + 2v_4$ $v_1 + v_4$ $v_3 + v_4$ $v_2 + v_3$ $v_3 + 2v_4$ $v_1 + v_2 + v_4$ $v_2 + v_3 + v_4$ $2v_3$ $2v_3 + v_4$ $v_2 + 2v_3$ $2v_1 + 2v_4$ $2v_3 + 2v_4$	$A_1 + E$ $A_1 + E$ $A_1 + E$ $A_1 + E$ $A_1 + E$ $A_1 + E$ $A_1 + E$ $A_1 + E$ $-(A_1 + E) + F_1$ $(A_1 + A_2 + 2E + F_1) + F_2$ $(A_1 + E) + F_2$ $(1A_1 + A_2 + 3E + 3F_1) + 5F_2$
Not in range Not in range Not in range	$2v_1 + v_3$ $v_1 + 2v_3$ $3v_3$	F_2 $(A_1 + E) + F_2$ $(A_1 + F_1) + 2F_2$

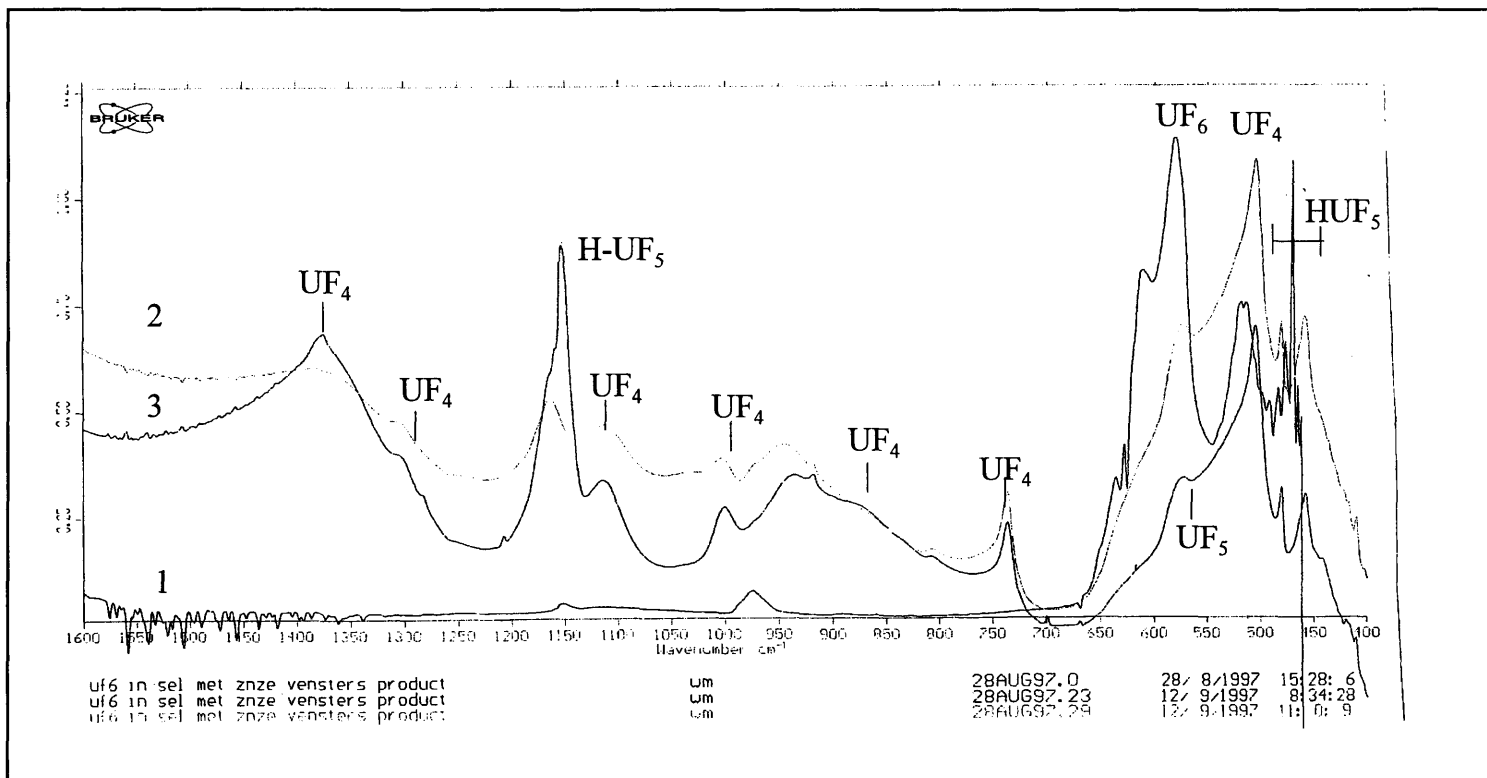


Fig. 68 (a): Uranium photolysis products formed by 16 μm infrared wavelength, 16R18, (1) Neat UF_6 (2) UF_6/H_2 (3) UF_6/CH_4 .

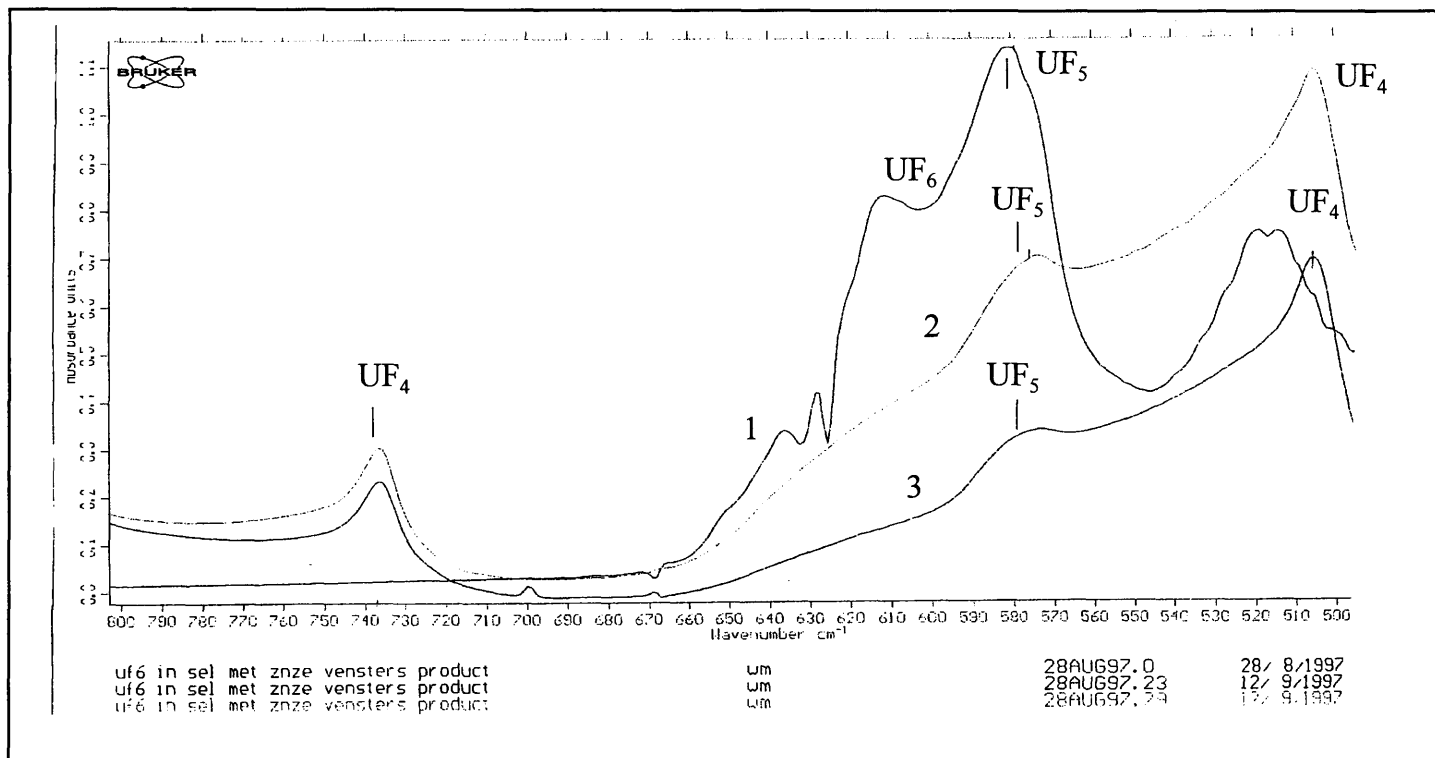


Fig. 68 (b): Expanded spectra 500 - 800 cm^{-1} .

DOCUMENT NUMBER	VERSION	PAGE	OF
LT100-000000-155-022		132	

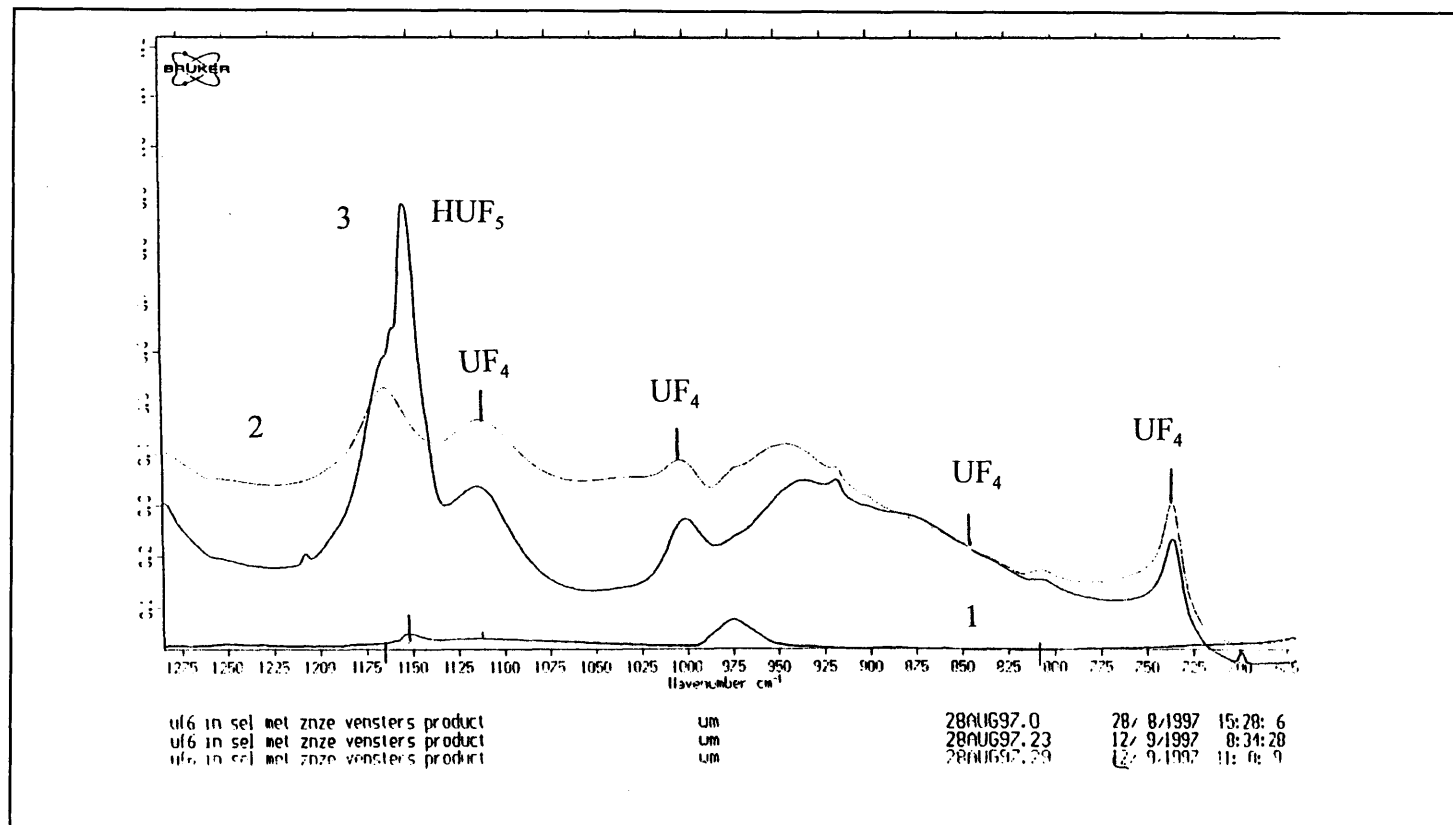


Fig. 68(c): Expanded spectra 700 - 1300 cm^{-1} .

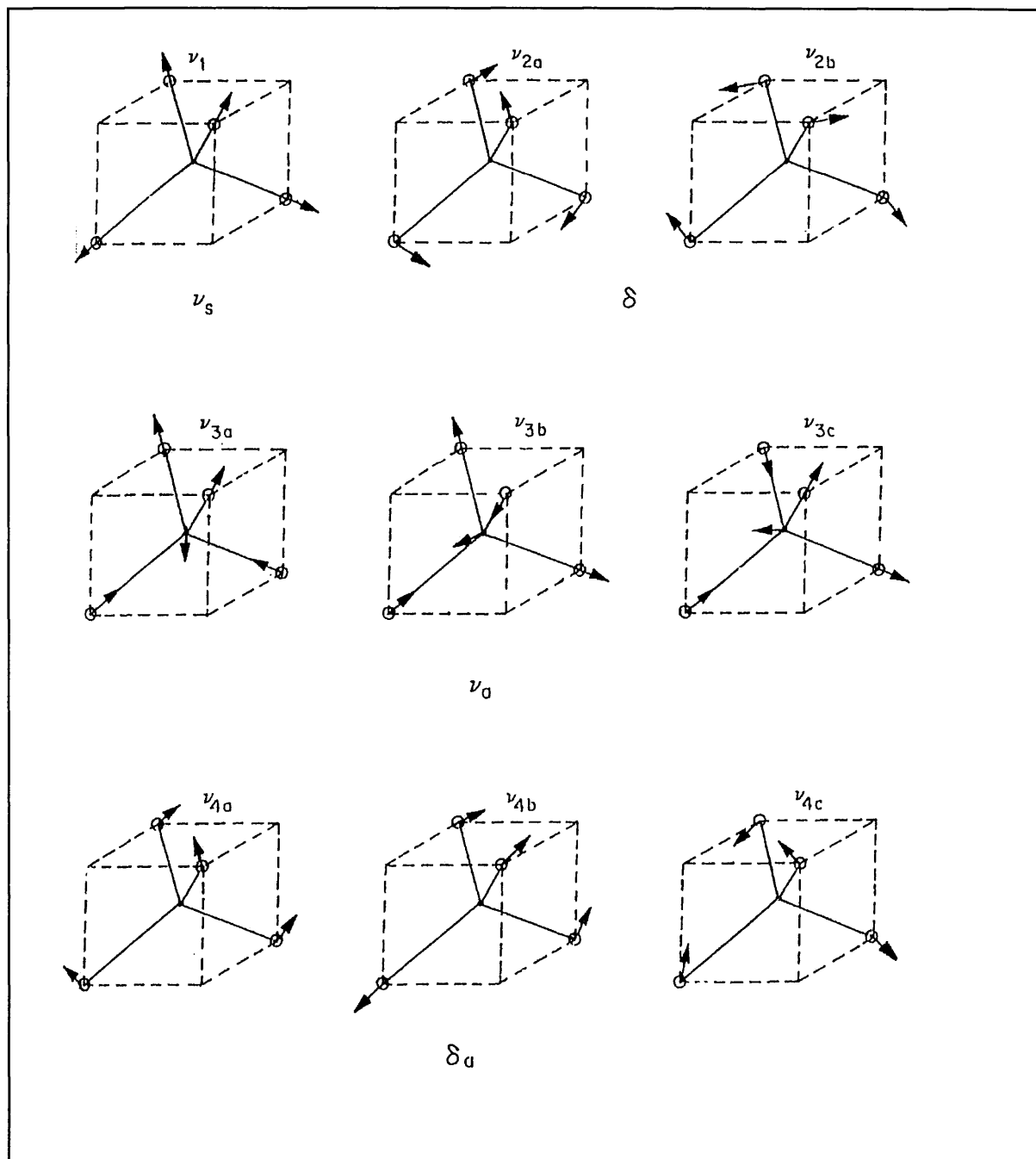


Fig. 69: Schematic presentation of the vibration modes of a tetrahedral molecule.

The allocation of the gas phase absorption peak of the strong ν_3 vibration at 520 cm^{-1} is consistent with, the observations of Catalano et al [86] and Kunze et al [87]. In the former study the reaction of SiH_4 (silane) with UF_6 was monitored under matrix isolation conditions. A gas phase

value of $\sim 520 - 530 \text{ cm}^{-1}$ for ν_3 for the suspected UF_4 molecule appeared at $\sim 506 \text{ cm}^{-1}$ due to solid surface effects. In the present case allowance is made for the decrease in values for the fundamental vibrations due to the solid ZnSe surface. A perusal of the plausibility of the allocated values for the fundamental vibrations for UF_4 can be performed if we investigate their interrelationships. On the assumption that the interaction between the nuclei can be described by a valence force model, which is applicable to CH_4 , the following relationships must hold [84].

$$\lambda_3 + \lambda_4 = \lambda_1 \left(1 + \frac{4m_Y}{3m_X} \right) + \frac{2}{3} \lambda_2 \left(1 + \frac{8m_Y}{3m_X} \right) \quad (5.5)$$

and

$$\frac{\nu_3\nu_4}{\nu_1\nu_2} = \frac{2}{3} \left(1 + \frac{4m_Y}{3m_X} \right)^{1/2} \quad (5.6)$$

where for the molecule XY_4 the mass of $M_X = 238 \text{ amu}$ and $M_Y = 19 \text{ amu}$. If the numerical values are inserted in wavenumbers in equation (5.5) a conversion factor of $5,8894 \times 10^{-2}$ is applicable. Hence

$$\begin{aligned} \lambda_3 + \lambda_4 &= 710 \text{ cm}^{-1} \\ &= \textit{right hand side} = 525,6 + 181,9 \\ &= 707,5 \text{ cm}^{-1} \end{aligned}$$

From equation (5.6) we have:

$$\begin{aligned} \frac{\nu_3\nu_4}{\nu_1\nu_2} &= 0,92 \\ &= \textit{right hand side} = 0,90 \end{aligned}$$

The designation of fundamental vibrations is thus plausible and supported by the valency force assumption. Furthermore, the energy connected with the U-F mode in the uranium fluorides are consistent with the normal pattern of decreasing frequency with decreasing valency:

$$\begin{array}{lll}
 UF_6 & \sim & 627 \text{ cm}^{-1} \quad (\text{VI oxidation state}) \\
 UF_5 & \sim & 575 \text{ cm}^{-1} \quad (\text{V oxidation state}) \\
 \text{and} & & \\
 UF_4 & \sim & 520 \text{ cm}^{-1} \quad (\text{IV oxidation state})
 \end{array}$$

During the investigation into the nature of the photolysis products an effort was made to record the Raman spectrum at the University of Pretoria. This, however, never precipitated due to the fact that the reaction holders could not be accommodated in the Raman spectrometer. Nevertheless, it is believed that the assignments of the fundamental vibrations of UF_4 and its identification is reasonable. This is also the first time that assignments for the monomeric specie has been done based on experimental observations.

The calculated value for the force constant for the U-F stretching band using the ν_3 harmonic frequency of 520 cm^{-1} is $3,02 \text{ m dyn}/\text{\AA}$. Using Badgers rule [88] and the force constant of $3,84 \text{ m dyn}/\text{\AA}$ for a UF_6 bond length of $1,99 \text{\AA}$ [78], we find a bond length of $2,16 \text{\AA}$ for UF_4 . For the case of UF_5 the angle between the diagonal and radial fluorines increases to 101° (90° in UF_6). This leads to a increase in F-F repulsion because the F atoms are more electronegative in UF_5 than in UF_6 . In the tetrahedral structure of UF_4 the F-F repulsion can be expected to be increased due to the angle of a regular tetrahedron being $\sim 110^\circ$. For UF_5 the radial bond length increases to $2,02 \text{\AA}$ and the according force constant decreases to $3,59 \text{ m dyn}/\text{\AA}$ [79]. The calculated bond length and force constant for UF_4 thus follows the trend and is deemed reasonable.

A check on the spectroscopic and molecular constants for UF_4 can be performed via the calculation of the reaction entropy. Using the following formula for statistical thermodynamics, the thermodynamic functions for UF_4 can be calculated.

$$S_{trans}^o = 3/2 R \ln M + 5/2 R \ln T - R \ln p + 5/2 R - 30,44 \quad (5.7)$$

$$S_{rot}^o = 3/2 R \ln M + 3/2 R \ln I - R \ln \sigma + 1119,50 \quad (5.8)$$

$$S_{vib}^o = R \ln \left(\frac{kT}{hv} \right) + R \quad (5.9)$$

where M is the molecular mass of UF₄; T will be taken as 1050 K to compare to the experimental value of entropy of Hildenbrand [62]; p is the pressure which is equal to 1 atmosphere at STP; σ is the symmetry number for a tetrahedral structure which is 12. The moment of inertia for the UF₄ molecule is calculated from the formula

$$I = 8/3 m r^2 \text{ with } m = 19 \text{ for the fluorine atom and } r = 2,16 \text{ \AA} \text{ as determined above. This value is then calculated as } 3,925 \times 10^{42} \text{ g/cm}^2.$$

Values for the standard entropy for gaseous UF₄ were subsequently calculated as:

$$\begin{aligned} S_{trans}^o &= 206,6 \text{ J deg}^{-1} \text{ mole}^{-1} \\ S_{rot}^o &= 111,5 \text{ J deg}^{-1} \text{ mole}^{-1} \\ S_{vib}^o &= 139,9 \text{ J deg}^{-1} \text{ mole}^{-1} \\ S_{tot}^o &= 458,0 \text{ J deg}^{-1} \text{ mole}^{-1} = 111 \text{ cal deg}^{-1} \text{ mole}^{-1} \end{aligned}$$

Hildenbrand [62] used the entropy of sublimation at 1050 K of 45,3 cal deg⁻¹ mole⁻¹ combined with the established entropy of UF₄ (s) of 74 cal deg⁻¹ mole⁻¹ to yield the entropy of UF₄ (g) at 1050K as 119,3 cal deg⁻¹ mole⁻¹. The large discrepancy of 8,3 cal deg⁻¹ mole⁻¹ between the experimental and calculated entropies cannot be accounted for from incorrect molecular and spectroscopic data. Rather it points towards a significant electronic partition function at 1050 K and/or it is unlikely that all the UF₄ was in the monomeric form. In the polymeric state the vibrational frequencies will be substantially reduced which in turn leads to an increased vibrational entropy contribution. The measurements of Kraser and Nürnberg [76] of the vibrational frequencies of UF₄ in a crystalline form supports this suggestion.

Lets now return to the spectra of figure 68. All the peaks for spectrum (a) when neat UF₆ is dissociated by 16 μm radiation are accounted for except two or three satellites that appear below

500 cm^{-1} . These satellites are not regarded as indicative of a different form of uranium bearing specie but merely as absorption by molecules in different surface positions [89]. Consider now the infrared spectrum, (b), which results subsequent to the photolysis of UF_6 with hydrogen gas present. A spectrum identical to figure 68(a) results with only one significant difference. A strong absorption appears at $\sim 1150 \text{ cm}^{-1}$. This cannot be allocated to the $\nu_2 + \nu_3$ binary combination mode of UF_6 , which is observed at 1157 cm^{-1} in the gas phase, because the strong ν_3 mode is not observed.

A possible and plausible explanation for the $\sim 1150 \text{ cm}^{-1}$ absorption feature is to allocate this to a U-H stretching frequency. Kunze et al [87] studied the spectroscopy when the alkali metals Li, Na and Cs are condensed with UF_4 and detected new bands arising. The ${}^6\text{Li}^+ - \text{UF}_4$ stretching mode is observed at $\sim 571 \text{ cm}^{-1}$ compared to the U-F stretching mode at 520 cm^{-1} . A shift to $\sim 1150 \text{ cm}^{-1}$ for the U-H stretching vibration is reasonable seen against the work of Kunze et al. The presence of a U-H mass peak, that will be discussed later on, further supports this conclusion.

In the third spectrum shown in figure 68 (c) we find a much different picture. This represents the products that are formed subsequently to dissociation in the presence of CH_4 . The strongest absorption peak at $\sim 575 \text{ cm}^{-1}$ can be readily allocated to UF_5 . An absorption at $\sim 625 \text{ cm}^{-1}$ with satellite peaks at slightly higher wavenumbers must belong to UF_6 absorbed onto the surface. The absorption features at the position of the UF_4 monomer vibration resembles to a very high degree the features of the products of the alkali-metal fluorides and UF_4 interaction. Even the double “spikes” on the UF_4 vibration is similar to the mentioned spectra [87]. It thus seems judicious to allocate this to $\text{HF} - \text{UF}_4$ or H UF_5 . Again the appearance of a U-H mass peak will be furnished as additional support for this conclusion.

5.2.2.2 ULTRAVIOLET AND NEAR INFRARED SPECTROSCOPY

The question at issue to answer is what characteristic absorption features in the UV/NIR region

DOCUMENT NUMBER	VERSION	PAGE	OF
LT100-000000-155-022		138	

can be connected to UF_5 and UF_4 . Although this can be answered for the solid crystalline phases, very little information exists for the monomeric species. As the latter form is found under the lower pressure conditions of MLIS and where in line analysis techniques are employed, this is a vital question that must be addressed.

There exists a paucity of information on this topic for mainly two reasons:

1. The reactive nature of both UF_5 and UF_4 makes it an extremely formidable task to observe the monomeric form.
2. Normally the nascent uranium bearing species following photolysis are vibrationally very hot. Consequently the absorption features are broad and the selective absorption of different species are destroyed.

It, therefore, seems sensible to first visit the application of theoretical models and investigate their predictions of the optical spectra of the compounds under discussion. For the case of UF_5 we will accept the work of Rosen and Fricke [62] who performed relativistic Dirac Slater calculations and indicated absorption features at $\sim 1,3 \mu\text{m}$ and $\sim 1,8 \mu\text{m}$ wavelengths. Experimental observations for UF_5 are in agreement with the $\sim 1,3 \mu\text{m}$ absorption [91]. For the UF_4 molecule we performed calculations to elucidate this question [80]. Some of the relevant obtained values are listed in the table 9 below.

Table 9: *Ab Initio* calculated transitions in NIR region [80].

UF_4	Calculated (μm)
	1,184
	1,187
	1,650

The experimental spectra obtained by Hancke [92] for a variety of uranium compounds, where the uranium is in the IV oxidation state, supports the calculated values. He recommended that the transition band between 1000 and 1150 nm be used to identify U(IV). The Gmelin Handbook [93] which covers a large number of U(IV) spectra also indicates the omnipresence of absorption features at 1000 to 1100 nm.

Hitherto, ionization of photolysis products at 532 nm, the frequency doubled wavelength of the Nd:YAG laser, has been tacitly interpreted as indicating the presence of UF_5 and the absence of ionization at this wavelength as the absence of UF_5 . Experimental observations, however, concerning the ionization characteristics do not support this picture. In an experiment conducted in a photo chamber, to allow the carrier gas argon to be gradually increased which cannot be easily accomplished in a mass spectrometer, the results of figure 70 were observed [94]. Note that 0,1 torr UF_6 (13,3 Pa) was employed and argon was added up to 10 torr (1,33 kPa).

In this experiment it was possible to ionize UF_6 only with a wavelength at 500 nm and this was unaffected by the carrier gas pressure. Addition of the dissociation of UF_6 , with a wavelength of 266 nm, and the subsequent MPI of UF_5 at the same wavelength of 500 nm, at a reduced intensity, clearly showed a decrease as the total pressure increased. A higher degree of vibrational relaxation of the UF_5 molecule therefore lead to the ionization features at wavelengths around 500 nm to diminish.

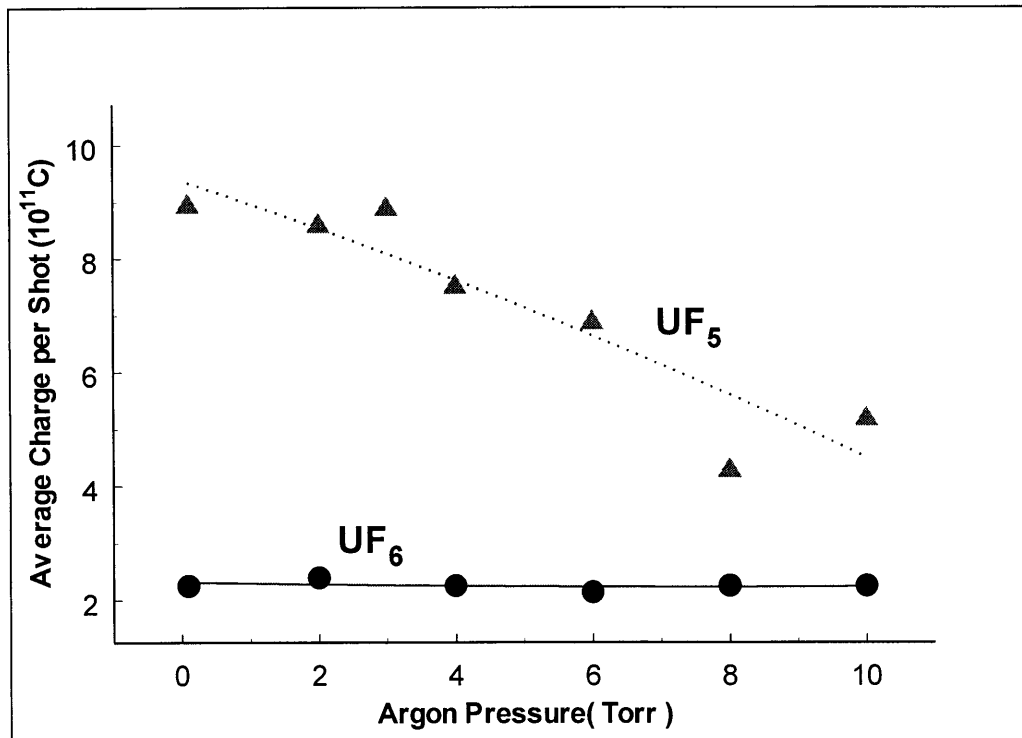


Fig 70: Ionization efficiency of UF₆ and UF₅ at ~500 nm wavelength as a function of pressure (reproduced from reference [94]).

We can conclude from the UV/NIR spectroscopy:

1. Ionization of uranium bearing compounds around 532 nm wavelength is not characteristic of the UF_5 specie. Vibrationally hot UF_5 , however, does absorb this wavelength.
2. Absorption features at $\sim 1,1 \mu m$ wavelength can be associated with the monomeric UF_4 specie.
3. Monomeric UF_5 exhibits a characteristic absorption feature at $\sim 1,3 \mu m$ wavelength.
4. *Ab initio* calculations support the experimental observations.

5.2.2.3 MASS SPECTROMETRY

In chapter IV a copious review of the application of mass spectrometry in the study of MLIS process was given. Recall here that the wavelength of the Nd:YAG laser was often used to ionize the uranium bearing compound after laser photolysis. However, this ionization process has been assumed to be that of the nascent UF_5 molecule. As a result of the present study it became clear that this is not the case and that rather UF_4 is ionized at this wavelength. An experiment to scan the ionization wavelength and observe the resultant fragmentation was planned. This was in an advanced state when the MLIS process was terminated.

Two additional observations relevant to the products formed must be reflected here. In figure 71 the secondary ion mass spectrum (SIMS) of laser photolysis products is shown. In figure 71(a) uranium product that have not been exposed to laser dissociation is shown and in figure 71 (b) the product of laser photolysis. A mass peak appears in (b) at the position one mass unit higher than U^+ . This has become an identification feature of laser photolysis products and has been observed without

DOCUMENT NUMBER	VERSION	PAGE	OF
LT100-000000-155-022		142	

exception. In chapter IV the presence of this U-H mass fragment was also confirmed in the gas phase in flight in the TOFMS when CH₄ or H₂ gas is present (see figure 44). This feature has not been explained before.

5.2.2.4 X-RAY PHOTOELECTRON SPECTROSCOPY (XPS) OF LASER PHOTOLYSIS PRODUCTS

X-Ray Photoelectron Spectroscopy (XPS) or Electron Spectroscopy for Chemical Analysis (ESCA) is the analysis of a core electron ejected from a sample surface after the absorption of an X-ray quantum, usually of Al or MgK α radiation. The kinetic energy of the photoelectron amounts to

$$E_{PE} = h\nu - E_x - \Delta_p \quad (5.10)$$

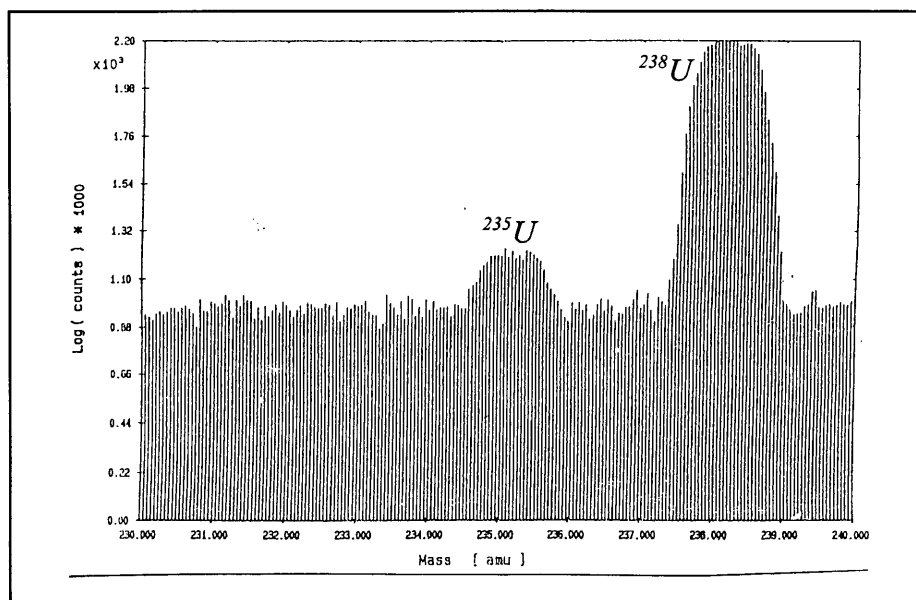
where E_x is the ground state core level energy and Δ_p depends on the chemical binding state of the atom (usually 10eV or less). A quantitative element analysis is possible and additional information on the binding state of the surface atoms is given by the chemical shift. The escape depth of the photo electrons with different initial energies determines the depth resolution, typically 40Å or less.

It is critically important to allow for sample charging effects when attempting to measure accurate chemical shifts. In some cases, the chemical shifts observed in core level XPS are not sufficient to identify the surface chemistry of a particular sample. With the routine use of monochromators in XPS and the high counting rates made possible by current spectrometer technologies, many analysts use valence bands for identification of materials. In many cases the valence bands are used as fingerprints for a sample, rather than for identifying specific molecular orbitals. Fingerprints of the valence bands may then be used to aid in both the identification of samples and the quantification of mixtures of different species.

X-Ray photoelectron spectra were obtained at room temperature on a PHI Quantum 2000 system (at the CSIR) system, using monochromatized Al K α radiation ($h\nu = 1486.6$ eV) [95]. Line broadening and peak shifts, resulting for nonconducting samples from the inhomogeneous charge buildup at the surface due to the emitted photo electrons was controlled by means of an adjustable low-energy electron flood gun. All the samples analysed were handled and stored under strictly dry nitrogen atmosphere. In spite of the precautions used during sample preparation and handling, most spectra revealed the presence of an oxygen peak. The reason for this is the high surface sensitivity of the technique, providing possible evidence of traces of water.

DOCUMENT NUMBER	VERSION	PAGE	OF
LT100-000000-155-022		144	

(a)



(b)

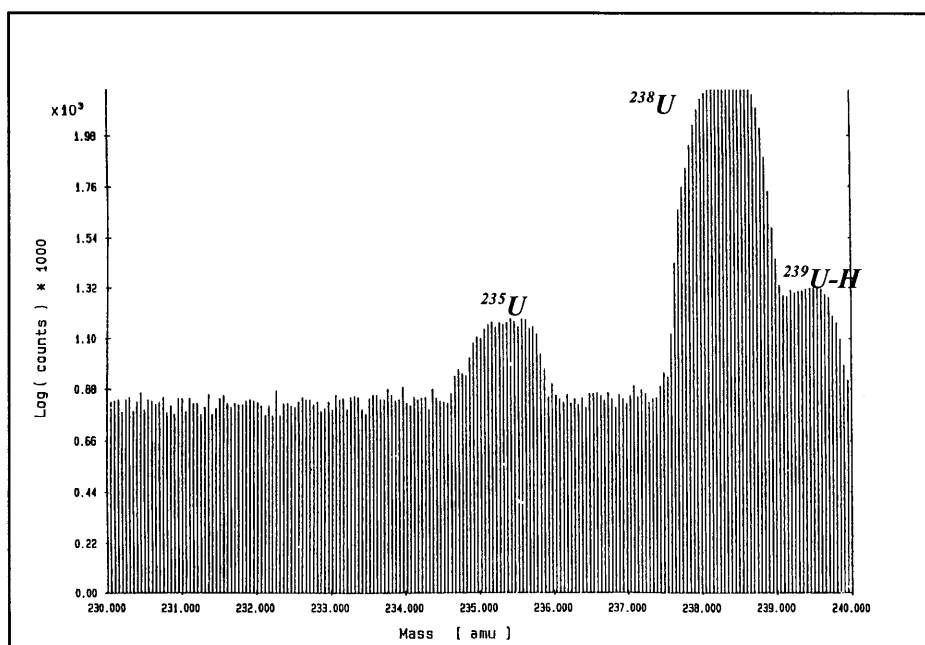


Fig. 71(a): Secondary Ionization Mass spectrometry (SIMS) of UF₆ products. (a) product formed from chemical reaction; (b) product formed from UF₆/CH₄ photolysis.

DOCUMENT NUMBER

VERSION

PAGE

OF

LT100-000000-155-022

145

XPS valence band spectra for UF_4 , UF_5 , UO_2F_2 and an unknown MLIS radiation sample are presented in figure 72. The illustrations corresponds to the raw data. The zero of the binding energy scale was set by the reference to the C_{1s} level at 285 eV.

Figure 72 shows a number of peaks: identification of these peaks is given in table 10. Having the fingerprint spectra for the different uranium complexes, one can attempt a qualitative identification of the MLS product on the filament. The oxide content of the MLIS product can be accessed by the peaks at $\sim 14,9$ and $\sim 23\text{eV}$, both of which are fairly weak.

It should be pointed out that the MLIS sample was kept in a desiccator and analysed within 24 hours after irradiation. The uranium peaks at ~ 2.5 , ~ 7 , ~ 19 and $\sim 29\text{eV}$ are pronounced and very much in agreement with that of UF_4 . The indications are that the MLIS product on the filament is a mixture of UF_4 and UO_2F_2 , favouring the UF_4 . The hydrolysis of UF_5 produces:

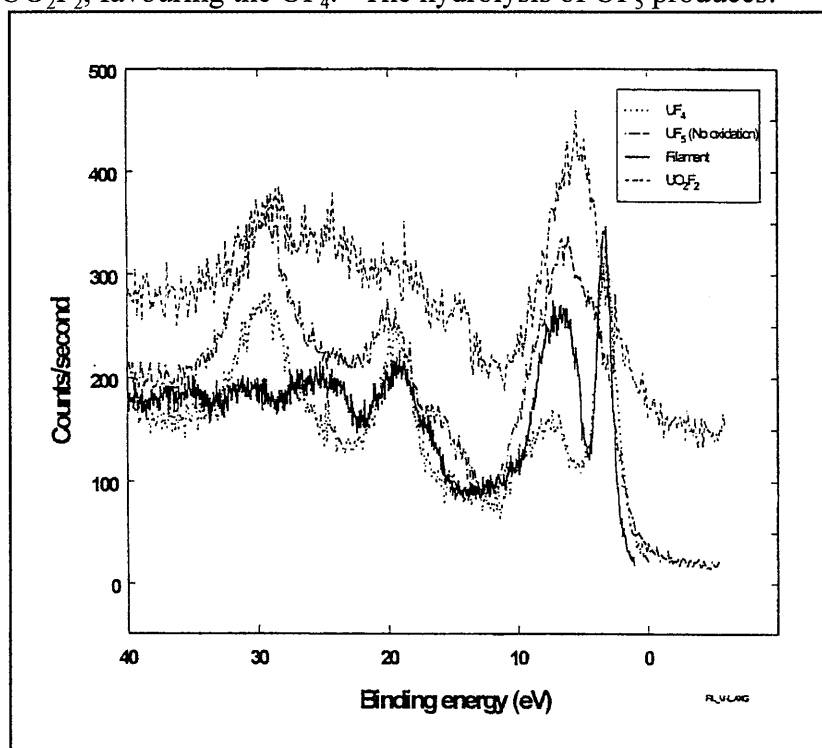
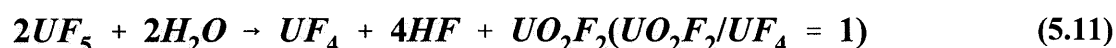


Fig. 72: Comparison of the valence spectra of UF_4 , UF_5 , UO_2F_2 and MLIS sample.

Table 10: Identification of uranium and ligand XPS transition

Level	Binding energy (eV)
U _{5f}	0.6 - 2.8
U _{7s} , U _{6d} , U _{5f} , and F _{2p}	3.6 - 7.0
UO ₂ ²⁺	14.9
U _{6p3/2}	17.1 - 20.3
O _{2s}	22.1 - 24.6
F _{2s}	27.2 - 30.1
U _{6p1/2}	29.2 - 30.9



5.2.3 OBSERVATION OF DISSOCIATION PRODUCTS IN A STATIC CELL BY He-Ne LASER BEAM SCATTERING

Light scattering of a continuous visible laser beam such as a He-Ne laser, by dimers and polymers of the uranium bearing compounds following laser photolysis is a very useful and convenient analytical technique. Such experiments were performed by Human at the AEC. His findings support very directly the proposed uranium reactions of the present study and will with permission be summarized here. A more comprehensive report is contained in reference [96].

The report reflects on observations made of laser light scattering when irradiating a static gas mixture of UF₆ in argon, with and without methane. Dissociation was instigated by UV laser, 266 nm from a quadrupled Nd:YAG laser, and the 16 μm pulsed source described previously. Two wavelengths were used, 16R18 and 16P20 where the former were kept well below dissociation threshold. The UF₆ pressures were typical in the 100 Pa region.

DOCUMENT NUMBER VERSION PAGE OF
 LT100-000000-155-022 147

With UV irradiation, light scattering of the He-Ne laser starts after a few seconds (~10 UV laser shots), grows within a few seconds to a bright cylindrical light source and then subsides slightly to a constant value. By moving the He-Ne laser beam away from the dissociating beam, it was noted that the scattering is confined to the path of the UV beam, except for some scattering below the UV beam, which is probably caused by product particles floating to the bottom of the cell. The time taken for the scattering signal to appear (called induction time) is explained as the time necessary for the UF₅ particle concentration to reach a critical concentration, at which the particles formed by polymerization reach a size large enough to cause appreciable light scattering. It was shown that the inverse of the induction time is directly proportional to the dissociation rate [97]. The constant value of scattering reached after some time is a balance between the production rate of UF₅ particles and the diffusion of particles out of the beam. After cessation of UV irradiation the scattering dies out in 5 - 10 seconds. These results were the same for both gas mixtures, i.e. with and without methane.

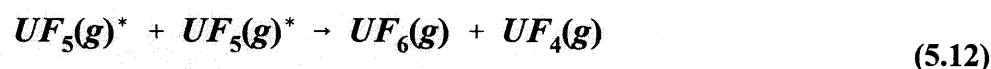
Observations with IR irradiation and the CH₄ gas mixture were as follows: the scattering takes only a few seconds longer to appear, but never reaches a steady value. Instead, the scattering at any particular point in the beam varies with each laser shot. It appears as if each laser shot either produces scattering particles or removes them from the particular volume viewed. The distribution of scattering particles in the cell (observed by moving the He-Ne beam in the cell) is more or less the same as with UV irradiation, i.e. confined to the dissociating beam. The scattering with the IR beam blocked behaves quite differently: it grows for approximately 15 seconds to a maximum and then dies in about 30 seconds.

With IR irradiation and the gas mixture without CH₄ the scattering signal behaves differently from the previous in two aspects: the scattering is spread over the whole volume of the cell and it takes about 5 minutes to die away after the IR is blocked. In both gas mixtures with IR irradiation, no

scattering signal is observed with only one wavelength present (confirming the choice of pulse intensities of the two wavelengths - they only give dissociation when acting together).

5.3 SECONDARY REACTIONS FOR URANIUM BEARING COMPOUNDS

On the basis of the experimental observations registered hitherto one can formulate with a high degree of certainty the reaction events following unimolecular decay. The only reverse reaction that produces UF_6 that has been considered here now, is the recombination of UF_5 and the F radical. We have to explain, however, the formation of UF_4 . The writer has put forward, for the first time, that the known disproportionation reaction



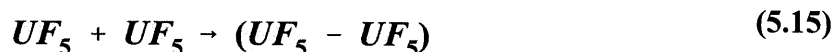
followed by



should also be considered and is indeed extremely important to explain the static cell behaviour. I would like to stress, however, that it is imperative not to equate the single shot chemistry and that in a static cell where the compounds are subjected to repeated laser pulses. It has unfortunately, unfoundedly so, been tacitly assumed that the two situations are identical. Together with reactions (5.12) and (5.13) we must consider, for the case of neat UF_6 , also



and



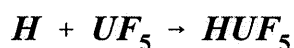
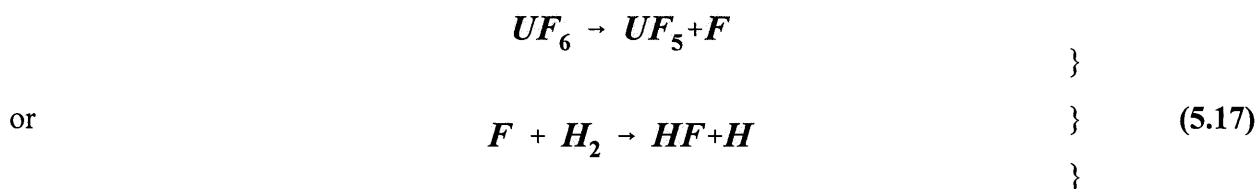
The formation energy of dimerization has been estimated as ~ 34 kcal/mole [98]. The activation energy to rupture the dimer bond by infrared laser, immediately after formation is thus ≤ 40 kcal/mole. The smaller sign provides for the fact that the dimer can contain substantial vibrational energy. It is important to remember here that if the total internal energy, including e.g. the translational energy of the F radical, just prior to a bimolecular reaction, exceeds the bond energy being formed, the same bond will simply rupture again by unimolecular decay in the absence of a collision partner to remove the excess energy. Therefore, after the unimolecular dissociation of UF_6 by multiphoton infrared absorption, vibrational relaxation of the UF_5 monomer and/or a reduction in the F radical translational energy is needed before recombination can occur. The bath of UF_6 molecules that did not participate in unimolecular dissociation is, however, vibrationally very hot with a wide distribution function for vibrational energy [99]. Cooling must thus proceed mainly via transfer of vibrational energy to scavenger- or carrier gases. In the case of UV laser dissociation the bath of unaffected UF_6 molecules remain at low vibrational energy. Rapid vibrational energy exchange between hot UF_5 and cold UF_6 will promote both reactions (5.14) and (5.15) by stabilizing the products $\text{UF}_6(\text{g})$ and UF_5 -dimers. It has been suggested that the dimerization proceeds at a rate of more than 10 times faster than recombination thereby negating to a large extent its influence [100]. Reaction (5.12) is endothermic by 32,7 kcal/mole whilst if reaction (5.13) is included it turns the combination reaction exothermic by 40,4 kcal/mole (considering the reaction on the surface of solid UF_4 particles).

It is important to note that the energy residing in two photochemically produced UF_5 molecules easily exceeds 32,7 kcal/mole - this will promote reaction (5.12). The dimerization reaction could be favoured on the basis of its exothermicity. The UF_5 monomer and dimer both absorb strongly the infrared radiation at roughly 16 μm and particular the 16P20 wavelength. This wavelength is close to resonance with the ~ 580 cm^{-1} vibration mode of monomer UF_5 . The hot vibrational temperatures will furthermore broaden the absorption features. For the dimer we have a broad absorption spectra in the same region. When we repeatedly radiate in a static cell with neat UF_6 we also repeatedly

DOCUMENT NUMBER	VERSION	PAGE	OF
LT100-000000-155-022		150	

vibrationally heat the UF_6 , monomeric and dimeric UF_5 . This clearly promotes reaction (5.12) and our end products become UF_6 and UF_4 . The infrared absorption features of UF_4 is well removed from this wavelength region and this stabilizes the formation thereof. Clearly the formation of UF_4 is a feature synonymous with repeated irradiation in static cells. For a single shot photolysis, when a dynamic system is used, as for a MLIS plant, the formation of UF_4 will be suppressed. The past practise to view the chemistry in static cells equivalent to that in dynamic systems created a lot of confusion, preventing the development of a clear picture of the dissociation process.

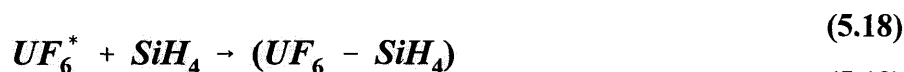
From the rates of vibrational energy relaxation, treated in chapter III, we know that the UF_5 molecule is cooled very fast when CH_4 is present. This is not the case for H_2 as scavenger/coolant. If we have a slow transfer of vibrational energy from the UF_6 molecule to H_2 we can expect the dominant features of the static cell irradiation to be similar to that in neat UF_6 . This is indeed the case. The presence of HF which is formed from the reaction between H_2 and the F radical allows the formation of a new chemical compound HUF_5 . This can originate in two ways



At least three different analytical techniques, i.e. infrared spectroscopy and secondary ionization mass spectrometry (both on solid product, and time-of-flight for gas phase), supported reactions (5.16) and (5.17). The ease with which the alkali metals (Li, K, Cs) and the alkali fluorides (LiF, KF, CsF) enter into similar bonds with the uranium fluorides, attests to the soundness of the

proposed reactions. Hydrogen, another group I element, is expected to show similar behaviour.

Refer now to the photolysis process when CH₄ is present. From the fast deactivation rate of the vibrational energy in CH₄ mixtures we can expect the formation of UF₅ dimers to be stabilized. Very little UF₄, if any, should originate from reaction (5.12). Our infrared spectroscopic analysis of the photolysis products collected on a window (see figure 67), nevertheless show the UF₄ characteristic vibration. This is almost certainly not in the monomeric form as with the prior two cases. A hypothesis put forward by Eerkens [101] to explain the bimolecular reaction between silane, SiH₄, and UF₆, should first be considered to clarify the interaction with CH₄. For the silane the following reactions were proposed to explain the experimental observations



Due to a lack of direct investigation of the reactions involving CH₄ we cannot positively claim that a similar scheme holds good. A few observations lend credibility, however, to such reactions also with CH₄:

1. The formation of UF₄ via the channels proposed for the situation of neat UF₆ and UF₆/H₂ mixtures, will be suppressed by the vibrational quenching of CH₄. Another mechanism therefore seems appropriate to explain the presence of UF₄ in these systems.
2. The U-H⁺ fragment was consistently detected for in-line measurements in a mass spectrometer when CH₄ is present during laser photolysis.

3. Infrared absorption spectra indicate the characteristic features of a HF-UF₄ compound similar to the alkali metal fluorides.
4. If the UF₆^{*} initially contains large amounts of vibrational energy, as it does in infrared multiphoton (as opposed to UV) excitation and dissociation, the HF molecule produced (5.21) will be left with enough vibrational energy to emit fluorescence. One can expect to see this emission delayed in time from the main burst of HF-fluorescence from the reaction.



This was indeed observed and will be discussed under the heading of the scavenger reactions (section 5.4)

The laser scattering measurements of Human merits a discussion in terms of the proposed reactions. The writer finds the trends of the measurements and the proposed reaction mechanisms to correlate extremely well.

- (a) In the static cell irradiations with a UV laser the unimolecular dissociation produces vibrationally hot UF₅. This will lose energy to the bath of UF₆ molecules that are vibrationally cold. This will promote the dimerization process of UF₅. The monomer and dimer of UF₅ do not absorb the subsequent laser pulses and it consequently cannot be further heated or fragmented. Dimerization proceeds nearly unaffected and is determined by the amount of monomeric UF₅ formed, the laser fluence, the working pressure etc.
- (b) When unimolecular dissociation is instigated by 16 μm radiation the effect of many laser pulses come into play. The repeated heating and fragmentation (from many laser pulses) of UF₅ and dimers maintain the species vibrationally hot. Furthermore, for neat UF₆ the

deactivation paths are limited to the bath of UF_6 that is also hot. Dimerization is inhibited by this heating process and we detect a prolonged growth rate as visualized by the scattered signal. Repeated growth and fragmentation cycles occur that accounts for the observed behaviour.

- (c) With CH_4 in the cell the scattering signal varies in the laser beam path. If our complex theory holds then this should be dependent on the internal energy content of the UF_6 molecule. This will vary as the intensity in a Gaussian beam varies. We can then expect spatial variations in scattering which was observed. These kind of effects will unfortunately be accentuated in a system that is repeatedly irradiated. In a flowing system it is reasonable not to expect the same contribution of effects.
- (d) In neat UF_6 the scattering signal spreads out over the cell volume. This is consistent with the slow vibrational cooling. Dimerization can thus occur well outside the laser beam. Here we must also include dimerization of UF_4 .

5.4 REACTIONS OF FLUORINE RADICAL WITH METHANE

It is appropriate to study also the reaction rate of the nascent F radical and the CH_4 scavenger and investigate what confirmation of the general picture can be extracted from the observations. An adequate description of the experimental setup was given in section 3.2. The same configuration was utilized to study the HF fluorescence that will be narrated here.

In figure 73 a HF fluorescence curve is shown after laser dissociation of the UF_6 by $16\ \mu\text{m}$ radiation. A UF_6 pressure of 50 Pa at ambient temperature was loaded and a five times higher CH_4 pressure was added. Similar to the previously described radiations, the yield per laser shot was $\sim 3\%$ or

<i>Document Number</i>	<i>Version</i>	<i>Page</i>	<i>of</i>
LT100-000000-155-016		154	

$$\begin{aligned}
 3\% \times 50 \text{ Pa} &= 1,5 \text{ Pa UF}_6 \\
 &= 2,65 \times 10^{14} \text{ molecules/cm}^3
 \end{aligned}$$

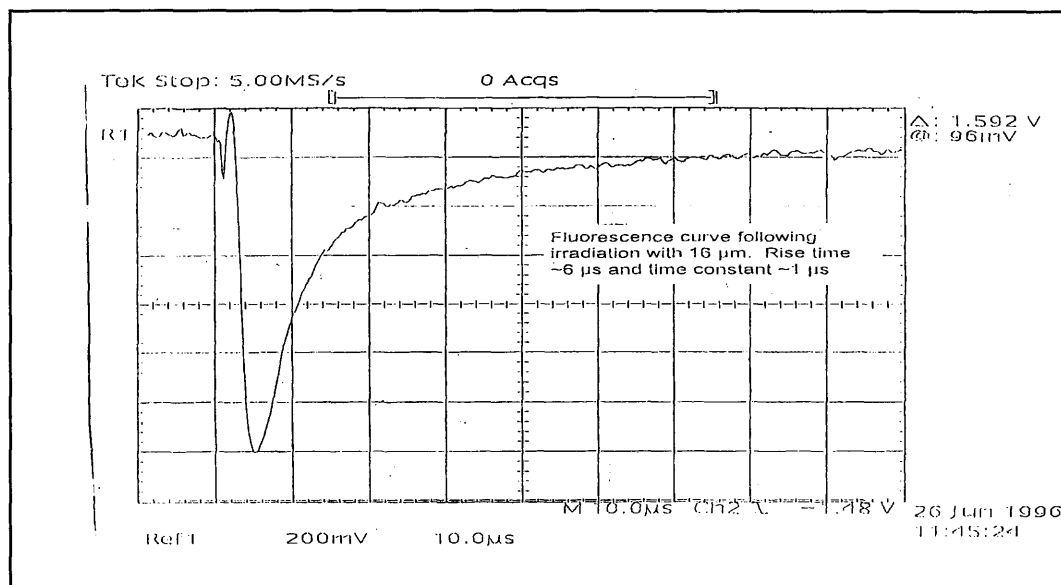


Fig. 73: Fluorescence curve following irradiation with 16 μm . Rise time $\sim 6 \mu\text{s}$ and detection time constant $\sim 1 \mu\text{s}$.

The CH_4 density was $\sim 7,24 \times 10^{14}$ molecules/ cm^3 . If we would describe again the reaction rate as second order then

$$\frac{1}{a - b} \ln \frac{b(a - x)}{a(b - x)} = k_{\text{CH}_4} t \tag{5.23}$$

This mathematical formulation is valid if $a \neq b$ which denotes the initial concentrations of F radicals and CH_4 molecules respectively [66]. From the rising part of our fluorescence curve we find that x is equal to 50% of the initial value after $\sim 2 \mu\text{s}$. A value for k_{CH_4} of

$$5,4 \times 10^{-11} \text{ cm}^3 \text{ molecules}^{-1} \text{ s}^{-1} = 3,25 \times 10^{13} \text{ cm mole}^{-1} \text{ s}^{-1}$$

can now be calculated.

In the temperature range 298 - 450 K the reaction rate has been studied mass spectrometrically, employing fluorine atoms produced by the $N + NF_2$ reaction, giving [102]

$$k_{CH_4} = 3,3 \times 10^{14} \exp(-4800/RT) \text{ cm}^3 \text{ mole}^{-1} \text{ s}^{-1}$$

with the activation energy in J mole^{-1} . The room temperature value, $4,8 \times 10^{13} \text{ cm}^3 \text{ mole}^{-1} \text{ s}^{-1}$ is slightly larger than the value determined from the fluorescence data. It must be remembered that the risetime of the fluorescence curve is slower than the real rate due to the limiting time response of the detector system. The true rate is therefore higher than the value determined here.

The Arrhenius coefficient from transition state theory for bimolecular reactions can be written as

$$A = e^2 \left(\frac{k_B T}{h} \right) \exp(\Delta S_c^+/R) \quad (5.24)$$

where ΔS_c^+ is the entropy change in going to the activated complex. In table 11 below values for similar reactions are shown:

Table 11: Molecule/radical reactions

Reaction	Temperature (K)	log A ($1 \text{ mole}^{-1} \text{ s}^{-1}$)
$CH_4 + I \rightarrow HI + CH_3$	630	11,7
$CH_4 + F \rightarrow HF + CH_3$	300	11,52
$H_2 + F \rightarrow HF + H$	300	11,1
$H_2 + I \rightarrow HI + H$	680	11,4

The rate constants can therefore be accurately predicted assuming very tight activated

complexes i.e. $E=0$. This implies that the reaction rate between CH_4 and F radical must be close to the bimolecular collisional frequency. Taking the hard sphere collisional diameters of the CH_4 and F complex as $\sim 4 \times 10^{-8} \text{ cm}$, (5.24) reduces to

$$k_Z = \pi d_{\text{CH}_4\text{-F}}^2 \left(\frac{8 RT}{\pi \mu_{\text{CH}_4\text{-F}}} \right)^{1/2} \quad (5.25)$$

where $\mu_{\text{CH}_4\text{-F}} = (16 \times 19)/(16 + 19) = 8,69 \text{ amu}$. Based on (5.25) we predict a rate of $2,58 \times 10^{11} \text{ liter mole}^{-1} \text{ s}^{-1}$ compared to the expected rate of $4,8 \times 10^{10} \text{ liter mole}^{-1} \text{ s}^{-1}$ at ambient temperature. This agreement is not as good as anticipated and suggests that the activation energy of 4800 J mole^{-1} is too large.

The prediction of the Arrhenius coefficient from transition state theory seems reasonable and in line with similar reactions. It is therefore recommended that the activation energy of $\leq 1 \text{ kJ/mole}$ be accepted as a more realistic value. The work of reference [102] warns about possible inaccuracy of the determined value.

A subsequent search into more data on the activation energy from the literature revealed that this reaction has indeed been studied utilizing different techniques. In table 12 a summary of the experimentally obtained activation energies is reflected. A value close to 1000 J mole^{-1} is thus supported and confirms that the value determined from the fluorescence of HF is reasonable.

Table 12: Reaction $\text{CH}_4 + \text{F} \rightarrow \text{HF} + \text{CH}_3$

Temperature K	E_a cal mole ⁻¹	Method	Reference
178 - 373	1210	F_2 + hydrocarbon	[103]
250 - 400	1150	$\text{N} + \text{NF}_2$	[102]
178 - 373	1210	F_2 + hydrocarbon	[104]
178 - 373	1850	Competitive method	[105]
250 - 450	2080	F_2 + hydrocarbons	[106]
~300	≤ 1000	Fluorescence	This work

This value of the activation energy will confirm a tight activated complex and a reaction rate very close to the collisional frequency. It also confirms the lack of any influence of steric effects on the reaction rate. The tetrahedral structure of the methane molecule is a highly symmetrical configuration which supports the absence of steric effects. It seems also that the rotational speed of the methane molecule furthermore negates the need for a specific configurational approach between the two species. If the proposed features of the CH_4/F reaction is reasonable it leaves little room for any significant contribution to the formation of HF molecules by reactions other than the discussed one.

5.5 REACTION OF VIBRATIONALLY HOT UF_6 AND METHANE

The fluorescence response of figure 73 was observed in the standard process gas mixture that also contains the carrier gas, argon, that constitutes ~70% of the mixture. In the absence of argon, some interesting features were observed that indicate a bimolecular reaction. Figure 74 shows the HF fluorescence response for a binary gas mixture of ~50 Pa UF_6 and ~266 Pa of CH_4 . The dissociation of the UF_6 is instigated by 16 μm radiation. A fast initial risetime similar to figure 73 is observed but the temporal shape following the peak of fluorescence signal is considerably different. Firstly, the decay time of the HF fluorescence signal is very fast, indeed

comparable to the initial risetime. Secondly, a smaller but significant pinnacle appears roughly 5-6 μs later than the first. This second burst of fluorescence can be reasonably tied up with a bimolecular reaction that produces an amount of excited HF subsequent to the fast scavenging reaction. The bimolecular reactions cited in equations (5.18) to (5.21) can be connected to this HF production. The presence of a bimolecular reaction between UF_6 and CH_4 for the case of infrared laser excitation is very significant in terms of the MLIS separation process. This reaction is absent when the photolysis proceeds via ultraviolet laser excitation. This aspect will be discussed under section 5. For the infrared laser excitation we have, however, a major difference in the vibrational energy of the UF_6 molecule (compared to UV) which enables it to react. The bimolecular features of the fluorescence response is not detected when argon is present, most probably due to collisions smoothing the effect. It has been advocated [107] that the HF fluorescence technique is an ideal method to establish the yield of the unimolecular dissociation reaction of UF_6 . A few precautions seem necessary when this is implemented. It is common to have residual HF as an impurity in industrial UF_6 . This can be removed but the process is quite cumbersome and it can become costly if the specification requires very low concentrations of HF impurity. A question that arises immediately relates to the influence of this HF on the HF fluorescence responses utilized to study the scavenger reaction. This background HF will be initially vibrationally cold and will have fast resonant vibrational energy exchange with the hot reaction product. It can be anticipated that the decay time and therefore the inflexion point of the HF response curve will be significantly influenced. In figure 75 this phenomenon is clearly demonstrated. For this purpose the prototype molecule SF_6 was used together with CH_4 . SF_6 was selected for this experiment because it was easier to purchase high purity SF_6 than to clean UF_6 to the desired level. Fixed concentrations of HF were loaded into the fluorescence cell in advance to the laser dissociation of SF_6 . The HF was selected for this experiment because it was easier to purchase high purity SF_6 than to clean UF_6 to the desired level. The HF was monitored by an infrared spectrometer and the concentration of HF is specified by the absorbance measured. For very small concentrations of added HF the peak of the fluorescence curve diminishes rapidly but evens out for higher concentrations. It is then imperative to take note of this influence and cater for it when the yield of the UF_6 dissociation

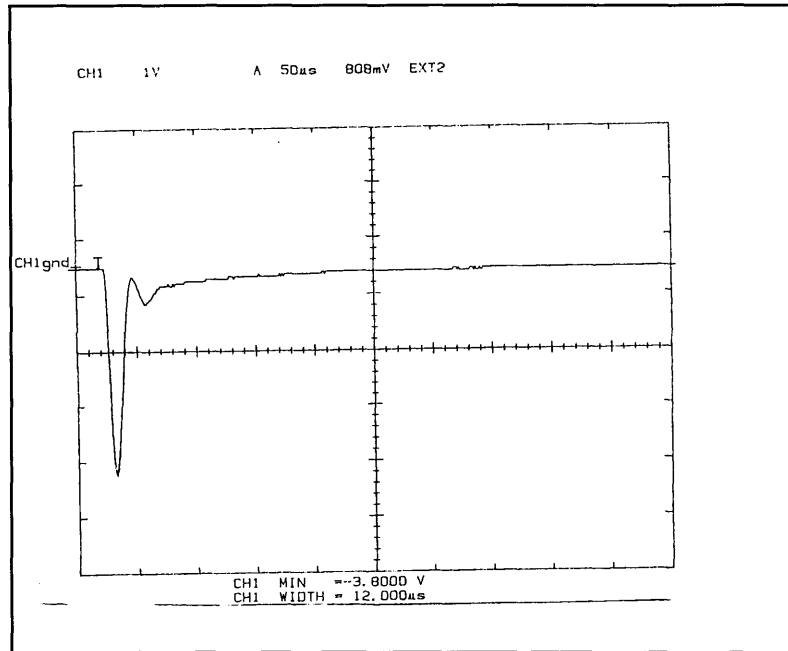


Fig 74: HF fluorescence versus time. Oscilloscope trace for $\sim 0,4$ torr (50 Pa) UF_6 and 2 torr (266 Pa) CH_4 . Temperature is 300 K and dissociation wavelength 16 μ m.

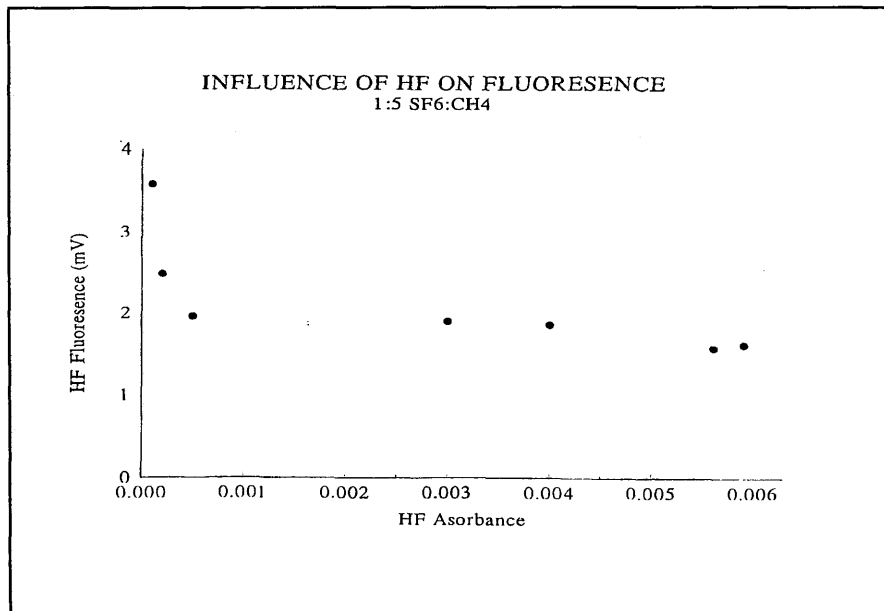


Fig. 75: Influence of HF concentration on the integrated peak fluorescence signal.

is monitored via HF fluorescence. Consider next the influence of the CH_4 concentration on the HF fluorescence response curve. As we have seen in chapter II the temporal rise and fall of the response can be narrated by a reaction- and decay time constant respectively. The former is normally much faster than the latter which is determined by the collisional deactivation of vibrationally excited HF. When the CH_4 content in an experiment is gradually increased we can anticipate an accelerated reaction rate between F and CH_4 . We should detect a monotonic rise in the amplitude of the inflexion point as this is applied. From figure 76 we see that this is indeed the case. A steep rise in the amplitude is observed up to a CH_4/UF_6 ratio of ~ 2 . Subsequently, however, we see an equally rapid drop up to about a ratio of ~ 4 followed by a decline in the steepness. This feature can be ascribed to the collisional decay segment of the HF response curve experiencing a rapid increase in rate. The sudden change after the inflexion point of figure 76 seems strange from this point of view. A similar change, when the collisional deactivation was measured by the Russian group in Troitzk [108], was observed. This was only observed in CH_4/UF_6 mixtures and not when N_2 or Argon was added.

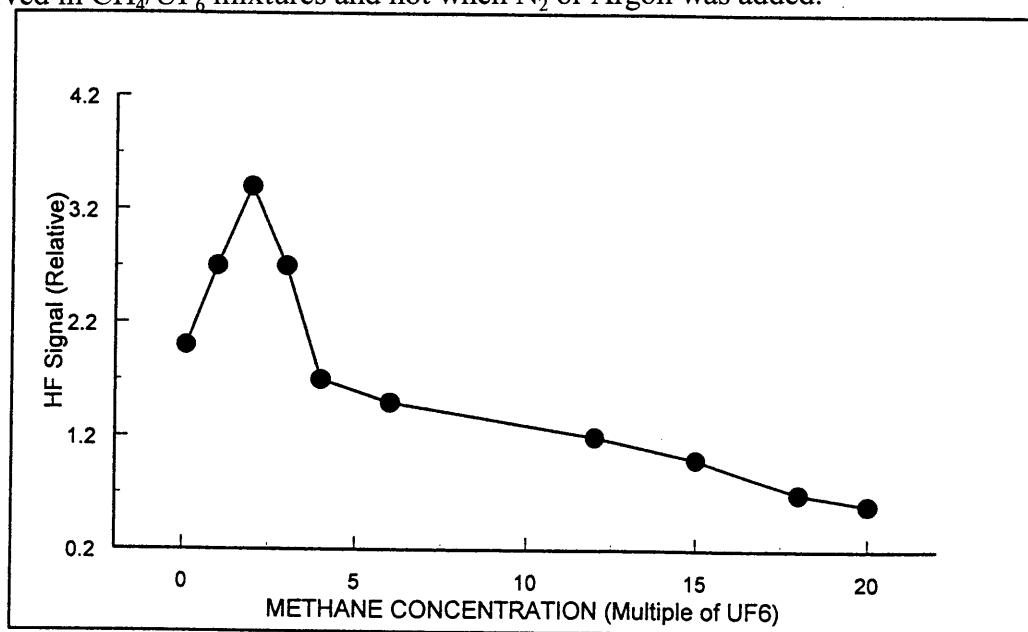


Fig. 76: HF signal as a function of methane concentration at room temperature (300°) for the 16R18 line at 500 mJ/cm².

Figure 77 shows the same kind of information but at a flow cooled temperature of ~ 100 K. This is the temperature where MLIS is operated. Although the general shape of the curve is the same as for ambient temperature, the rapid decline after the CH_4/UF_6 ratio of ~ 2 is absent. How do we explain these observed features? From chapter II we know that the vibrational exchange between two species, if it is of a long range nature, increases as the temperature drops to 100 K. The vibrational quanta for $\nu_3(\text{CH}_4)$ and HF are very close to each other. Furthermore, HF has a very high dipole moment, ca 1,91 Debye, which promotes the dipole-dipole mechanism. If this view is correct we would expect the influence of CH_4 at the flow cooled temperature to be more prominent than at ambient temperature. It, therefore, seems more apparent that this phenomenon must be ascribed to a bimolecular reaction.

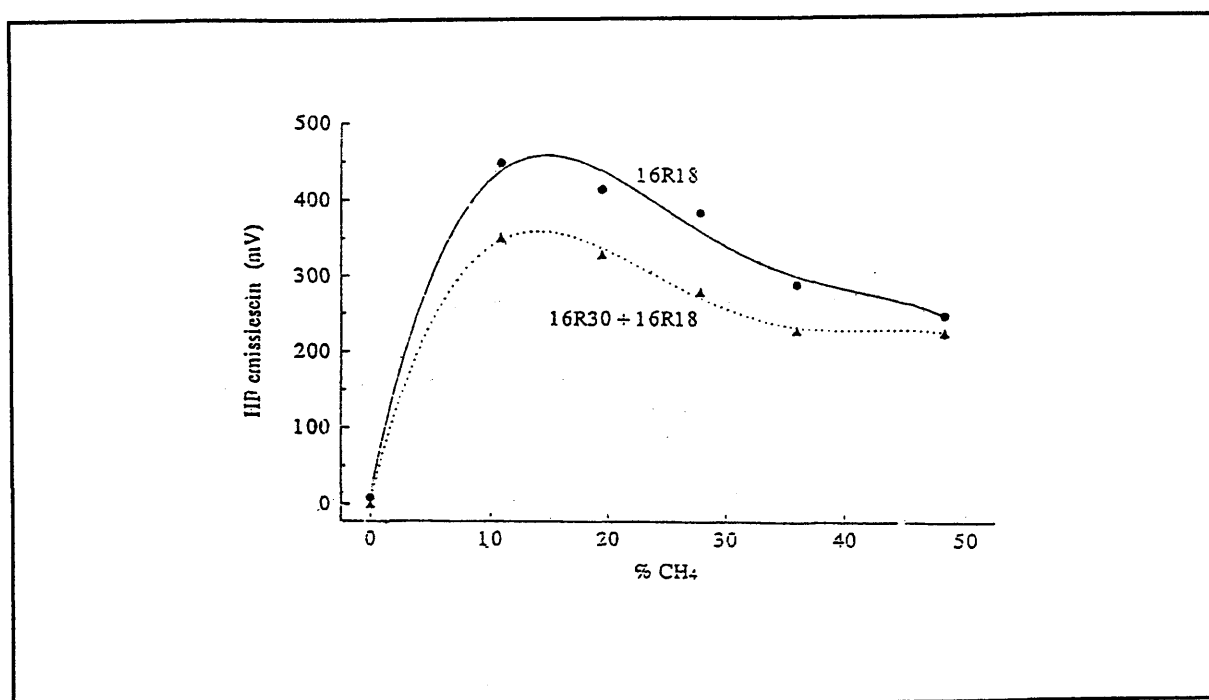


Fig. 77: HF fluorescence signal as a function of methane concentration at flow cooled temperature (~ 100 K) for the 16R18 line at ~ 500 mJ/cm².

Figure 77 illustrates another interesting feature. HF fluorescence response curves for two laser excitation conditions are depicted. The two laser wavelengths 16R30 and 16R18 are utilized for excitation and dissociation. When they operated in tandem, 16R30 first in time, a larger portion of UF_6 molecules are excited and dissociated because the 16R30 wavelength is in resonance with the $^{238}\text{UF}_6$ absorption. Although a higher concentration of vibrationally hot UF_6 results, the overall HF fluorescence production is significantly lower. This would seem to indicate that more HF is “captured” into some reaction which prevents it from emitting photons. Our bimolecular reaction hypothesis is thus further supported, i.e. UF_6^* reacts with CH_4 which releases HF only partly and slowly.

A final feature of the HF fluorescence response merits some attention. Consider the situation when neat UF_6 is dissociated in our fluorescence cell. This obviously contains some HF impurity. A HF fluorescence signal can be detected from this HF as is illustrated in figure 78. The vibrational activation must surely result from vibrational energy transfer between hot UF_6 and the cold HF present. The temporal response covers a wide time span. When the decay region is plotted as the natural logarithm against time a linear response is evident (look at figure 79). A single exponential decay process is operational with a characteristic relaxation rate of $\sim 84 \mu\text{s torr}$. The important issue here is that the UF_6 relaxes very slowly when in a neat gas. This is consistent with our previous observation that also UF_5 in a vibrationally hot UF_6 bath relaxes slowly. The two molecules should react very similar due to their close relationships in vibrational modes.

5.6 REACTIONS OF THE METHYL RADICAL

In the section 5.4 it was confirmed that the $\text{CH}_4 + \text{F}$ reaction proceeds very rapidly. We have also shown that the rate constant can be quantitatively verified from the time response of the HF fluorescence signal originating from this reaction. We can conclude that other reactions that compete to annihilate the F radicals are of minor importance, i.e. do not contribute to any significant degree to the overall depletion. It is thus reasonable to allocate a minor role to the

DOCUMENT NUMBER	VERSION	PAGE	OF
LT100-000000-155-022		163	

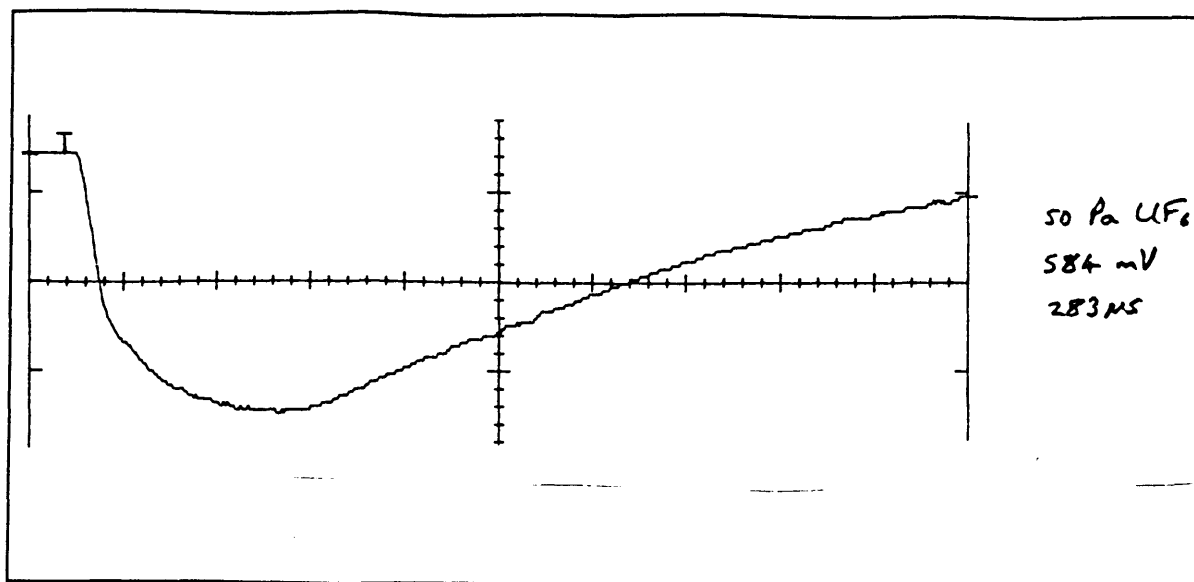


Fig. 78: HF fluorescence signal in neat UF₆. HF as residual impurity present.

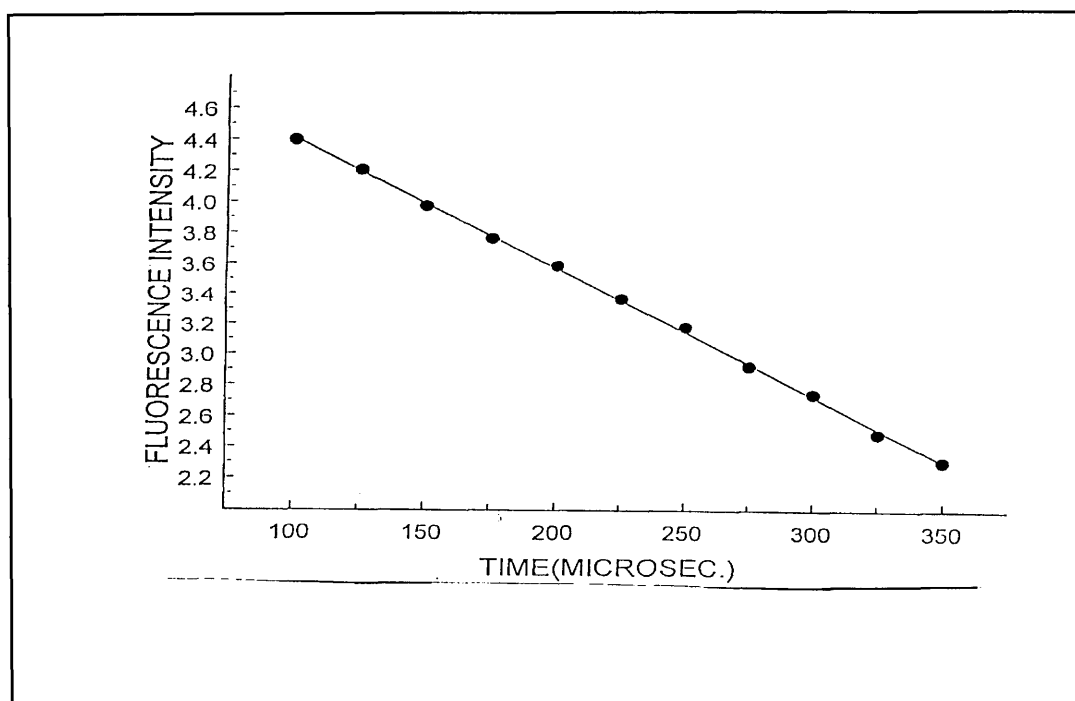


Fig. 79: Semilog plot of HF fluorescence decay in figure 3(a). The slope gives a relaxation rate of ~85 μs torr.

reaction



to remove the [F]. The formation of CH₃F cannot therefore, be explained to any significant amount as originating from reaction (5.26). It is important to note that this is applicable even for low CH₄ /UF₆ ratio mixtures. This observation is significantly different for dissociation instigated by an ultraviolet laser. For the latter case relatively large amounts of CH₃F are formed for low CH₄ /UF₆ ratio mixtures and we need to comprehend this. If the radical reaction (5.26) is insignificant after infrared laser photolysis we need to establish why it is so much different for ultraviolet laser photolysis.

The recombination reaction of methyl radicals to form ethane is a well studied and documented reaction, for various reasons [109]. In the MLIS reaction scheme context it is important in terms of annihilating the methyl radicals and preventing other possible interactions. There exists no direct evidence that the methyl radical reacts with UF₆ although we cannot exclude the possibility. It is not possible to unambiguously state that the bimolecular reaction with UF₆, that we know exists, involves CH₄ itself and not CH₃.

5.7 SECONDARY REACTIONS FOLLOWING DISSOCIATION BY ULTRAVIOLET LASER

The photochemistry of UF₆ following ultraviolet laser photolysis is moderately well documented. Compared with the data collected for the ultraviolet case, the available literature on the photochemistry after infrared laser photolysis is meager. This paucity of information is not surprising when one considers that the dissociation by ultraviolet laser was first chosen for enrichment studies but was later abandoned when it proved less viable than dissociation by infrared lasers. Nevertheless, these earlier efforts and the fact that the ultraviolet laser route seemed less promising, put much more information into the scientific domain than the infrared laser route. To explain the accounted features for the ultraviolet laser photochemistry it was not

necessary to perform experimental measurements as ample literature data is available. However, against the new evidence put forward in this dissertation for the infrared photochemistry it is imperative to reconsider many of the explanations furnished in the past. This section will reflect on the writer's contribution to the interpretation of the data. Although there are differences between the two photolysis processes, many aspects are common to both. The photochemistry following dissociation by UV-laser, 266 nm and 248 nm, will be scrutinized. These are the wavelengths emitted by the third harmonic of the Nd:YAG laser and the KrF laser respectively.

The absorption spectrum of UF₆ between 420 and 200 nm consists of three broad features. The first of these, the A band, is a weak feature that extends from 420 to 340 nm, at ambient temperature, with a peak near 375 nm. The peak absorption cross section in this region is about $2 \times 10^{-20} \text{ cm}^2$. The second feature, the B band, extends from 340 to about 240 nm. The absorption is more intense in this region and is about $1,5 \times 10^{-18} \text{ cm}^2$ at 260 nm. The most intense feature, the C band, extends from about 240 nm to below 200 nm. The cross section at the peak, about 214 nm is about $1,7 \times 10^{-17} \text{ cm}^2$.

The wavelength of the KrF laser, 248,3 nm, the photolysis source very often utilized in experiments, lies within the B band. At this position of wavelength the cross section is about

$$\sigma(\text{KrF}) = 1,7 \times 10^{-18} \text{ cm}^2$$

Another wavelength often used for the photolysis of UF₆ is 266 nm obtained from a Nd:YAG laser. At this wavelength the cross section is about

$$\sigma(266 \text{ nm}) = 1,15 \times 10^{-18} \text{ cm}^2$$

The measured enthalpy of formation of all possible reaction products allow for only one reaction pathway at the two wavelengths under discussion, the simple bond cleavage reaction (see also table 13):



PHOTON AND BOND ENERGIES RELEVANT TO UF₆ UV PHOTOCHEMISTRY

Table 13: Relevant energies

Relevant Energies	kcal/mole	eV
248 nm photon	115,3	5
266 nm photon	107,5	4,67
Bond energy UF ₆ (UF ₅ -F)	68,8	3
Bond energy UF ₅ (UF ₄ -F)	102,4	4,45
Bond energy H-F	130	5,8
Bond energy F-F	37	1,6
Bond energy C-H	102	4,4
Bond energy C-F	139	6
Bond energy H-H	108	4,72
Bond energy N≡N	225	9,8
Bond energy UF ₅ - UF ₅	40	1,7

1 eV ~ 23 kcal/mole

The next possible reaction, dissociation to UF₄ and F₂, requires wavelengths shorter than 216 nm if only single photon events are considered. This aspect is a very important point of departure and an expansive discussion is appropriate.

In support of the statement that only UF₅ is formed immediately following UV photolysis, the following observations relate:

1. The energy balance between the available photon energies, table 6, and the bond strength of the UF₅ - F bond does not allow for UF₄ to be formed.
2. The work of Kroger et al [110] on the photolysis products in molecular beams and the distribution of the internal energies between the UF₅ and F products, rules out the

possibility of direct two photon absorption at the laser fluences, a few tens of mJ/cm^2 , employed in typical dissociation experiments. At high laser fluences it is possible for the UF_6 molecule to absorb two photons simultaneously but not at the conditions that the experiments were performed - the fragmentation distribution also did not support such a mechanism.

3. A question also arises whether a UF_5 photo product that is in an excited vibrational state can absorb a UV photon during the initial laser pulse with subsequent dissociation to UF_4 . Radiation with a continuous UV lamp or laser under matrix isolated conditions in the absence of methane, rules this out [89]. In an experiment of this nature, lower UV fluences are compensated for by longer irradiations times. Under such conditions UF_5 monomer was detected as the only uranium bearing compound after photolysis.

The work of Kroger et al [110] supports the postulate of direct dissociation in the wavelength region under discussion. They utilized pulses from a frequency quadrupled Nd:YAG laser at 266 nm to photo dissociate UF_6 in an effusive beam. They measured the velocity and angular distribution of the fluorine-atom product with a quadruple mass filter. The detection of fluorine atoms in this experiment verified that the unimolecular dissociation producing UF_5 and F is the dominant photochemical reaction at 266 nm. The velocity distribution was bimodal and the angular distribution was slightly anisotropic. These both support a direct dissociation mechanism [110]. Furthermore, the fluorine atom velocities were much greater than one would expect from dissociation after internal conversion to the ground electronic state [110]. From the angular distribution the authors concluded that the absorbing molecule could have rotated only about 10° before dissociation. This implies that the dissociation process is completed in less than one nanosecond while the rapid, direct photo dissociation implies a primary quantum yield of unity.

The quantum yield of a photolysis reaction is determined by measuring the total number of molecules of UF_6 removed by the photolysis reaction and the total number of

ultraviolet quanta absorbed by the UF_6 sample. The quantum yield as usually reported in the literature is the ratio of these two quantities. Careful measurements [100] performed at 248 nm wavelength for both Ar and CH_4 diluents gave values of unity. This observation furthermore negates any evidence for a recombination reaction between the photolysis products, UF_5 and F, whereby a decrease in quantum yield would result.

An apparent quantum yield of $\sim 0,6$ was quoted in one paper [98]. I would like to make a few comments on this issue:

1. A decrease in quantum yield cannot result from recombination of photolysis products for 266 nm if it is not present for 248 nm, about 2728 cm^{-1} apart.
2. If pre-dissociation plays a significant role at 266 nm this would indeed be a surprising result. Pre-dissociation in large molecules, e.g. UF_6 , is usually thought to lead to total randomization of the vibrational motion, before bond breaking occurs. The distribution of the fragment translational energy should thus be, exponential. This is not so, as quoted by Kroger et al [110]. No experimental proof of incomplete randomization of the motion exists as far as the writer's knowledge goes.
3. If the quantum yield at 266 nm would indeed be $\sim 0,6$ this should support a viable enrichment scheme. A further enrichment factor of ~ 2 could then be obtained by utilizing a 266 nm beam as dissociation laser. After infrared radiation, which sets up the initial selectivity, of 4-5 photons of $16 \mu\text{m}$ to give the difference of $\sim 2728 \text{ cm}^{-1}$ between 248 nm and 266 nm, a laser at 266 nm will then dissociate the vibrationally excited UF_6 molecules twice more efficient than the unexcited molecules. Measurements in the wavelength region under discussion show no such effects [111].
4. Detailed measurements of the ultraviolet absorption cross sections in the 260 nm band of vibrationally excited by a $16 \mu\text{m}$ laser, have shown that the UV cross section changes are the smallest at the band origin and increase towards longer wavelengths. This trend

is in complete agreement with the theoretical model of a transition from a ground electronic state to a dissociative upper potential surface [111]. Maximum changes in the absorption cross section therefore occur in the wings of the UV absorption bands as might be expected when UF_6 molecules are vibrationally excited. The theoretical explanation for this observation is that the Franck-Condon factor for a transition from a ground vibrational state to the continuous vibrational function for an upper dissociative electronic state has a Gaussian form for an isolated absorption band.

The abovementioned observations clearly support the conclusion that absorption at 266 nm is dominantly to a directly dissociative state. A quantum efficiency of $\sim 0,6$ therefore seems indeed very odd. The further elaboration on the present topic will accept the picture of fast dissociation at both 248 nm and 266 nm based on the mentioned experimental evidence that supports this feature.

It has been pointed out that the dissociation time from a directly dissociative state is shorter than one nanosecond. The following features need to be stressed:

- (i) The dissociation of UF_6 following UV photolysis is entirely of unimolecular nature. The UF_6 molecule therefore reacts like an isolated molecule and CH_4 or any carrier gas plays no role in the dissociation dynamics.
- (ii) All bimolecular reactions are excluded in the primary dissociation reaction because none can proceed at a rate of 10^9s^{-1} at the conditions where MLIS is executed.
- (iii) The only uranium bearing compound that is initially formed is UF_5 .

Let us consider again the possibility of a bimolecular reaction contributing to the depletion of UF_6 during ultraviolet laser photolysis. Some simple reaction kinetics of a bimolecular interaction can be formulated. For the reaction

$$A + B \rightarrow \text{products } P \text{ we have}$$

$$\frac{d[P]}{dt} = \frac{-d[A]}{dt} = \frac{-d[B]}{dt} = k[A][B]$$

A test, very easily executed, examines the concentration dependence of the bimolecular reaction. If the reaction is entirely unimolecular, as is contemplated for the UV photolysis of UF_6/CH_4 mixtures, no dependence on $[\text{CH}_4]$ should exist. In figure 80 the result of a UF_6 depletion experiment in a static cell is shown. The declining UF_6 pressure was measured with a FTIR spectrometer and the yield per laser shot calculated. An increase in the $[\text{CH}_4]/[\text{UF}_6]$ ratio had no measurable effect on the depletion of UF_6 . It demonstrates that no bimolecular reaction between

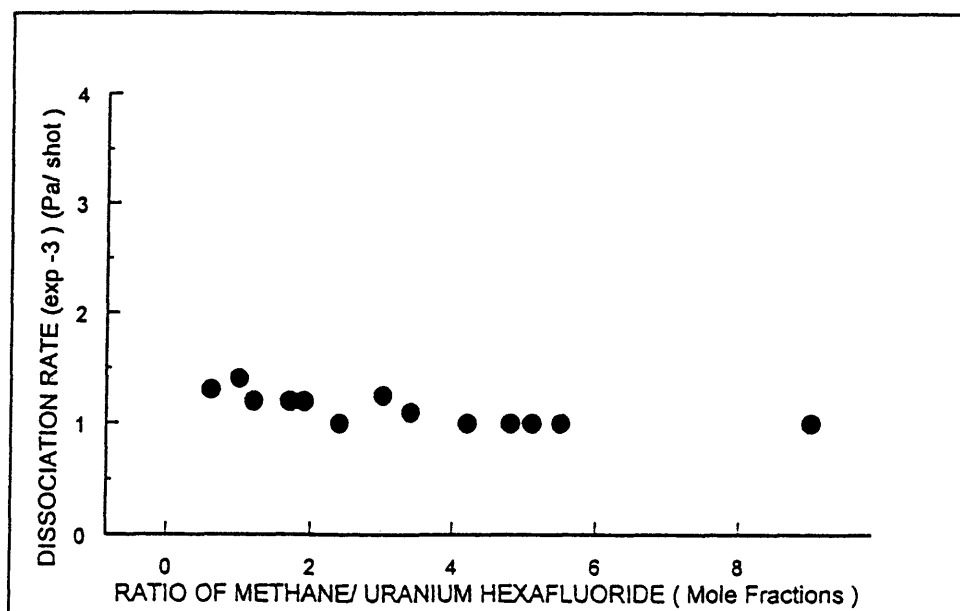


Fig. 80: Dissociation rate of UF_6 as a function of CH_4 content.

UF_6 and CH_4 occurs for ultraviolet, 248 nm, photolysis. Consider with this observation also the

following. We measured the HF fluorescence response for 266 nm in a UF₆/CH₄ mixture of 1 : 5. For a standard mixture and total pressure the yield increases in a linear fashion (look at figure 81) if the laser fluence is increased. This simple observation subscribes to another important issue. An increased dissociation of UF₆ also produces more CH₃ which is a product of the very fast CH₄/F reaction. Nevertheless, no detectable influence of the following reaction is observed:

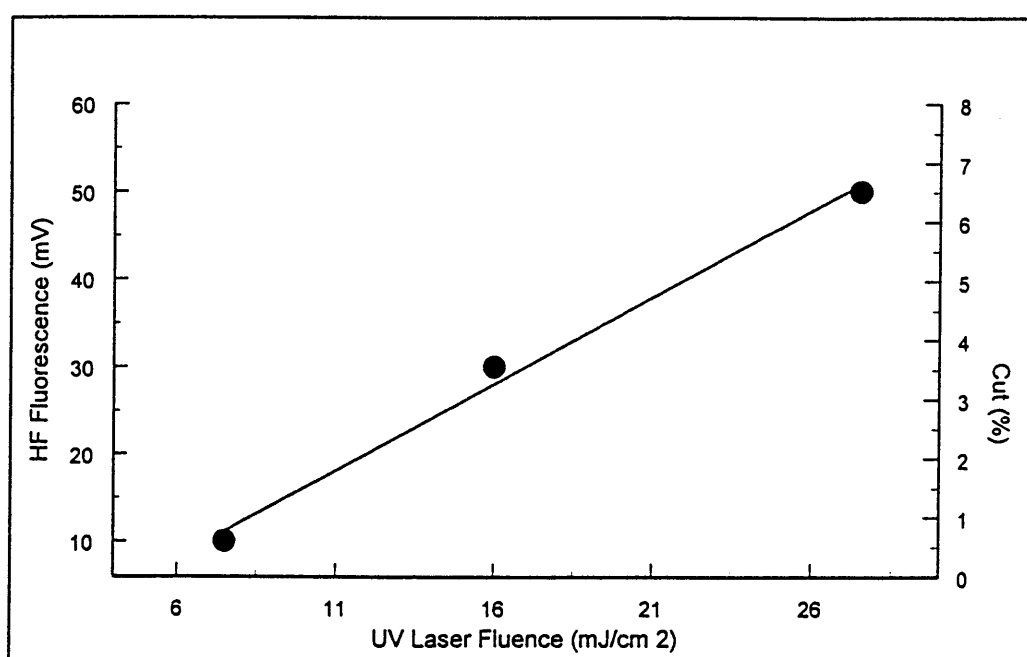
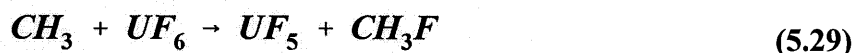


Fig. 81: Fluence dependence of UF₆ dissociation by UV laser (266 nm).

This reaction has been held responsible for the deterioration of the nascent separation factor achieved in isotopically selective infrared multiphoton dissociation of UF₆. The presence of CH₃F has been tacitly regarded as an indication of the reaction (5.29) proceeding. A branching ratio derived from the C₂H₆/CH₃F ratio has often been used to quantify the negative effect of CH₃F formation [112]. There seem to be no scientific grounds for this assumption and it is based on a postulated secondary reaction sequence and contributions which have not been experimentally verified.

Some observations during the HF fluorescence process when an ultraviolet laser is used will be reflected. In figure 82 we can look at the fluorescence response at a total pressure of 350 Pa with 5% UF₆, 20% CH₄ and the balance argon. The expected decay curve is observed. For comparison a similar response with only UF₆/CH₄ present is depicted in figure 83.

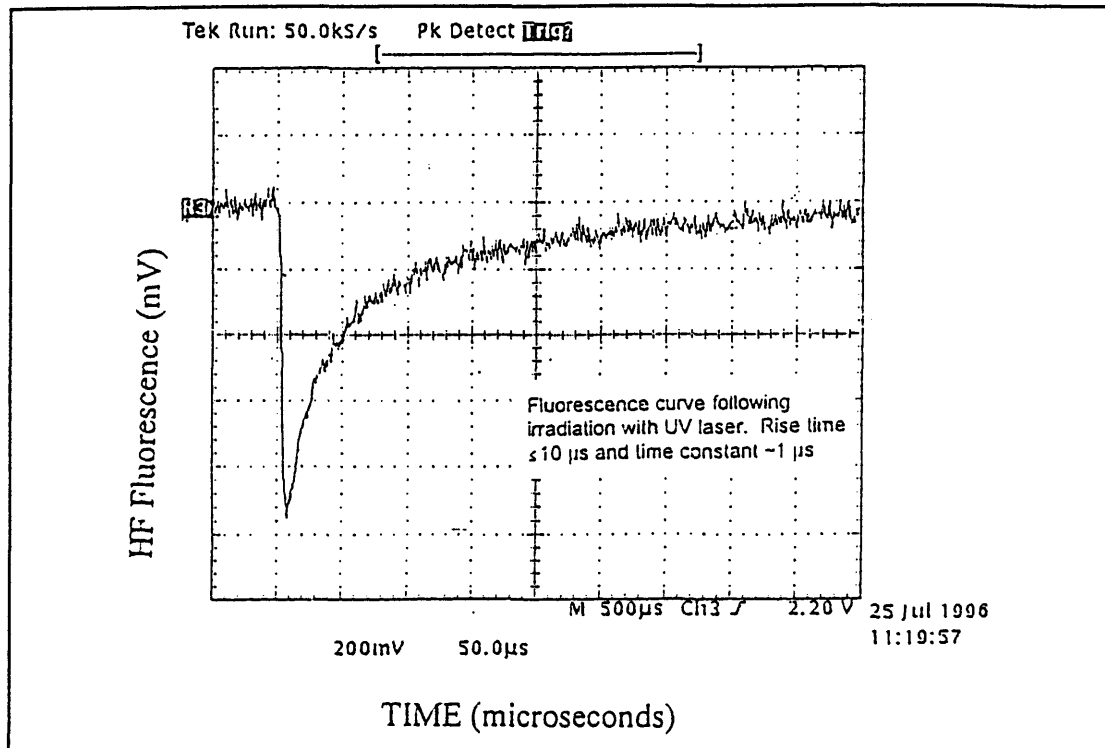


Fig. 82: Fluorescence curve following irradiation with UV laser. Rise time $\leq 10 \mu s$ and time constant $\sim 1 \mu s$.

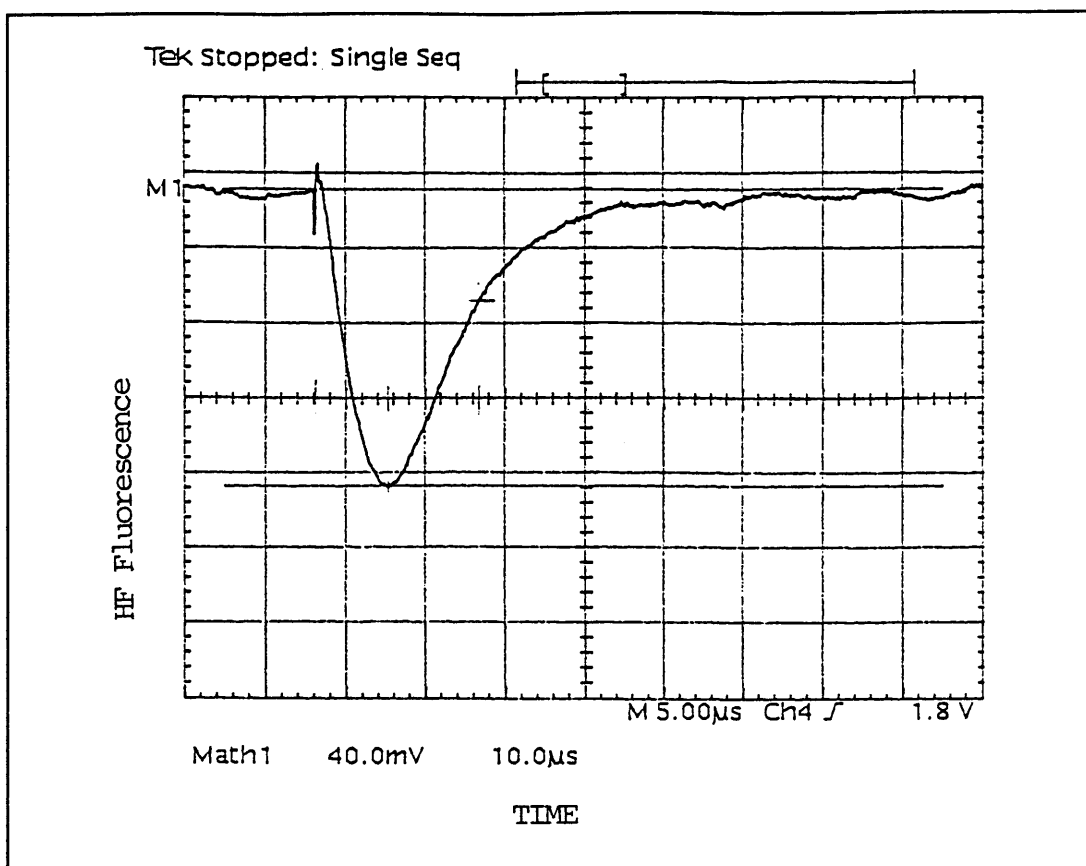
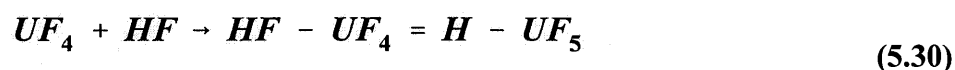
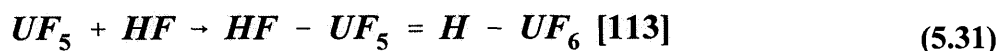


Fig. 83: HF Fluorescence response after UV laser dissociation of UF_6/CH_4 mixture. Pressure 350 Pa; $CH_4 : UF_6 = 5 : 1$; 5% UF_6 .

For the same conditions of detector setup the amplitude of the signal is much reduced, the decay time is faster and no second bump appears, as was detected for the infrared case (other features are similar). In the present case then, the UF_6/CH_4 reaction is absent (as proposed via 5.18 to 5.21) and the fast exchange of energy between CH_4 and HF significantly reduces the signal. Remember here that after ultraviolet photolysis, the undissociated UF_6 remains vibrationally cold. The mechanism involving a complex between UF_6 and CH_4 that was proposed for infrared photolysis is not applicable for the ultraviolet photolysis. Even so, a compound with a U-H bond is also observed in the mass spectra of UV photolysis products. This compound can be formed as follows:



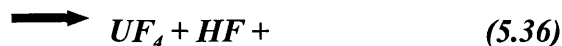
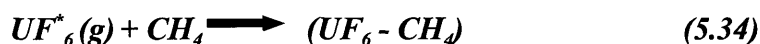
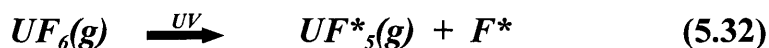
or



These reactions are in principle also possible after infrared photolysis.

How then does UF_4 originate after UV photolysis?

A very important observation is the measurement of a fluorine to uranium F/U, ratio of ~4,8 measured repeatedly in static experiments by W Meyer [68]. This result led to the labelling of the UF_{5-X} compound that has been consistently analysed in experiments. To explain this phenomenon a uranium compound containing uranium in the four, (IV), oxidation state must be present. At this point it will be stated that roughly 25% of the photoproduct UF_5 reacts bimolecularly to produce UF_4 and the observations that support this will then be scanned. We thus have for UV photolysis:



UF_4 (~25%) + UF_5 (75%) = F/U ratio of 4,75. This will explain the observed ~4,8 ratio measured.

In putting forward the reaction sequence, rations (5.32) to (5.36), we take note of the following observations:

1. The quantum efficiency of the summation of reactions must be 1. Therefore, any UF_6 resulting from reaction (5.33) must undergo further reaction to maintain the quantum

efficiency criterium.

2. The $\text{UF}_6(\text{g})$ formed from the disproportionation of vibrational hot UF_5 , is similarly vibrationally very hot.
3. Consequently the $\text{UF}_6(\text{g})^*$ may react via the proposed $(\text{UF}_6 - \text{CH}_4)$ complex as for the infrared situation. The U-H bond fragments in the mass spectra can be explained via this reaction.
4. It is also possible and probable that condensation of UF_4 and HF contributes to the U-H compound phenomenon.
5. The absence of a second smaller burst of HF fluorescence, observed for the infrared photolysis, stems most probably from the fact that we have substantially less vibrationally excited UF_6 , and thus HF from this source. Collisional deactivation of the HF would smooth this feature.

Support for the 1:3 ratio of $\text{UF}_4 : \text{UF}_5$ comes from the measured fragment recoil energy distribution derived from the F atom flight time as shown in figure 84 - from the work presented in reference [110]. This distribution presents the translational energy residing in the F fragments and clearly shows a 1 : 3 ratio for a lower translational energy distributed around a mean of ~ 7 kcal/mole and a higher translational energy distributed around a mean of 17 kcal/mole. Note here that if a lower translational energy resides in a F-atom, a corresponding higher vibrational energy resides in the internal energy of the UF_5 fragment from energy conservation considerations. The available energy is 40 kcal/mole as indicated in figure 84 that must be divided between the two modes referred to.

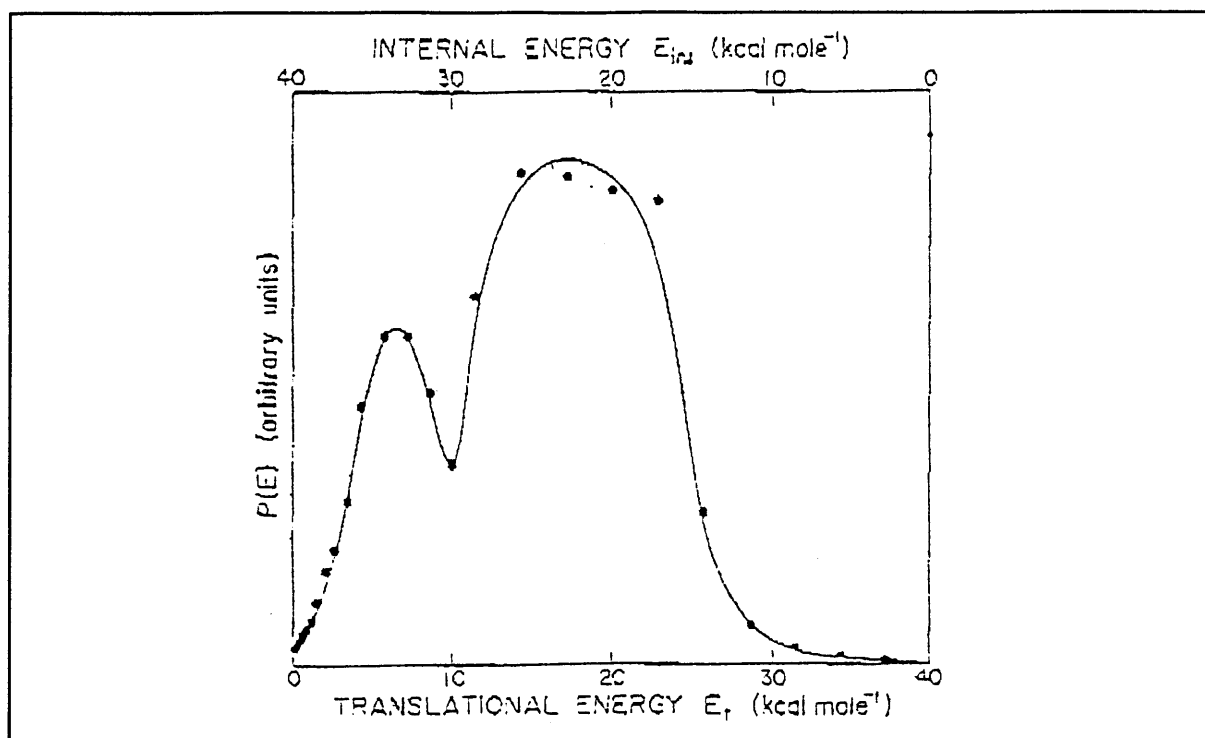
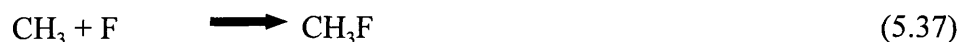


Fig. 84: Fragment recoil energy distribution derived from the F atom flight time in a time-of-flight mass spectrometer [110].

The vibrational energy of the ~25% portion of UF_5 monomers, formed in the photolysis process, contains between any two molecules involved in a bimolecular collisional well in excess of the activation energy of the disproportionation reaction. In competition with this reaction will be the vibrational deactivation which decreases the average energy to below the activation energy, estimated at ~32,7 kcal/mole [114]. Only the monomers at the high end of the vibrational distribution will proceed to react to form UF_4 and UF_6 . This phenomenon can surely not be unique. One can expect that for a UF_6/H_2 mixture where the vibrational deactivation is slower than for CH_4 , the statistical chance for reaction (5.33) to proceed would be increased. This was indeed observed [115]. Subbiah et al performed photolysis of UF_6/H_2 mixtures in the A-X band, and measured a U(IV) concentration of ~30%.

The formation of CH_3F and C_2H_6 following UV photolysis needs to be reconsidered. Consider the secondary radical reactions



It was concluded that CH_3F is formed entirely via this step. Experimentally it was observed that when the $\text{CH}_4 / \text{UF}_6$ ratio is decreased the % of CH_3F relative to C_2H_6 increases up to ~50% depending on the yield of UF_6 dissociation by laser. This hypothesis is based on two assumptions:

1. At small $\text{CH}_4 / \text{UF}_6$ ratio mixtures the lifetime of the F radical is much longer. This “encourages” the reaction of CH_3/F to proceed.
2. The rate constant for reaction (5.37) needed to fit the experimental data is

$$\begin{aligned} K_{\text{CH}_3\text{F}} &\sim 4 \times 10^{-9} \text{ cm}^3 \text{ molecule}^{-1} \text{ s}^{-1} \\ &= 2,4 \times 10^{15} \text{ cm}^3 \text{ mole}^{-1} \text{ s}^{-1} \quad [68] \\ &= 2,4 \times 10^{12} \text{ liter mole}^{-1} \text{ s}^{-1} \end{aligned}$$

The experimentally measured rate constant for reaction (5.37) determined by mass spectrometry, F atoms produced from the reaction of NF_2 with active nitrogen, showed an upper limit of [102]

$$3 \times 10^{13} \text{ cm}^3 \text{ mole}^{-1} \text{ s}^{-1}$$

The value used by W Meyer [68] to explain the trends of reaction (5.37) is more than two orders faster than the experimentally observed value. An upper value to the rate constant can be derived from the collisional theory which implies that the bimolecular rate constant cannot exceed the collisional frequency of the two fragments. We have already seen in our discussion of fission processes that the “looseness or tightness” of the transition state depends intimately on the nature of the potential interaction between the two fragments separating. The same reasoning must apply to the two species taking part in a bimolecular reaction. For the radical recombination of CH_3 and F we expect the transition state to be loose corresponding to the reverse of the simple

bond fission reaction, i.e. the rupture of the C-F bond in CH₃F. For the structure of the activated complex the model previously cited for C-H bond rupture in CH₄ is appropriate. In such a model the CH₃ radical has a planar structure with the C-F bond extended to ~2,8 times the normal equilibrium length of 1,33 Å or 3,724 Å. the collisional frequency with a collisional diameter of this extended bond length will define a rate constant:

$$\begin{aligned}
 k_{CH_3F} &= 4,57 \times 10^{-12} \times (3,724)^2 \times \left(\frac{300}{8,38} \right)^{\frac{1}{2}} \text{ cm}^3 \text{ molecule}^{-1} \text{ s}^{-1} \\
 &= 3,791 \times 10^{-10} \text{ cm}^3 \text{ molecule}^{-1} \text{ s}^{-1} \\
 &= 2,28 \times 10^{14} \text{ cm}^3 \text{ mole}^{-1} \text{ s}^{-1}
 \end{aligned}$$

The rate constant utilized by W Meyer [68] is then more than an order higher than the upper boundary derived from collisional theory. Furthermore, it is clear that steric effects must be included which reduce the experimental value by another order of magnitude (compare [102]).

The lifetime of the F radical at ratios of CH₄ /UF₆ from ~0,5 to 2 needs to be evaluated. From the HF fluorescence response we can see that, in the range considered, the peak of fluorescence never appeared beyond 10 μs. This is substantially shorter than the lifetimes calculated in the referenced work (see table 14).

Table 14: Comparative lifetimes for F radical

CH ₄ /UF ₆	F Lifetime (5% yield)	F Lifetime (10% yield)	F Lifetime (15% yield)	Reference
0,5	50 μs	60 μs	69 μs	[68]
0,5	≤ 10 μs	≤ 10 μs	≤ 10 μs	this work

The writer therefore concludes that neither of the two assumptions, i.e. the F lifetime and the rate constant, is supported by the results of this dissertation. How do we then explain the increased formation of CH₃F as we decrease the CH₄ /UF₆ ratio? A plausible explanation lies in the

deactivation effect than CH_4 has on the lifetime of vibrational hot UF_6 and also UF_5 . The proposed disproportionation reaction of vibrationally hot UF_5 to UF_4 and UF_6 is very much dependent on the CH_4 content. This reaction is promoted at low CH_4 content mixture as it leaves the UF_5^* for a larger time with enough energy that exceeds the activation energy. The UF_6 formed as a result of this reaction also contains excess energy. Vibrationally hot UF_6 , also slowly deactivated when the CH_4 content is low, forms a complex with CH_4 as proposed in reactions (5.18) to (5.21). This is then responsible for the increased production of CH_3F at low CH_4 content mixtures. A quantitative assessment of the formation of CH_3F is not possible presently because more data is needed to execute such an exercise.

5.8 CONCLUSIONS

In summary a number of conclusions derived in this dissertation, which differ profoundly from previous views on the laser photolysis and photochemistry of UF_6 , will be reflected.

1. The presence of the uranium compound, UF_4 , in the laser photolysis products of UF_6 has unambiguously been identified. This is applicable for both infrared and ultraviolet laser photolysis.
2. UF_4 in the monomeric phase has for the first time been identified to have a tetrahedral structure and the four fundamental vibrations have been allocated. It seems reasonable to describe the internuclear forces in terms of the valency force model. The U-F force constant and bond length has been established.
3. The formation of UF_4 most probably results from the disproportionation reaction of vibrationally hot UF_5 monomers. This reaction is more important than the recombination of UF_5 monomer and F radical.

4. In a neat UF_6 gas photolysis by infrared laser the uranium bearing compound is dominantly UF_4 . It is proposed that a smaller amount of HUF_5 , is also produced from the co-condensation of UF_4 and residual HF impurity.
5. Photolysis by infrared laser of UF_6/H_2 mixtures produce similar products to the neat case. An additional amount of HUF_5 is formed due to the increased presence of HF. The HF is formed in copious amounts via the scavenging reaction of H_2 and F.
6. Photolysis of UF_6/CH_4 mixtures produce predominantly UF_5 . This feature is the result of the fast deactivation of vibrationally warm UF_5 monomers by CH_4 to levels of internal energy below the activation energy for the disproportionation reaction to proceed readily. Absorption features of the $\text{HF-UF}_4 = \text{HUF}_5$ compound are evident.
7. A $\text{UF}_6 - \text{CH}_4$ complex between vibrationally hot UF_6 and CH_4 is implicated following the proposed SiH_4 equivalent reactions. This branches into CH_3F and HF fragments. HF can be identified from a second burst of HF fluorescence.
8. Absorption features in the near infrared (NIR) spectrum at $\sim 1,1 \mu\text{m}$ wavelength can be connected to the monomeric UF_4 .
9. Absorption features around 500 nm in the visible spectrum are not characteristic of monomeric UF_5 .
10. The presence of a U-H bond is confirmed by mass spectrometry both in the nascent product and solid samples.
11. XPS spectroscopy confirms the presence of UF_4 in photolysis products.
12. The proposed uranium reactions correlate with scattering experiments with He-Ne laser of temporal formation of photolysis products.

13. There is a great danger in equating the results of static cell irradiations, i.e. repeated laser shots, with the photolysis results in dynamic systems. This has previously blatantly been done.
14. The CH_4/F reaction is very rapid and can quantitatively be analysed by the temporal response of the HF fluorescence. An activation energy ~ 1000 J/mole is derived.
15. The CH_3/F radical combination reaction is unimportant for the formation of CH_3F .
16. Previous assumptions on which the increased formation of CH_3F at low CH_4/UF_6 ratio mixtures were based, are both unfounded.
17. The internal energy content of nascent photolysis products is extremely important to determine the secondary reactions. Equally important is the rate of deactivation in various environments to promote or inhibit secondary reactions.
18. For the CH_4/F reaction a “loose” activated complex, similar to equivalent molecule/radical reactions, gives a good description of the transition state.
19. The HF fluorescence should be treated with care.

CONCLUSIONS

CONCLUSIONS

In this dissertation a large volume of new experimental work has been reported and extensive complimentary theoretical descriptions are put forward. It contributes significantly to create a much better picture of the infrared laser photolysis of UF₆ as applied to laser isotope separation.

It seems appropriate to reflect on the aims envisaged at the onset of the study as summarized in section 1.4.

One of the outstanding achievements is the applications of the RRKM theory and transition state description to successfully predict the unimolecular dissociation rates after laser excitation. Excellent agreement with published experimental work has been demonstrated. This result is based on a sound scientific methodology which makes guess work unnecessary. Two previous attempts in the scientific literature suffered from the lack of a sound mathematical foundation. The additional finding that the dissociation rates are approximately two orders faster than previously anticipated has an extremely beneficial impact on the techno-economic viability of the laser separation process.

The technique of HF fluorescence was successfully applied to measure the nature and rate of vibrational energy transfer between UF₆ molecules. It is proposed for the first time, that a long range interaction between UF₆ molecules is responsible for very fast vibrational energy exchange. The unimolecular dissociation rate, however, is even faster and the effect of vibrational energy quenching can be neglected at the gas densities envisaged. Nevertheless, the proposed mechanism of energy exchange seems to have an influence on secondary reactions as detected by the HF fluorescence technique (chapter V).

The study into the molecular beam method to measure real time dissociation rates were very fruitful to clarify the aspects of the mass spectrometric detection of UF₆ (and its photoproducts).

DOCUMENT NUMBER	VERSION	PAGE	OF
LT100-000000-155-022		183	

In itself, the method did not produce the result anticipated initially - mainly due to the demise of the MLIS project at the AEC. Instead thermal dissociation data were used to calibrate the theoretical description of the unimolecular dissociation of UF_6 .

A large number of aspects concerning the secondary chemical reactions, after photolysis, were investigated and clarified. Some significantly new explanations were put forward. The lingering concern about the interactions of the uranium bearing compound has satisfactorily been addressed. The findings of this dissertation do not predict a loss of isotopic selectivity via reactions previously envisaged. At the end of chapter V the reader will find a summary of the detailed findings.

There are certainly outstanding issues at the end of this project. However, they are of a nature that will not significantly impact on the industrial viability of the I R laser separation of uranium isotopes. In the author's opinion the important aspects of the multi-photon infrared photolysis of UF_6 have been clarified.

At the end of this document there are copies of the scientific contributions that appeared (will appear) in the scientific literature. There have been two papers at international conferences in Harare (Zimbabwe) and Sydney (Australia) marked respectively paper II and III. Furthermore, two full length papers have been accepted for publications in international journals (paper I and IV)

REFERENCES

REFERENCES

REFERENCES

1. R.B. Hall, *Laser Focus*, p 57, September 1982.
2. P.J. Robinson and K.A. Holbrook, *Unimolecular Reactions*, Wiley-Interscience Press, 1972, p68.
3. R.G. Gilbert and S.C. Smith, *Theory of Unimolecular and Recombination Reactions*, Blackwell Scientific Publications, 1990.
4. F.A. Lindemann, *Trans.Faraday Soc.*, 17, p598, 1922.
5. G. Herzberg, *Molecular Spectra and Molecular Structure*, Van Nostran, Princeton N.J., 1945.
6. J.H. Levy, J.C. Taylor and P.W. Wilson, *J.Chem. Soc. Dalton Trans.*, 3, p219, 1976.
7. E. Tschuikow-Roux, *J. Phys. Chem.*, 72, p1009, 1968.
8. W.Forst, *J.Chem. Phys.*, 48, p3665, 1968.
9. E.V. Waage and B.S Rabinovitch, *Chem. Rev.*, 70, p377, 1970.
10. D.L. Bunker and M. Pattengill, *J. Chem. Phys.*, 48, p772, 1968.
11. J. Subbiah, S.K. Sarkar, K.V.S. Rama-Rao and J.P. Mittal, *Indian J.Phys.*, 54B, p121, 1980.
12. Annual Report of Laser Spectroscopy Department, Russian Academy of Sciences for the AEC, 1997.
13. K.P. Schug, H.C. Wagner, *Zeitschrift fur Physikalische Chemie Neue Folge*, Bd. 108, S. 173-184, 1977.
14. P.L. Hildenbrand, *J.Chem. Phys.*, 46, p98, 1967.
15. L.H. Jones and S. Ekberg, *J. Chem. Phys.*, 67, No 6, p2591, 1977.

DOCUMENT NUMBER	VERSION	PAGE	OF
LT100-000000-155-022		185	

16. B.J. Krohn, W.B. Person and J. Overend, *J.Chem.Phys.*, 65, No 3, p969, 1976.
17. J.L. Lyman, *J.Chem. Phys.*, 67, No 5, p1868, 1977.
18. M.C. Gower and K.W. Billman, *Optics Comm.*, 20, No 1, p123, 1977.
19. R.V. Ambartsumyan, Yu A. Garokhov, V.S. Letokhov and G.N. Makarov, *Jetp. Lett.*, 21, No 6, p171, March 1975.
20. H.J. Gerritsen and M.E. Heller, *Appl.Opt. Suppl.*, No 2, p73, 1965.
21. J.T. Yardley, *Introduction to Molecular Energy Transfer*, Academic Press Inc., London, p146, 1980.
22. R.C. Oldenberg, W.W. Rice and F.B. Wampler, *J. Chem. Phys.*, 69, No 5, p2181, 1978.
23. F.B. Wampler, R.C. Oldenberg and W.W. Rice, *Chem.Phys.Lett.*, 54, No 3, p554, 1978.
24. See reference 21, p15.
25. R.D. Levine and R.B. Bernstein, *Molecular Reaction Dynamics and Chemical Reactivity*, Oxford University Press, 1987.
26. W.J. Moore, *Physical Chemistry*, Prentice-Hall, Englewood Cliffs, New Jersey, 1972.
27. See reference 21, p18.
28. S.P. van Heerden, E.G. Rohwer and E Ronander, To be published.
29. E.G. Rohwer, Ph.D. dissertation, University of Stellenbosch, Stellenbosch, South Africa, January 1992.
30. M.D. Nunes, Ph.D. dissertatation, University of Pretoria, Pretoria, 1989.
31. M.Gilbert, J.M. Wulersse, P. Isnard and G. Salvetat, *Proceedings of SPIE Conference, Laser Applications in Chemistry*, Vol 669, p10, 1986.
32. Internal Progress Report, AEC of South Africa, September 1993.
33. See reference 31.

DOCUMENT NUMBER	VERSION	PAGE	OF
LT100-000000-155-022		186	

34. B.H. Mahan, J. Chem. Phys., 46, p98, 1976.
35. Rosenstock H.M., Wallenstein M.B., Wahrhaftig A.L. and Eyring H., Proc. Natl. Acad. Sci. USA 38, p 667, 1952.
36. Cooks R.G., Beynon J.H., Caprioli R.M and Lestr G.R., Metastable Ions, Elsevier, Amsterdam, 1973.
37. Letokhov V.S., Laser Spectroscopy of Highly Vibrationally Excited Molecules, Adam Hilger Press, Bristol, 1989.
38. Dittner P.F. and Datz S., J. Chem. Phys., Vol 68, No 5, March 1978, p 2451.
39. Beaukamp J.L., J. Chem. Phys., 64, p 929, 1976.
40. Ronander E., Internal AEC report LT100-000000-155-013, August 1996.
41. Frenkel J., Z.Phys., 25, p 1, 1924
42. Stuke M, Reisler H and Wittig C., Apply. Phys. Lett., Vol 39, No 3, August 1981, p 201.
43. Armstrong D.P., Harkins D.A., Compton R.N., and Ding D, J. Chem. Phys., 100, No 1, January 1994, p 28.
44. S. Kato, Y. Okada, S Satooka, H. Tashiro and K. Takeuchi, Proceedings of International Symposium on Isotope Separation and Chemical Exchange Uranium Enrichment, Tokyo, (Oct-Nov 1990) 141.
45. Y. Kuga, S. Satooka, H. Tashiro and K. Takeuchi., Proceedings of International Symposium on Isotope Separation and Chemical Exchange Uranium Enrichment, Tokyo, (Oct-Nov 1990) 133.
46. Y. Okada, S. Kato, S. Satooka, H. Tashiro and K. Takeuchi, J Nucl. Sci. Technology., 32, no 11, (Nov 1995) 1174-1180.
47. Y. Okada, S. Kato, K. Sunouchi, S. Satooka, H. Tashiro and K. Takeuchi, Appl. Phys. B62, (1996) 77-81

48. M. Stuke, H. Reisler and C. Wittig, *Appl. Phys. Lett.*, 39, (1981) 201.
49. J.S. Chou, D. Sumida, M. Stuke and C. Wittig, *Laser Chem.*, 1, no 1, (1982) 1-7
50. A.S Sudbo , P.A Schulz, D.J. Krajnovich, Y.T. Lee and V.R Shen, *Opt. Lett.*, 4, no 7, (1979) 219
51. D.P. Armstrong, Ph.D. dissertation, The University of Tennessee, Knoxville, Tennessee, (1992).
52. D.P. Armstrong, D.A. Harkins, R.N. Compton and D. Ding, *J. Chem. Phys.*, 100, no 1, (1994) 28.
53. H.G.C. Human, AEC of South Africa, private communication.
54. P. Rabinowitz, A. Kaldor, A. Gnauck, R.L. Woodin, and J.S. Gethner, *Optics Lett.* 7, no 5, (1982) 212-214.
55. M. Gilbert, J.M. Weulersse, P. Isnard and G. Salvetat, Congress of the Society of photo-optical instrumentation Engineers (SPIE), Quebec (Canada), (June 1986).
56. E. Ryabov, Russian Institute of Spectroscopy, private communication.
57. M. Menghini, P. Morales, P. Dore and M.I. Schisano, *J. Chem. Phys.*, 84, no 11, (1986) 6521.
58. P. Dore, M.I. Schisano, M. Menghini and P. Morales, *Chem. Phys. Lett.*, 116, no 6, (1985) 521-524.
59. Contracted to the University of Stellenbosch.
60. J. J. Katz and E. Rabinowitch, *The chemistry of Uranium*, Daver, New York (1951), p 389.
61. A. S. Wolf, J. E. Posey and K. E. Rapp, *Inorg. Chem.*, Vol 4 (1975), p 751.
62. D. L. Hildenbrand, *J. Chem. Phys.*, 66 (1977), p 4788.
63. Y. Kuga, S. Satooka and K. Takeuchi, *Applied Physics B*, Vol 63 (1996), p 293.

64. Courtesy of C. J. Liebenberg.
65. Figures produced by C. J. Liebeberg.
66. W.J. Moore, *Physical Chemistry*, Longmans, London (1985), p 534.
67. J. L. Lyman and R. Holland, *J. Phys. Chem.*, Vol 91 (1987), p 4821.
68. W.C.M.H. Meyer, Ph.D. dissertation, University of Pretoria, Pretoria (RSA) (1992).
69. J. Onoe, N. Uehara, Y. Iimura, T. Oyama, O. Suto, Y. Shimazaki and K. Takeuchi, *Journal of Nuclear Materials*, Vol 207 (1993), p 205.
70. Spectra produced by W.C.M.H. Meyer, AEC of South Africa
71. J.G. Conway, *J. Chem. Phys.*, Vol 31 (1959), p 1002.
72. V.S. Ezhov, R.A. Akishim and N.G. Rambidi, *Zh. Strukt. Khim.*, Vol 10 (1969), p 571.
73. L.N. Gorokhov, V.K. Smirnov and Yu S Khodeev, *Zh. Fiz. Khim.*, Vol 58 (1984), p 1103.
74. K.H. Lau and D.L. Hildenbrand, *J. Chem. Phys.* Vol 76 (1982), p 2646.
75. A.A. Belyaeva and Yu M. Golubev, *Opt. Spectrosc. (USSR)*, Vol 63 No 3 (1987), p 299.
76. W. Krasser and H.W. Nürnberg, *Spectrochimica Acta*, Vol 26A (1970), p 1059.
77. J.H. Prior, Ph.D dissertation, University of Port Elizabeth (1987).
78. R.S. McDowell, L.B. Asprey and R.T. Paine, *J. Chem. Phys.*, Vol 61 (1974), p 3571.
79. L.H. Jones and S. Ekberg, *J. Chem. Phys.*, Vol 67 No 6 (1977), p 2591.
80. Calculations done on request by M. Govender, AEC of South Africa.
81. J.M Dyke, N.K. Fayad, A. Morris and J.R. Trickle, *J. Chem. Phys.*, Vol 72 (1980), p 3822.
82. V.M. Kovba and I.Y. Chikh, *Zh Strukt Khim.*, Vol 24 (1983), p 172.

83. V.N. Bukhmarina, Yu B Predtechenskii and V.G. Shklyarik, *Opt. Spectrosk.*, Vol 62 (1987), p 1187.
84. G. Herzberg, *Infrared and Raman Spectra of Polyatomic Molecules*, Van Nostrand Reinhold Co, New York, 1945.
85. Yu N. Tumanov, *Russian Journal of Inorganic Chemistry*, Vol 13 No 6 (19968), p 782.
86. E Catalano, R.E. Barletta and R.K. Pearson, *J. Chem. Phys.*, Vol 70 No 7 (1979), p 3291.
87. K. R Kunze, R.H. Hauge and J.L. Margrave, *J. Chem. Soc. Dalton Trans.*, (1978), p 433.
88. R.M. Badger, *J. Chem. Phys.*, Vol 3 (1935), p 710.
89. R. T Paine, R.S. Mc Dowell, L.B. Asprey and L.H. Jones, *J. Chem. Phys.*, Vol 64 (1976), p 3081.
90. A. Rosen and B. Fricke, *Chem. Phys. Lett.*, Vol 61 No 1 (1979), p 75.
91. K. C Kim and G.A. Laguna, *Chem. Phys., Lett.*, Vol 82 No 2 (1981), p 292.
92. Hancke, MSc dissertation, Rand Afrikaans Universiteit (1987).
93. *Gmelin Handbook, Omnity - Gesellschaft Nachf. Leopold Zechnall, Stuttgart (1966).*
94. P. Dore, M.I. Schisano, M. Menghini and P. Morales, *Chem. Phys. Lett.*, Vol 116 No 6 (1985), p 521.
95. Courtesy of H. J. Strydom, AEC of South Africa.
96. H.G.C. Human, personal communication, AEC of South Africa.
97. E. Borsella, F. Catoni and G. Freddi, *J. Chem. Phys.*, Vol 73 No 1 (1980), p 316.
98. W.B. Lewis, F.B. Wampler, E.G. Huber and G.C. Fitz-gibbon, *J. of Photochemistry*, Vol 11 (1979), p 393.
99. Institute of Spectroscopy, Annual Report Troitzk, Russia (1993).

DOCUMENT NUMBER	VERSION	PAGE	OF
LT100-000000-155-022		190	

100. J.L. Lyman, g. Laguna and N.R. Greiner, J. Chem. Phys. Vol 82 No 1 (1985), p 175.
101. J.W. Eerkens, D.G. Garrett, B.C. Olson, K.J. Falk and J.H. Wang, United States Patent 5666639, Sept. 9, 1997, P 34.
102. H.G. Wagner, J. Warnatz and C. Zetzsch, An. Asoc. Quim. Argent., Vol 59 (1971), p 169.
103. G.C. Fettis, J.H. Knox and A.F. Trotman-Dickenson, J. Chem. Soc., (1960) p 1064.
104. G.C. Fettis, J. H. Knox and A.F. Trotman-Dickenson, Canadian J. Chem., Vol 38 (1960), p 1643.
105. R. Foon and G.P. Reid, Trans. Faraday Soc., Vol 67 (1971), p 3513.
106. R. Foon, G . P. Reid and K.B. Tait, J. Chem. Soc., Faraday Trans., 1, Vol 68 (1972), p 1131.
107. Y. Okada, K. Sunmouchi, S. Kato, S. Satooka, H. Tashiro and K. Takeuchi, j. Nuclear Science and Tech., Vol 31 No 2 (1994), p 40.
108. Semi-annual Report of the Laser Spectroscopy Department, Russian Academy of Sciences, Troitzk, Moscow (1995).
109. M.R. MacPherson, M.J. Pilling and M.J.C. Smith, Chem.Phys.Lett., Vol 94 No 4 (1983), p 430.
110. P.M. Kroger, S.J. Riley and G.H. Kwei, J. Chem. Phys., Vol 68 No 9 (1978), p 4195.
111. Y. Kuga, S. Satooka and K. Takeuchi, Appl. Phys. B63, (1996), p 293.
112. A.L. Myerson and J.J. Chludzinski, J.Che., Vol 85 (1981), p 3905.
113. J. Subbiah, S.K. Sarkar, K.V.S. Rama Rao and J.P. Mittal, Indian J. Phys., Vol 54 (1980), p 121.

DOCUMENT NUMBER	VERSION	PAGE	OF
LT100-000000-155-022		191	

APPENDIX A

APPENDIX A

COMPUTING THE DENSITY OF VIBRATIONAL STATES

Many occasions arise in which it is useful and necessary to determine the vibrational state density. In the context of this dissertation the need to evaluate this quantity is imperative to compute the unimolecular dissociation rate of UF_6 for the laser instigated process. The role of recombination and bimolecular reactions in the final yield of the dissociation reaction also utilizes the density of vibrational states.

The simplest approximation to the sum and densities of vibrational states is obtained by treating the molecule as a set of classical harmonic oscillators. Some corrections to the obtained mathematical formulations are, however, necessary to make the expressions useful. This will be considered in the following analysis:

In the simplest case we may consider a molecule made up of s normal modes of identical frequency ν and containing N quanta of excitation. From elementary statistical arguments the number of different ways to distribute N indistinguishable quanta among s oscillators is [A1]

$$\eta = \frac{(N + s - 1)!}{N!(s - 1)!} \quad (A1)$$

In the limit that N is large, or ν is small, we can estimate the quantity in A1 as follows by utilizing Stirling's approximation for large N

$$\ln N! = N \ln N - N \quad (A2)$$

Taking then $\ln \eta$ and also for large N , i.e. $N \gg s$, we find

$$\eta \sim N^{s-1}/(s - 1)! \quad (A3)$$

Now, if we take the density of states just as

$$\rho(E_v) = \eta/h\nu \tag{A4}$$

and we replace N with $E_v/h\nu$ where E_v is the amount of internal vibrational energy, then

$$\rho(E_v) = \frac{E_v^{s-1}}{(s-1)! (h\nu)^s} \tag{A5}$$

This is a classical expression which is valid in the limit as $h\nu$, the quantum energy, is small or E_v is large. It is very convenient for rapid estimations.

Improvements to expression A5 have been suggested by Marcus and Rice [A2]. They suggested that since a quantized oscillator with a non-fixed energy E_v has a total vibrational energy above the ground state of $E_v + E_z$, where E_z is the zero-point energy and is equal to $\frac{1}{2}h\nu$, we should compare the density of vibrational energy states at $(E_v + E_z)$ rather than at E_v . The classical expression A5 must thus be modified to give the Marcus-Rice approximation:

$$\rho(E_v) = \frac{(E_v + E_z)^{s-1}}{(s-1)! \prod_i h\nu_i} \tag{A6}$$

where

$$E_z = \sum_{i=1}^s (\frac{1}{2}h\nu_i)$$

Although this approximation is an improvement to the classical expression, A5, it is still not accurate and leads to an over-estimation of the number of states at any level.

A further significant improvement was suggested by Rabinovitch and Diesen [A3] followed by elaborations by Whitten and Rabinovitch. The first two researchers deliberated that only an appropriate fraction of the zero-point energy should be added to E_v and introduced the empirical

factor \mathbf{a} into expression A6 giving.

$$\rho(E_{\nu}) = \frac{(E_{\nu} + aE_z)^{(s-1)}}{(s-1)! \prod h\nu_i} \quad (\text{A7})$$

The factor \mathbf{a} has a value between 0 and 1 and the comparison of expression A7 with the result of direct counts of the density of states, makes it possible to determine the appropriate value of \mathbf{a} required to give a correct result for a given molecule at any energy level. Values for \mathbf{a} have been determined for a number of cases and the importance of this approach depends on the consequent ability to predict suitable values for \mathbf{a} for unknown cases. We shall evaluate this parameter for UF_6 .

First, we introduce a further elaboration by the researchers Whitten and Rabinovitch [A4]. The typical variation of \mathbf{a} with increasing internal vibrational energy of a molecule, is to increase, approaching unity at high energies. This is in accord with the classical approximation of equation A6. It was found empirically that the values of \mathbf{a} depend only on the distribution of the molecular vibrational frequencies, i.e. the values of \mathbf{a} are lower for a molecule whose vibrations have widely different frequencies than for one containing many vibrations but with a small spread in the actual frequencies. Whitten and Rabinovitch introduced a dispersion factor which quantifies the standard deviation:

$$\beta = \frac{s - 1}{s} \frac{\langle \nu^2 \rangle}{\langle \nu \rangle^2} \quad (\text{A8})$$

The modified frequency dispersion parameter β is defined by the ratio of the mean frequency, $\langle \nu \rangle$, and the mean-square frequency $\langle \nu^2 \rangle$, of a molecule. The value of the parameter β varies from about unity for molecules with a narrow frequency spread to about two for molecules with a wide frequency spread. As an illustration of this feature the β values for the molecules SF_6 , UF_6 and $\text{Ni}(\text{CO})_4$ are tabulated in table A1. The value for β for UF_6 was calculated from the vibrational frequencies given in reference [A5] which are representative values derived from a number of papers as cited in the reference. It remains to define a simple analytical relationship between \mathbf{a}

and β and to evaluate its applicability to the case of UF_6 to correctly describe the density of vibrational states.

Table A-1

Values of β for different compounds

Molecule	Vibrational Frequencies (cm ⁻¹)	β
SF_6	965 (3) 772 642 (2) 617 (3) 525 (3) 370 (3)	1,03
UF_6	668,2 534,5 (2) 627,7 (3) 187,5 (3) 201 (3) 143 (3)	1,28
$\text{Ni}(\text{CO})_4$	2057 (3) 2040 545 (3) 460 (2) 422 (3) 381 300 (3) 79(5)	2,04

To this purpose it was found more illustrative to use the reduced energy $E' = E_v/E_z$ rather than the vibrational energy E_v itself. Whitten and Rabinovitch put forward the following analytical relationship

$$a = 1 - \beta W(E') \quad (\text{A9})$$

where $W(E')$ is a unique function of E' described adequately by the following equations

$$W = 5E' + 2,73E'^{0,5} + 3,51^{-1} \text{ for } 0,1 < E' < 1$$

and

$$W = \exp(-2,4191 E'^{0,25}) \text{ for } 1 < E' < 8 \tag{A10}$$

Finally, then the density of vibrational states, which we will now denote by $\rho(E_v)$, may be obtained by:

$$\rho(E_v) = \frac{(E_v + aE_z)^{S-1}}{(S-1)! \prod_i h \nu_i} \left[1 - \beta \frac{dW}{dE'} \right] \tag{A11}$$

This completes what has become known as the Whitten-Rabinovitch approximation that has been utilized extensively to determine the densities of vibrational states. Tardy et al [A6] have deduced a more complex and slightly more accurate form of this equation, A11. The direct counting of vibrational states utilizing the Beyer-Swinehart algorithm [A7] has also been proposed but will not be utilized for the case of UF₆. The extensive use of the Whitten-Rabinovitch approximation necessitates an analysis for our case.

The Microsoft Program AXUM was used to compute the density of vibrational states for UF₆ with the following inputs data:

1. Table A-2 contains the frequencies corresponding to the six fundamental vibrational modes.

Table A-2 - UF₆ (O_h point group) fundamental vibrational frequencies

i*	Spectroscopic	ν _i (cm ⁻¹)	Assignments
	Notation		
1	A _{1g}	668,2	ν (U-F) stretch
2 (2)	E _g	534,5	ν (F-U-F) stretch
3 (3)	F _{1u}	627,7	ν (U-F) stretch
4 (3)	F _{1u}	187,5	δ (F-U-F) bend
5 (3)	F _{2g}	201	δ (F-U-F) bend
6 (3)	F _{2u}	143	δ (F-U-F) bend

*degeneracy in parenthesis

2. β = 1,28
3. E_z = 2598 cm⁻¹
4. S = number of modes = 15

Two sets of computational results were produced. A range of 2000 to 5000 cm⁻¹ for the vibrational energy were produced to compare to the direct spectroscopical analysis that follows later and a range of 5000 cm⁻¹ to 30 000 cm⁻¹. The dissociation energy of UF₆ is taken as 68,8 kcal/mole [A8] which equates to 24 195 cm⁻¹. The latter range therefore extends to about 25% above the dissociation level (figure A1).

As stressed previously the corrections that incorporate the parameters W and β were necessitated to correct for the density of vibrational levels at lower energies which for UF₆ lies typically below 5 000 cm⁻¹. The computation showed that W decreases from a value of 0,1 at E_v = 2000 cm⁻¹, i.e. E' = 0,77, to W = 0,06 at E_v = 5000 cm⁻¹, E' = 1,92, and at E_v = 12700, E' = 4,89, it is for all practical purposes zero (look at table A-3).

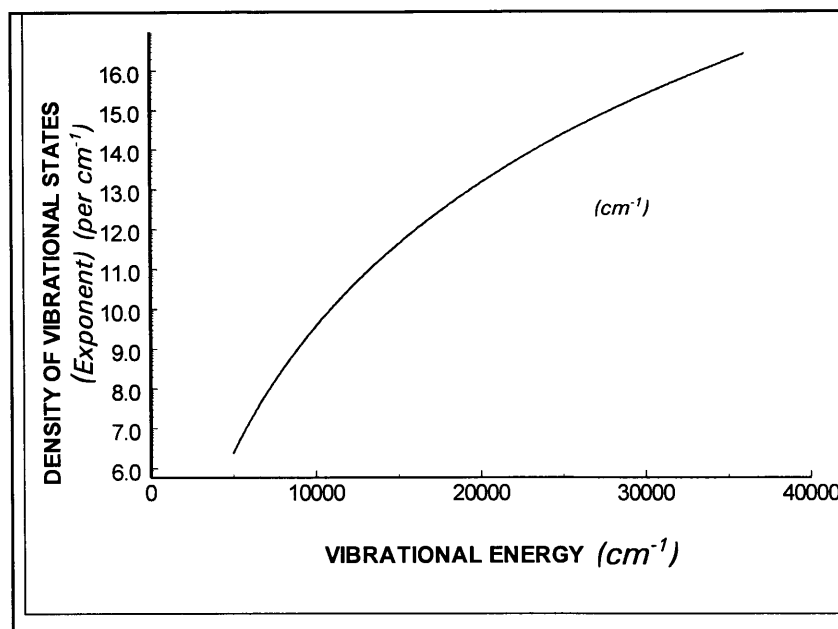


Fig. A1 - Density of vibrational states for the UF_6 molecule

Table A-3 Computational values for the parameters W and a for the molecule UF₆

Vibrational Energy (cm ⁻¹)	E'	W	a
2000	0,77	0,10	0,87
3000	1,15	0,08	0,90
4000	1,54	0,07	0,91
5000	1,92	0,06	0,93
6000	2,31	0,05	0,94
7000	2,73	0,04	0,94
8000	3,08	0,04	0,95
9000	3,46	0,04	0,05
10000	3,85	0,03	0,96
12000	4,62	0,03	0,96
14000	5,39	0,03	0,97
16000	6,16	0,02	0,97
18000	6,93	0,02	0,97

Furthermore, the value of the derivative of W with respect to E' as contained in expression A11 has the value 0,02 at E_v = 5000 cm⁻¹ and at E_v = 12800 cm⁻¹ becomes zero. It is therefore superfluous to include the correction in the square brackets of the expression A11 as it contributes nothing to the obtained values for the density of vibrational states in the case of UF₆. The writer consequently searched for a much simpler expression which also eases the computational process. It turns out that equation A7 is adequate to describe the density of states for UF₆ in the range higher than 5000 cm⁻¹ if the definition of a is altered as follows:

$$a(E_v) = (E_v - 350)/E_v \quad (\text{A12})$$

Comparative values for ρ(E_v) for the range 5000 cm⁻¹ to 14000 cm⁻¹ are shown in table A4

Table A-4 Comparative values for the density of vibrational states for UF₆

Energy level (cm ⁻¹)	Whitten-Rabinovitch Approximation	Proposed expression A12 For parameter a
5000	2,49 x 10 ⁶	2,44 x 10 ⁶
6000	1,54 x 10 ⁷	1,50 x 10 ⁷
7000	7,62 x 10 ⁷	7,39 x 10 ⁷
8000	3,17 x 10 ⁸	3,10 x 10 ⁸
9000	1,15 x 10 ⁹	1,12 x 10 ⁹
10000	3,75 x 10 ⁹	3,66 x 10 ⁹
11000	1,11 x 10 ¹⁰	1,10 x 10 ¹⁰
12000	3,03 x 10 ¹⁰	2,98 x 10 ¹⁰
13000	7,76 x 10 ¹⁰	7,64 x 10 ¹⁰
14000	1,87 x 10 ¹¹	1,87 x 10 ¹¹

The Whitten-Rabinovitch approximation has been extensively tested for the majority of cases and very good agreement, with direct count approaches. This is so for molecules with substantial vibrational energy. For lower vibrational energies significant deviations, up to 40%, have been illustrated for simple molecules [A9]. There are many examples [A10] for the density of levels of molecules of comparable size to be a factor of 3 to 10 larger than ρ_{WR} calculated using the Whitten-Rabinovitch approximation. An example is the molecule ketene, CH₂CO. It is necessary to understand and be able to predict these unexpectedly large densities of states in order for RRKM theory to be completely quantitative and predictive.

In the following section we shall compare the methodology offered hitherto to a direct spectroscopical method to establish the validity of the former approach.

DENSITY OF VIBRATIONAL STATES (ALTERNATIVE METHOD)

GENERAL

Consider a polyatomic molecule assembled from N nuclei. We would need 3N coordinates to describe their motion: there are 3N degrees of freedom in the molecular system. Six of the

degrees of freedom are appropriated to the translational and rotational motion of the molecule and this leaves $(3N-6)$ degrees of freedom to specify the vibrational motions. For a linear molecule this number turns out to be $(3N-5)$ vibrational degrees of freedom.

Therefore the UF_6 molecule, which is of the spherical top type and belongs to the highly symmetrical O_h point group, has 15 normal modes of vibration since the number N of nuclei is seven. It is, however, sufficient to consider only six different modes: ν_1 , ν_2 , ν_3 , ν_4 , ν_5 , and ν_6 , since the molecule exhibits two-fold and three-fold degeneracies (look at table A-1). A schematic diagram of these modes are shown below in figure A2.

These modes may be divided into two categories representing respectively the stretching modes ν_1 , ν_2 and ν_3 as well as the bending modes ν_4 , ν_5 , and ν_6 . For UF_6 the former group covers the energy range 0,066eV to 0,083 eV, i.e. 534 cm^{-1} to 668 cm^{-1} , whilst the latter group covers the energy range 0,018 eV to 0,025 eV, i.e. 143 cm^{-1} to 201 cm^{-1} .

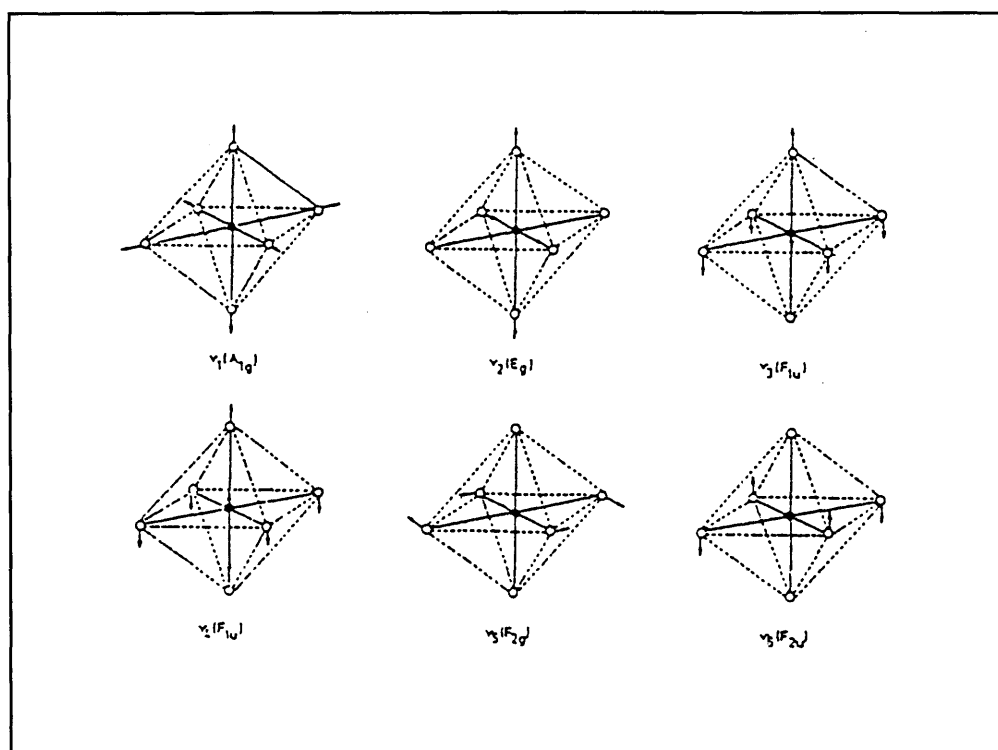


Fig. A2 - Fundamental modes of vibration for an XY_6 type spherical-top molecule. The symbols in parentheses represent symmetry species.

The observed infrared spectrum for molecules such as UF₆ exhibits transitions of the type $\nu_i + \nu_j - \nu_i$ near to the ν_j band. These are called “hot bands” which originates from vibrationally excited states ν_i to upper states $\nu_i + \nu_j$. These hot-bands complicate the spectral analysis for room temperature UF₆. Consequently an observed spectrum for UF₆ is mainly caused by the superposition of many hot-bands rather than by the normal series of transitions from the vibrational ground state.

DESCRIPTION OF VIBRATIONAL STATES

In the vibrational spectrum we have, in addition to the mentioned six fundamental modes, also overtones, i.e. $2\nu_3, 3\nu_3, \dots$, and combination tones, $\nu_i + \nu_j$ etc. The population of molecules in thermal equilibrium is generally given by the Boltzmann distribution law

$$P_i = (\text{cons}) D_i \exp(-E_i / k_B T) \quad (\text{A13})$$

where D_i = the degeneracy or total statistical weight of the i -th state

E_i = energy of the i -th state.

If we take P_i to be the fractional population, i.e. set the summation of P_i over all states equal to unity, then equation A13 can be rewritten as:

$$P_i = \frac{D_i}{Z} \exp(-E_i / k_B T) \quad (\text{A14})$$

In this formulation Z is a function of temperature T , and physically represents the “effective” number of states.

On the assumption the molecular vibrations are harmonic, the energy E_i can be presented as a linear combination of the fundamental vibrations

$$E_i = \sum_{\beta=1}^6 V_{\beta i} E_{\beta} \quad (\text{A15})$$

where $V_{\beta i}$ is the vibrational quantum number of the i -th state and E_{β} the harmonic energy of the fundamental vibration β . The degeneracy D_i should be represented by the product of statistical weights $g_{\beta i}$ of the fundamental vibrations

$$D_i = \prod_{\beta=1}^6 g_{\beta i} \quad (\text{A16})$$

The statistical weights $g_{\beta i}$ is given according to the following relations:

$$g_{\beta i} = \begin{cases} 1 & \text{for } \beta = 1 \\ V_{\beta} + 1 & \text{for } \beta = 2 \\ \frac{1}{2}(V_{\beta} + 1)(V_{\beta} + 2) & \text{for } \beta = 3,4,5 \text{ and } 6 \end{cases} \quad (\text{A17})$$

The degeneracy D_i can therefore be simplified to

$$D_i = \frac{1}{16} (V_2 + 1) \prod_{\beta=3}^6 (V_{\beta} + 1)(V_{\beta} + 2) \quad (\text{A18})$$

In terms of the harmonic oscillator assumption it can be shown [A11] that the summation that defines the vibrational partition function, $Z_v(T)$ can be analytically carried out to yield

$$Z_v(T) = \prod_{\beta=1}^6 [1 - \exp(-E_{\beta}/k_B T)]^{-d_{\beta}} \quad (\text{A19})$$

where d_{β} is the degeneracy of the fundamental vibration β namely

$$d_{\beta} = \begin{cases} 1 & \text{for } \beta = 1 \\ 2 & \text{for } \beta = 2 \\ 3 & \text{for } \beta = 3,4,5,6 \end{cases} \quad (\text{A20})$$

A computational approach to describe the density of vibrational states can now be derived [A11].

For a given energy E let $G(E)$ be the summation over all the vibrational states up to E , including E . We can then express as follows:

$$G(E) = \sum_{0 < E_i < E} D_i \quad (\text{A21})$$

where D_i is the degeneracy of the i -th state as expressed in A16. If we now consider the number of vibrational states in an energy range from E to $E + dE$ which is defined as $G(E + dE) - G(E)$ and in the limit when dE tends to zero we find that

$$G(E + dE) - G(E) = \frac{dG}{dE} dE = g(E)dE \quad (\text{A22})$$

where $g(E)$ will represent the density of vibration states. Following this definition we express

$$g(E) = \frac{d}{dE} G(E) \quad (\text{A23})$$

In practice we find that $G(E)$ varies according to a stepwise function for very low vibrational energy ranges, i.e. in the discrete levels of the UF_6 molecule. The vibrational density level rises very fast for higher levels and we may assume a smooth function for $G(E)$. We accordingly express $G(E)$ as

$$\ln G(E) = P_n (\ln E) \quad (\text{A24})$$

where $P_n(x)$ is a polynomial of the fifth order,

$$P_5(x) = A_0 + A_1x + A_2x^2 + A_3x^3 + A_4x^4 + A_5x^5 \quad (\text{A25})$$

Hence, the density of vibrational states, $g(E)$, can be written as:

$$g(E) = \frac{P_5' (\ln E)}{E} \exp [P_5 (\ln E)] \quad (\text{A26})$$

with P'_5 the first derivative of P_5 with respect to E .

Utilizing the expressions put forward in this section we can calculate the density of vibrational states and subsequent to that perform a least squares fit to find the coefficients of P_5 in the region 2000 cm^{-1} to 5000 cm^{-1} . This was done with the purpose of comparing our results with the Whitten-Rabinovitch approximation where the latter is most likely to be inaccurate [A12].

This exercise was performed using the microsoft program AXUM and the coefficients specified in table A5.

Table A-5 - :Coefficients of polynomial P_5 for UF_6 [A11].

$2000 \text{ cm}^{-1} \leq E \leq 5000 \text{ cm}^{-1}$					
A_0	$A_1 \times 10$	$A_2 \times 10^2$	$A_3 \times 10^4$	$A_4 \times 10^3$	$A_5 \times 10^4$
-5,0	5,872	-4,957	4,974	5,816	-1,437

If we now compare the results of the spectroscopic approach and the Whitten-Rabinovitch approximation, for the the energy range 2000 cm^{-1} to 5000 cm^{-1} , we find that the values are in excellent accord as verified by table A-6. Therefore it is concluded that the Whitten-Rabinovitch description can be used with confidence for the molecule UF_6 . The simplified definition for the parameter \mathbf{a} in expression A12 also greatly simplifies the computational procedure.

Table A-6: Comparison of the Whitten-Rabinovitch methodology and the spectroscopical approach for the density of vibrational states for UF_6 .

Energy Level (cm^{-1})	Whitten-Rabinovitch	Spectroscopical Approach
2000	$1,14 \times 10^3$	$1,13 \times 10^3$
3000	$2,57 \times 10^4$	$2,50 \times 10^4$
4000	$3,10 \times 10^5$	$2,99 \times 10^5$
5000	$2,51 \times 10^6$	$2,44 \times 10^6$

APPENDIX A - REFERENCES

- A1. **Gilbert R G and Smith SC, Theory of Unimolecular and Recombination Reactions, Blackwell Scientific Publications (1990).**
- A2. **Marcus RA and Rice OK, J. Phys. Coll. Chem., Vol 55, p894 (1951).**
- A3. **Rabinovitch and Diesen. See disccsion in Rabinovitch BS and Setser DW, Adv. Photochem, Interscience (New York) Vol 3 (1964).**
- A4. **Whitten G Z and Rabinovitch BS, J. Chem Phys., Vol 38, p2466 (1963).**
- A5. **Robinson P.J. and Holbrook KA, Unimolecular Reactions, Wiley-Interscience: New York (1972).**
- A6. **Tardy DC, Rabinovitch BS and Whitten GZ, J. Chem. Phys. Vol 48, p1427(1968).**
- A7. **Beyer T and Swinehart D F, Comm. Assoc. Computt. Mechanics, Vol 16, p379 (1973).**
- A8. **Hildenbrand DL, J. Chem. Phys, Vol 66, p4788 (1977).**
- A9. **Polik W F Guyer DR and Moore CB, J. Chem.Phys, Vol 92, p3453 (1990).**
- A10. **Choi YS and Moore CB, J.Chem Phys. Vol 94, p5414 (1991).**
- A11. **Jackson D, Los Alamos Scientific Laboratory Report, number LA-6025-MS (1975).**

DOCUMENT NUMBER	VERSION	PAGE	OF
LT100-000000-155-022		206	

APPENDIX B

APPENDIX B

ROTATIONAL PARTITION FUNCTION AND MOMENTS OF INERTIA FOR UF₆

1. ROTATIONAL PARTITION FUNCTION

If a molecular system is capable of existing in a series of quantized energy levels which we can denote by E_0, E_1, E_2, \dots , then the general definition of the partition function, Q , for the molecule is defined as

$$\begin{aligned} Q &= g_0 \exp(-E_0/kT) + g_1 \exp(-E_1/kT) + \\ &\quad g_2 \exp(-E_2/kT) + \dots \\ &= \sum_{i=0}^{\infty} g_i \exp(-E_i/kT) \end{aligned} \quad (B1)$$

where g_i is the degeneracy or statistical weight of the energy level E_i . This can also be seen as the number of physically distinguishable quantum states of that energy. For a given system the numerical value for Q depends only on the temperature and the zero energy chosen for the system. If the zero energy is downshifted by an amount of ΔE and all the energies increased by ΔE , each term in expression B1 must be multiplied by $\exp(-\Delta E/kT)$ which implies that Q must be simply multiplied by the same factor. The different degrees of freedom commonly considered for molecular systems are the electronic, vibrational, rotational and translational and the respective partition functions are denoted Q_e, Q_v, Q_r and Q_t . It can be easily shown that if the energies are simply additive, i.e. the total energy can be written as $E_{\text{tot}} = E_e + E_v + E_r + E_t$, then the total molecular partition function is the product of the individual partition function

$$Q_{\text{tot}} = Q_e \cdot Q_v \cdot Q_r \cdot Q_t \quad (B2)$$

The rotational energy levels of a molecule may be obtained by solving the Schrödinger equation. There is, fortunately, a short-cut if we apply the classical expression for the energy of a body that

rotates around some arbitrary axis, say x.

$$E = \frac{1}{2} I_{xx} \omega_x^2 \tag{B3}$$

Where ω_x denotes the angular velocity about the x-axis and I_{xx} is the moment of inertia. The two subscripts on I is for a technical reason which we shall accept for the moment. A body that can rotate about three axis, x, y and z, has energy.

$$E = \frac{1}{2} I_{xx} \omega_x^2 + \frac{1}{2} I_{yy} \omega_y^2 + \frac{1}{2} I_{zz} \omega_z^2 \tag{B4}$$

Further discussion is more convenient if we consider the different types of molecules. For our purpose the spherical top molecules, e.g. UF_6 and CH_4 , are of interest and we shall consider them only. Our target molecules have structures as depicted in figure B1.

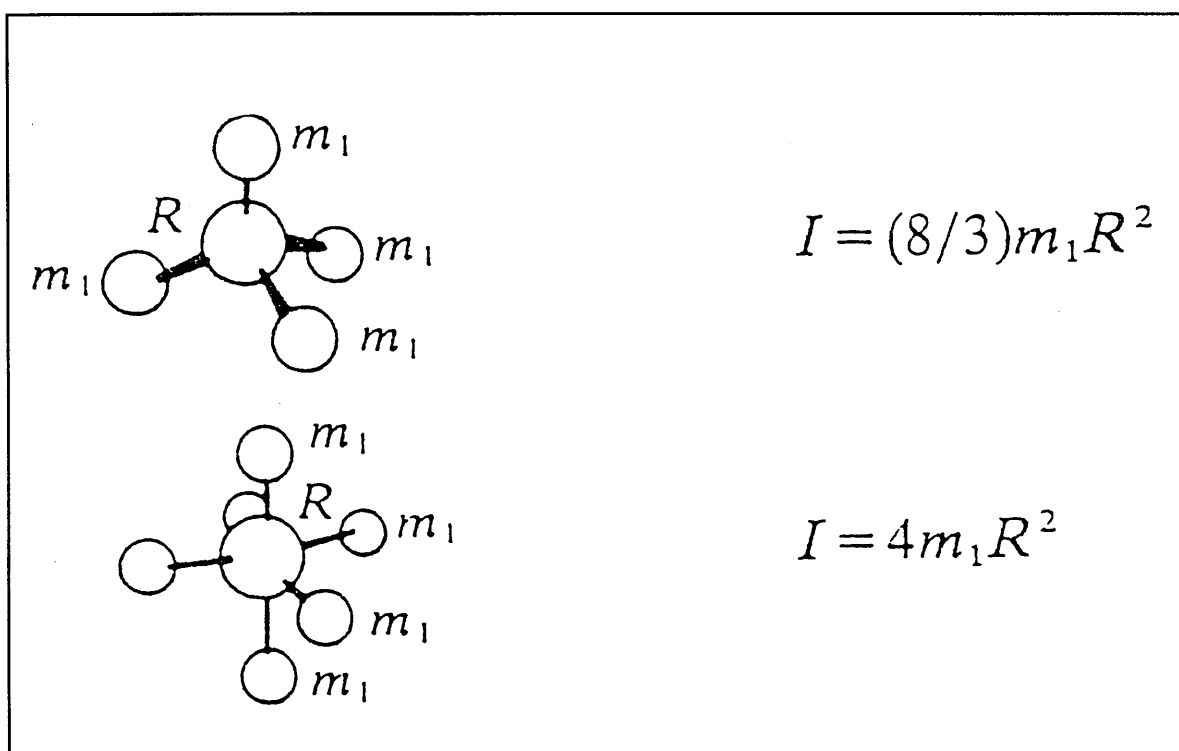


Fig.B1 - Molecular structures of CH_4 and UF_6 . The moments of inertia per principal axis are indicated.

For spherical top molecules all three moments of inertia are the same, i.e. $I_{xx} = I_{yy} = I_{zz}$. Consequently expression B4 reduces to

$$E = (1/2I) (J_x^2 + J_y^2 + J_z^2) = J^2/2I \quad (B5)$$

This is the classical expression with J^2 being the square of the magnitude of the classical angular momentum. For the quantum expression we introduce the result that the magnitude of the angular momentum is confined to the values $[J(J + 1)]^{1/2} \hbar$ where $J = 0, 1, 2, \dots$. Therefore the energies of a rotating spherical top molecule is limited to the values

$$E_J = J(J + 1) \hbar^2 / 2I \quad J = 0, 1, 2, \dots \quad (B6)$$

The factor $\hbar^2/2I$ is usually equated to B the rotational constant and then expression B6 is written as

(B7)

$$E_J = BJ(J + 1)$$

It must be noted that B has the units of energy, e.g. ergs. In practice we more often use wave numbers to indicate the magnitude of B . Heavy molecules such as UF_6 have very low values of rotational constants, e.g. $B = 0,0555 \text{ cm}^{-1}$ [B1]. To convert from ergs to wave numbers we use the conversion formula.

$$B = h/4\pi c I \quad (B8)$$

Where c = speed of light in cm/s.

In the expression B7 the rotational energy was evaluated after assuming that the molecular rotation energy would be fixed and independent of molecular vibration. However, the rotational energy can be corrected for centrifugal distortion. For a non-rigid rotor we have to add the stretching effect arising from the centrifugal force to expression B7. This is accomplished by adding the following

term [B2]:

$$E_J = B J(J + 1) - D J^2(J + 1)^2 \quad (\text{B9})$$

Where D is known as the centrifugal distortion constant and can be found from the evaluation of the infrared spectra of the molecule. The centrifugal force causes the moment of inertia to increase if the molecule rotates faster, hence the negative sign for the added term. Furthermore, the rotational constant also differs from vibration to vibration. Thus we find that it can be realistically represented by an expression of the type [B2].

$$B_v = B_e - \sum_{\beta} \alpha_{\beta} (V_{\beta} + d \beta/2) \quad (\text{B10})$$

where α_{β} is called the vibration-rotation constant and B_e is the rotational constant corresponding to the equilibrium bond length. We find that, when the effect of the centrifugal distortion for UF_6 is analyzed, the correction for the rotational population is very small. Typically the magnitude of D is of the order 10^{-12} eV. The rotational constant, B_v , for UF_6 differs only by 6×10^{-8} eV between the lower and upper vibrational states of the ν_3 stretching vibration. This effect will thus be ignored in defining the rotational partition function.

Proceeding now from expressions B1 and B7 we can define the rotational partition function for a nonsymmetric linear molecule

$$Q_r = \sum_j (2J + 1) \exp [-BJ(J + 1)/k_B T] \quad (\text{B11})$$

An equivalent expression is to replace the summation by an integration over a continuous range of energy and in the limit that $B \ll kT$ we can use the approximation

$$Q_r = \int_0^{\infty} (2J + 1) \exp [-BJ(J + 1)/k_B T] dJ \quad (\text{B12})$$

$$\text{to obtain } Q_r = k_B T / B \quad (\text{B13})$$

For a symmetric linear molecule the levels $J = 1, 3, 5$ etc are missing by symmetry. Thus, we may write for a linear molecule

$$Q_r = k_B T / \sigma B \quad (\text{B14})$$

where σ is a symmetry number equal to 1 for non symmetric molecules and 2 for symmetric molecules. As an extension to the formulations considered hitherto we may write for a polyatomic molecule

$$Q_r = \frac{\sqrt{\pi}}{\sigma} \left(\frac{k_B T}{A} \right)^{1/2} \left(\frac{k_B T}{B} \right)^{1/2} \left(\frac{k_B T}{C} \right)^{1/2} \quad (\text{B15})$$

where the rotational constant $A = B = C$ for a spherical top molecule, e.g. UF_6 and CH_4 . Some of the commonly used expressions for Q are summarized in table B1.

Table B1: Commonly used expressions for Q and $\langle E \rangle / k_B T$ for vibrational and rotational degrees of freedom; the corresponding molar entropies are given by $S = R \ln Q + r \langle E \rangle / k_B T$

Type of motion	Degrees of freedom	Q	$\langle E \rangle / k_B T$
Simple harmonic oscillator	1	$[1 - \exp(-h\nu/k_B T)]^{-1}$	$\frac{(h\nu/k_B T)}{\exp(h\nu/k_B T) - 1}$
Free internal rotation	1	$\pi^{1/2} (8\pi^2 k_B T / h^2)^{1/2} I^{1/2}$	$1/2$
Overall rotation of linear molecule	2	$(8\pi^2 k_B T / h^2) I$	1
Overall rotation of non-linear molecule ^a	3	$\pi^{1/2} (8\pi^2 k_B T / h^2)^{3/2} (I_A I_B I_C)^{1/2}$	$3/2$
p independent rotations (Marcus expression) ^b	$r = \sum_{i=1}^p d_i$	$\left[\prod_{i=1}^p \Gamma(1/2 d_i) \right] (8\pi^2 k_B T / h^2)^{1/2 r} \prod_{i=1}^p e_i^{1/2 d_i}$	$1/2 r$

^a Expression for Q applies strictly to spherical tops ($I_A = I_B = I_C$) and symmetric tops ($I_A \neq I_B = I_C$), and approximately to asymmetric tops ($I_A \neq I_B \neq I_C$).

A contribution to the rotational partition function from the nuclear spin has been neglected so far. Due to coupling between the nuclear spin and the angular momentum additional energy levels can appear dependent on the magnitude of the nuclear spin. This leads to an extension to the density of rotational states and thus the partition function. It was shown [B2] that for a XY_n spherical top molecule these terms are incorporated as follows:

$$Q_r = [(2I_y + 1)^n / \sigma] (k_B T)^{3/2} \left(\frac{\pi}{ABC} \right)^{1/2} \quad (\text{B16})$$

where I_y is the nuclear spin of atom Y and σ the classical symmetry number (look at table B1). For UF_6 one takes $I_y = \frac{1}{2}$; $n = 6$ and $\sigma = 24$.

To determine the rotational partition function we need to establish the moments of inertia. As can be seen from figure B1 for UF_6 .

$$I_A = I_B = I_C = \sum_i m_i R_i^2 = 4mR^2$$

With $m = 19$ the mass of the fluorine atom and $R =$ equilibrium bond length of $1,99 \text{ \AA}$ [B3]. It is common to express the moment of inertia in amu \AA^2 . Alternatively it can be expressed in g cm^2 where $\text{amu \AA}^2 = 1,6604 \times 10^{-40} \text{ g cm}^2$ and the appropriate value of $(8\pi^2k/h^2)$ from table B1 is then $2,4831 \times 10^{38} \text{ g}^{-1} \text{ cm}^{-2} \text{ K}^{-1}$. The rotational partition function for UF_6 is presented in figure B2 as a function of temperature.

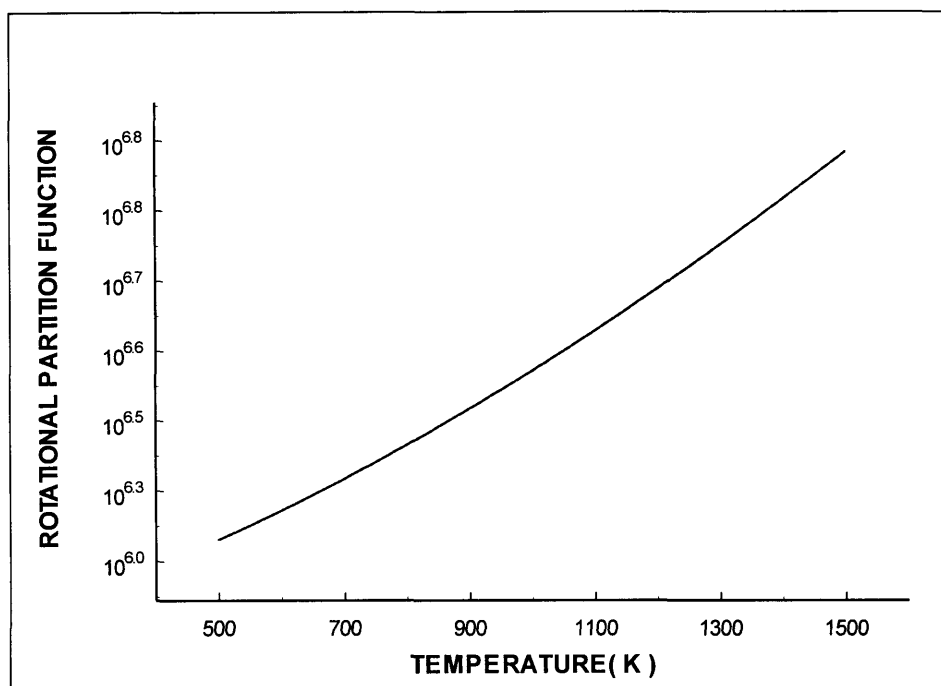


Fig.B2 - Rotational partition function for UF_6 as function of temperature

APPENDIX B - REFERENCES

- B1. Mc Dowel RS, Aprey LB and Paine RT, *J. Chem. Phys.*, Vol 61, No. 9, p3571 (1974).
- B2. Jackson D, Los Alamos Scientific Laboratory Report, number LA-6025-MS (1975).
- B3. Krohn B J, Person W B and Overend J, *J. Chem. Phys.*, Vol 65, No 3, p969 (1976).

DOCUMENT NUMBER	VERSION	PAGE	OF
LT100-000000-155-022		215	

PAPERS

PAPER I

**LASER ISOTOPE SEPARATION AND THE CONCEPT OF
SEPARATION WORK**

E RONANDER, E R ROHWER, S P VAN HEERDEN

**Accepted for Publication in
The Japanese Journal of Nuclear Science**

LASER ISOTOPE SEPARATION AND THE CONCEPT OF SEPARATIVE WORK

Einar Ronander

*Atomic Energy Corporation of South Africa Limited, P O Box 582, Pretoria, 0002,
South Africa*

Egmont R Rohwer

University of Pretoria, Pretoria, 0002, South Africa

Stephanus P van Heerden

*Atomic Energy Corporation of South Africa Limited, P O Box 582, Pretoria, 0002,
South Africa*

Number of pages : 21

Number of figures : 4

ABSTRACT

The concept of separative work is scrutinized to determine its applicability to specify the separation performance of quantum-based processes with relatively large separation factors. It is suggested that the traditional value function, defined for the infinitesimal case, i.e. small separation factors, is not mathematically valid and should not be employed directly. Substituting the separating element with a suitable, imaginary cascade of conventional stages, in conjunction with cascade theory, is a valid approach to determine separation work and capacity in terms of the traditional value function.

Keywords: *separative work, quantum based process, value function, infinitesimal case, cascade, capacity, Taylor expansion, AVLIS, MLIS, feed, tails, product.*

I. INTRODUCTION

The nuclear fuel cycle is presently based on uranium hexafluoride being utilized in industrial enrichment enterprises. Since the inception of uranium enrichment for commercial purposes, separative work units (SWU's) have been used to specify the capacity (SWU/yr) of a plant and, as a commercial support, the added value of enriched uranium.

At the moment the diffusion process for the enrichment of uranium isotopes is the dominant commercial process with the centrifugal method trailing at roughly ten percent of market share. Diffusion and aerodynamic processes, however, are handicapped due to their low enrichment factors and hence, to their opulent energy consumption factors. It has therefore been accepted in the industry that the technology that should ultimately prevail at the beginning of the next century is the isotopic separation by laser. Two different approaches referred to as AVLIS (Atomic Vapour Laser Isotope Separation) and MLIS (Molecular Laser Isotope Separation) have emerged over the last two decades which are very different in their principles and their performances compared to the statistically based processes. Axiomatic with these quantum processes are high enrichment factors and single stage operation with the result that no cascading is required. This is augmented by the desirable feature of high mass throughput. These qualities make the laser processes strong contenders to dominate the enrichment market in future.

Separation and cascade theory have been adapted to adequately describe the existing commercial techniques where the enrichment per step is very small and does not differ much from unity. It has subsequently been pointed out [1,2(a)] that the SWU concept is meaningless as a measure of the separative work performances of laser based

processes. If these notions were to be upheld, the enrichment industry that will thus emulate in the near future seems set for the introduction of a new parameter to evaluate the enrichment performance. The leading players in the enrichment market have all opted for the AVLIS route and it thus seems likely to discontinue the use of uranium hexafluoride as merchant product.

However, cognisance should be taken of the propensity of tradesmen not to simply abandon a well established and proven industry, e.g. the manufacturing of uranium hexafluoride, and cotton onto new technology and terminology. In spite of several statements as to the incorrect use of the SWU concept when describing the laser enrichment technique, scientists and economists have given this an unanimous support by continuing to apply it. There is at present a general realization that the mathematically simplified concept of the elementary value function, derived for extremely small increments of enrichment, cannot be used directly in the case of high separation factors.

Progress with the laser enrichment processes has been more gradual and time consuming than initially anticipated. Nevertheless, the separation factors have been measured [3,4,5] and the industrial development has advanced to a stage that the economical viability can be realistically reassessed. The magnitude of the remaining technological uncertainties necessitates the debate on the measurement of the separation performance, dormant for some time now, be reopened. A reevaluation of the present definition of separative work is called for before the new enrichment processes are prematurely abandoned.

This paper will endeavour to analyse the concept of separative work as it pertains to laser isotope separation.

II. SEPARATIVE WORK

A common framework to treat all fractionation processes, independently of the particular separation method employed or the particular isotope to be separated, has been developed [6(a), 7]. This is fundamentally based on obtaining material balances for a single step or stage in a cascade. Furthermore the amount of separation in the specific step or stage is defined. The nomenclature proposed in the literature will be followed to facilitate direct comparison [2].

As a general approach an enrichment element can be treated as a "black box" into which flows material of a certain isotopic composition and out of which flow two streams, one containing a higher percentage and the other a lower percentage of the desired isotope relative to the feed stream. Figure 1 depicts this phenomenon schematically. It depicts an enrichment element with input, (feed = F) and outputs (product = P, tails = W). N_F , N_p and N_w denote the fraction of ^{235}U present in each stream. If the feed material is of natural abundance, then $N_F = 0,0072$. Furthermore, the relative abundance R is defined by

$$R = N/(1 - N) \quad (1)$$

The effect of a separative element on this ratio is given by the single stage separation factor, q, defined by

$$q = R_p/R_w \quad (2)$$

For many processes this number is only slightly larger than one, so it is more often

$$g = q - 1 \quad (3)$$

convenient to deal with the small quantity.

called the separation gain. The enrichment factor, α , of an element or stage is defined by the ratio between the relative abundances in the feed and product streams

$$\alpha = R_p / R_F \quad (4)$$

Similar to the definition of (3)

$$\varepsilon = \alpha - 1$$

is defined.

The requirements that there should be a mass balance both for the total flow and the respective isotopes will, in the absence of any chemical losses, uphold the following relations:

$$F = P + W \quad (6)$$

$$\begin{aligned} FN_F &= PN_p + WN_w \\ &= \theta FN_p + (1 - \theta) FN_w \end{aligned} \quad (7)$$

where θ is the ratio of the product flow to feed flow, usually called the cut.

The fundamental property which is being changed by the separation process is entropy. Entropy is a measure of the disorder of a system, and the product and tails from a separative element constitute a slightly less disordered system than the incoming feed material. In other words, the isotopes have been partially separated so they are approaching the more orderly state of total separation. The second law of thermodynamics states that work is required to achieve any decrease in the entropy of a system. Therefore the separation element can be visualized as doing work to increase order. The entropy change per unit of feed product by a separative element is given by

[2].

$$\Delta S = \frac{1}{2} K g^2 \theta (1 - \theta) N_F (1 - N_F) \quad (8)$$

where K is a constant. Note that this relationship has been derived and is valid only for $g \ll 1$.

The energy consumption is extremely important in comparing the costs of various enrichment techniques and in estimating the cost of producing reactor fuel. Consequently the energy efficiency of separation should be high. To define this efficiency, we can compare separation energies for obtaining "pure" ^{235}U with the entropy change associated with mixing one kilogram of ^{235}U with 138 kilograms of ^{238}U to obtain 139 kilograms of the natural assay material. This entropy change is 60 kJ. The energy spent to separate these isotopes by gaseous diffusion exceeds this value by 10^7 [6(b)]. This means that the work to create order is done extremely inefficiently, most of the energy being ultimately dissipated as heat. The specific energy consumption, i.e. the photons consumed for AVLIS to achieve 5% enrichment, amounts to about 0,06 to 0,1 MJ/kg of natural feed material [8] and that for MLIS 0,4 to 0,5 MJ/kg [9]. This must obviously still be correlated with the efficiency for producing the necessary photon flux which for a plant will be less than 1 percent.

Two aspects of the concept of entropy, are not desirable when designing a plant consisting of many enrichment stages:

1. There is no simple connection between the energy requirements for a separating element and the entropy change it creates.
2. The entropy change depends on the composition, N_F , of the feed material.

As a substitute the concept of separative work or separative power was invented (unit = kilogram separative work units = kg SWU). It stems from the fact that energy is spent to increase the concentration of the desired isotope in the product stream. Thus this flow would have a higher "value" than the feed stream. This value will be a function of mass fraction:

$$V = V(N)$$

Furthermore, the following two properties were assumed

1. If $V(N)$ represents the value of one unit of the material, the value of P units will be $PV(N_p)$.
2. For the case of a small enrichment factor, the increase in value produced by the separating element is independent of the isotopic concentration in the feed material.

The total separative work done by a plant consequently is

$$\Delta V = PV(N_p) + WV(N_w) - FV(N_f) \quad (8)$$

The mathematical manipulation that follows after equation 8, to derive the expression for the value function, makes two approximations that are not generally true for all enrichment processes. To satisfy requirement 2 stated above, $V(N_w)$ and $V(N_p)$ are expressed in a Taylor series about $V(N_f)$:

$$V(N_p) = V(N_f) + \frac{(N_p - N_f)}{1!} V'(N_f) + \frac{(N_p - N_f)^2}{2!} V''(N_f)$$

and

$$V(N_w) = V(N_F) + \frac{(N_w - N_F)}{1!} V'(N_F) + \frac{(N_w - N_F)^2}{2!} V''(N_F)$$

This will hold good if $(N_p - N_F) \ll 1$ and $|N_w - N_F| \ll 1$ which, for a high enrichment factor as is possible for the laser processes, will not be a good approximation. Secondly, because of the special importance of cascades when the enrichment factor is very nearly unity and thus

$$\alpha - 1 = \epsilon \ll 1$$

an approximation

$$N_p - N_F = \epsilon N_F (1 - N_F) \quad (9)$$

is employed and subsequently a value function is derived:

$$V(N) = (2N - 1) \ln R \quad (10)$$

This is referred to as the elementary value function and is valid for the "infinitesimal" case.

The definition for the separative work performed by a plant or element is clearly of a general form and can be applied to any process. The subsequent mathematical manipulation has, however, been adapted for a very special case. Contrary to belief the separative work is not proportional to the energy consumption of any enrichment process. It can certainly be correlated and is expressed as kWh/kg SWU. Note that for all the known techniques the bulk of the energy consumed to perform this separative work is spent outside the actual separating elements. With the diffusion and aerodynamic processes the flows of UF_6 circulating inside a cascade are considerable. To transport these huge volumes from one separating element to another without performing separative work remains the handicap of these statistical processes. The efficiency of the compressors required to handle the gaseous UF_6 , increases with size,

with the result that the energy part per SWU varies within one multistage plant. The relatively low efficiency that is associated with the production of laser photons, dominate the energy consumption in quantum techniques. The irradiation zone where the actual separative work is performed is not the culprit.

Although the concept of separative work and the value function are not necessary for the optimum design of a plant it is a very useful unit to measure enrichment capacity and to compare different processes. Clearly the expression for the value function, equation 10, has a limited accuracy. In appendix A, another expression of the value function is derived:

$$V(N) = (2N - 1) - \ln(N/0,5) \quad (11)$$

This expression for the value function suffers from the same limitations as expression 10 but is easier to manipulate mathematically. Figure 2 shows a graphical presentation of the value function in 11 and 10 as a function of the ^{235}U fraction N . Equation 11 produces "values" that are substantially lower than that calculated by equation 10. It should be pointed out that it is the change in "value" given by equation 8 which is important and this is consistently less than 5% smaller than the calculated work when the traditional definition (equation 10) is employed.

Both equations 10 and 11 are derived under the approximation that $V(N_p)$ and $V(N_w)$ can be expanded into a Taylor series around $V(N_f)$. The series, however, is truncated after the second order term. The truncation error involved in using this finite summation to approximate the sum of an infinite series needs to be examined. This can more easily be accomplished for the expression in 11. The remainder term or summation of the terms that is ignored can be written as (see appendix B):

$$R_k(N) = \sum_{k=3}^{\infty} \frac{1}{k} (1 - N_p / N_F)^k \quad (12)$$

This summation will, however, not converge to any finite number unless ($N_p < 2N_F$). This puts a limitation on the interval ($N_p - N_F$) in which the Taylor series truncation can be sensibly applied.

Figure 3 illustrates some conclusions that might be drawn if equations 10 and 11 are used beyond their range of validity, for large enrichment factors. The separation work performed for each kilogram of feed material of natural isotopic abundance, is plotted for a constant tails assay of 0,2%, a feed mass flow of 1265 ton uranium, and an increasing product assay. Although the separation work differs only by a few percent in the range presented, the horizontal line would seem to indicate that the single step enrichment factor requirements of a plant designed for a given separation capacity (equivalent to that of an alternative multistep facility), can vary greatly. Clearly this would also lead to contradictions in the plant specification of feed and product composition. This will be discussed in the following section.

III. CASCADING

An alternative approach to calculate the separation work of our "black box" enrichment element is to use the well known cascade theory. You can simply imagine the element with a high enrichment factor as a cascade arrangement with many stages for which the enrichment factor per stage is small and the expression for the value function holds good. A summation over all the stages of the separation work performed will represent that of the single step high enrichment factor process.

The basic concept of a cascade is illustrated in figure 4(b) which shows how natural feed

material enters at one point and is transported to the first enriching stage where it is separated into a product and waste flow. If the enrichment factor is small the isotopic concentration in the waste flow is still close to natural abundance. To recover this a stripping section, i.e the sum of all the stages below the feed line in figure 4(b), is necessary. Above the horizontal line the enriching section operates to acquire the necessary enrichment. All the stages contain an array of elements, the number of which is proportional to the mass flow of the specific stage. An ideal cascade is arranged in such a way that streams of different isotopic concentrations do not mix i.e. there is no mixing entropy [2].

If the feed is assumed to enter stage $n = 0$ and the product to emerge from stage S , then [2(c)]

$$R_P = \alpha^{S+1} R_F \quad (13)$$

Similarly, if the last stage of the stripping section is number T , it follows that

$$R_W = \alpha^{-T} R_F \quad (14)$$

These equations can now be used to compute the total number of stages (which equals $S + T + 1$) required in an ideal cascade, once the product and tails assays are specified and the enrichment factor is known:

$$S + T + 1 = \frac{\ln(R_P / R_W)}{\ln \alpha} \quad (15)$$

The cut per stage will be taken as 0,5 which is characteristic of a symmetric cascade. For the chosen case, the enriched and depleted streams are each sent forward or backward by one stage. The enrichment factor can be chosen to be any small value to attain the desired "plant" enrichment. For our comparative calculations $\alpha = 1,0408$ will be employed for convenience as this value was used for illustrative purposes in

reference 2 and this facilitates direct comparison.

The amount of material to be handled by each stage, for a given output of final product, is needed to establish the separation work for each stage. If L_n is taken to be the flow rate of material into the n -th stage of an ideal cascade, then to a very good approximation [2(c)]

$$L_n = \frac{4P}{g} \frac{(N_p - N_n)}{N_n(1 - N_n)} \quad (16)$$

in the enriching section and

$$L_n = \frac{4W}{g} \frac{(N_n - N_w)}{N_n(1 - N_n)} \quad (17)$$

in the stripping section. Equations 16 and 17 define the optimum mass flow per stage when the cascade is running in total reflux conditions, i.e. $P = 0$, when there is no withdrawal of product from the cascade. The respective mass flows per stage follows a profile for the cascade such as is presented in figure 4(a). In this diagram, the vertical dimension is the stage number and the horizontal dimension is the total mass flow in each stage.

It is emphasized again that a laser process and a cascade with equivalent external operating conditions must produce the same separation work. After all, the value function is defined as being only dependent on N . Figure 3(a) illustrates the difference compared to the capacity calculated with the value functions when it is applied as a single step enrichment. Although the capacity for the three cases that are presented in figure 3 are not much different, the single step enrichment factor as stated before can differ greatly. If process engineers do not heed the mathematical constraints of the elementary value function, wrong conclusions will be drawn as to the requirements of

single step separation factors. These may vary between 50 and 20 for the case under discussion (i.e. for a required capacity of 1500 ton SWU/yr and a waste assay of 0,2%).

IV. CONCLUSIONS

In this paper the methodology to calculate the separation work capacity of future laser plants is scrutinized. The large enrichment factors of these processes necessitates a different approach to simply utilizing the well-known elementary value function definition in a single step enrichment. The latter approach should be limited to conditions where the product assay does not exceed twice the feed assay and preferably much smaller. It is suggested that a cascade arrangement with similar external conditions should more correctly represent the separation work performed and provide a more realistic assessment of the required single step enrichment factor.

If treated in the prescribed manner the concept of separative work remains a very useful parameter and can be maintained to describe processes with large enrichment factors.

REFERENCES

1. Sauzay, G., *Some characteristics of SILVA and their Implications for the Nuclear Fuel Cycle.*, Nuclear Europe, 9/1986.

2. Krass, A. S., Boskma, P., Ebzen, B and Smit, W. A., *Uranium Enrichment and Nuclear Weapons Proliferation* (Taylor and Francis Ltd, London and New York, 1983).
 - (a) - p. 98
 - (b) - p. 94
 - (c) - p. 104

3. Meyer-Kretschmer, G. and Schweizer, G., *Status of the MLIS Project in the Federal Republic of Germany, Proceedings of the International Symposium on Isotope Separation and Chemical Exchange Uranium Enrichment, October 29 - November 1, 1990, Tokyo, Japan.*

4. Takeuchi, K., Tashiro, H., Midorikawa, K., Kato, S., Oyama, T., Satooka, S., Tashiro, K., Suzuki, E., Endoh, S. and Nanba, S., *Research on the Verification of the Process of Laser Uranium Enrichment using Riken's Molecular Method*, Laser Science Research, No. 10 (1988).

5. Strydom, H. J., Human, H. G. C., Green, C. R., Rohwer, E. R., Michaelis, M. M., *Uranium Isotope analysis by laser desorption time-of-flight mass spectrometry and secondary ion mass spectrometry*, Proceedings of the 13th International Mass Spectrometry Conference (Budapest), 29 August - 2 September 1994.

6. Villani, S. (ed), Topics in Applied Physics, Vol. 35, *Uranium Enrichment* (Springer - Verlag, New York, 1979).
 - (a) Brigoli, B., Cascade Theory, p. 13.
 - (b) Robinson, C. P. and Jensen, R., *J. Laser Methods of Uranium Isotope Separation*, p. 267.

7. Cohen, K., *The Theory of Isotope Separation as Applied to the Large Scale Production of ²³⁵U* (Mc Graw-Hill, New York, 1951).

8. Stern, R. C., Paisner, J. A., *Atomic Vapor Laser Isotope Separation*, First International Laser Science Conference, November 18-22, 1985. Dallas USA.

9. Ronander, E., *Internal Report for AEC of South Africa*, August 1995.

APPENDIX A

The separative work produced by a generalized element such as the schematic presentation of figure 1 shows, results in a net change in value:

$$\Delta V = PV(N_P) + WV(N_W) - FV(N_F) \quad (\text{i})$$

$$= P[V(N_P) - V(N_F)] + W[V(N_W) - V(N_F)] \quad (\text{ii})$$

Expanding $V(N_P)$ and $V(N_W)$ as a Taylor series about $V(N_F)$:

$$V(N_P) = V(N_F) + \frac{N_P - N_F}{1!} V'(N_F) + \frac{(N_P - N_F)^2}{2!} V''(N_F) \quad (\text{iii})$$

$$V(N_W) = V(N_F) + \frac{N_W - N_F}{1!} V'(N_F) + \frac{(N_W - N_F)^2}{2!} V''(N_F) \quad (\text{iv})$$

The termination of the series expansion after the second order term is by choice and implies that the enrichment factor is small.

Substituting equation (iii) and (iv) into equation (ii):

$$\begin{aligned} \Delta V &= V'(N_F)[P(N_P - N_F) + W(N_W - N_F)] \\ &+ \frac{1}{2} V''(N_F)[P(N_P - N_F)^2 + W(N_W - N_F)^2] \end{aligned} \quad (\text{v})$$

The coefficients of $V(N_F)$ and $dV(N_F)/dN$ vanish by virtue of the assumption that matter is conserved. Therefore

$$\Delta V = \frac{1}{2} V''(N_F) [P(N_P - N_F)^2 + W(N_W - N_F)^2] \quad (\text{vi})$$

To make this change in value independent of N_F , the feed isotopic concentration, the following substitution is performed:

$$\begin{aligned}
1 + \epsilon &= \alpha = R_p/R_F \\
&= \frac{N_p}{1 - N_p} \cdot \frac{1 - N_F}{N_F}
\end{aligned}
\tag{vii}$$

From this relationship follows

$$N_p - N_F = \epsilon N_F (1 - N_p) \tag{viii}$$

For the derivation of the infinitesimal case where the condition $\epsilon \ll 1$ is included, an approximation is used

$$N_p - N_F = \epsilon N_F (1 - N_F) \tag{ix}$$

Equations (viii) and (vi) produce the following relationship

$$\Delta V = \frac{1}{2} V''(N_F) N_F^2 (1 - N_p)^2 [P\epsilon^2 + Wg^2] \tag{x}$$

and if

$$\begin{aligned}
V''(N_F) &= 1/N_F^2, \\
(1 - N_p)^2 &\sim 1
\end{aligned}$$

the net change will be independent of N_F . This approach suffers from the same limitations as the derivation for the traditional value function and is performed purely for convenience. The comparison between the two functions, however, turns out to be surprisingly good. The expression

$$\frac{d^2V(N)}{dN^2} = \frac{1}{N^2}$$

is much simpler to handle for further manipulation e.g. higher order derivatives.

To find the value function thus the differential equation

$$\frac{d^2V(N)}{dN^2} = \frac{1}{N^2} \quad (\text{x i})$$

must be solved. The two integration constants that emerge from the double integration, say C_0 and C_1 , can be solved if the requirement

$$V(N_F) = \frac{dV(N_F)}{dN} = 0 \text{ is assumed at } N_F = 0,5.$$

Thus

$$\begin{aligned} V(N) &= C_1 + C_0 N - \ln N \\ &= (2N - 1) - \ln \left(\frac{N}{0,5} \right) \end{aligned} \quad (\text{x ii})$$

APPENDIX B

The Taylor series for $V(N_P)$ about N_F is represented by the infinite series by taking the limit of $V_k(N)$ as $k \rightarrow \infty$:

$$V_k(N_P) = \sum_{k=0}^{\infty} \frac{V^k(N_F)}{k!} (N_P - N_F)^k$$

In the derivation of the value function (equation 11) this series was truncated after the second order. The remainder term (or truncated error), which generally refers to the error involved in using a truncated or finite summation to approximate the sum of an infinite series, can be established:

$$R_k(N) = \sum_{k=3}^{\infty} \frac{V^k(N_F)}{k!} (N_P - N_F)^k$$

The relationship in Appendix A gives

$$V^2(N) = 1/N^2$$

From this follows

$$V^3(N) = -2/N^3$$

$$V^4(N) = +6/N^4$$

$$V^5(N) = -24/N^5 \text{ ---etc.}$$

Thus

$$\begin{aligned} R_k(N) &= \sum_{k=3}^{\infty} (-1)^k \frac{(k-1)!}{k!} \left(\frac{N_P - N_F}{N_F} \right)^k \\ &= \sum_{k=3}^{\infty} \frac{1}{k} \left(1 - \frac{N_P}{N_F} \right)^k \end{aligned}$$

FIGURE CAPTIONS

1. Schematic of an enrichment element. The input (feed = F) and outputs (product = P, tails = W) mass flows as indicated with their corresponding ^{235}U -fractions N_F , N_P and N_W respectively.
2. Elementary value function (a) $V(N) = (2N - 1) \ln R$ and (b) $V(N) = (2N - 1) - \ln(N/0,5)$.
3. Separation work capacity for a quantum process with increasing product assay.
 - (a) $N_F = 0,0072$; $\alpha = 1,0408$, cut (θ) = 0,5, Feed = 1265 ton uranium and constant tails assay (N_W) of 0,002. Appropriate cascade arrangement.
 - (b) Single step enrichment: Feed = 1265 ton uranium; $N_F = 0,0072$; $N_W = 0,002$; value function $V(N) = (2N-1)\ln R$.
 - (c) Similar to (b) with value function $V(N) = (2N-1) - \ln(N/0,5)$
4. Schematic of cascade arrangements with (a) enriching and stripping sections and (b) detail mass flow connections for a ideal symmetric cascade.

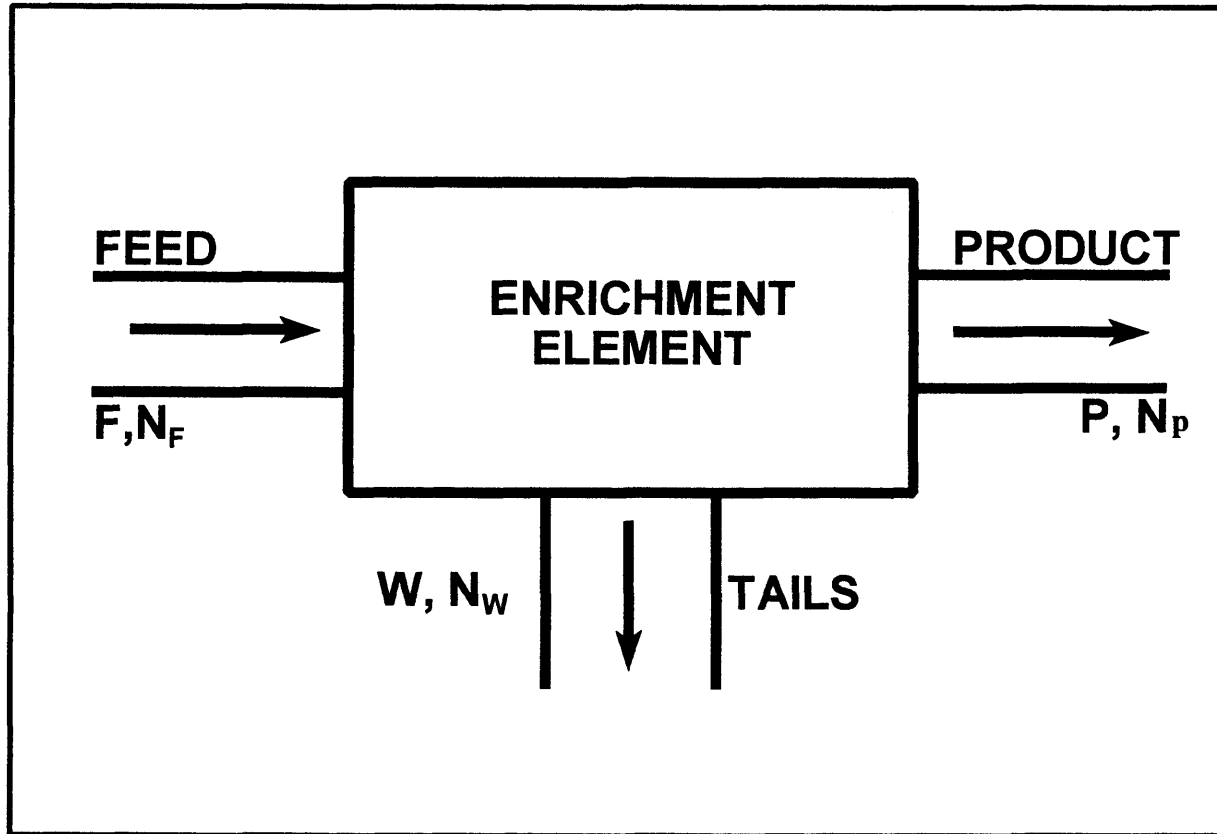


Fig. 1 Schematic of an enrichment element. The input (feed = F) and outputs (product = P , tails = W) mass flows as indicated with their corresponding ^{235}U -fractions N_F , N_P and N_W respectively.

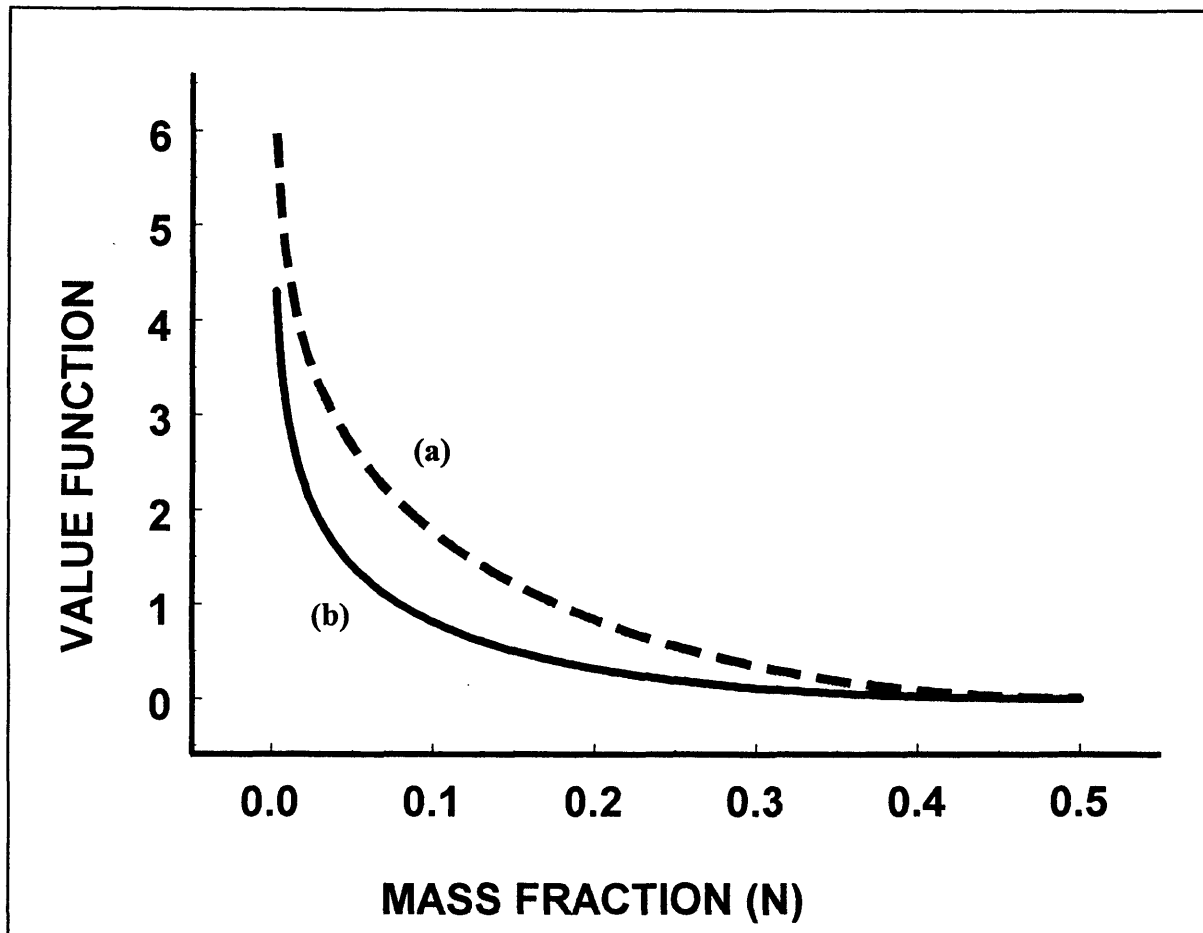


Fig 2. Elementary value function (a) $V(N) = (2N - 1)\ln R$ and (b) $V(N) = (2N - 1) - \ln(N/0,5)$

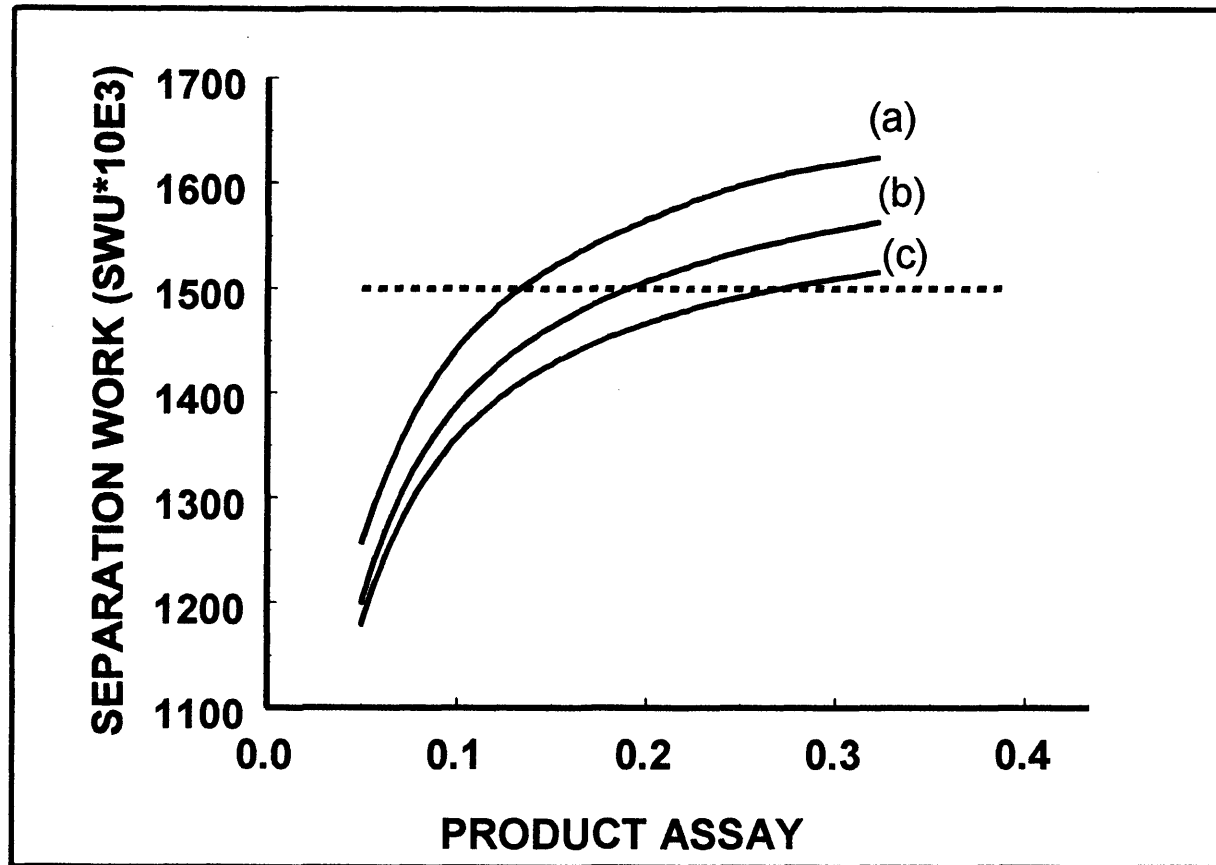


Fig. 3 Separation work capacity for a quantum process with increasing product assay
 (a) $N_F = 0,0072$; $\alpha = 1,0408$, $CUT(\theta) = 0,5$, Feed = 1265 ton uranium and constant tails assay (N_W) of 0,002. Appropriate cascade arrangement.
 (b) Single step enrichment: Feed = 1265 ton uranium; $N_F = 0,0072$; $N_W = 0,002$; value function $V(N) = (2N-1) \ln R$.
 (c) Similar to (b) with value function $V(N) = (2N-1) - \ln(N/0,5)$

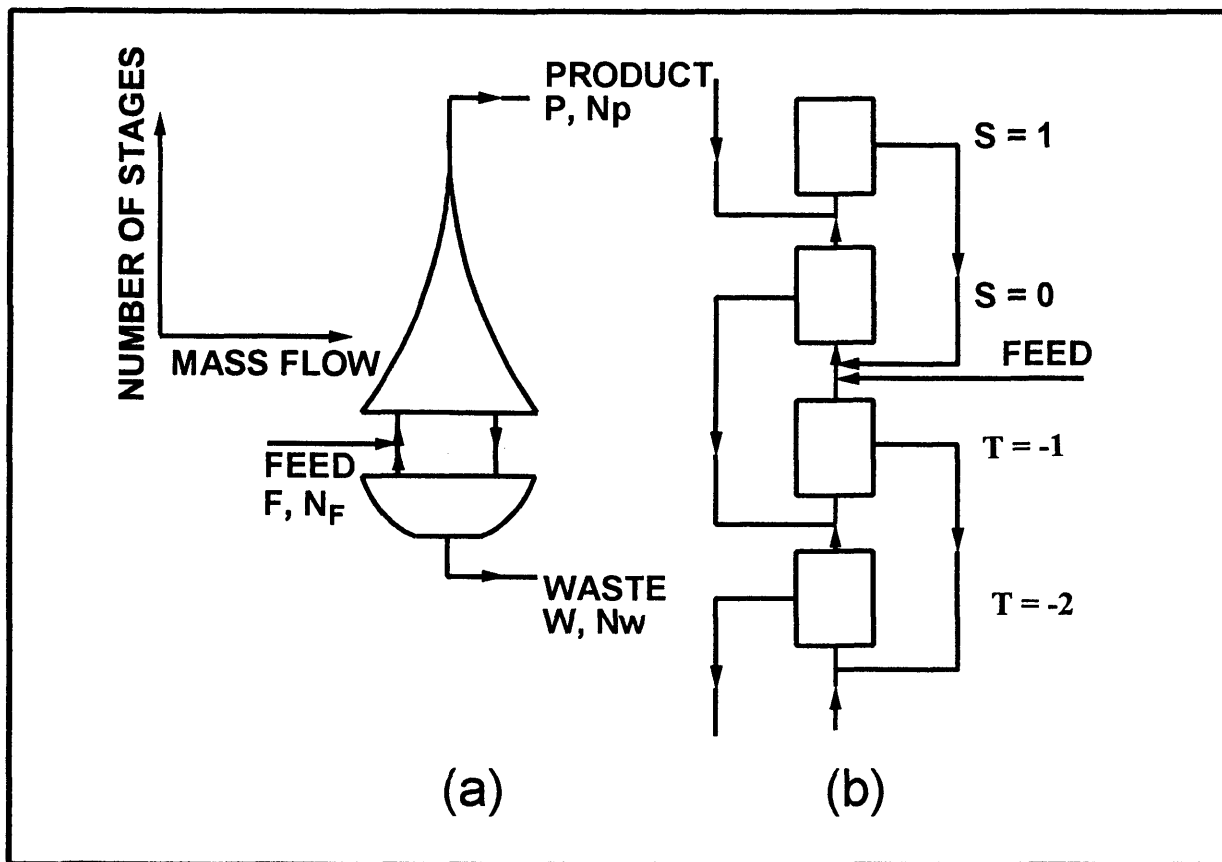


Fig. 4 Schematic of cascade arrangements with (a) enriching and stripping sections and (b) detail mass flow connections for an ideal symmetric cascade.

PAPER II

THE TEA-CO₂ LASER IN THE CHEMICAL INDUSTRY

E RONANDER AND R ROHWER

**Presented at the second International Workshop on Physics and
Modern applications of Lasers
6-14 September 1993
Harare-Zimbabwe**

THE TEA-CO₂ LASER IN THE CHEMICAL INDUSTRY

Einar Ronander

Atomic Energy Corporation of South Africa, Pelindaba, Pretoria

Erich Rohwer

Department of Physics, University of Stellenbosch, Stellenbosch

ABSTRACT

Laser induced chemistry has received much attention in the past few years. The economics of such applications are dominated by the cost of photons and the quantum yield of the specific reaction. For a typical multiple-IR-photon process the quantum yield can be as low as 10^{-2} which emphasises the importance to develop laser systems that can produce laser photons at relatively low cost.

At the South African Atomic Energy Corporation, we have for the past decade been involved in the development of high pulse frequency, high average power TEA-CO₂ lasers for the application in the field of industrial synthesis. Due to the cost of laser photons, however, the present applications are limited to the separation of high value added isotopes, the synthesis of pharmaceuticals, the purification of chemicals, the chemical modification of surfaces, the generation of catalytic intermediates, etc. Much of the attention, however, has been focused on the application to separate the isotopes of uranium via a multi-wavelength infrared irradiation scheme. The progress that has been made towards the establishment of CO₂-lasers and laser chains for industrial use, has been quite outstanding.

INTRODUCTION

In recent years a number of uses of lasers for industrial scale chemical applications has been put forward and investigated. These applications include isotope separation, the purification of chemicals, the chemical modification of surfaces and the generation of catalytic intermediates. Over and above this, lasers can be widely applied in the very important area of laser based analytics for process control. The applicability of lasers to industrial scale synthesis is determined by economical considerations. In figure 1 [1] the selling price of some of the relevant chemicals are presented and it indicates that for most high volume chemicals, this is substantially below US \$1 per mole of product. It is also shown that some

isotopes have a selling price of US $\$10^4 - 10^8$ per mole. These high value added products are therefore very good candidates of laser based processes. A product with a relatively high intrinsic value of importance to the nuclear industry is isotopically enriched uranium. The latter has a value of ca. US $\$100$ per mole of product. Due to the increased costs of modern medicines the laser syntheses of some pharmaceuticals are becoming more attractive.

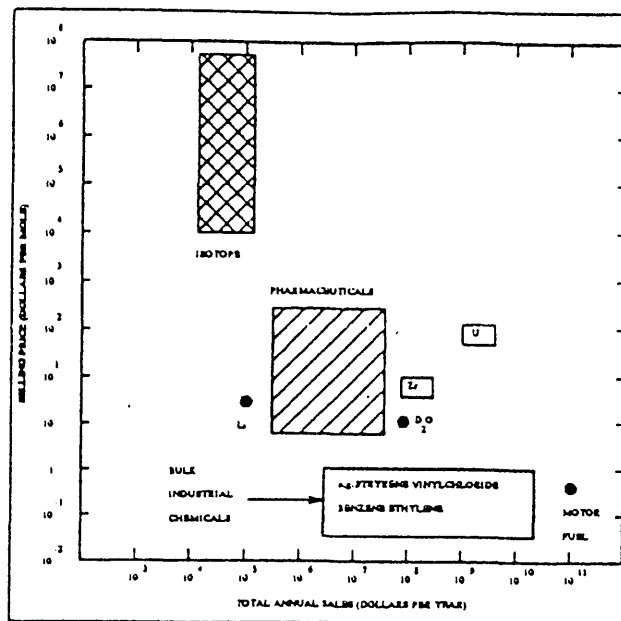


FIGURE 1: Selling price compared with annual sales of some selected chemical in the USA.

Two aspects that dominate the economy of laser based processes are the quantum yield of the specific reaction and the cost of the laser photons. For a typical multiple-IR-photon process the quantum yield can be low and values between 10^{-1} to 10^{-2} are common. The quantum yield of a chemical reaction can be substantially increased if chain reactions are involved or if the laser photon interacts only with one minor component of the process. An example of the latter is the selective removal of H_2S from synthesis gas, $CO + H_2$, using an ArF laser. The second area of concern namely the reduction of the cost of laser photons has been intensely researched at the South African Atomic Energy Corporation for the past decade. An analysis of the costs of different lasers shows that although it takes approximately 10 CO_2 laser photons to total 1eV the cost is nevertheless lower than for any other laser.

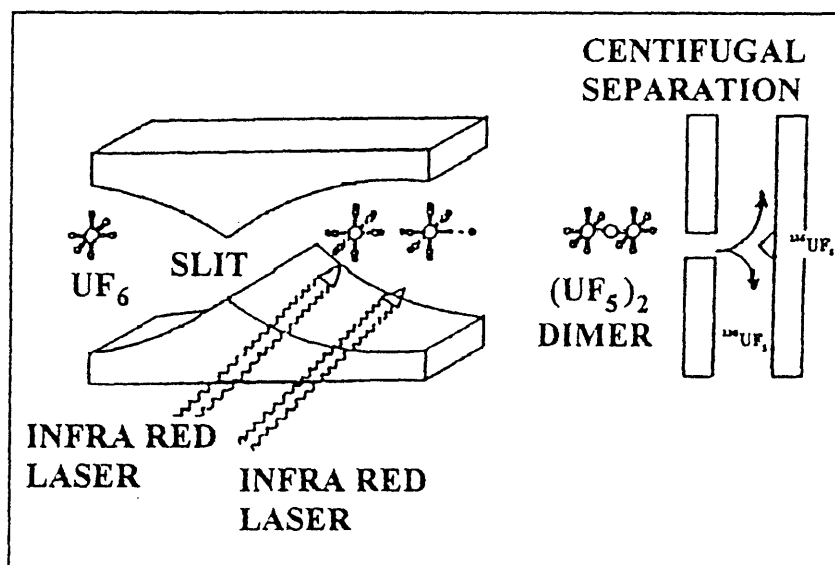
ISOTOPE SEPARATION

A number of commercial opportunities exists for isotope selective laser chemistry. For the purpose of this discussion only those isotopes that can be separated with the TEA CO_2 laser will be considered. Table 1 summarizes some of the more important cases.

ELEMENT	APPLICATIONS	LASER PROCESS
HYDROGEN	² H 0.015% na. Heavy water reactors, research applications.	T/H separated by TEA CO ₂ laser decomposition of CF ₃ H
	³ H Lumiglow sources	T/D separated by TEA CO ₂ laser decomposition of CCl ₃ H
BORON	¹⁰ B 19.78% na. Safety devices and control rods of nuclear reactors and neutron counter tubes.	TEA CO ₂ laser dissociation of BCl ₃ .
CARBON	¹² C Isotopically pure form has special thermal properties (higher conduction) and used in the growth of diamond and DLC coatings.	TEA CO ₂ laser dissociation of CF ₂ HCl (Freon 22). Single step process: 99.99% ¹² C and 72% ¹³ C. Two step process: ¹³ C > 95%
	¹³ C 1.11% na. Medical, biological and agricultural tracer studies and accelerator beam particles.	TEA CO ₂ dissociation of CF ₂ Cl ₂ (Freon 12) with HI as co-reagent. CF ₂ H ₂ product 97% enriched.
NITROGEN	¹⁵ N 0.37% na. Medical, biological and agricultural tracer studies and accelerator beam particles.	TEA CO ₂ laser dissociation of NH ₃ .
OXYGEN	¹⁷ O 0.037% na. 50% enrichment used for ¹⁷ O NMR, medical diagnostics and studying properties of high T _c superconductors. Both ¹⁷ O and ¹⁸ O used as accelerator beam particles.	TEA CO ₂ laser dissociation of di-isopropyl ether.
	¹⁸ O 0.204% na. CO ₂ lasers for LIDAR applications in atmospheric window, production of ¹⁸ F for positron emission tomography (PET) from ¹⁸ O (p,n) ¹⁸ F, PET appears to be a growing medical market.	
SULPHUR	³⁴ S 4.22% na. Environmental pollution dilution studies of SO ₂ and drug metabolism.	TEA CO ₂ dissociation of SF ₆ .
	³⁶ S 0.014% na.	
MOLYBDENUM	⁹⁸ Mo 23.78% na. Required for ^{99m} Tc generator, produced by ⁹⁸ Mo (n,λ) ⁹⁹ Mo.	TEA CO ₂ laser dissociation of MoF ₆ .

TABLE 1: Laser processes for isotope separation

The best known example of isotope separation is enriched uranium that is used in light water reactors. A process based on the TEA CO₂ laser has been proposed. This is being referred to as the MLIS process which is an acronym for molecular laser isotope separation. In the MLIS process multi-photon absorption in the ν_3 band of UF₆ is used to selectively excite the ²³⁵UF₆ isotope and finally dissociate the UF₆ molecule. Gaseous UF₆ is used since this is the only uranium compound with a sizeable vapour pressure at reasonable temperatures and fluorine as the sole partner exists only as a single isotope. Due to the complexity of the vibrational and rotational spectrum at ambient temperatures, the UF₆ molecule has to be flow cooled to below 100°K. This is accomplished by the adiabatic expansion through a nozzle. The resultant molecular beam moves at a high speed of approximately 450 m/s. As a consequence a laser repetition rate of 12kHz and average output power of several kilowatt is required to irradiate all the UF₆ (figure 2).



High power, high repetition rate infrared lasers of multi-kilowatt output, however, are not currently commercially available. For this reason we embarked on an intense development program stretching back to ca. 1983.

FIGURE 2: MLIS Schematic

THE TEA CO₂ LASER

Since non-linear processes like the multi-photon dissociation of molecules depends strongly on peak power and the thresholds for most applications mentioned hitherto is beyond that which continuous wave CO₂ lasers can produce, TEA CO₂ lasers are a logical choice. For the MLIS process an additional frequency conversion step is necessary to convert the 10,6μm to 16μm by stimulated rotational Raman scattering. Figure 3 shows the schematic layout

applicable in the latter case and indicates some of the important parameters. These parameters are generally advantageous to any photochemical process that employs the TEA CO₂ laser. The present state of art at the AEC employs a TEA CO₂ laser that can operate at repetition frequencies up to 2kHz and delivers 1,5 Joule per pulse as a free running oscillator. This represents an average output of 3kW of optical power. When the oscillator is injection locked to produce a single longitudinal mode pulse and amplified in a MOPA chain as depicted in figure 3, the output increases to 4kW. In this configuration the pulse length is about 60 ns and barely has a tail and the beam quality is very good. [2] The capital cost of a 3kW CO₂ laser is ca US \$ 100/watt output and the unit running cost ca US \$ 14/kWh. These costs can be further reduced.

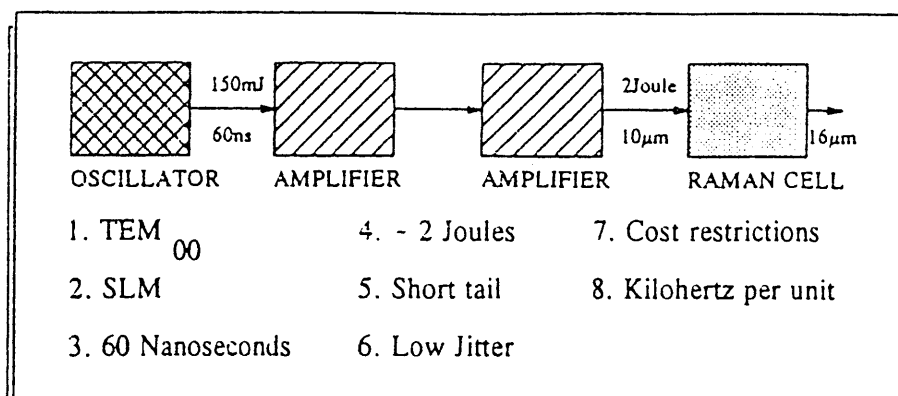


FIGURE 3: Schematic CO₂ -laser system for MLIS

CONCLUSION

Multikilowatt average power TEA CO₂-laser have been firmly established in the last decade in the RSA. These devices operate at levels adequate for many photochemical applications.

REFERENCES

1. R.B. Hall, "Lasers in industrial chemical synthesis", Laser Focus, pp. 57-62, September 1982.
2. E Ronander and E G Rohwer, "A multikilowatt TEA-CO₂ Laser system for molecular laser isotope separation", SPIE , Vol 1810, Gas Flow and Chemical lasers, pp. 49-52, 1992..

PAPER III

**A LONG-RANGE DIPOLE-DIPOLE INTERACTION
MECHANISM FOR THE VIBRATIONAL ENERGY
EXCHANGE IN SF₆ AND UF₆**

E RONANDER AND R ROHWER

**Presented at the XX International Quantum Electronics Conference
14-19 July 1996
Sydney-Australia**

A long-range dipole-dipole interaction mechanism for the vibrational energy exchange in SF₆ and UF₆

E Ronander, *ER Rohwer, CJ Liebenberg, *Atomic Energy Corporation of South Africa Limited, PO Box 582, Pretoria, 0002, South Africa*

The molecular route for the separation of uranium isotopes utilises the technique of flow cooling to decrease the vibrational and rotational temperatures of UF₆ in order to enhance the optical selectivity obtainable in the first selective step of a multifrequency irradiation scheme. This selectivity in the subsequent photodynamics when the molecule is excited through the quasicontinuum to dissociation, impacts critically on the specific energy consumption and the techno-economics of the separation process. A high density is favoured in the irradiation zone. However, this introduces the aspect of vibrational energy transfer between molecules, with resultant loss in isotopic selectivity. It is therefore imperative to establish a consummate picture of the influence of vibrational exchange processes, during and after the laser pulses, on the photodynamics of UF₆.

Experimental measurements performed with a pump and probe technique will be reported. Beams, generated via stimulated Raman scattering in parahydrogen, are employed. The intensity of a HF-fluorescence signal, generated by dissociating UF₆ in the presence of a suitable hydrogen containing

molecule or scavenger, was monitored. The time between pump and probe was suitably delayed in a stepwise manner to study the vibrational de-excitation. The results indicate very fast exchange of vibrational energy at the low temperatures. The rate of exchange is influenced by the gas composition, ie carrier gas and scavenger, and rates of 10 to 50 nanoseconds Torr are demonstrated in typical process gas mixtures. A striking feature of the vibrational exchange for both SF₆ and UF₆, is an increased rate of exchange as the temperature is decreased. Thus, contrary to common belief, the low temperature, (60 to 80 K), prevailing in the irradiation zone, increases rather than decreases the role of intermolecular vibrational energy transfer in the photodynamics. The energy transfer rates are compared to the unimolecular rate of decay for the UF₆ molecule as predicted by RRKM theory for up to 40% over excitation.

The most obvious theory for V-V energy transfer is derived from an exponential repulsive interaction between harmonic oscillators. In the case of resonant transfer, the integrated probability for V-V energy transfer is directly proportional to the absolute temperature. Mahan [1] was first to point out that an alternative mechanism, referred to as long-range dipole-dipole interactions, could induce near resonant V-V transfer in molecules with a strong induced dipole moment. In such cases the attractive part of the interaction potential introduces considerable Fourier components into the interaction potential. An expansion of the dipole moments in a Taylor series relative to the normal vibrational coordinate, confirms that if the dipole derivatives are nonzero, the dipole-dipole potential can indeed couple molecular vibrational states. According to this model, the integrated probability for V-V transfer, exhibits an inverse proportionality to the temperature as is detected experimentally.

1. BH Mahan, *J. Chem. Phys.*, 46, p.98 (1967)

**University of Pretoria, Pretoria 0002, South Africa*

**A LONG-RANGE DIPOLE-DIPOLE INTERACTION
MECHANISM FOR THE VIBRATIONAL ENERGY
EXCHANGE IN SF₆ AND UF₆**

Einar Ronander

*Atomic Energy Corporation of South Africa Limited,
P O Box 582, Pretoria, 0001, South Africa
Telephone (27-12-316 2754), Fax (27-12-316 2236)*

Egmont R Rohwer

*University of Pretoria, Pretoria, 0001, South Africa
Telephone (27-12-420 2518), Fax (27-12-43 2863)*

Christo J Liebenberg

*Atomic Energy Corporation of South Africa Limited, P
O Box 582, Pretoria, 0001, South Africa
Telephone (27-12-316 2759), Fax (27-12-316 2236)*

INTRODUCTION

The molecular route for the separation of uranium isotopes utilizes the technique of flow cooling to decrease the vibrational and rotational temperatures of UF_6 in order to enhance the optical selectivity obtainable in the first selective step of a multi frequency irradiation scheme. This intrinsic selectivity and the subsequent photodynamics when the molecule is excited through the quasi continuum of vibrational levels to dissociation, impacts critically on the specific energy consumption, expressed as megajoules/kilogram feed material (MJ/kg_F), and the techno-economics of the separation process. A high molecular density is favoured in the irradiation zone. However, this introduces the aspect of vibrational energy transfer between molecules with the resultant loss in isotopic selectivity. It is therefore imperative to establish a consummate picture of the influence of vibrational exchange processes, during and after the laser pulses, on the photodynamics of UF_6 .

In our studies into the dissociation dynamics of UF_6 , we have gathered evidence that attractive forces that influence the exchange process over longer distances on the intermolecular potential curve play a significant role at low temperatures.

The Rice-Ramsberger-Kassel-Marcus (RRKM) theory can be used to predict the unimolecular decay rate of UF_6 . Hitherto the influence of collisional transfer of vibrational energy has been neglected as this is regarded as too slow in the density and temperature regions applicable to MLIS. If the over excitation of a large polyatomic molecule is substantially above the dissociation level, the decomposition will be rapid and the competition of collisional energy transfer processes can be negligible. A higher over excitation, however, occurs at the expense of increased specific energy consumption. A comprehensive study to relate the predictions of the RRKM theory with experimentally measured dissociation rates, which will include collisional effects, has been undertaken to understand the photodynamics of UF_6 better. This paper will deal only with the mechanism of vibrational energy transfer which is very important to allow a proper description of its influence on the selectivity.

Figure 1 shows schematically the ground electronic state of UF_6 together with the excited electronic states that give rise to fluorescence via the A-X- and B-X-bands. The origins of the different fluorescence signals studied are as follows:

1. After infrared multiphoton excitation in the ground electronic state, UF_6 dissociates with the formation of a fluorine radical. Adding an appropriate scavenger gas leads to the formation of excited HF which subsequently relaxes by fluorescence and emits 2-3 μm wavelength photons.
2. Excitation with a 248 nm photon, KrF-laser, to the B-X-band, which is a directly dissociative state, is followed by very fast unimolecular decay of UF_6 and a similar reaction to 1 can be utilized to obtain a HF fluorescence signal.
3. Excitation to the A-X-band with a 395 nm photon gives rise to UF_6 fluorescence which peaks in intensity at 420 nm.

This paper deals with the experimental configuration to obtain 1 and relates some results whilst 2 and 3 were previously reported.

RESULTS

A. HF FLUORESCENCE - DISSOCIATION WITH $16\mu\text{m}$

Experiments to characterize the HF fluorescence signal at ambient temperatures were first performed. Figures 2 (a) and (b) depict the time response of the signal in a static condition in the flow cooling nozzle, first without any scavenger gas added, figure 2(a). In figure 2(b) a small amount of scavenger gas and argon as carrier gas has been added to a total pressure of $\sim 9,8$ torr (1300 Pa). The slow relaxation process in figure 2(a) corresponds to a $p \tau \sim 85 \mu\text{s torr}$ where p = pressure in torr and τ is the characteristic relaxation time derived from figure 3. This relaxation is derived by ignoring the first $\sim 100 \mu\text{s}$ where clearly

another process interferes. The addition of less than 0,023 torr of scavenger gas has a significant effect on the fluorescence dynamics in the first 50 μ s and a clear fluorescence peak evolves which is shown in figure 2(a-b). Under these conditions the second fluorescence decay shortens significantly and is a function of scavenger gas pressure. If the scavenger gas concentration is further increased the amplitude of the first part of the signal increases less dramatically and only a \sim 15% increase results from a \sim 2 torr (250 Pa) scavenger gas pressure. Adding argon to the mixture, figure 2(b), the fluorescence signal is suppressed.

Two-frequency dissociation measurements were subsequently performed under flow cooled conditions. An appropriate delay time was introduced between the two 16 μ m beams and the corresponding fluorescence signal was monitored. These type of results are illustrated in figure 4. From this data the relaxation time for vibrational relaxation can be derived. The striking feature; see table 1; is that the relaxation process at \sim 100 K is very fast and substantially exceeds the relaxation rate at room temperature. Furthermore the level of excitation with λ_1 , as shown in figure 4, impacts on the characteristic time. Table 1 summarizes our results together with relevant data from published literature.

Table 1

Vibrational Relaxation rates of multiphoton excited UF₆.

Gas Composition	Temperature	p.τ	Reference
UF ₆ UF ₆	100 K	0,25 μ s torr	2
UF ₆ /H ₂ /Ar	300 K	2,9 μ s torr	1
UF ₆ /H ₂ /Ar	90 K	0,85 μ s torr	1
UF ₆ /Hydrocarbons/Ar	300 K	2,5 μ s torr	this work
UF ₆ /Hydrocarbons/Ar	100 K	0,75 μ s torr*	this work
UF ₆ /Hydrocarbons/Ar	100 K	0,45 μ s torr**	this work

Different levels of excitation * $\phi\lambda_1 = 40\text{mJ/cm}^2$

** $\phi\lambda_2 = 160\text{mJ/cm}^2$

B. HF FLUORESCENCE - DISSOCIATION WITH 248 nm

Fluorescence data was also obtained after dissociation of the UF_6 molecule with 248 nm. Under these conditions the UF_6 molecule possesses a relatively small amount of vibrational energy but a large amount of electronical excitation. Figure 5 presents the HF fluorescence signal when a scavenger gas is added. Only the faster signal, compare the multi photon infrared data, is detected and it has the same rise time as in the case when dissociation occurs as a result of infrared radiation. A rate coefficient of $\sim 5,2 \times 10^5 \text{ s}^{-1} \text{ torr}^{-1}$ can be deduced from the rise time. This is consistent with the reaction between F and H_2 for which values reported in the literature vary from $5,4 \times 10^5$ to $> 10^6 \text{ s}^{-1} \text{ torr}^{-1}$. This rate can thus reasonably be associated with the removal of fluorine atoms by hydrocarbons which subsequently causes the fluorescence signal. A characteristic decay time of $\sim 4,5 \mu\text{s torr}$ is derived from the fluorescence decay time in figure 5.

DISCUSSION AND CONCLUSIONS

The schematic presentations of figures 1 and 6 facilitate a discussion of the reported results and its significance in terms of the dissociation dynamics. Figure 6 illustrates the distribution of the vibrational energy for a polyatomic molecule, e.g. UF_6 and SF_6 , at the onset of dissociation after excitation with infrared photons. A bimodal distribution is seen which is the result of the different rates of excitation in the discrete levels and the quasi continuum. The molecules that dissociate first are those in the high energy tail of the distribution curve that exceeds the dissociation energy. Typical rates of dissociation for UF_6 are $\sim 2 \times 10^6$ and $5 \times 10^7 \text{ sec}^{-1}$ at respectively 10 and 15 times $16 \mu\text{m}$ photons excitation above the dissociation energy which lies at $24\,197 \text{ cm}^{-1}$. This dissociation rate is a very sensitive function of the degree of over excitation.

In a selectivity experiment a concentration gradient in the minor isotope, ^{235}U , will exist across the vibrational distribution curve (derived from the fact that mass balance must prevail). Therefore the high energy tail will contain a higher ^{235}U -isotope concentration. Consequently, the resonant transfer of vibrational energy at high levels of excitation

becomes very important. This resonant transfer will not change the shape of the distribution curve and will not be detectable with the techniques used hitherto to study vibrational relaxation. The role of a scavenger gas can, however, produce much insight into the mechanism of the transfer.

From the results of the HF fluorescence signal in pure UF₆ the following picture emerges. The relatively long time decay of figure 2(a) is as a result of vibrational-vibrational transfer of energy from highly excited UF₆ to HF molecules. The latter is present as an impurity in the UF₆ - this was confirmed by chemical analysis. It is possible that the F atom that recoils from the dissociation process, contains sufficient energy to have the same role. However, this is ruled out by the absence of the slow transfer process when dissociation is instigated by 248 nm. In the latter case the remaining UF₆ contains a low amount of vibrational energy. The faster process clearly represents the reaction of F atoms with the scavenger gas, where the relaxation rate of ~4,5 μs torr is typical of vibrational-vibrational (V-V) transfer processes.

The striking results of this study are:

- 1. The dramatic effect of scavenger gases on the fluorescence signals especially at low temperature and***
- 2. The fact that at low temperatures the exchange of vibrational energy is much faster than at 300 K.***

The second aspect is consistent with results in a hydrogen scavenger media reported in the literature [1]. An increase of 3-6 times in the vibrational relaxation rate, dependent on the level of pre-excitation, results from a decrease in temperature from ambient to ~100K. This represents an equivalent increase in the effective cross-section. This clearly indicates that a long range exchange process must be dominant at low temperatures.

It must be kept in mind that the resonant transfer of vibrational energy between UF₆ molecules can be faster than the actual relaxation times measured in our experiments. Only a change in the vibrational distribution function will be detectable with e.g.

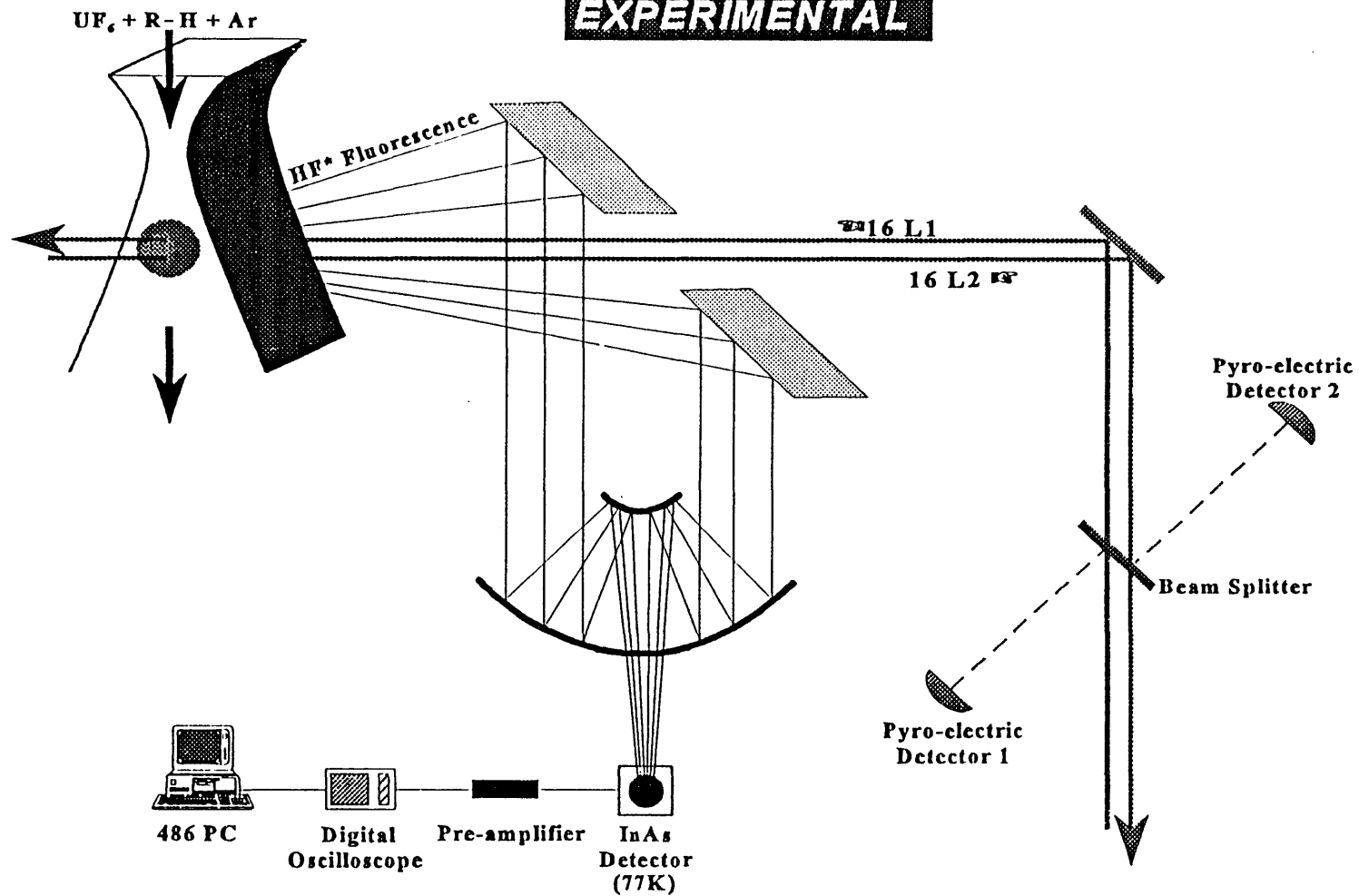
fluorescence and absorption techniques. Selectivity experiments, in turn, will be sensitive to exchange processes which will affect the dissociation rate of the specific isotope. Our results show that a high degree of vibrational excitation combined with a low thermal velocity, i.e. translational energy, advances the rate of vibrational energy exchange. Clearly, the contact time between molecules is advantageous to this process.

The most obvious theory for V-V energy transfer is derived from an exponential repulsive interaction between harmonic oscillators. In this case the integrated probability for V-V energy transfer is directly proportional to the absolute temperature. Mahan [3] was the first to indicate that an alternative mechanism, referred to as long-range dipole-dipole interactions, could induce near resonant V-V transfer in molecules with a strong induced dipole moment. In such cases the attractive part of the interaction potential introduces considerable Fourier components to the interaction potential. An expansion of the dipole moments in a Taylor series relative to the normal vibrational coordinate, confirms that if the dipole derivatives are non-zero, the dipole-dipole potential can indeed couple molecular vibrational states. According to this model, the integrated probability for V-V transfer, exhibits an inverse proportionality to the temperature, as was detected experimentally. Therefore the "collisions" under consideration in this paper are not of the head-on type but are subtle encounters in which one molecule simply passes another with a rather large distance, typically 5-10Å, between them.

REFERENCES

1. Gilbert M, Weulersse J M, Isnard P and Salvetat G, *Proceedings of SPIE Conference, Laser Applications in Chemistry*, Vol 669, 1986, p. 10.
2. Alimpiev S S, Karlov N V, Nabiev Sh Sh, Nikiforov S M, Prokhorov A M and Sartakov B G, *Sov. J. Quantum Elec.*, Vol 11, No 3, March 1987, p. 375.
3. Mahan B H, *J. Chem. Phys.*, Vol 46, 1967, p. 98.

EXPERIMENTAL



Schematic presentation of experimental configuration to measure HF fluorescence.*

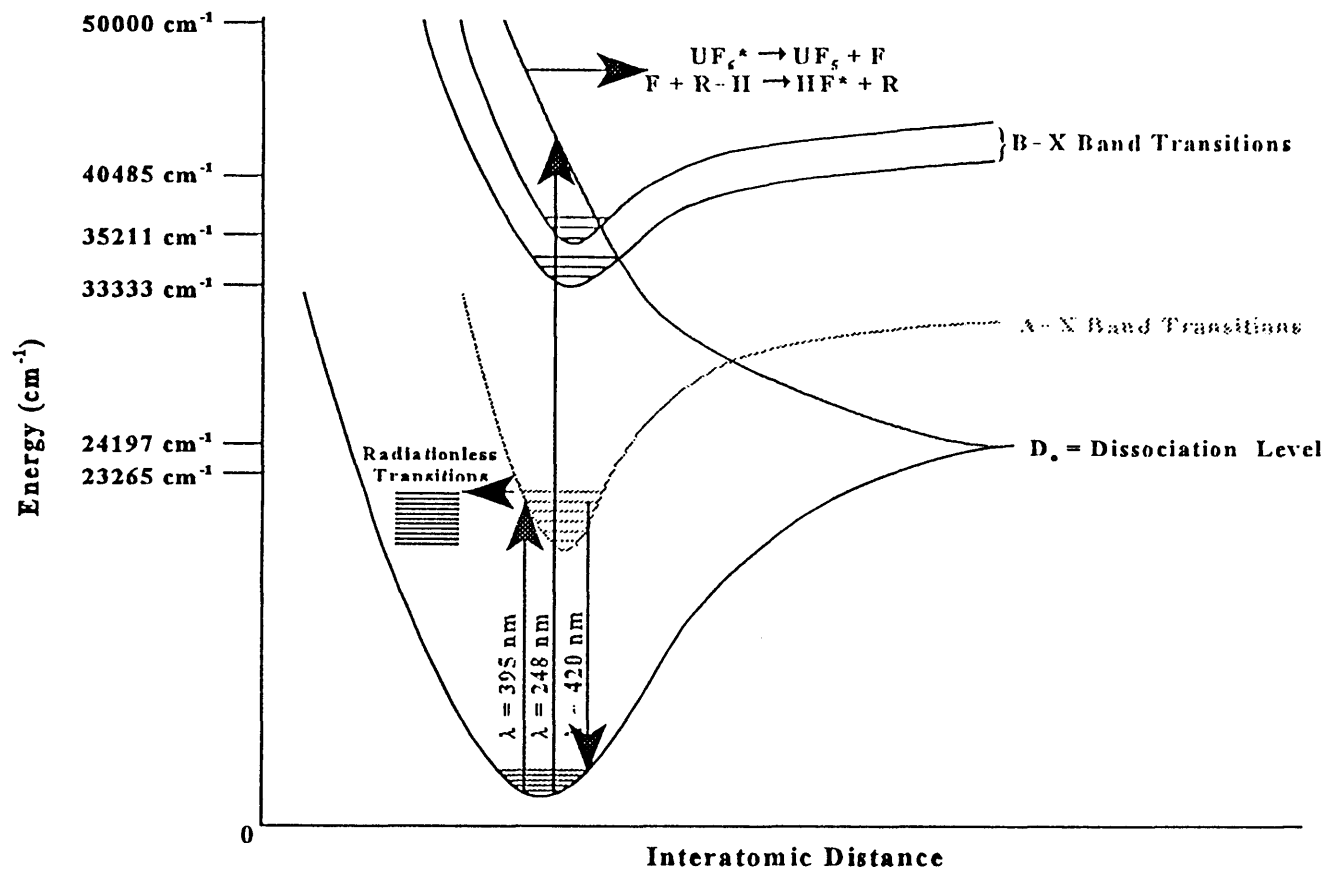


Figure 1: Schematic presentation of the excitation transitions giving rise to fluorescence in UF_6 .

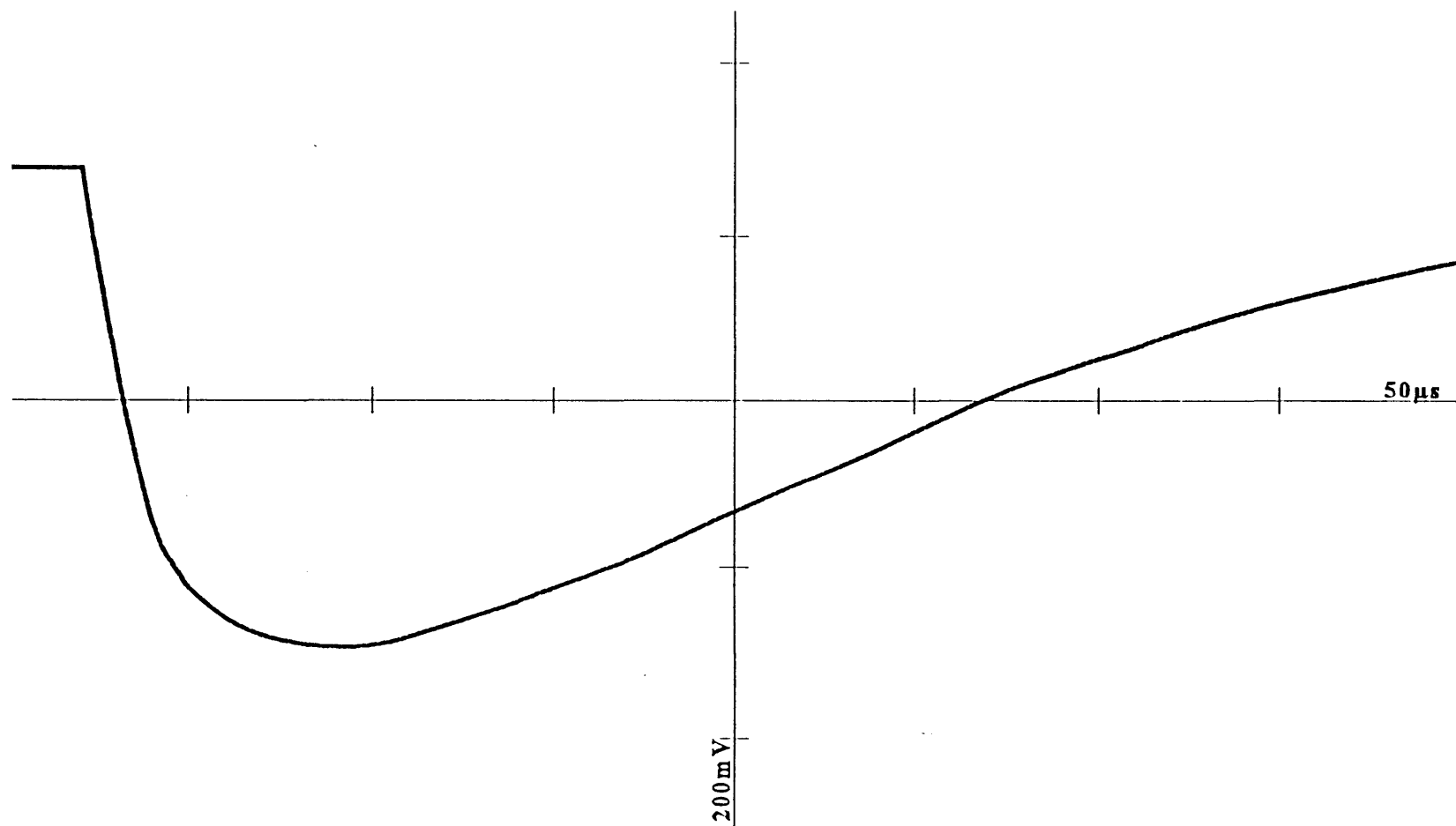


Figure 2(a): HF fluorescence versus time. Oscilloscope trace for $\sim 0,4$ torr (50Pa) UF_6 . HF as impurity. Temperature is 300K and dissociation wavelength $16\mu m$.

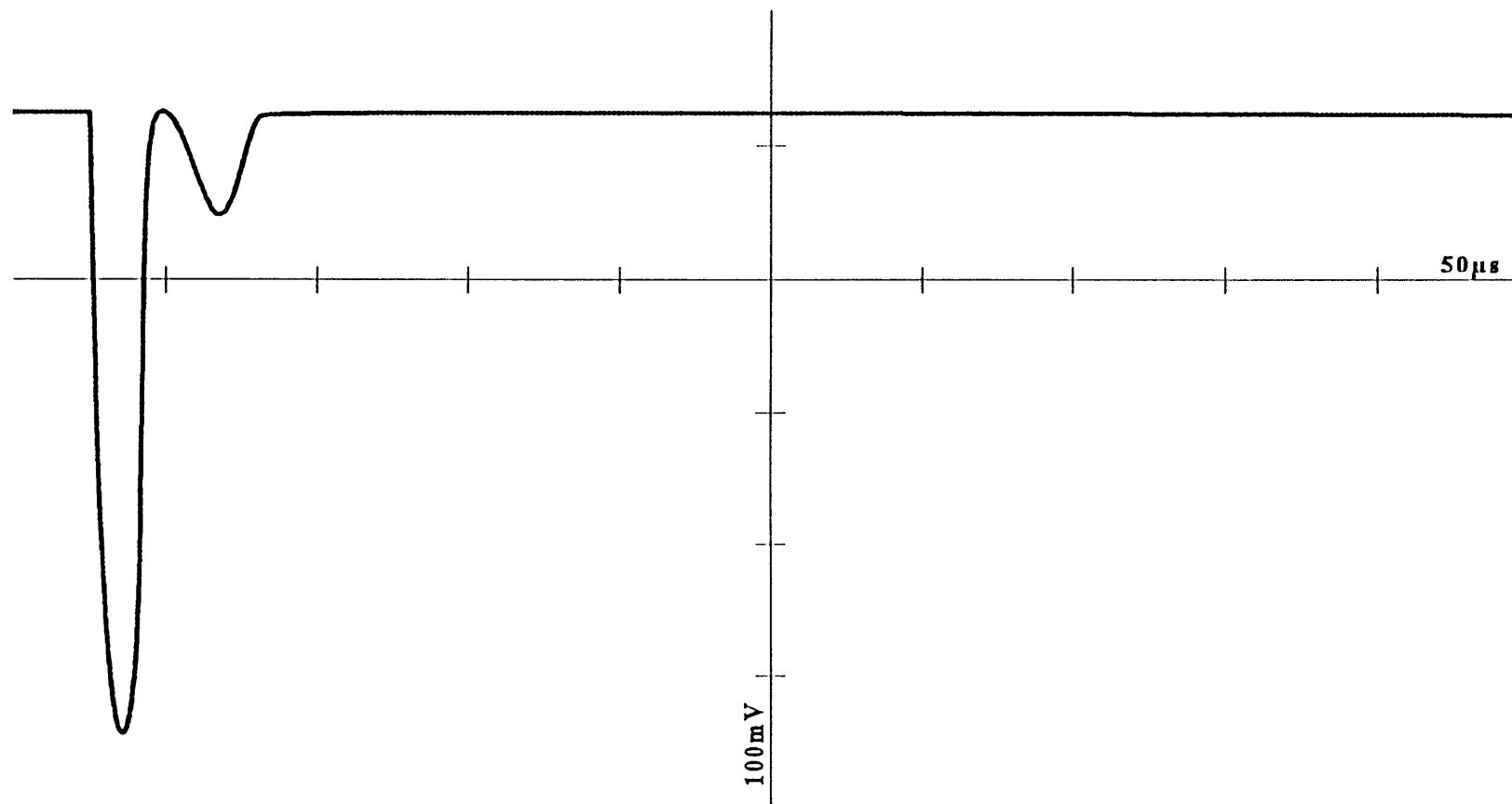


Figure 2(b): HF fluorescence versus time. Oscilloscope trace for ~0,4 torr (50Pa) UF_6 , 2 torr (266Pa) scavenger gas and Argon added to 9,8 torr (1300 Pa). Temperature is 300K and dissociation wavelength $16\mu\text{m}$.

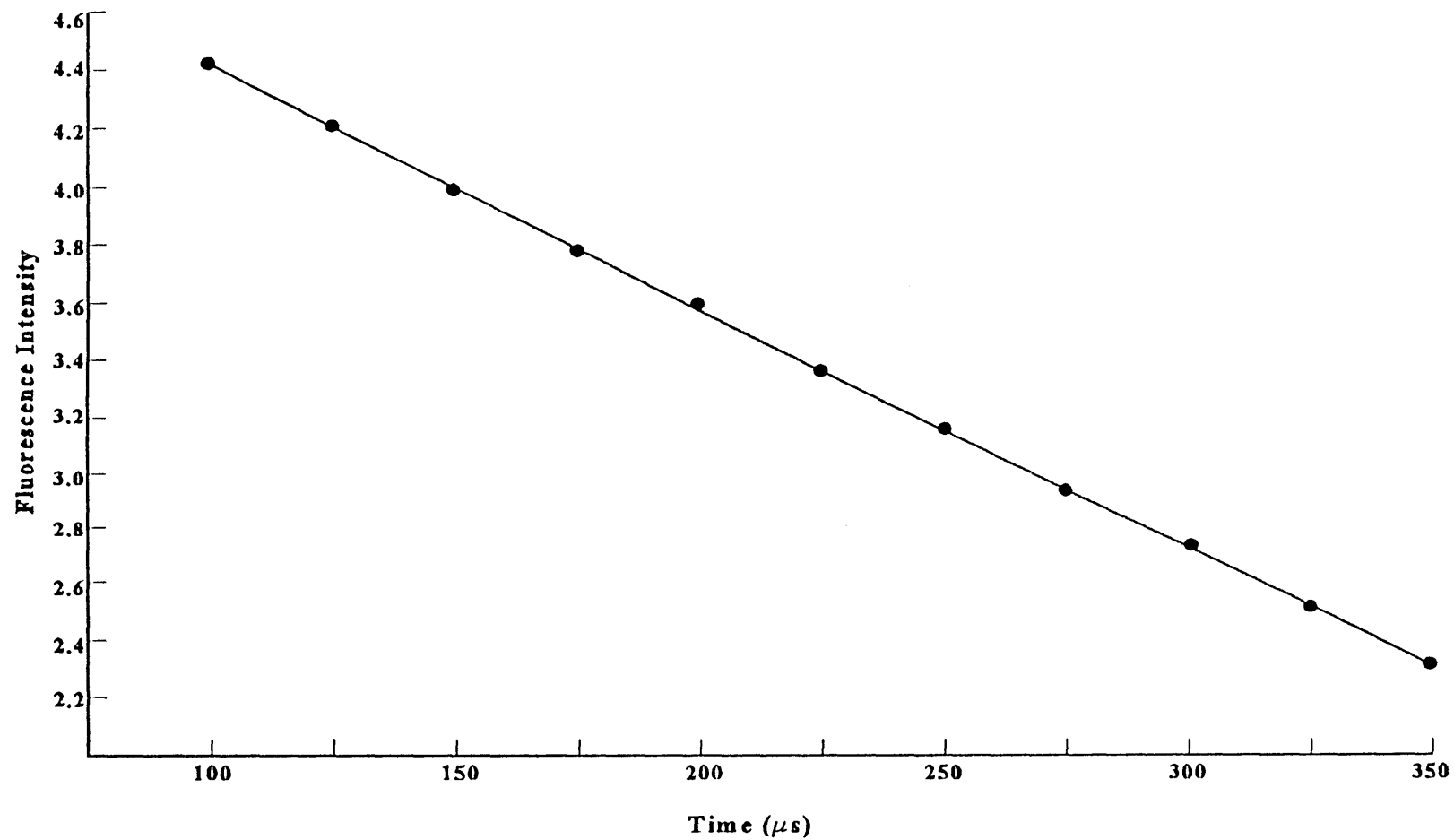


Figure 3: Semilog plot of HF fluorescence decay in figure 2(a). The slope gives a relaxation rate of $\sim 85 \mu s$ torr.

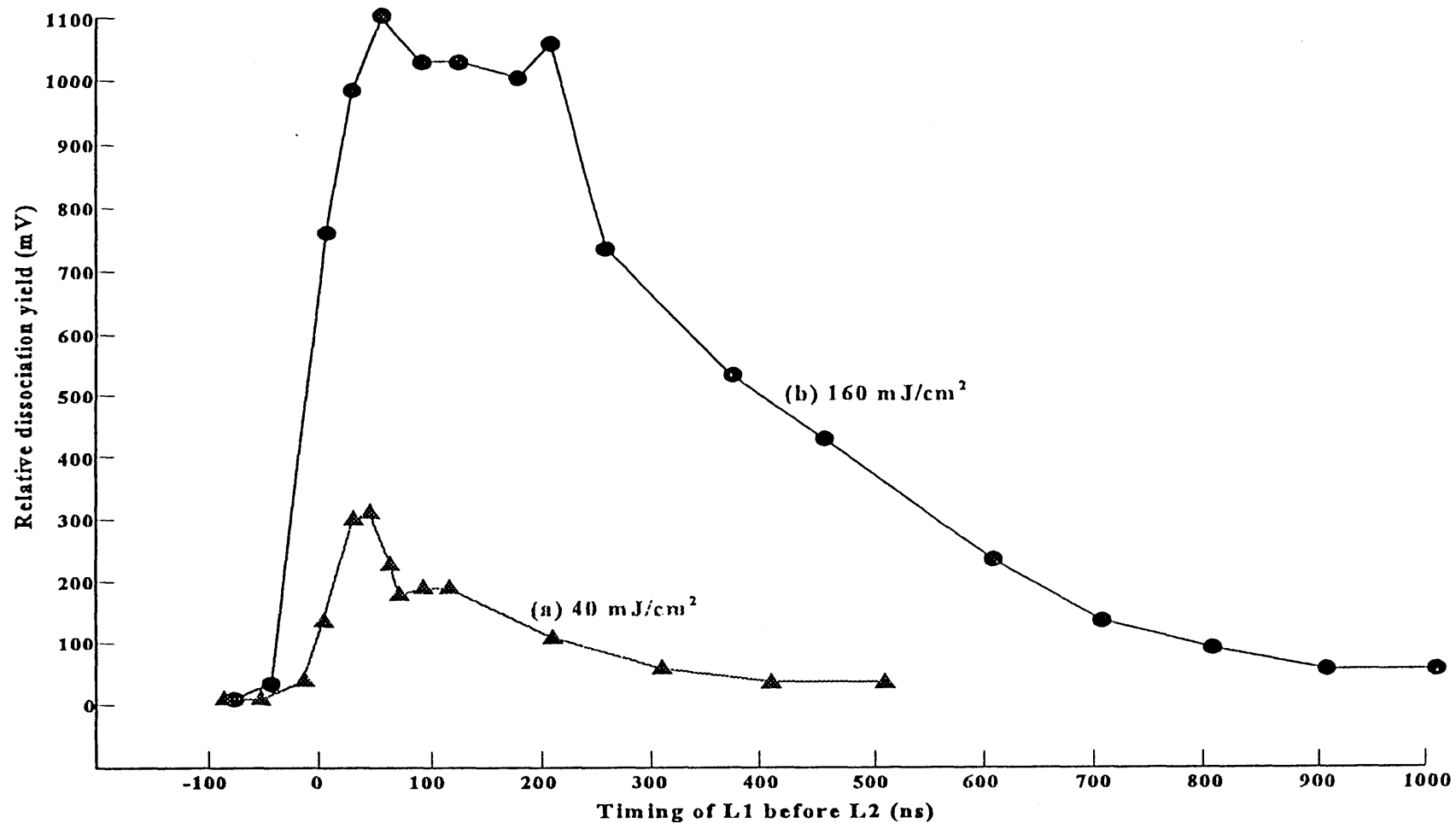


Figure 4: Peak HF fluorescence versus delay time between two 16 μ m wavelengths. The two plots are for different intensities of first wavelength (a) 40 mJ/cm² (b) 160 mJ/cm².

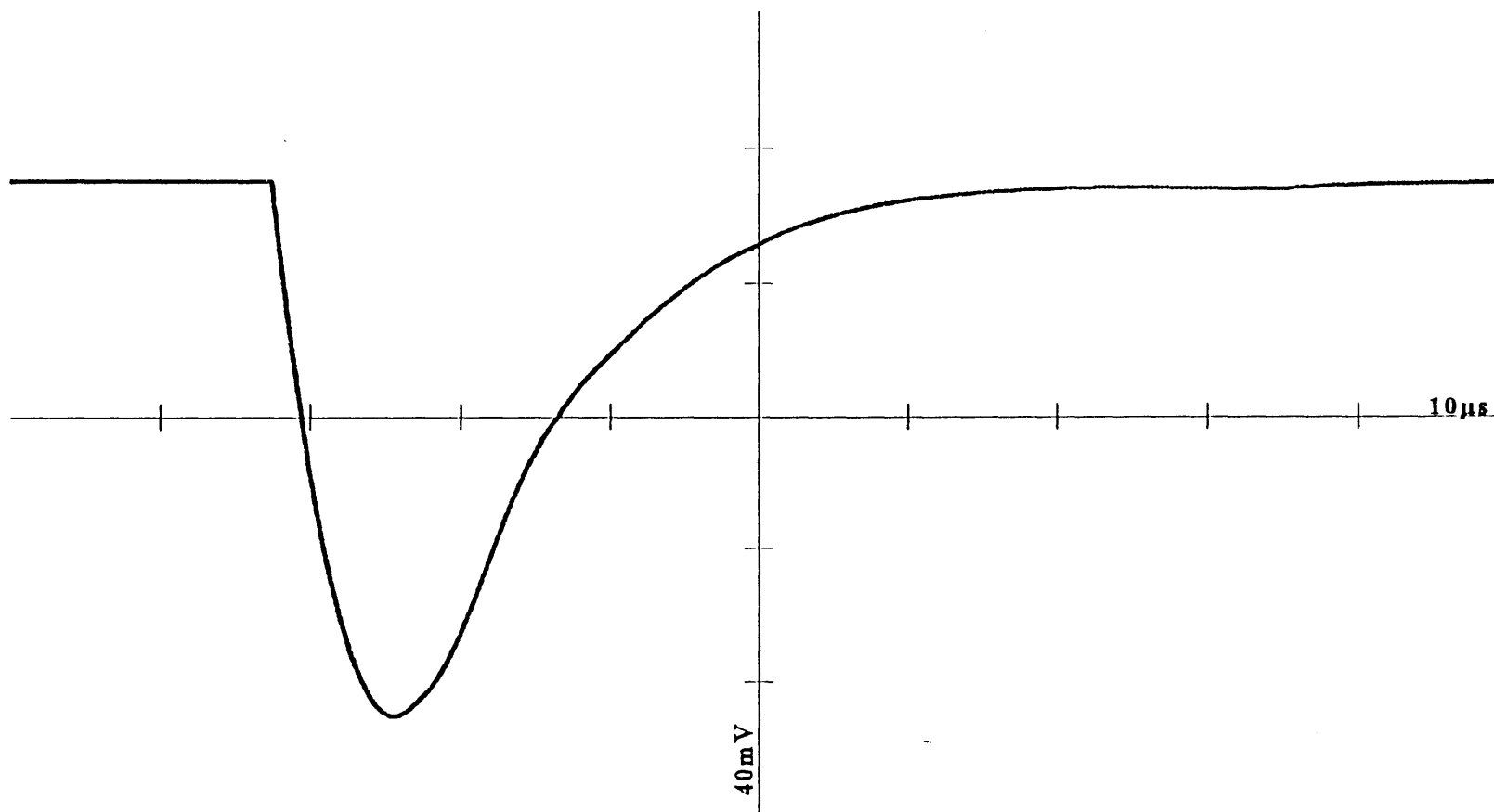


Figure 5: HF fluorescence versus time. Oscilloscope trace for ~0,4 torr (50Pa) UF₆ and 2,3 torr (300Pa) scavenger gas. Temperature is 300K and dissociation wavelength 248 nm.

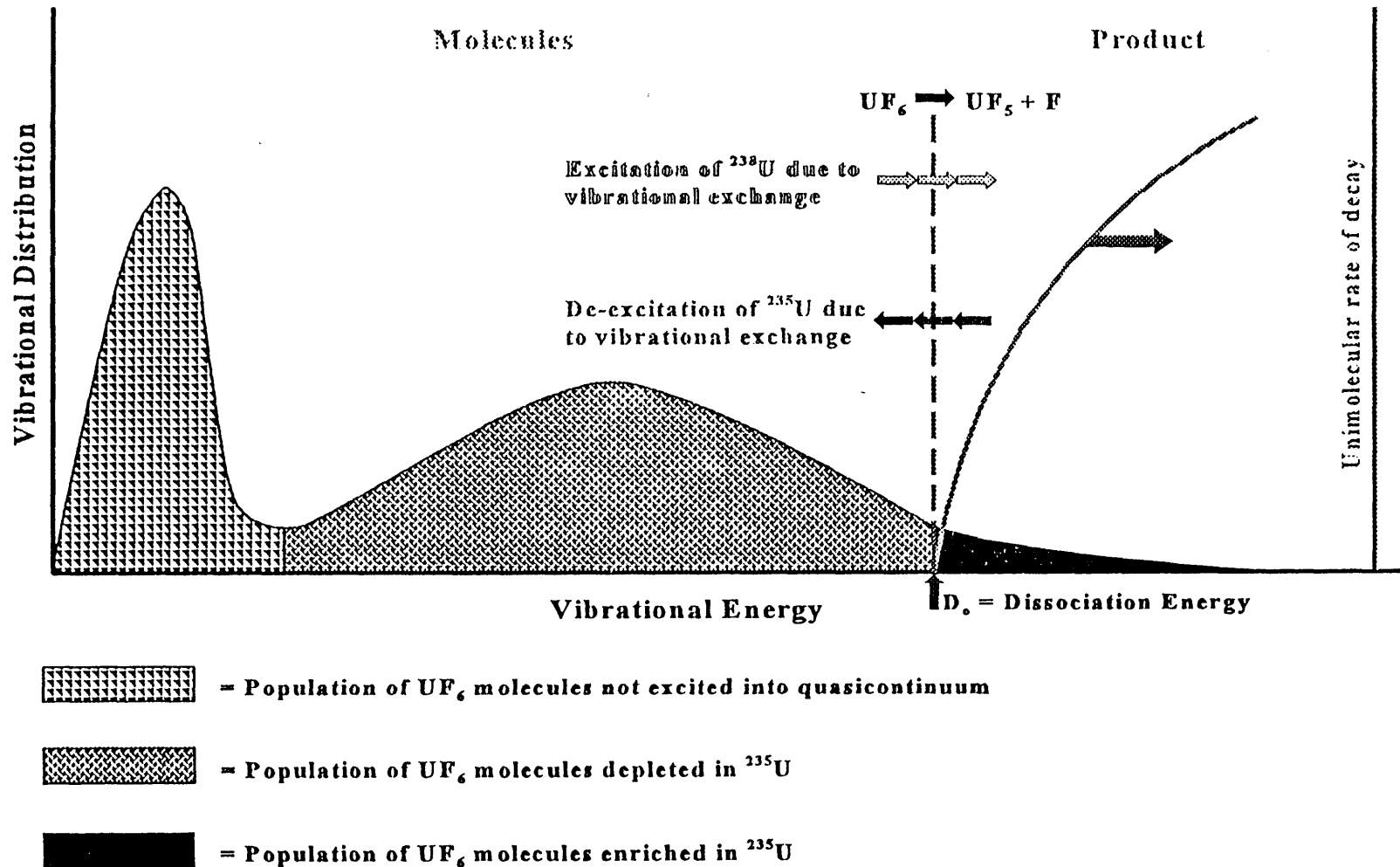


Figure 6: Schematic of the bi-modal vibrational distribution function of UF_6 at the onset of dissociation after excitation by multiphoton infrared absorption.

PAPER IV

**MULTIPHOTON INFRARED DISSOCIATION OF UF₆ AND
THE SUBSEQUENT IONIZATION OF THE PHOTO
FRAGMENTS IN A TIME-OF-FLIGHT MASS
SPECTROMETER**

E RONANDER, C LIEBENBERG, E R ROHWER

**Accepted for Publication in
International Journal of Mass Spectrometry and Ion Processes**

**MULTI PHOTON INFRARED DISSOCIATION OF UF₆ AND THE
SUBSEQUENT IONIZATION OF THE PHOTO FRAGMENTS IN A TIME-
OF-FLIGHT MASS SPECTROMETER**

E Ronander
Atomic Energy Corporation of South Africa Ltd
P O Box 582, Pretoria, 0001
South Africa

C J Liebenberg
Atomic Energy Corporation of South Africa Ltd
P O Box 582, Pretoria, 0001
South Africa

E R Rohwer
The University of Pretoria, Pretoria, 0001
South Africa

ABSTRACT

Some phenomena that relate to the analysis of a large polyatomic molecule and the nascent photo fragments formed subsequently to multi photon infrared dissociation in situ in a time-of-flight mass spectrometer are reported. Although the molecule UF_6 will be considered to convey the ideas, the processes involved are of a general nature and could possibly apply to many large polyatomic molecules. The analysis pertains specifically to the determination of e.g. isotopic concentrations, the yield of a photo reaction, concentrations of specific species etc, which all impacts critically on the viability of a laser isotope separation process.

This paper shows that the simplified picture of the dissociation and ionization processes by laser as being separate issues are not at all valid. The vibrational content of the molecule strongly influences the subsequent ionization cross section and leads to erroneous results for the selectivity. The selective ionization of the UF_5 product specie by laser in a time of flight mass spectrometer can therefore not be achieved in the simple fashion as previously proposed.

Keywords: cross sections, dissociation, mass spectrometry, Time-of-flight (TOF), laser ionization, vibrational energy

INTRODUCTION

This paper will address some phenomena that relate to the analysis of a large polyatomic molecule and the photo fragments formed subsequently to multi photon infrared absorption. The analysis pertains specifically to the time-of-flight mass spectrometer technique when it is utilized to determine, e.g. isotopic concentrations, the yield of a photo reaction, concentrations of specific species etc. Although the molecule UF_6 will be considered to convey the ideas, the processes involved are of a general nature and may possibly apply to many large polyatomic molecules.

A number of papers [1-4] have recently discussed the direct and real time determination of the separation factor obtained after the multi photon infrared dissociation of UF_6 . The approach is based on the selective ionization of the nascent UF_5 product by direct irradiation in a time of flight mass spectrometer. This methodology followed on earlier experimental observations [5,6] which showed that in the case of the dissociation of UF_6 by 266 nm via the B-X band, the UF_5 product can be selectively ionized by radiation at 532 nm. It was subsequently argued that if the ionization laser is set to a fluence, where no ion signal is detected, in the absence of infrared absorption the selectivity of the technique is guaranteed. This is an unfounded conclusion and not in line with the general picture of multi photon excitation and dissociation as it has precipitated over the last two decades. To facilitate a background for the discussion of the present issues, a short review of the salient properties of the infrared multi photon excitation in the ground electronic state of a polyatomic molecule will be given.

In the course of the multi photon excitation (MPE) of polyatomic molecules a molecule passes

through three very distinct regions labelled the initial region of discrete vibrational levels followed by the quasi continuum and the continuum that extends roughly from above the level of dissociation. Experimental observations on the multi photon dissociation (MPD) of SF₆ and UF₆, like other simple bond rupture reactions, are consistent with the RRKM statistical theory for the description of unimolecular reactions in MPD. In the quasi continuum the internal energy is randomized among all the vibrational modes on a timescale much shorter than the dissociation lifetime. At the onset of dissociation, after the excitation by many infrared photons, the vibrational distribution function of all the molecules in the irradiation zone takes the form as depicted schematically in figure 1. The RRKM theory shows that a substantial over excitation above the dissociation energy is required in order for a large molecule to dissociate, i.e. have a short dissociation lifetime. Thus, when the rate of the dissociation process becomes negligible the internal energy of the irradiated molecules is still substantial. If this energy is largely contained in the irradiation area, which is the case for the conditions prevailing when a laser time-of-flight mass spectrometer is utilized for UF₅ analyses, the following phenomena must surely influence the results:

1. The dissociation of vibrationally hot UF₆ molecules by the ionization laser, at fluences below the threshold for photo dissociation of cold UF₆. An additional amount of UF₅ is formed.
2. The direct ionization of vibrationally hot UF₆ molecules of which the photo ionization cross section differs markedly from vibrationally cold molecules. The additional ions detected are indistinguishable from those used for the detection of UF₅. The change in the photo ionization cross section for MPE SF₆ in a molecular beam has been used to

probe the vibrational energy distribution of SF₆ [7]. Clearly, the simplified picture of the dissociation and ionization processes as totally isolated events, can lead to erroneous interpretation of MS results.

EXPERIMENTAL

Infrared multi photon excitation (IR-MPE) of room temperature UF₆ was studied using 16 μm pulses to excite the strong fundamental ν₃ vibrational mode of UF₆. These pulses were focussed into the ionization region of a linear Time-of-Flight Mass Spectrometer (TOF-MS), followed by MPI of the dissociation products and mass selection of the resulting ions.

The experimental geometry was such that the direction of gas flow, laser pulses and flight tube were perpendicular to each other. A mixture of a small percentage UF₆ and some carrier gas was prepared in a reservoir and recirculated to maintain its composition. From here the gas mixture was slowly but continuously introduced through a 4 mm diameter orifice into the ionization chamber of the TOF-MS, which was evacuated by a 2000 liter/sec turbo molecular pump. The typical background pressure increased slightly to ~5 x 10⁻⁵ mbar. This arrangement was suitable for ambient temperature measurements but for flow cooled experiments the setup illustrated in figure 2 was utilized.

A CO₂ oscillator and amplifiers arranged in a master oscillator power amplifier (MOPA) configuration together with the Raman conversion technique was used to generate the 16 μm wavelength radiation. The oscillator was injection mode locked by a CW CO₂ laser, producing a smooth single longitudinal cavity mode. The Raman cell was a Herriot type design with 26

pass as operated at 77K with Giqued nitrogen and the scattering gas was para-H₂. The 16 μm output had a Gaussian transverse profile, with a M² beam quality factor of <2. It was focussed inside the TOF-MS with a 1/e² beam radius of 2 mm. At the exit of the ionization chamber, the beam was reflected by a LiF window, and the energy monitored by a Lambda Physic energy meter. A correction was made to relate this value to the actual energy at the centre of the ionization region.

The source for the ionization wavelength was the fundamental, multimode 1064 nm output of a Nd:Yag laser, or alternatively its second harmonic, 532 nm. These pulses were introduced into the TOF-MS, collinearly with the 16 μm, but from the opposite direction. The pulses were focussed by a 300 mm quartz lens to produce fluences of 200-300 J/cm², respectively. Extreme care was exercised to ensure that the laser fluence was below the MPI threshold of UF₆. The fluences in the focal volume were varied using quartz plate stacks or by adjusting the focal length of the lens. The ionization laser intensity was also monitored in situ by placing a pyroelectric detector in the reflected portion from a LiF window.

A time delay of 0-2 μs was introduced between the 1064 nm pulses and the preceding 16 μm pulses. The ions formed in the volume between the repeller plate and extraction grid as a result of MPD and subsequent MPI were accelerated through a ground grid into the field-free flight tube of the TOF-MS, onto a multichannel plate (MCP) detector. The TOF mass spectra are dominated by the parent U⁺ and U²⁺ ions, of which the ratio could be varied by changing the ionization laser power density. The effective mass resolution at the U²⁺ peak was >300. The output of the MCP detector, together with the respective energy signals were connected to a 540 Tektronix digital storage oscilloscope. Data acquisition and detection were carried out for each

photo ionization event. The signal amplitude of the U^+ ion was taken as an indication of the relative MPE/MPD/MPI yield.

RESULTS

The time-of-flight mass spectra (TOFMS) of UF_6 , using the focussed light from the Nd:YAG laser or its second harmonic, $\lambda = 532$ nm, is dominated by the single and multiple charged uranium ions and not the UF_x^+ fragment ions. This surprising result has been reported previously [5,6,8,9] and has led to the postulate of the “giant resonance” transitions [8,9]. Our spectra agree in general with the qualitative features of the previously reported data. However, we also found some distinctly different aspects. The first prominent feature is that the laser fluences employed were at least two orders of magnitude lower than that utilized in reference [9]. This probably stems from the fact that the M^2 parameter was not included in the estimation of the spot size in the latter study, leading to an underestimation of the beam diameter. Whilst only weak ion signals were obtained with the Nd:YAG laser at $\sim 7.6 \times 10^{12}$ W/cm² in the mentioned study, we could detect the mass spectra from $\sim 3 \times 10^{10}$ W/cm². The same feature applies when ionization is instigated by $\lambda = 532$ nm. The detected ion signals were similar to that reported in references [8, 9] namely U^{2+} , U^+ , and UF_2^+ with the addition of a clear signal at UF^{++} . The latter was approximately one third the strength of the UF^+ ion signal which in turn was \sim six percent of the dominant signal at U^+ . In the configuration when the ionization is applied downstream of the pre-excitation or dissociation laser, shown in figure 2, the presence of a hydrocarbon scavenger plays a dominant role in the strength of the ion signals [10]. In this position no ion signals were detected when 532 nm radiation was used to ionize the nascent photo fragments of UF_6 even when HF-fluorescence from the formed F radical and a scavenger confirmed that dissociation

was indeed occurring. The UF_5 photo fragments produced by, e.g. the 266 nm photo dissociation of UF_6 can contain as much as 1,5 eV of vibrational energy, derived from energy conservation, and at this point it was suspected that this internal energy, can play a significant role to overcome the UF_5 ionization potential of especially in the collinear experimental setup. If this is applicable to the ionization cross section of the UF_5 photo product then the vibrational content after multi photon infrared excitation of the parent UF_6 molecule, must show an equally significant effect on its own ionization cross section. The approach to decrease the MPI laser energy to below the threshold of cold UF_6 ionization would then cease to guarantee the selectivity of the ionization for the photo fragments. The magnitude of the dominant U^+ -ion signal was chosen to monitor the influence of a few parameters on the ionization process. Figure 3 displays the ion signals for a constant Nd:YAG laser (1064 nm) fluence, mJ/cm^2 , whilst the fluence of the 16 μm laser is scanned for various wavelengths in the collinear arrangement. The notation, e.g. 16R30 refers to 16 μm wavelengths derived from the R30 line of the 10,6 μm branch of the CO_2 laser. Prior to the accumulation of the TOF MS spectra, the fluence of the Nd:YAG laser was decreased to the point where no ion signals could be detected when the ionization laser was acting on its own. UF_6 was introduced together with a carrier gas, e.g. helium or argon, where the former constituted 1-5% of the mixture. The mixture was introduced by effusive inlet consequently the temperature was at ambient. A small delay of $\sim 10\text{-}20$ ns between the excitation laser and ionization laser was introduced. It is well-known that the different 16 μm wavelengths will excite UF_6 with different efficiencies in the discrete region [11,12]. Note that there appears to be virtually no threshold fluence and even values of 10 mJ/cm^2 causes an ion signal which rises rapidly as the fluence of the infrared laser increases. If single wavelength dissociation of UF_6 at room temperature is desired, substantially higher fluences are required. A fluence of 10 mJ/cm^2 mildly excites a UF_6 molecule, nevertheless this

has a pronounced effect on the ion signals. In figure 4 similar trends are depicted for UF_6 molecules that have been flow cooled to ca 100 K. The ionization process, however, is now not performed in a collinear manner but downstream, with a time delay of $\sim 500 \mu\text{s}$ after the infrared radiation pulse. In this instance, a clear threshold fluence is applicable for each 16 μm wavelength. It is clear from the abovementioned trends that the ion yield is significantly affected by the pre-excitation of the UF_6 molecule and the consequences for isotopic analysis after infrared multi photon dissociation will be discussed under the appropriate section.

We observed the same trends for the ion yield if the second harmonic at 532 nm was introduced as ionization laser. In the latter case the efficiency of ionization is substantially better, as has been reported before [8, 9]. In figure 5 the case for the collinear radiation is depicted. To accentuate the effect even more, a series of graphs is shown in figure 6 where different Nd:YAG ionization fluences are selected and the infrared excitation varied. For any selected ionization fluence the pre-excitation strongly influences the ion yield. Plotting the data on a log scale for the ion signal illustrates clearly the variable “threshold” fluence for the IR dissociation laser to overcome the ionization potential.

Some simple calculations on the average vibrational temperature at the downstream position, to elucidate the contribution of pre-excitation at this position, is desirable. We first assume that the irradiated UF_6 molecules remain largely in the irradiated dimensions as they move downstream. This is a reasonable assumption as the Rayleigh scattering technique, which detects the uranium photo fragments after clustering [10], has previously illustrated this feature. Furthermore, the probing of the distribution of energy pumped into UF_6 molecules, by Raman scattering techniques [13], have confirmed an average vibrational temperature shortly after

irradiation, and at less than ten percent dissociation, of approximately 2000 K. At high temperatures the UF_6 molecules can “store” 15 kT of energy in the vibrational modes whilst all the other modes of energy is equal to $3/2$ kT, i.e. rotational and translation. For the case of UF_6 in He, say 5% of the former and an initial flow cooled temperature of ~ 100 K, an equilibrium temperature of 700-800 K will result. From our experimental observations it is certain that such a increase in temperature will affect the ionization signal significantly compared to the flow cooled temperature situation. If a scavenger gas is added, the resultant temperature will be slightly less due to its increased thermal capacity.

DISCUSSION AND CONCLUSIONS

A discussion of the reported observations should be directed along the giant resonance hypotheses of Armstrong et al [8,9] and the schematic presentation of figure 7. The giant resonance proposal has been discussed at length in reference [9] and will not be repeated here. Suffice it to say that the efficient excitation of UF_6 molecules to a level of ~ 50 eV is proposed via a resonance with energy in the range of 12-14 eV above the ground state UF_6 . This highly excited molecule then ionizes and fragments, via multiple channels into U^{m+} and UF_x^+ etc. The prominence of the atomic ions seems to be supported by this approach. Figure 7 serves to highlight the different processes involved when dissociation and/or excitation of a UF_6 molecule occur prior to ionization. In the case of UV, 266 nm, excitation the initial vibrational energy distribution is very narrow, representative of either room temperature or flow cooled temperatures. At a wavelength of 266 nm the excitation is to the A-X band and at this wavelength dissociation occurs from the excited electronic states by pre-dissociation [14]. Upon dissociation substantial vibrational, energy, up to 1,5 eV, resides in the UF_5 fragment thereby

placing it in the quasi continuum. The remaining UF_6 , in the ground electronic state remains at low levels of vibrational excitation. When the ionization laser is tuned to interact preferentially on the UF_5 photo fragments, selectivity for ionization is possible by virtue of the lower ionization potential, and the vibrational excitation level of the UF_5 molecule. It is also conceivable that if a relatively high pressure of a buffer gas, e.g. Argon, is added to this system that it will affect the ionization yield of the UF_5 , but not UF_6 as was experimentally observed [15].

The action of multi photon processes involving the simultaneous annihilation of 266 nm and an ionizing wavelength, e.g. 532 nm, has previously been excluded if neither of the lasers on it's own caused any detectable ion signals. These hypotheses assume that excitation by 266 nm is to a directly dissociative state which is, in our opinion a debatable issue. The result of reference 15 indicates that pre-dissociation clearly plays a role. The pre-dissociative process requires some time and if the ionization process is instigated whilst a molecule is in the excited state, it follows from our observations and the giant resonance proposal that this pre-excitation will have a significant influence on the ion signals. A model that can be applied to the ionization process is the similarity of the discrete levels and quasi continuum of the vibrational levels in the ground electronic state. The "ease" with which the first resonance in the giant resonance model can be reached, should strongly influence the entire multi photon process. This is similar to the case where even mild pre-excitation of the vibrational levels in the multi photon infrared dissociation process has a strong influence on the dissociation yield. From the discussion hitherto it follows that the selective laser ionization of the UF_5 molecule, immediately after its formation by 266 nm photolysis of UF_6 , is suspect.

Considering the situation when pre-excitation and dissociation proceed via multi photon infrared

absorption. The RRKM theory predicts that an over excitation, of 40 to 50 percent above the dissociation energy of 3 eV is required for a UF_6 molecule to dissociate in a short enough time. At the point where the rate of dissociation approaches zero, the average vibrational energy is still substantial, as depicted in figure 7(b). Due to the distribution of the vibrational energy a long high energy tail is characteristic of this process with the result that a portion of the UF_6 molecules can have internal energies up to 4 eV. The UF_5 photo fragment receives less internal energy after dissociation than in the case when dissociation is instigated via 266 nm. Reducing the intensity of the ionization laser to the point where vibrationally cool UF_6 is not detectable, does not guarantee the absence of a signal from the vibrationally excited molecules. The opposite is indeed true, not only does our experimental observation show a significant loss of ionization selectivity of the uranium bearing photo fragment to be analysed, it also implies that incorrect enrichment factors are derived by this method. The findings of this study have a general impact on the interpretation of molecular beam studies performed by laser ionization MS. The yields of reactions are influenced by many parameters, including the change in ionization cross section following pre-excitation.

REFERENCES

1. S. Kato, Y. Okada, S. Satooka, H. Tashiro and K. Takeuchi, Proceedings of International Symposium on Isotope Separation and Chemical Exchange Uranium Enrichment, Tokyo, (Oct-Nov 1990) 141.
2. Y. Kuga, S. Satooka, H. Tashiro and K. Takeuchi., Proceedings of International Symposium on Isotope Separation and Chemical Exchange Uranium Enrichment, Tokyo, (Oct-Nov 1990) 133.
3. Y. Okada, S. Kato, S. Satooka, H. Tashiro and K. Takeuchi, J Nucl. Sci. Technology., 32, no 11, (Nov 1995) 1174-1180.
4. Y. Okada, S. Kato, K. Sunouchi, S. Satooka, H. Tashiro and K. Takeuchi, Appl. Phys. B62, (1996) 77-81
5. M. Stuke, H. Reisler and C. Wittig, Appl. Phys. Lett., 39, (1981) 201.
6. J.S. Chou, D. Sumida, M. Stuke and C. Wittig, Laser Chem., 1, no 1, (1982) 1-7
7. A.S. Sudbo, P.A. Schulz, D.J. Krajnovich, Y.T. Lee and V.R. Shen, Opt. Lett., 4, no 7, (1979) 219
8. D.P. Armstrong, Ph.D. dissertation, The University of Tennessee, Knoxville, Tennessee, (1992).
9. D.P. Armstrong, D.A. Harkins, R.N. Compton and D. Ding, J. Chem. Phys., 100, no 1, (1994) 28.
10. H.G.C. Human, AEC of South Africa, private communication.
11. P. Rabinowitz, A. Kaldor, A. Gnauck, R.L. Woodin, and J.S. Gethner, Optics Lett. 7, no

- 5, (1982) 212-214.
12. M. Gilbert, J.M. Weulersse, P. Isnard and G. Salvétat, Congress of the Society of photo-optical instrumentation Engineers (SPIE), Quebec (Canada), (June 1986).
 13. E. Ryabov, Russian Institute of Spectroscopy, private communication.
 14. M. Menghini, P. Morales, P. Dore and M.I. Schisano, J. Chem. Phys., 84, no 11, (1986) 6521.
 15. P. Dore, M.I. Schisano, M. Menghini and P. Morales, Chem. Phys. Lett., 116, no 6, (1985) 521-524.

FIGURE CAPTIONS

- Fig.1 - Schematic presentation of the vibrational distribution function for a poly-atomic molecule such as UF_6 following multi photon infrared excitation. The molecules containing internal energy exceeding the dissociation energy, D_0 , can dissociate according to the RRKM theory.
- Fig.2 - Schematic of the experimental configuration utilized to study the role of vibrational pre-excitation on the ionization spectra of UF_6 .
- Fig.3 - TOFMS signals for UF_6 when ionization is instigated by a Nd:YAG laser (1064 nm) at a constant fluence of $\sim 200 \text{ J/cm}^2$. Pre-excitation is by $16 \mu\text{m}$ radiation for various wavelengths: (a) 16R20 (b) 16R22 (c) 16R28 (d) 16R30. Measurements are for UF_6 at ambient temperature in a co-linear arrangement.
- Fig.4 - TOFMS signals for UF_6 when ionization is instigated by a Nd:YAG laser (1064 nm) at a constant fluence of $\sim 200 \text{ J/cm}^2$. Pre-excitation is by $16 \mu\text{m}$ radiation at various wavelengths: (a) 16R16 (b) 16R20 (c) 16R24 (d) 16R30. Measurements are for UF_6 flow cooled to ca 100 K. A time delay of $\sim 500 \mu\text{s}$ was introduced between pre-excitation and ionization signals.
- Fig.5 - TOFMS signals for UF_6 when ionization is instigated by a Nd:YAG laser at 1064 nm, (a), and the second harmonic of the Nd:YAG laser at 532, (b), respectively. Pre-excitation is by $16 \mu\text{m}$ radiation at the 16R18 line. The respective fluences of the ionization lasers are $\sim 100 \text{ J/cm}^2$, (a), and 10 J/cm^2 , (b). The measurements are for UF_6 at ambient temperature in a co-linear arrangement.
- Fig.6 - TOFMS signals, presented on a log scale, for UF_6 when ionization is instigated by a Nd:YAG laser (1064 nm) at a different fluence: (a) 280 J/cm^2 , (b) 225 J/cm^2 , (c) 185 J/cm^2 and (d) 145 J/cm^2 . Pre-excitation is by $16 \mu\text{m}$ radiation at 16R18 line. Measurements are for UF_6 at ambient temperature in a co-linear arrangement.

Fig.7 - Schematic presentation of the vibrational energy distribution for UF_6 when excitation is instigated by a ultraviolet laser at 266 nm, (a), and multi photon excitation of a infrared laser at 16 μm wavelength, (b).

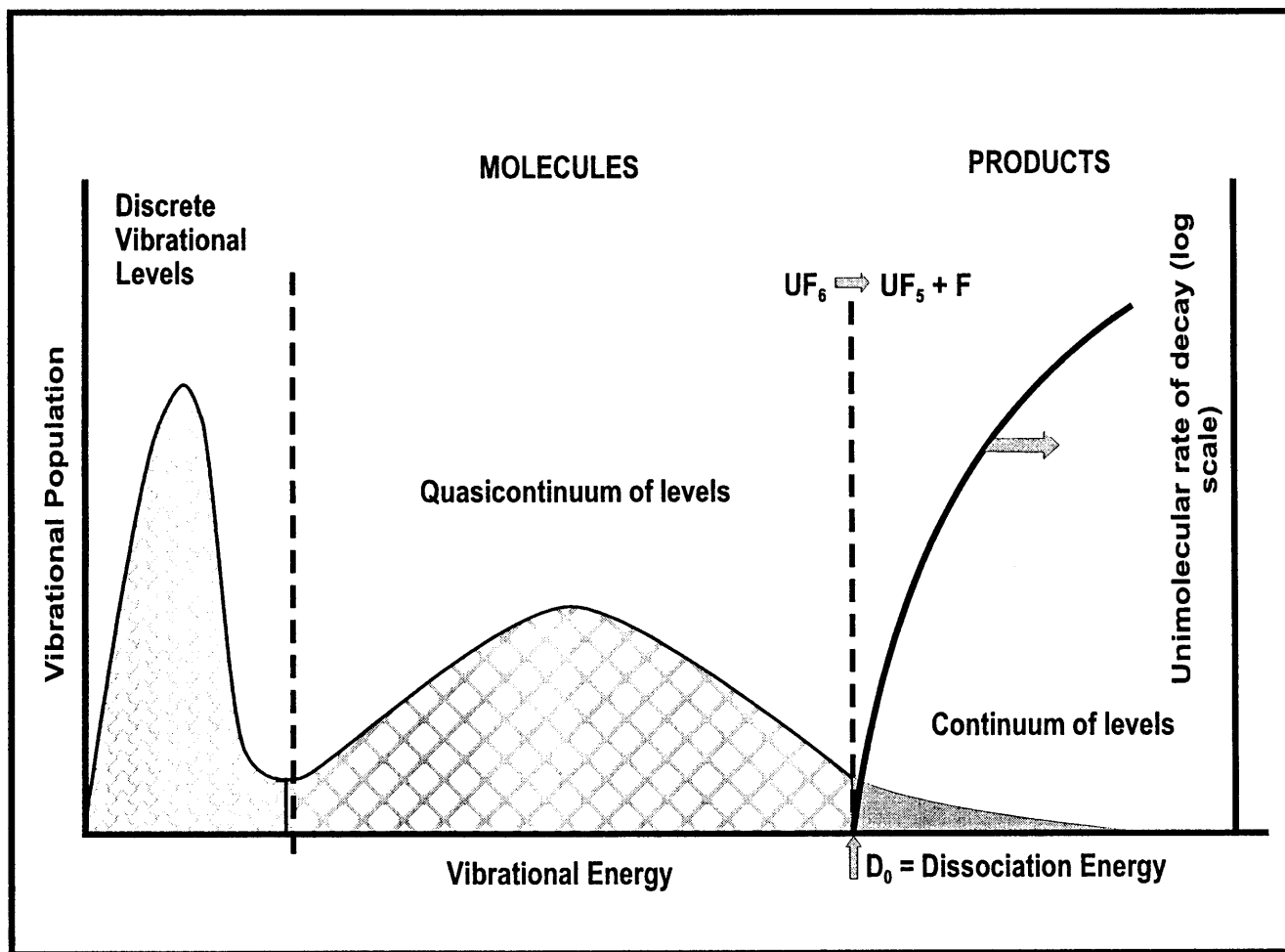


FIGURE 1

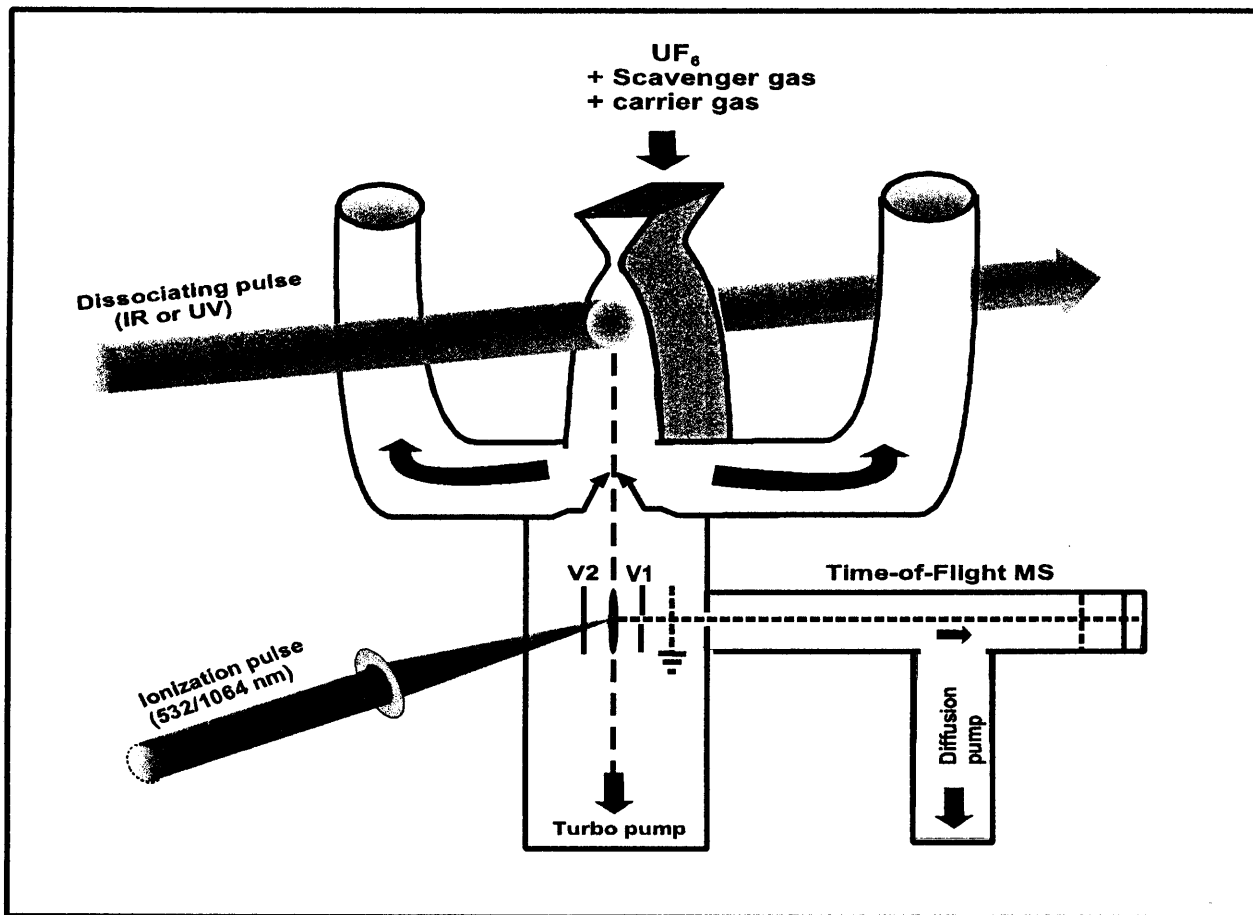


FIGURE 2

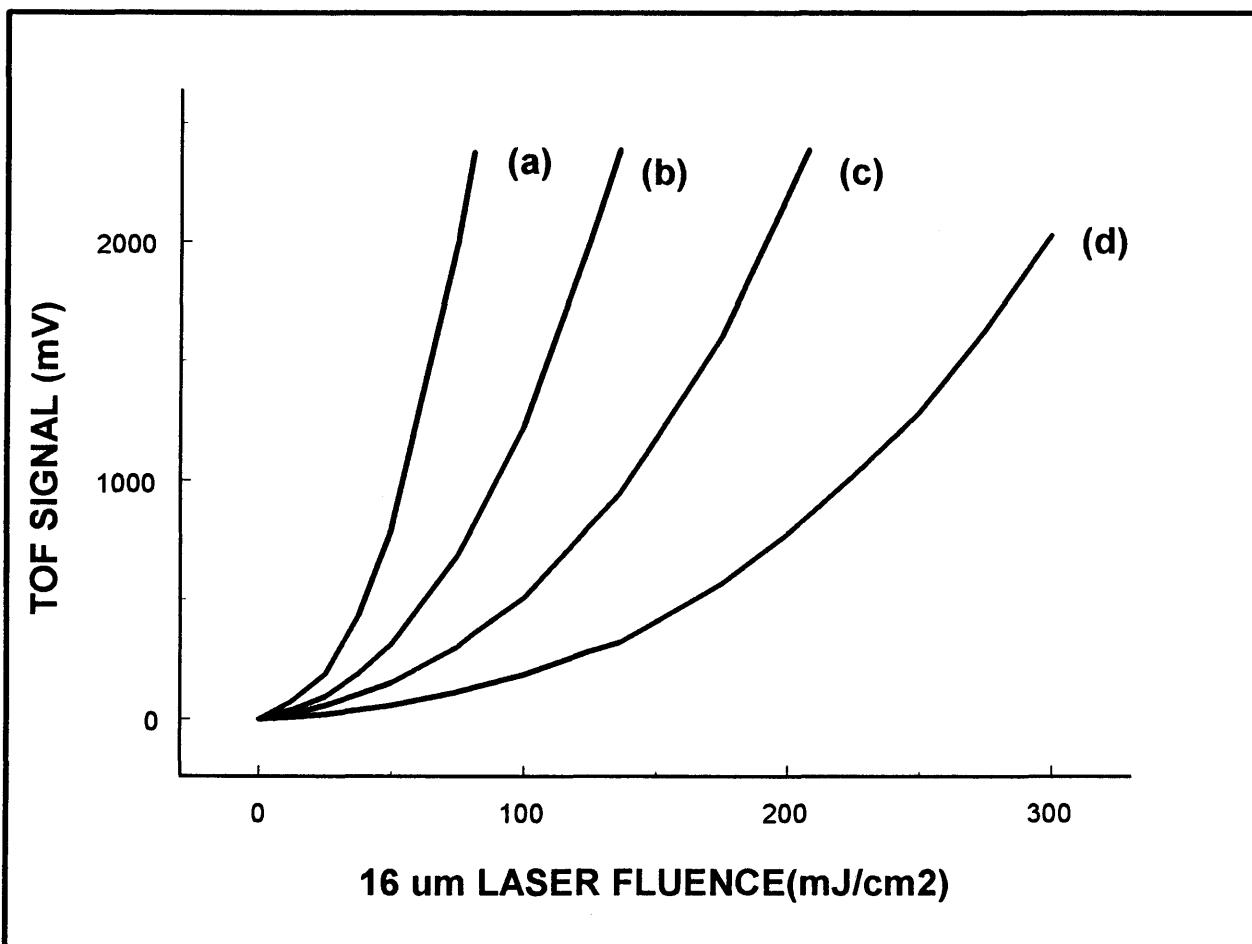


FIGURE 3

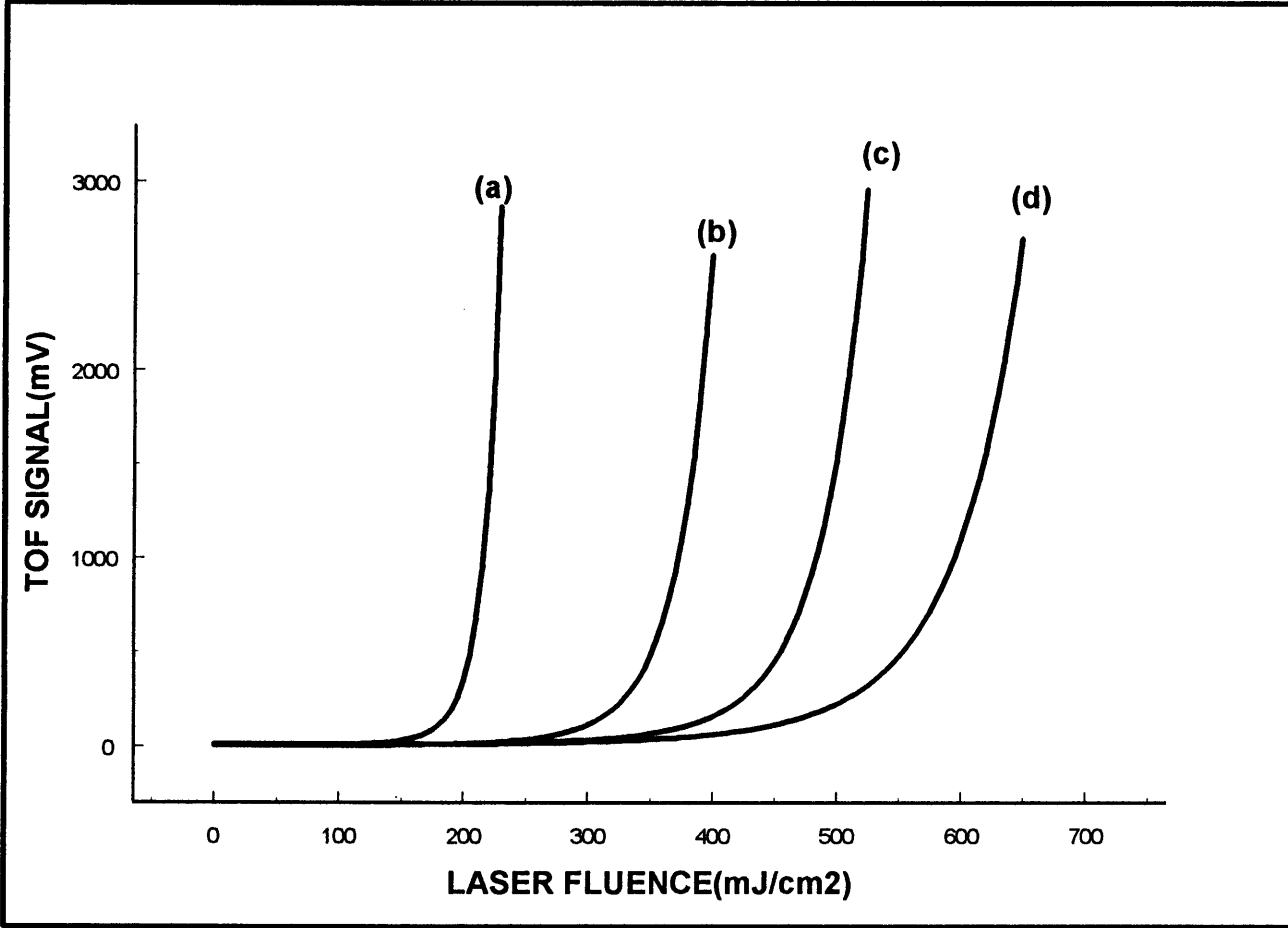


FIGURE 4

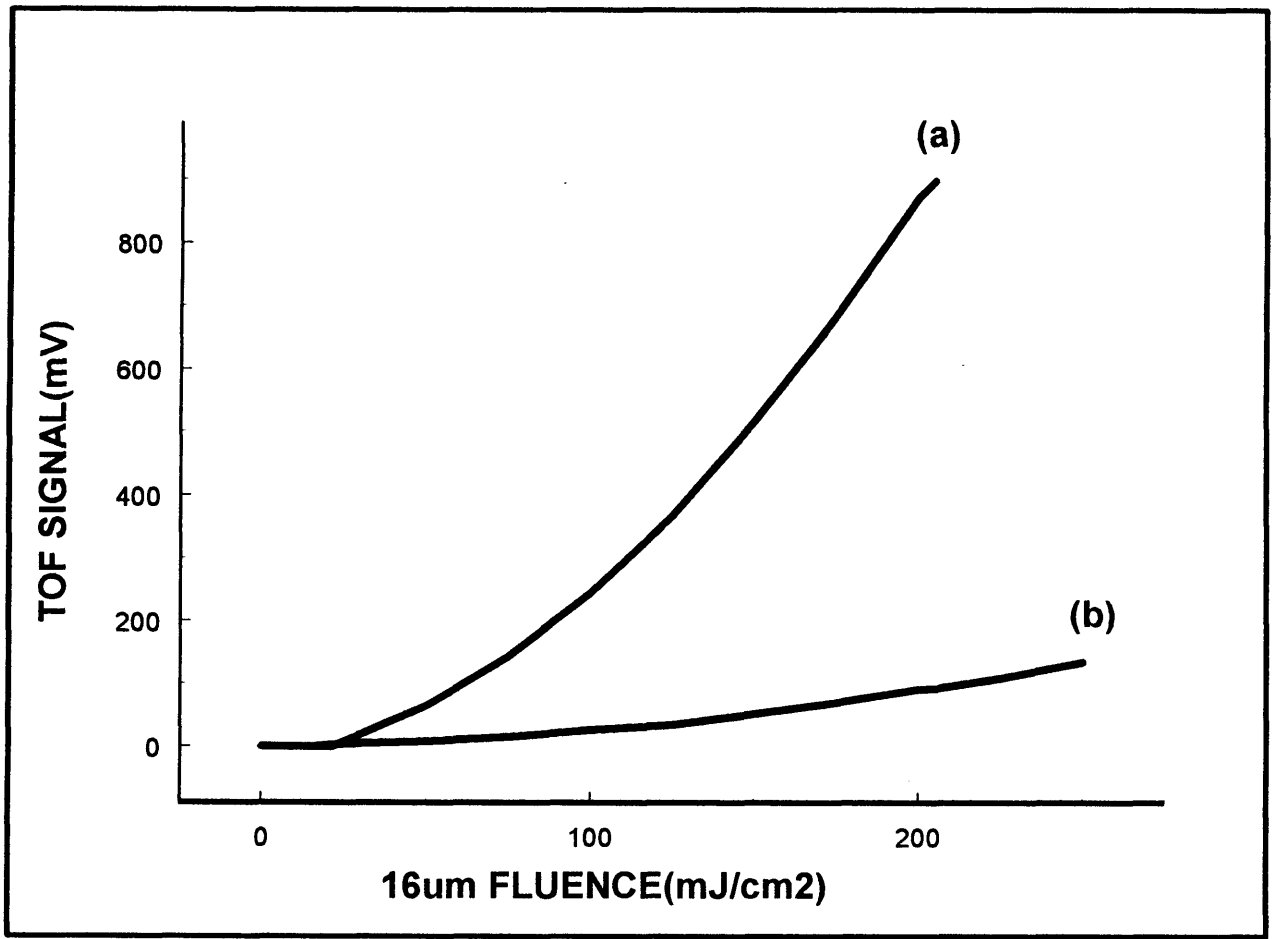


FIGURE 5

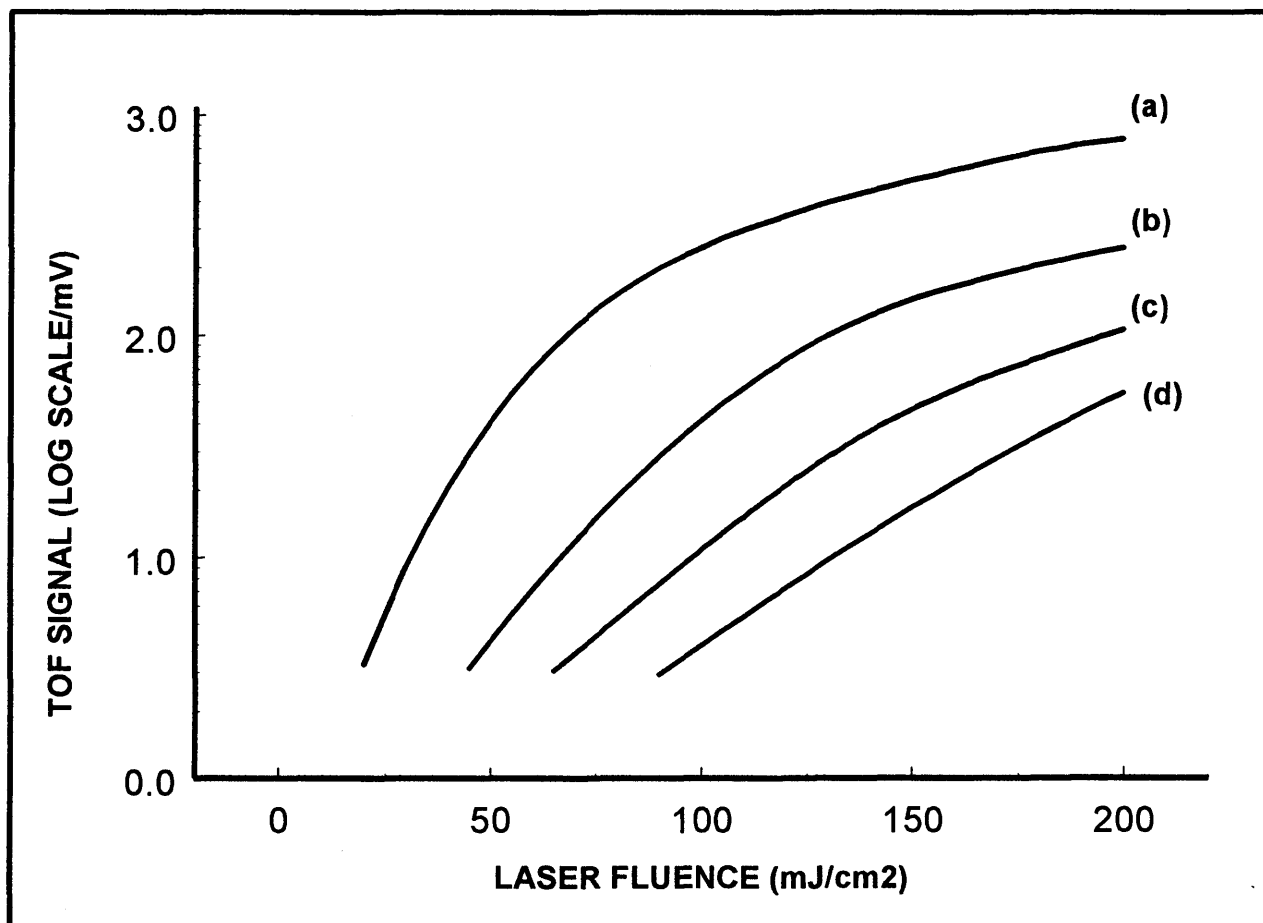


FIGURE 6

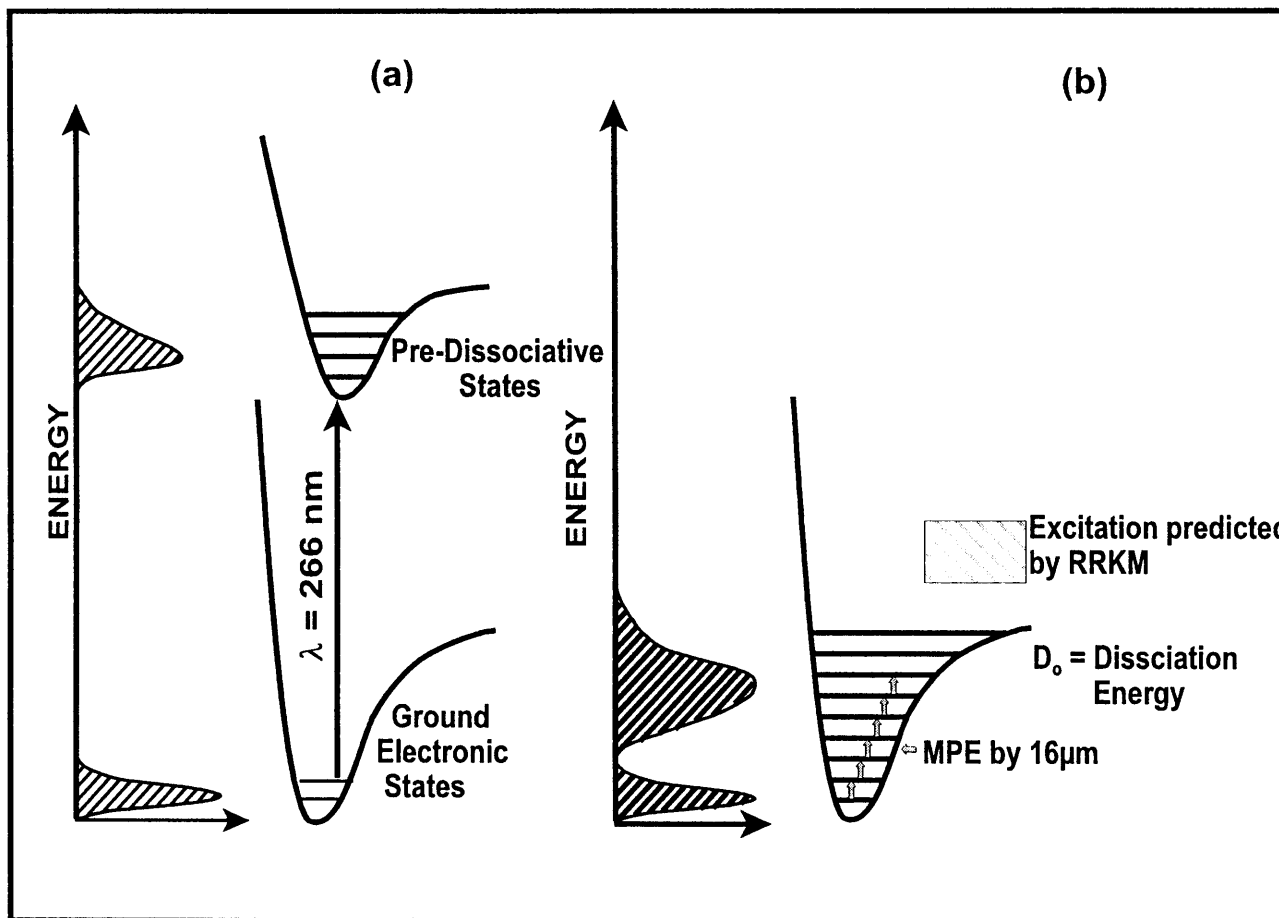


FIGURE 7